Expanding the Toolbox for Probing Dynamic Behavior in Covalent Adaptable Networks

Nicholas J. Bongiardina

B.S., Chemical Engineering, University of Colorado Boulder, 2016

M.S., Materials Science and Engineering, University of Colorado Boulder, 2018

A thesis submitted to the Materials Science and Engineering Program at the University of

Colorado for the Degree of Doctor of Philosophy Materials Science and Engineering

2022

Committee Members:

Dr. Christopher Bowman

Dr. Yifu Ding

Dr. Ryan Hayward

Dr. Jeffery Stansbury

Dr. Timothy White

Bongiardina, Nicholas, J. (Ph.D., Materials Science and Engineering)

Expanding the Toolbox for Probing Dynamic Behavior in Covalent Adaptable Networks

Thesis directed by Professor Christopher N. Bowman

Covalent Adaptable Networks are an important and growing class of polymer materials that enable reconfiguration of what would otherwise be a static three-dimensional network through the incorporation of dynamic bonds. Such adaptability enables the design of stimuli responsive materials and crosslinked networks that can processed and reprocessed in ways that are typically attributed to linear and branched polymers.

Two areas were explored in this thesis with respect to covalent adaptable networks. The first was the development and characterization of the thiol-ene-disulfide polymerizations of linear disulfides, which combines the thiol-ene and disulfidation reactions in one network-forming system to make tunable dynamic materials. The second was implementation of dielectric analysis to characterize the dynamic behavior of various dynamic networks. this was done to understand the impact of thiol substitution on dynamic thioester reactions and explore the utility of DEA as a tool for understanding the differences in dynamic for different mechanisms of dynamic bonding, A combination of FTIR, DMA, NMR, rheology, and stress relaxation were implemented to develop and study these materials and techniques.

It was found that thiol-ene-disulfide photopolymerizations were a viable approach for making dual-cure and dynamic networks. A thorough kinetics analysis showed that the thiol-ene reaction is about 30 times faster than the disulfide-ene reaction, producing a dual-cure system with spatial and temporal control. Inherent to this approach, radical-disulfide exchange slowed the thiol-ene step, and the specific thiol/disulfide pair significantly impacted the rate of both the thiol-ene and disulfide-ene stages of the polymerization, depending on the relative stability of the thiyl radical formed by the thiol and disulfide. Exchange also enabled shrinkage stress reduction during the polymerization and induced stress relaxation that could be controlled by network structure and choice of disulfide core.

Although thiol substitution has been shown to have little impact on thiol-ene the thiol-ene reaction, it was found to have a significant impact on dynamic reactions involving thioesters. In networks only capable of thioester exchange, stress relaxation was significantly slower for the secondary thiol/thioester networks than for the primary analogues. Dielectric analysis indicated that the slowed rate was due to a combination of steric hinderance, which slows nucleophilic attack onto the thioester, and the decrease in polarity associated with the large number of additional methyl groups, which is known to create a less conducive environment for thioester exchange in general. For thiol-anhydride-ene networks, which are capable reversible addition and reversible exchange, substitution biased dynamic bonding toward the reversible thiol-anhydride addition at a given temperature.

Finally, analysis of dielectric and stress relaxation spectra showed that DEA can detect differences between reversible addition and reversible exchange mechanisms. Time-temperature-superposition of dielectric spectra for Diels-Alder (addition), thioester (exchange), and thiol-anhydride (both) networks showed that the spectra were superimposable if the equilibrium number of crosslinks was not significantly impacted by the temperature.

Dedication

To my mom, dad, stepfather, and sister who have tirelessly supported me throughout my childhood, undergraduate, and graduate school journey. I would not be here without them.

Acknowledgments

First and foremost, I would like to thank my advisor, Christopher Bowman, for being such an important part of my journey through both my undergraduate and graduate programs. I first met Chris when he taught my undergraduate kinetics course, and I was so struck by his enthusiasm for teaching that I walked into his office mid-semester through the semester and asked to do a senior thesis project in his lab the following year. When I decided to go grad school and stay here at CU, he encouraged me to make sure that I found the right research group even if it wasn't his. But ultimately choosing his group was an easy decision, and I would not be here without his reassurance, guidance, and support.

I am thankful to have been awarded the Ruth L. Kirschstein NRSA Predoctoral Fellowship from the National Institute of Health. This fellowship was a significant source of funding my research and education at the University of Colorado Boulder.

I would not have made it through the last five and a half years without my all friends. I would have fully lost my sanity if not for Katelyn Long. Whether we talk about science, our favorite TV shows, or your hilarious/therapeutic writing project, you have helped enormously and I could not be more grateful that you (and your dogs) are a part of my life. I'd also like to thank Alina Martinez; you have been my partner in crime in the lab since day one. It has been a wild journey and our venting sessions have been sanity inducing throughout. I can't wait to see what you do next. Dani Konetski, you were the first friend I made in lab as a bright-eyed senior undergraduate. You made me feel welcome, have taught me so much, and you were my fellow morning person until Katelyn had drank enough coffee to tolerate our cheery morning demeanor. Lastly, Josh Kamps and Shafer Soars were late additions to the lab who somehow tolerated my rantings and raving about politics at lunch for the last three years.

I have also been lucky to have incredible mentors along the way. Dr. Janet DeGrazia taught me materials and energy balances and helped me get my first job working in a lab. Dr Christine Hrenya, who took me on as a sophomore for my first research experience. And all of the wonderful faculty in chemical engineering at CU Boulder who helped give me the tools to be an engineering student and researcher

along the way. In grad school, Dr. Ben Fairbanks, Dr. Heidi Culver, Dr. Jasmine Sinha, Dr. Maciej Podgorski, Dr. Sudhi Mavila, Dr. Alexa Kuenstler, Dr. Matthew McBride, and Dr. Brady Worrell have all given me incredible help and advice throughout the years and I would have been lost without them.

Finally, I'd like to thank my credible family. My parents, Jodi and Richard, have always supported and encouraged me in whatever I wanted to do. They created a stable and healthy homes for my sister and I even after they split up. My stepfather, Mitch, has been a third parent to me and I'm so thankful for him as well. And of course Io need to thank my sister, Alessandra. I'm lucky that I have a sister who is also my best friend, who I can talk to about anything and everything, and who helped keep me sane for 5 months of quarantine during the COVID-19 pandemic.

Table of Contents

List of Figures

List Of Tables

Chapter 1 - INTRODUCTION

1.1 *Introduction to Covalent Adaptable Networks*

Polymers are ubiquitous materials that permeate all aspects of modern life. They are made up of long chains of repeating units, and the nature of those units and how they are connected dictate their properties and ultimately their utility. Polymers make up a huge proportion of the functional materials we see and rely on every day, ranging from soda bottles to food and product packaging, to vehicle tires, to aircraft wings and wind turbine blades. In general, most polymers are classified into two categories based on the topology of the constitutive polymer chains: thermoplastics or thermosets (**Figure 1.1**). Each possesses specific advantages and disadvantages derived from their structure and connectivity.

a) Thermoplastics   a) Thermosets

Linear   **Branched**   **Crosslinked**
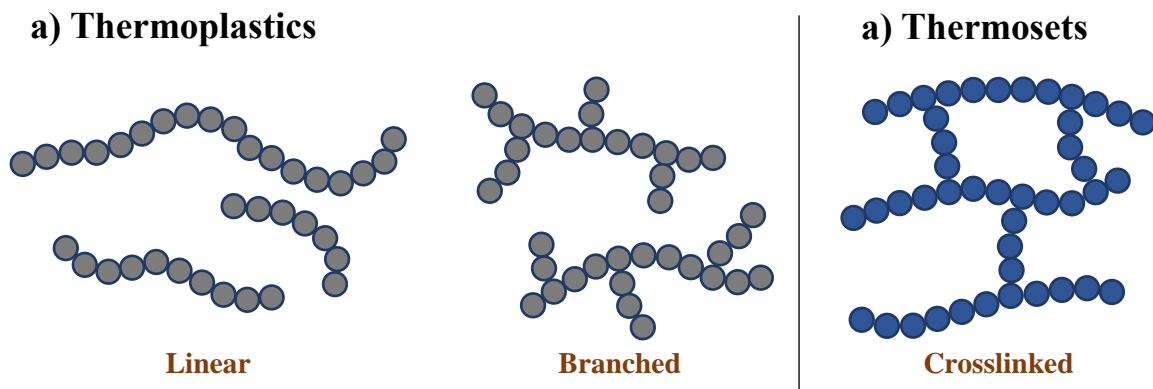
Figure 1.1: A representation of the types of the types of polymer chains that make up the two general classes of polymers, where a) Thermoplastics are broadly made up of linear and branched polymer chains and b) thermosets are made up of polymer chains that are covalently bonded, or crosslinked, together.

Thermoplastics are the more common class of plastics that we use in everyday life and make up the plastics that are numbered for recycling, such as low-density polyethylene (LDPE) used for plastic bags and poly(ethylene terephthalate) (PET) for beverage bottles. They consist of linear or branched polymer chains that are held together by non-covalent interactions that may include any combination of chain entanglements, other non-specific Van Der Waals forces, hydrogen bonding, and other non-covalent interactions depending to type and structure of a given polymer or polymer mixture. Thermoplastics are ubiquitous in commercial plastics and consumer materials because these non-covalent interactions enable facile processing into the desired shape. Upon heating, the linear or branched chains overcome the forces

holding them together and slide past each other under an applied force. This mobility makes thermoplastic amenable to a variety of processing techniques such as injection molding or extrusion to convert the synthesized polymer into the desired product[1, 2]. A major benefit of thermoplastics is that, when properly separated, they can be recycled upon heating to make new products and reduce single-use plastic waste, although at the current time, only about 9% of plastics are recycled and most are downcycled into materials of lower quality[3]. However, the non-covalent interactions associated with thermoplastics often, though not exclusively, limit them to lower temperature applications and uses that don't involve prolonged exposure to solvent or chemical conditions that can solvate or degrade these materials over time. In addition, the mechanical strength and longevity of thermoplastics can be limited due the strength of their intermolecular interactions and are frequently less suitable for structural materials or long-term wear and tear.

In contrast, thermosets are made of polymer chains that are connected by covalent bonds, forming a three-dimensional network. Their covalently crosslinked structure results in robust mechanical properties and better resistance to solvents and chemical exposure. This makes thermosets extremely attractive for structural materials and composite matrices that must survive conditions and/or mechanical forces for which thermoplastics are unsuitable – such as permanent and structural adhesives, lightweight composites used in aerospace and wind-power, and bottles used for chemical storage among others. However, it is extremely difficult to repurpose/recycle or even degrade many thermosets at end-of-life because their covalently crosslinked structure prevents flow upon heating, meaning that any reprocessing requires irreversible breaking of covalent bonds.

Given the strengths and weakness of thermoplastics and thermosets, a great deal of work over the past several decades has been devoted to developing covalently bonded materials with reconfigurable bonds to bridge the gap of these two classes of polymers. The result has become a rich and growing class of dynamic polymer materials called covalent adaptable networks (CANs)[4-6]. These crosslinked networks incorporate dynamic covalent chemistries that, when triggered under a chosen set of conditions, enable bond reconfiguration in what would otherwise be considered a static, three-dimensional network. An approach

centered on dynamic bonds opens the door to generate stimuli-responsive materials and products with the robust properties sought out in thermosets with many of the processability characteristics of thermoplastics. Both the development and implementation of new dynamic polymers and a better understanding of how dynamic bonds impact polymer chain dynamics are of great interest to improving the design of CANs for a growing range of applications.

The number of available dynamic bonds has expanded tremendously in recent years. Bond reconfiguration can be active either during or after polymerization depending on the choice of dynamic bond, polymerization chemistry, and stimulus. CANs are classified based on their dynamic bonding mechanism. The most common classification is based on the mechanism of bond reconfiguration and the resulting impact on network structure. These categories are reversible addition (dissociative chemistries) and reversible exchange (associative chemistries) (**Figure 1.2**).
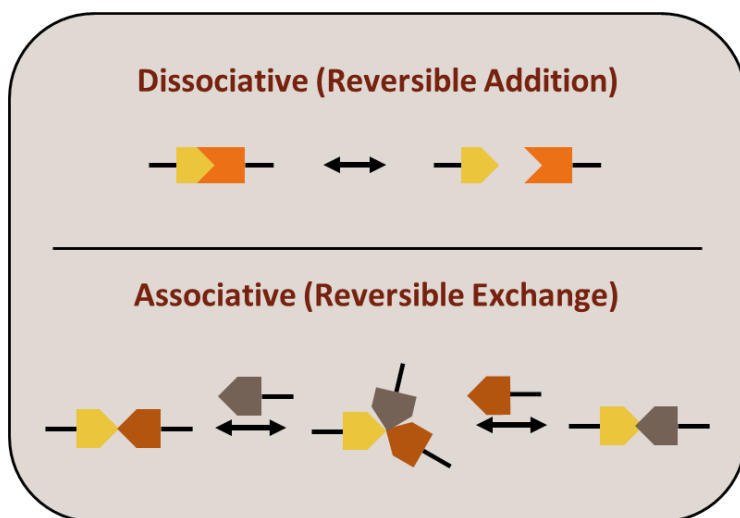
Figure 1.2: Schematic of a) dissociative/reversible addition and b) associative/ reversible exchange bond in covalent adaptable networks.

Reverible addition involves the breaking-then-reforming of the dynamic bond under the applied stimulus. During this process, the overall chain mobility is increased due to partial or complete de-gelation of the network, which allows the chains to rearrange until the stimulus is removed. The network then returns to a crosslinked state with different topology than the initial network. This results in high chain mobility as bonds continuously break and reform. A variety of dissociative bonds have been explored, including Diels-

Alder[7, 8], dimerization of anthracene[9] and cinnamates[10, 11], urethane and urea bonds[12, 13], and thiol-Michael adducts[14, 15]. These and other bonds can be simulated by light, heat, and/or the appropriate catalysts to activate bond reconfiguration depending on the choice of chemistry that suits the application. Reversible addition CANs are well suited for recycling and self-healing behaviors in bulk because the number of crosslinks can be significantly reduced, or the material can be temporarily depolymerized into a liquid state. These processes can be performed repeatably so long as the relevant functional groups aren't consumed by side reactions and too many non-dynamic covalent bonds are not broken during processing.

In contrast, in reversible exchange the dynamic bond mechanism is the opposite of dissociative chemistries; bond-formation followed by bond-breaking. Here, the dynamic bond is activated by a catalyst or an active center, then the dynamic bond and active center are regenerated to rearrange network topology without significantly changing the total number of crosslinks. Because the overall number of bonds is maintained, reversible exchange CANs can be locally welded or even repaired without compromising the properties of the entire material, or reformed or molded into a new shape. Some dynamic reactions used to produce associative CANs include addition fragmentation chain transfer (AFT) of allyl sulfides or trithiocarbonates[16, 17], transesterification[18], thiol-thioester exchange (TTE)[19-22], and imine exchange[23, 24]. Incorporation of associative bonds into CANs enables bond rearrangement either during and/or after polymerization. For example, AFT has been implemented in materials for dental restoration (fillings for cavities) to reduce polymerization shrinkage stress, increasing the functional lifetime of the restoration without deleterious effects on the material properties of the restoration[25-27].

A notable subcategory of CANs that is often attributed to associative chemistries are "vitrimers"[28]. Vitrimers are generally thought of as thermally activated associative networks that undergo flow like that of strong glass formers, meaning that the increase in the viscosity of the network due to bond rearrangement with respect to temperature follows an Arrhenius relationship. For vitrimers, flow is possible at temperatures for which (1) the dynamic chemistry is active and (2) the network possesses sufficient mobility such that bond exchange results in productive rearrangement of polymer chains. For example, imine-

exchange vitrimers have been used to make carbon fiber composites that can be repeatably remodeled into various shapes by heating he part to activate imine-exchange and reconfigure the matrix topology, resulting in a stable and robust part upon cooling[23, 24, 29-31]. Broadly speaking, associative CANs and vitrimers can be reprocessed or recycled by adding sufficient excess of one functional group-containing monomer to de-gel the network. Monomer containing the complementary functional group can then be added to re-crosslink the recovered monomer mixture. For example, in a polythiourethane network used to make carbon fiber composites, excess of the thiol monomer can be added to return the network to a liquid state to recover both the carbon fibers and the monomer/macromer mixture. The mixture can then be repolymerized with additional isocyanate monomer[32]. While "vitrimeric" behavior is most often attributed to associative networks, dissociative networks can also show many of these characteristics under relevant processing conditions[33].

Some dynamic bonds may undergo either or both associative and dissociative reactions depending on the reaction conditions, including thiol-anhydride adducts that are capable of both thioester exchange and ring-opening/closing reactions[34, 35], boronic esters[36, 37], disulfides[38, 39]. These networks often possess complex rheological properties depending on which dynamic mechanism prevails under a given set of conditions. As mentioned above, the properties of dissociative networks can be quite similar to associative networks if the equilibrium number of dissociated crosslinks is small and the bond kinetics are fast under the relevant reprocessing conditions. Under such conditions, the crosslinking density is essentially unchanged and the dynamic breaking/reforming of bonds induces the same viscoelastic behavior that is typically attributed to associative networks that fit the "vitrimer" paradigm[33]. Characterization of the impact of different dynamic bonding mechanisms and combinations thereof is important to fully understand and leverage dynamic bonding in CANs.

1.2 *Disulfide Chemistries in Dynamic Networks*

Disulfides are pervasive bonds in biological and polymeric systems. They play a crucial role in protein folding[40], are industrially relevant for processes such as the vulcanization of rubber[41], and are one of the

oldest known and most well-studied dynamic bonds[42-44]. These are versatile dynamic bonds because they can be triggered by light, heat, or basic/nucleophilic catalysis depending on specific disulfide structure and neighboring functional groups. Aromatic disulfides, for example, are thermally labile and have been used to induce self-healing upon heating via a metathesis mechanism (**Figure 1.3a**)[38]. Disulfides may also undergo radically mediated dynamic bonding. Many disulfides can be homolytically cleaved into thiyl
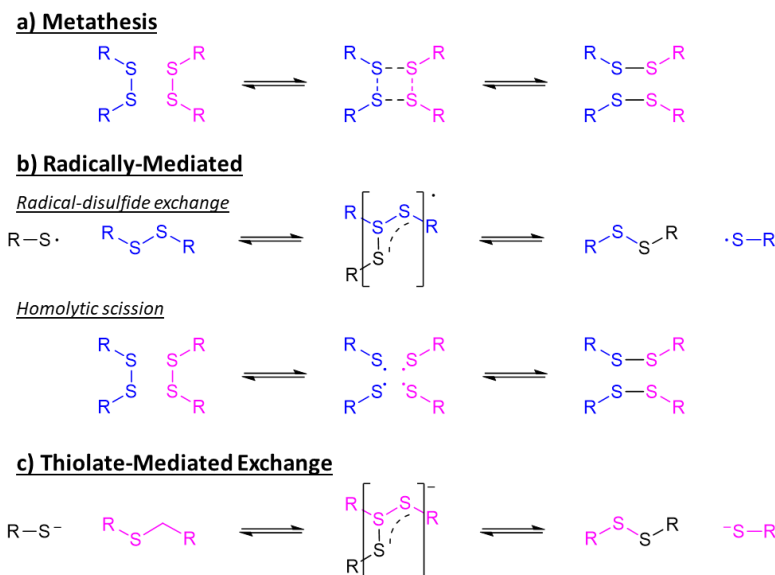
Figure 1.3: Various mechanisms of bond exchange for disulfides: a) Metathesis of two disulfides, b) radical-mediated exchange, and thiolate-mediated exchange.

radicals by direct irradiation with ultraviolet light, which can dynamically break and reform via a dissociative mechanism or exchange with another disulfide via an associative mechanism[39]. Thiyl radicals can also be produced through activation by a photoinitiator to generate the radicals that participate in radical-disulfide exchange (**Figure 1.3b**)[45]. In addition, thiolate-mediated thiol-disulfide exchange can be catalyzed by base or nucleophile (**Figure 1.3c**)[46]. This process is analogous to radical-mediated exchange, where the thiolate anion is produced through either the deprotonation of thiol by a base or the nucleophilic attack of a disulfide by a sufficiently potent nucleophile.

Certain disulfides are also polymerizable by cascading homopolymerization reactions so form poly sulfides or the disulfidation of alkenes to form thioacetals. Lipoates and 1,3-dithiolanes are cyclic disulfides

that have been used to form polydisulfides through a ring-opening homopolymerization[47-51] and have also been implemented in ring-opening disulfidation of alkeness[52, 53] by an analogous mechanism to the thiol-ene reaction[54, 55]. This is an attractive scheme because of the perfect atom economy and ring-opening reactions can be leveraged to reduce shrinkage stress during polymerization[26, 56]. However, the scope of inexpensive and commercially available starting materials is rather narrow, limiting the diversity of potential disulfide-containing monomers and therefore the tunability of material properties polymer networks made with this approach. Recently, certain linear disulfides have been found to react via the same disulfidation mechanism with vinyl ethers[57]. In that study, a variety of linear disulfides flanked by different functional groups were evaluated, and disulfides derived from thioglycolic acid were found to be particularly reactive, reaching near 100% conversion in the shortest time, which those derived from mercaptopropionates and sulfones also reached reasonably high conversions.

1.3 *Dielectric Analysis in Polymer Networks*

The experimental approaches for studying the dynamic behavior of CANs typically revolve around mechanical measurements such as dynamic mechanical analysis (DMA)[58], stress relaxation and creep compliance[59, 60], and/or self-healing that involves rheological or tensile testing on broken-then-healed specimens[61]. In particular, for DMA a sample is subjected to an oscillating mechanical strain and the phase lag between the input strain, and the output stress on the sample is measured to determine properties such as the storage and loss modulus, which correspond to the ability of the material to store or dissipate energy, respectively. The changes in these moduli are a consequence of the chain relaxations and their macroscopic effects on the material. DMA is frequently conducted with isothermal frequency sweeps utilized to measure relaxations, such as those which correspond to the glass transition, or T_g. However, this the frequency range for such experiments is typically quite limited due to instrumentation restraints (up to about 100 Hz), and DMA cannot directly probe chain-level dynamics.

Another experimentally analogous tool in polymer science is dielectric analysis (DEA), which can be leveraged to investigate chain-level dynamics. Much like DMA, DEA uses an oscillating input to measure

a complex response (in the mathematical sense) related to the storage and dissipation of energy to characterize time-dependent responses in the material of interest (**Figure 1.4**). Instead of an oscillating strain, an oscillating electric field is applied to the sample to determine the timescales at which dipole moments in the backbone of the polymer chains and side groups reorient themselves in response to the electric field. This provides a window into polymer chain and segment-level mobility. In addition, DEA enable much wider frequency windows to measure dynamic behavior. While standard dynamic mechanical analyzers can reach frequencies of 100 Hz, standard dielectric spectrometers can reach frequencies of 10^6 Hz. This enables the observation of more relaxation processes at a given temperature than mechanical techniques like DMA can access.
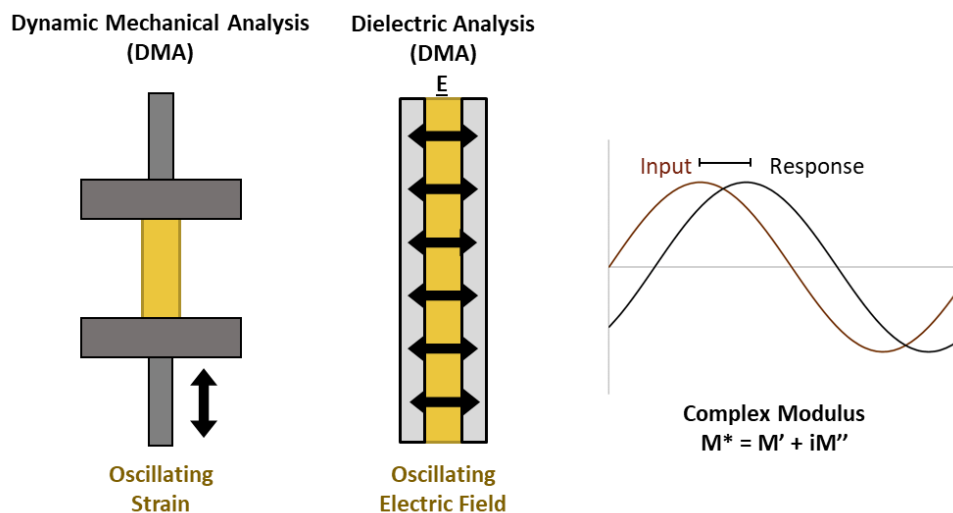
Figure 1.4: Representation of the standard configuration of dynamic mechanical analysis (DMA) and dielectric analysis (DEA), showing how both techniques utilize an oscillating input and measure the response to measure a complex quantity, shown here is the complex modulus.

Considering the relaxations themselves, different relaxation modes appear at different frequencies. Faster modes arise from short-range cooperativity such as the rotation of a side group or short chain segments. These relaxations appear at higher frequencies at a given temperature. Slower relaxation modes arise from long-range cooperative motions such as the segmental chain motions that are associated with the T_g (called the α-relaxation). These modes will appear at lower frequencies at a given temperature. Each relaxation mode will generally have its own temperature dependence, and different relaxation modes will be convoluted when two or more modes are equally fast at a given temperature or temperature range. This

is often the case for the α-relaxation and other relaxations due to shorter range motions of sides chains (often called β-relaxations). At temperatures well above the T_g, segmental motions are just as fast as side chain motions, and their respective peak in dielectric spectra will overlap. As temperature is decreased both the α-relaxation and β-relaxation peaks move to lower frequencies. But because cooperative segmental motions become more inhibited near and below the T_g, the two distinct peaks are observed in the dielectric spectra. DEA has been implemented to study chain and side group relaxations in a wide variety of materials including epoxy-resins[62], natural and synthetic rubbers[63, 64], dental restoratives[65], composites[66, 67], and supramolecular networks[68].

However, little work has been done using DEA to assess polymer dynamics in CANs, which exhibit distinct time/temperature dependent behavior compared to equivalent non-dynamic networks due to viscoelasticity introduced by dynamic bonds. Studies of supramolecular networks offer the closest analogy to CANs because hydrogen bonding can be strongly analogized to dynamic bonds, especially for dissociative networks. For example, Tress et al.[68] used dielectric spectroscopy to identify distinct peaks corresponding the α-relaxation in addition to the terminal chain-end relaxations that correspond to hydrogen bonding, which they called the α*-relaxation. The difference in the relaxation times at various temperatures was used to determine the activation energy of the α*-relaxation. This work also showed that relaxation times for the hydrogen-bonding process measured by dielectric were significantly faster than those measured by shear rheology, showing that a given hydrogen bonding pair can break and reform many times before they find new partners that results in a productive relaxation event. While this framework may prove useful assessing relaxations in CANs, peaks in the dielectric spectra that can be directly attributed to dynamic bonding have not been readily identified in CANs[34, 35].

Given the interest in recyclable, repurposable, self-healing, and responsive polymer materials[69], an improved understanding of chain dynamics in CANs is important in materials design. This is especially relevant in the context of an ongoing conversation in the literature regarding the distinctions between associative and dissociative CANs. Specifically, whether the distinction between associative and

dissociative CANs are important at relevant processing conditions for dissociative networks. Meaning conditions at which bonds are dynamically breaking and reforming but the reduction in crosslinking is small, generating dynamic behaviors that have generally been attributed to associative CANs[33, 70].

1.4 *Overview of Present Work*

The goal of this thesis is to build out the toolbox for making and characterizing covalent adaptable networks. Disulfides have been utilized and studied extensively in dynamic networks for more than half a century[42-44]. In addition, there have been studies of network formation of cyclic disulfides via ring-opening homopolymerization[47-50] as well as disulfidation with alkenes[52, 53]. Cyclic disulfides show excellent reactivity in these crosslinking polymerizations due to ring strain, but that reactivity makes these monomers unstable to premature homopolymerization. Linear disulfides, devoid of such ring strain, should be much more stable monomers that their cyclic counterparts and be suitable for disulfidation. Indeed, Kamps et al.[57] demonstrated that certain linear disulfides can be efficiently copolymerized with vinyl ethers. This work expands upon disulfidation (or disulfide-ene) in a copolymerization between thiols and disulfides with vinyl ethers produce a two-stage polymerization scheme, one that is controlled by the relative rate of thiol-ene and disulfide-ene polymerization. A thorough kinetics analysis of these reactions using FTIR was performed to characterize the relative reaction rates of thiol-ene and disulfide-ene in these combined polymerizations. Furthermore, the radically-mediated bond dynamics of these networks were studied to (1) understand the role of radical disulfide exchange both during both stages of the polymerization as well as post-polymerization stress relaxation and (2) expand the scope of linear disulfides and thiol monomers used to synthesize these materials.

This thesis also expanded upon previous work by Podgorski et al.[34, 71] investigating dynamic thioester reactions and by Long et al.[72, 73] studying how thiol substitution impact thiol-x reactions to investigate the role of thiol/thioester substitution on dynamic networks using DEA. Primary and secondary thiols and thioesters were synthesized and implemented in dynamic thioester networks to (1) study how substitution impacts exchange rates in these materials and (2) use these different substitutions as probes to

measure the differing dielectric response induced by changes in network polarity. First, model studies using NMR were used to characterize the relative reactivity of these networks at equilibrium. Next, stress relaxation and DEA were used to study how that substitution effects dynamic thioester reactions in thiol-ene and thiol-anhydride-ene networks. Lastly, this work aims to take a broader look at DEA as a tool for evaluating bond dynamics in different types of CANs. Namely, DEA and rheological stress relaxation measurements were used to study networks capable of reversible addition, reversible exchange, and both reversible addition and exchange reactions.

1.5 References

1. Giles Jr, H. F.; Mount III, E. M.; Wagner Jr, J. R., *Extrusion: the definitive processing guide and handbook*. William Andrew: 2004.

2. Rosato, D. V.; Rosato, M. G., *Injection molding handbook*. Springer Science & Business Media: 2012.

3. Parker, L. A Whopping 91 Percent of Plastic Isn't Recycled. https://www.nationalgeographic.org/article/whopping-91-percent-plastic-isnt-recycled/.

4. Podgórski, M.; Fairbanks, B. D.; Kirkpatrick, B. E.; McBride, M.; Martinez, A.; Dobson, A.; Bongiardina, N. J.; Bowman, C. N., Toward Stimuli-Responsive Dynamic Thermosets through Continuous Development and Improvements in Covalent Adaptable Networks (CANs). *Advanced Materials* **2020,** *32* (20), 1906876.

5. Khan, A.; Ahmed, N.; Rabnawaz, M., Covalent Adaptable Network and Self-Healing Materials: Current Trends and Future Prospects in Sustainability. *Polymers* **2020,** *12* (9), 2027.

6. Kloxin, C. J.; Scott, T. F.; Adzima, B. J.; Bowman, C. N., Covalent Adaptable Networks (CANs): A Unique Paradigm in Cross-Linked Polymers. *Macromolecules* **2010,** *43* (6), 2643-2653.

7. Gandini, A., The furan/maleimide Diels–Alder reaction: A versatile click–unclick tool in macromolecular synthesis. *Progress in Polymer Science* **2013,** *38* (1), 1-29.

8. Chen, X.; Dam, M. A.; Ono, K.; Mal, A.; Shen, H.; Nutt, S. R.; Sheran, K.; Wudl, F., A Thermally Re-mendable Cross-Linked Polymeric Material. *Science* **2002,** *295* (5560), 1698-1702.

9. Chandross, E. A.; Ferguson, J.; McRae, E. G., Absorption and Emission Spectra of Anthracene Dimers. *The Journal of Chemical Physics* **1966,** *45* (10), 3546-3553.

10. Egerton, P. L.; Hyde, E. M.; Trigg, J.; Payne, A.; Beyton, P.; Mijovic, M. V.; Reiser, A., PhotocycloadditioninLiquidEthylCinnamateandinEthylCinnamateGlasses.ThePhotoreactionasaProbeintotheMicromorphologyoftheSolid. *Journal of the American Chemical Society* **1981,** *103*, 3859-3863.

11. Jin, B.; Song, H.; Jiang, R.; Song, J.; Zhao, Q.; Xie, T., Programming a crystalline shape memory polymer network with thermo- and photo-reversible bonds toward a single-component soft robot. *Science Advances* **2018,** *4* (1), eaao3865.

12.   Ying, H.; Zhang, Y.; Cheng, J., Dynamic urea bond for the design of reversible and self-healing polymers. *Nature Communications* **2014,** *5* (1), 3218.

13.   Velankar, S.; Pazos, J.; Cooper, S. L., High-performance UV-curable urethane acrylates via deblocking chemistry. *Journal of applied polymer science* **1996,** *62* (9), 1361-1376.

14.   Zhang, B.; Digby, Z. A.; Flum, J. A.; Chakma, P.; Saul, J. M.; Sparks, J. L.; Konkolewicz, D., Dynamic Thiol–Michael Chemistry for Thermoresponsive Rehealable and Malleable Networks. *Macromolecules* **2016,** *49* (18), 6871-6878.

15.   Van Herck, N.; Maes, D.; Unal, K.; Guerre, M.; Winne, J. M.; Du Prez, F. E., Covalent Adaptable Networks with Tunable Exchange Rates Based on Reversible Thiol–yne Cross-Linking. *Angewandte Chemie* **2020,** *132* (9), 3637-3646.

16.   Fenoli, C. R.; Wydra, J. W.; Bowman, C. N., Controllable Reversible Addition–Fragmentation Termination Monomers for Advances in Photochemically Controlled Covalent Adaptable Networks. *Macromolecules* **2014,** *47* (3), 907-915.

17.   Sowan, N.; Cox, L. M.; Shah, P. K.; Song, H. B.; Stansbury, J. W.; Bowman, C. N., Dynamic Covalent Chemistry at Interfaces: Development of Tougher, Healable Composites through Stress Relaxation at the Resin-Silica Nanoparticles Interface. *Advanced Materials Interfaces* **2018,** *5* (18).

18.   Montarnal, D.; Capelot, M.; Tournilhac, F.; Leibler, L., Silica-Like Malleable Materials from Permanent Organic Networks. *Science* **2011,** *334* (6058), 965-968.

19.   Wang, C.; Mavila, S.; Worrell, B. T.; Xi, W. X.; Goldman, T. M.; Bowman, C. N., Productive Exchange of Thiols and Thioesters to Form Dynamic Polythioester-Based Polymers. *Acs Macro Letters* **2018,** *7* (11), 1312-1316.

20.   Worrell, B. T.; Mavila, S.; Wang, C.; Kontour, T. M.; Lim, C. H.; McBride, M. K.; Musgrave, C. B.; Shoemaker, R.; Bowman, C. N., A user's guide to the thiol-thioester exchange in organic media: scope, limitations, and applications in material science. *Polymer Chemistry* **2018,** *9* (36), 4523-4534.

21.   Worrell, B. T.; McBride, M. K.; Lyon, G. B.; Cox, L. M.; Wang, C.; Mavila, S.; Lim, C. H.; Coley, H. M.; Musgrave, C. B.; Ding, Y. F.; Bowman, C. N., Bistable and photoswitchable states of matter (vol 9, 2804, 2018). *Nature Communications* **2018,** *9*.

22.   Sowan, N.; Lu, Y.; Kolb, K.; Cox, L. M.; Long, R.; Bowman, C. N., Enhancing the toughness of composites via dynamic thiol–thioester exchange (TTE) at the resin–filler interface. *Polymer Chemistry* **2020**.

23.   Lei, X. F.; Jin, Y. H.; Sun, H. L.; Zhang, W., Rehealable imide-imine hybrid polymers with full recyclability. *Journal of Materials Chemistry A* **2017,** *5* (40), 21140-21145.

24.   Liu, Y. J.; Tang, Z. H.; Chen, Y.; Wu, S. W.; Guo, B. C., Programming dynamic imine bond into elastomer/graphene composite toward mechanically strong, malleable, and multi-stimuli responsive vitrimer. *Composites Science and Technology* **2018,** *168*, 214-223.

25.   Park, H. Y.; Kloxin, C. J.; Abuelyaman, A. S.; Oxman, J. D.; Bowman, C. N., Stress Relaxation via Addition-Fragmentation Chain Transfer in High T-g, High Conversion Methacrylate-Based Systems. *Macromolecules* **2012,** *45* (14), 5640-5646.

26.   Park, H. Y.; Kloxin, C. J.; Abuelyaman, A. S.; Oxman, J. D.; Bowman, C. N., Novel dental restorative materials having low polymerization shrinkage stress via stress relaxation by addition-fragmentation chain transfer. *Dental Materials* **2012,** *28* (11), 3-9.

27.   Park, H. Y.; Kloxin, C. J.; Fordney, M. F.; Bowman, C. N., Stress relaxation of trithiocarbonate-dimethacrylate-based dental composites. *Dental Materials* **2012,** *28* (8), 888-893.

28.   Denissen, W.; Winne, J. M.; Du Prez, F. E., Vitrimers: permanent organic networks with glass-like fluidity. *Chemical science* **2016,** *7* (1), 30-38.

29.   Taynton, P.; Ni, H. G.; Zhu, C. P.; Yu, K.; Loob, S.; Jin, Y. H.; Qi, H. J.; Zhang, W., Repairable Woven Carbon Fiber Composites with Full Recyclability Enabled by Malleable Polyimine Networks. *Advanced Materials* **2016,** *28* (15), 2904-2909.

30.   Taynton, P.; Yu, K.; Shoemaker, R. K.; Jin, Y. H.; Qi, H. J.; Zhang, W., Heat- or Water-Driven Malleability in a Highly Recyclable Covalent Network Polymer. *Advanced Materials* **2014,** *26* (23), 3938-3942.

31.   Zhu, C. P.; Xi, C.; Doro, W.; Wang, T. Y.; Zhang, X.; Jin, Y. H.; Zhang, W., Tuning the physical properties of malleable and recyclable polyimine thermosets: the effect of solvent and monomer concentration. *Rsc Advances* **2017,** *7* (76), 48303-48307.

32.   Cui, C.; Chen, X.; Ma, L.; Zhong, Q.; Li, Z.; Mariappan, A.; Zhang, Q.; Cheng, Y.; He, G.; Chen, X.; Dong, Z.; An, L.; Zhang, Y., Polythiourethane Covalent Adaptable Networks for Strong and Reworkable Adhesives and Fully Recyclable Carbon Fiber-Reinforced Composites. *ACS Applied Materials & Interfaces* **2020,** *12* (42), 47975-47983.

33.   Elling, B. R.; Dichtel, W. R., Reprocessable Cross-Linked Polymer Networks: Are Associative Exchange Mechanisms Desirable? *ACS Central Science* **2020,** *6* (9), 1488-1496.

34.   Podgórski, M.; Mavila, S.; Huang, S.; Spurgin, N.; Sinha, J.; Bowman, C. N., Thiol–Anhydride Dynamic Reversible Networks. *Angewandte Chemie International Edition* **2020,** *59* (24), 9345-9349.

35.   Podórski, M.; Spurgin, N.; Mavila, S.; Bowman, C. N., Mixed mechanisms of bond exchange in covalent adaptable networks: monitoring the contribution of reversible exchange and reversible addition in thiol–succinic anhydride dynamic networks. *Polymer Chemistry* **2020,** *11*, 5365-5376.

36.   Cash, J. J.; Kubo, T.; Bapat, A. P.; Sumerlin, B. S., Room-Temperature Self-Healing Polymers Based on Dynamic-Covalent Boronic Esters. *Macromolecules* **2015,** *48* (7), 2098-2106.

37.   Smithmyer, M. E.; Deng, C. C.; Cassel, S. E.; LeValley, P. J.; Sumerlin, B. S.; Kloxin, A. M., Self-Healing Boronic Acid-Based Hydrogels for 3D Co-cultures. *ACS Macro Letters* **2018,** *7* (9), 1105-1110.

38.   Martin, R.; Rekondo, A.; Ruiz de Luzuriaga, A.; Cabañero, G.; Grande, H. J.; Odriozola, I., The processability of a poly(urea-urethane) elastomer reversibly crosslinked with aromatic disulfide bridges. *Journal of Materials Chemistry A* **2014,** *2* (16), 5710-5715.

39.   Michal, B. T.; Jaye, C. A.; Spencer, E. J.; Rowan, S. J., Inherently Photohealable and Thermal Shape-Memory Polydisulfide Networks. *ACS Macro Letters* **2013,** *2* (8), 694-699.

40.   Wedemeyer, W. J.; Welker, E.; Narayan, M.; Scheraga, H. A., Disulfide Bonds and Protein Folding. *Biochemistry* **2000,** *39* (15), 4207-4216.

41.   Craig, D., The Vulcanization of Rubber with Sulfur. *Rubber Chemistry and Technology* **1957,** *30* (5), 1291-1346.

42.   Green, M. S.; Tobolsky, A. V., A NEW APPROACH TO THE THEORY OF RELAXING POLYMERIC MEDIA. *Journal of Chemical Physics* **1946,** *14* (2), 80-92.

43.   Takahashi, Y.; Tobolsky, A. V., Chemorheological study on natural rubber vulcanizates. *Polymer Journal* **1971,** *2* (4), 457-467.

44.   Tobolsky, A.; MacKnight, W.; Takahashi, M., Relaxation of disulfide and tetrasulfide polymers. *The Journal of Physical Chemistry* **1964,** *68* (4), 787-790.

45.   Matxain, J. M.; Asua, J. M.; Ruipérez, F., Design of new disulfide-based organic compounds for the improvement of self-healing materials. *Physical Chemistry Chemical Physics* **2016,** *18* (3), 1758-1770.

46.   Pepels, M.; Filot, I.; Klumperman, B.; Goossens, H., Self-healing systems based on disulfide– thiol exchange reactions. *Polymer Chemistry* **2013,** *4* (18), 4955-4965.

47.   Huang, S.; Shen, Y.; Bisoyi, H. K.; Tao, Y.; Liu, Z.; Wang, M.; Yang, H.; Li, Q., Covalent Adaptable Liquid Crystal Networks Enabled by Reversible Ring-Opening Cascades of Cyclic Disulfides. *Journal of the American Chemical Society* **2021,** *143* (32), 12543-12551.

48.   Zhang, X.; Waymouth, R. M., 1,2-Dithiolane-Derived Dynamic, Covalent Materials: Cooperative Self-Assembly and Reversible Cross-Linking. *Journal of the American Chemical Society* **2017,** *139* (10), 3822-3833.

49.   Liu, Y.; Jia, Y.; Wu, Q.; Moore, J. S., Architecture-Controlled Ring-Opening Polymerization for Dynamic Covalent Poly(disulfide)s. *Journal of the American Chemical Society* **2019,** *141* (43), 17075-17080.

50.   Sakai, N.; Matile, S., Stack Exchange Strategies for the Synthesis of Covalent Double-Channel Photosystems by Self-Organizing Surface-Initiated Polymerization. *Journal of the American Chemical Society* **2011,** *133* (46), 18542-18545.

51.   Choi, C.; Self, J. L.; Okayama, Y.; Levi, A. E.; Gerst, M.; Speros, J. C.; Hawker, C. J.; Read de Alaniz, J.; Bates, C. M., Light-Mediated Synthesis and Reprocessing of Dynamic Bottlebrush Elastomers under Ambient Conditions. *Journal of the American Chemical Society* **2021,** *143* (26), 9866-9871.

52.   Tong, C.; Wondergem, J. A. J.; Heinrich, D.; Kieltyka, R. E., Photopatternable, Branched Polymer Hydrogels Based on Linear Macromonomers for 3D Cell Culture Applications. *ACS Macro Letters* **2020,** *9* (6), 882-888.

53.   Suzuki, T.; Nambu, Y.; Endo, T., Radical Copolymerization of Lipoamide with Vinyl Monomers. *Macromolecules* **1989,** *23*, 1579-1582.

54.   Cramer, N. B.; Reddy, S. K.; O'Brien, A. K.; Bowman, C. N., Thiol− ene photopolymerization mechanism and rate limiting step changes for various vinyl functional group chemistries. *Macromolecules* **2003,** *36* (21), 7964-7969.

55.   Cramer, N. B.; Davies, T.; O'Brien, A. K.; Bowman, C. N., Mechanism and modeling of a thiol− ene photopolymerization. *Macromolecules* **2003,** *36* (12), 4631-4636.

56.   Ge, J.; Trujillo-Lemon, M.; Stansbury, J. W., A mechanistic and kinetic study of the photoinitiated cationic double ring-opening polymerization of 2-methylene-7-phenyl-1, 4, 6, 9-tetraoxa-spiro [4.4] nonane. *Macromolecules* **2006,** *39* (26), 8968-8976.

57.   Kamps, J.; Soars, S.; Fairbanks, B. D.; Bowman, C. N., Photodisulfidation of Linear Disulfides and Alkenes: Reaction Scope and Kinetics (Submitted to Tetrahedron).

58.   Porath, L. E.; Evans, C. M., Importance of Broad Temperature Windows and Multiple Rheological Approaches for Probing Viscoelasticity and Entropic Elasticity in Vitrimers. *Macromolecules* **2021**.

59.   Liu, W.; Schmidt, D. F.; Reynaud, E., Catalyst selection, creep, and stress relaxation in high-performance epoxy vitrimers. *Industrial & Engineering Chemistry Research* **2017,** *56* (10), 2667-2672.

60.   Chen, M.; Zhou, L.; Wu, Y.; Zhao, X.; Zhang, Y., Rapid stress relaxation and moderate temperature of malleability enabled by the synergy of disulfide metathesis and carboxylate transesterification in epoxy vitrimers. *ACS Macro Letters* **2019,** *8* (3), 255-260.

61.   Amamoto, Y.; Kamada, J.; Otsuka, H.; Takahara, A.; Matyjaszewski, K., Repeatable photoinduced self-healing of covalently cross-linked polymers through reshuffling of trithiocarbonate units. *Angew Chem Int Ed Engl* **2011,** *50* (7), 1660-3.

62.   Jilani, W.; Mzabi, N.; Gallot-Lavallée, O.; Fourati, N.; Zerrouki, C.; Zerrouki, R.; Guermazi, H., Dielectric relaxations investigation of a synthesized epoxy resin polymer. *The European Physics Journal Plus* **2015,** (130).

63.   Carrertero-Gonzalez, J.; Ezquerra, T. A.; Amnuaypornsri, S.; Toki, S.; Verdejo, R.; Sanz, A.; Sakdapipanich, J.; Hsiao, B. S.; López–Manchado, M. A., Molecular dynamics of natural rubber as revealed by dielectric spectroscopy: The role of natural cross–linking. *Soft Matter* **2010,** (6), 3636-3642.

64.   Hernández, M.; Grande, A. M.; van der Zwaag, S.; García, S. J., Monitoring Network and Interfacial Healing Processes by Broadband Dielectric Spectroscopy: A Case Study on Natural Rubber. *ACS Appl Mater Interfaces* **2016,** *8* (16), 10647-56.

65.   Lovell, L. G.; Berchtold, K.; Elliot, J. E.; Lu, H.; Bowman, C. N., Understanding the kinetics and network formation of dimethacrylate dental resins. *Polym. Adv. Technol.* **2001,** *12* (6), 335-345.

66.   Tsangaris, G. M.; Psarras, G. C.; Kouloumbi, N., Electric modulus and interfacial polarization in composite polymeric systems. *Journal of materials Science* **1998,** (33), 2027–2037.

67.   Yang, J.; Melton, M.; Sun, R.; Yang, W.; Cheng, S., Decoupling the Polymer Dynamics and the Nanoparticle Network Dynamics of Polymer Nanocomposites through Dielectric Spectroscopy and Rheology. *Macromolecules* **2020,** *53* (1), 302-311.

68.   Tress, M.; Xing, K.; Ge, S.; Cao, P.; Saito, T.; Sokolov, A., What dielectric spectroscopy can tell us about supramolecular networks⋆. *The European Physical Journal E* **2019,** *42* (10), 133.

69.   Zheng, N.; Xu, Y.; Zhao, Q.; Xie, T., Dynamic Covalent Polymer Networks: A Molecular Platform for Designing Functions beyond Chemical Recycling and Self-Healing. *Chemical Reviews* **2021,** *121* (3), 1716-1745.

70.   Scheutz, G. M.; Lessard, J. J.; Sims, M. B.; Sumerlin, B. S., Adaptable Crosslinks in Polymeric Materials: Resolving the Intersection of Thermoplastics and Thermosets. *Journal of the American Chemical Society* **2019,** *141* (41), 16181-16196.

71.   Podgórski, M.; Spurgin, N.; Mavila, S.; Bowman, C. N., Mixed mechanisms of bond exchange in covalent adaptable networks: monitoring the contribution of reversible exchange and reversible addition in thiol–succinic anhydride dynamic networks. *Polymer Chemistry* **2020**.

72.   Long, K. F.; Wang, H.; Dimos, T. T.; Bowman, C. N., Effects of Thiol Substitution on the Kinetics and Efficiency of Thiol-Michael Reactions and Polymerizations. *Macromolecules* **2021**.

73.   Long, K. F. B., N. J.; Mayordomo, P.; Olin, M. J.; Oretega, A. D.; Bowman, C. N., Effects of 1°, 2°, and 3° Thiols on Thiol–Ene Reactions: Polymerization Kinetics and Mechanical Behavior. *Macromolecules* **2020,** *53* (14), 5805-5815.

Chapter 2 - OBJECTIVES

2.1: Overview

Covalent adaptable networks are an important class of polymer materials whose mechanical and dynamic properties can be tuned by the choice of chemistry, bonding mechanism, and stimulus. This thesis focuses on (1) expanding the toolbox of dynamic network-forming polymerizations by introducing the thiol-ene-disulfide polymerization and substituted thiols into dynamic thioester networks and (2) further expanding dielectric analysis as a tool for characterizing dynamic behavior in CANs. This research implements fourier transform infrared spectroscopy, dynamic mechanical analysis, stress relaxation, dielectric analysis, and rheology to explore these focuses.

2.2: Specific Aim 1 – Develop disulfidation polymerizations of linear disulfides for creating and studying dynamic networks.

The purpose of this aim is to implement and characterize thiol-ene-disulfide polymerizations for dual-cure polymers and covalent adaptable networks.

2.2.1: Aim 1.1 – Characterize thiol-ene-disulfidation polymerization reaction kinetics.

The purpose of this sub-aim is to experimentally measure functional group conversion for thiol-ene-disulfide polymerizations and model the reaction kinetics. A new monomer containing a disulfide core flanked with vinyl ethers was synthesized and used to characterize the reaction kinetics for increasingly complex polymerization systems. First characterizing the polymerization of this monomer by itself, then monofunctional thiols, and finally multifunctional thiols. A kinetics model based on a combined thiol-ene and disulfide-ene polymerization schemes was implemented to quantify the difference in reaction rate between the two reactions. Mechanical testing including DMA and rheology were also used to characterize the material properties and gelation, respectively.

2.2.2: Aim 1.2 – Implement thiol-ene-disulfidation polymerizations for covalent adaptable networks.

The purpose of this sub-aim is to investigate the role that radical-disulfide exchange plays in thiol-ene-disulfide networks. A new disulfide-core monomer was introduced to expand the scope of disulfides that are viable in this polymerization scheme. Stress relaxation and fourier transform infrared spectroscopy (FTIR) were used to characterize the impact of disulfide exchange during both the thiol-ene and disulfide-ene stages of the polymerization as well as post polymerization stress relaxation.

2.3 Specific Aim 2: Implement dielectric analysis as a tool for characterizing the structure-property relationships of dynamic materials.

The purpose of this aim is to implement DEA to characterize structure-property relationships in covalent adaptable networks.

2.3.1: Aim 2.1 – Characterize the effect of thiol substitution on dynamic thioester reactions with mechanical and dielectric analysis.

The purpose of this sub-aim is to investigate how thiol/thioester substitution impacts dynamic thioester reactions. Model NMR studies, DMA, stress relaxation, and DEA were used to show differences in relaxation rates for primary and secondary thiol/thioester materials. This analysis was done for two kinds of dynamic thioester networks: thiol-ene networks that are only capable of reversible addition and thiol-anhydride-ene networks that are capable of both reversible addition and reversible exchange.

2.3.2: Aim 2.2 – Implement dielectric analysis to investigate different dynamic bonding mechanisms in comparison to macroscopic mechanical measurements:

The purpose of this sub-aim is to use investigate DEA as a tool for studying covalent adaptable networks and develop methodologies for analyzing their dielectric spectra. Two different types of dielectric probes, ITO coated glass and interdigit probes, were implemented to better understand how test conditions impacts the observed relaxations in CANs. Rheology and DEA were used to study whether time-temperature-superposition of using dielectric spectra can be leveraged to study dynamic networks.

2.4 Flory-Huggins Parameters for Thiol-ene Networks using Hansen Solubility Parameters

The purpose of this objective is to measure the Flory-Huggins interaction parameter for a thiol-ene networks of varying crosslinking density and polarity in organic solvents. Experimental measurements were compared to theoretical prediction using Hansen solubility parameters to assess the viability of this approach for predicting swelling in thioether-containing materials. Swelling and DMA were used to measure the Flory-Huggins parameter and the Hansen Solubility Parameters in Practice (HSPiP) software was used for predicted values.

Chapter 3 – SPATIAL AND TEMPORAL CONTROL OF PHOTO MEDIATED DISULFIDE-ENE AND THIOL-ENE CHEMISTRIES FOR TWO-STAGE POLYMERIZATIONS

3.1: Abstract

A new strategy is reported for the design and synthesis of high sulfur containing materials for potential use in covalent adaptable networks and optical materials by combining photomediated thiol-ene and disulfide-ene based polymerization reactions. Taking advantage of the relative reaction rates to differentiate sequentially between the thiol-ene and disulfide-ene conjugations, these reactions were performed semi-orthogonally to produce polymer networks of controlled architecture. Kinetic analysis demonstrates that the thiol-ene reaction is approximately 30 times faster than the disulfide-ene reaction, enabling spatial and temporal manipulation of material properties via dual-cure networks and photopatterning. A two-stage polymerization approach was implemented with increases in modulus in the second stage of 2-3 orders of magnitude accompanied by increases in the glass transition temperature of more than 15°C. Additionally, the thiol-ene reaction in the presence of a disulfide yields materials capable of simultaneous network development and stress relaxation through dynamic bond exchange during *in situ* polymerization.

3.2: Introduction

Over the last 50 years, sulfur-based chemistries have been widely applied to the field of polymer science and related applications.[1–4] Many of these chemistries involve thiol-X 'click-reactions' due to the high selectivity, rapid rates, and tolerability to various reaction conditions.[5–10] Other widely utilized sulfur-containing bonds include polysulfides which have been employed in vulcanization of rubbers since the 19th century.[11–14]

The disulfide bonds, in particular, are intriguing covalent bonds that have been well studied in the literature, especially due to their crucial role in protein stability.[15] Although the disulfide bond is relatively

19

strong (with a bond dissociation energy of roughly 60 kcal/mol), many disulfides are susceptible to cleavage by electrophiles, nucleophiles, reducing agents, free-radicals, and even directly by specific wavelengths of light.[16–20] The unique chemistry surrounding disulfides has resulted in a recent surge of the incorporation of disulfides into polymeric systems. Polymers containing disulfides have been used for: stress relaxation, self-healing adaptable networks, controlled drug release, chain transfer agents, increase of refractive index through the introduction of sulfur atoms, latent protection of thiols, and ring opening polymerizations of 1,2-dithiolanes and 1,2-dithianes.[14,20–31]

The disulfidation of alkenes utilizing linear disulfides has generally been accomplished with transition metal catalysis, limiting its utility in polymeric systems.[32–35] However, Bowman and coworkers recently reported the photo-induced radical-mediated disulfidation of vinyl ethers with various linear disulfides (**Figure 3.1a**). The mechanism of this reaction parallels that of the thiol-ene/yne reactions (**Figure 3.1b**), yielding thioacetal products in analogy to the thiol-yne bis thioether reaction products (**Figure 3.1c**), providing 100% atom economy and overall pseudo-first order kinetics with respect to the disulfide. Although the reactions are similar, it was demonstrated that the thiol-ene reaction exhibits a significantly faster reaction rate as compared to the disulfide-ene reaction.[36]
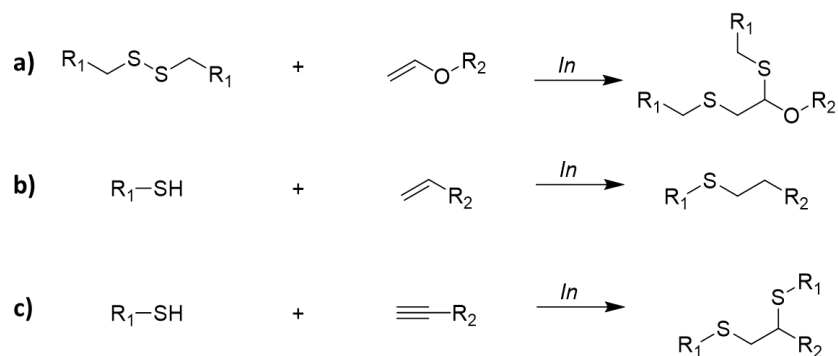
Figure 3.1: Radical conjugation reactions between unsaturated carbon-carbon bonds and thiols or disulfides in the presence of an initiator. a) Disulfidation of vinyl ethers, b) Thiol-ene reaction, and c) Thiol-yne reaction.

Furthermore, it was hypothesized that combining the thiol-ene and disulfide-ene reactions in a polymeric system (**Figure 3.2**) would enable dual-cure (or two stage) polymerization systems with spatial and temporal control over material properties. This approach will also enable dynamic covalent bond

exchange, due to the inherent disulfide exchange mechanisms, as is necessary for covalent adaptable networks (CANs).[20] This work focused on a monomer containing a linear disulfide flanked with vinyl ethers (DSDVE), enabling polymerization of the monomer with multifunctional thiols via the radical-medicated thiol-ene reaction and subsequent disulfidation of the alkenes (**Figure 3.3**).
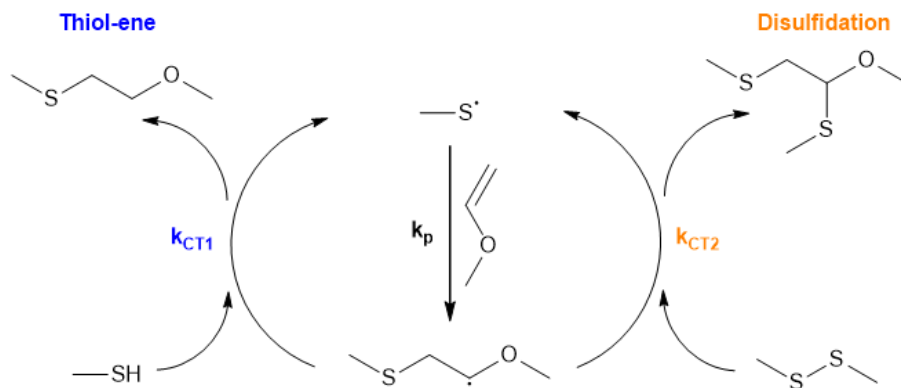
Figure 3.2: Schematic of the competing thiol-ene and disulfide-ene reactions utilized in this paper.

The disulfide monomer DVSDVE was designed to enable several key characteristics of the linear disulfidation reaction. The molecule contains a dithioglycolate core, which has been previously shown to be the most effective functional group for the disulfidation reaction, achieving fast reaction rates and high overall yields. Additionally, the pendent vinyl ether groups are vital because only vinyl ethers were shown to react on reasonable timescales in this disulfidation reaction scheme. Vinyl ethers also show excellent reactivity in the thiol-ene reaction. Finally, the butyl chains were incorporated such that the monomer would both be a liquid and miscible with the other components used herein.[36]

3.3: Experimental section
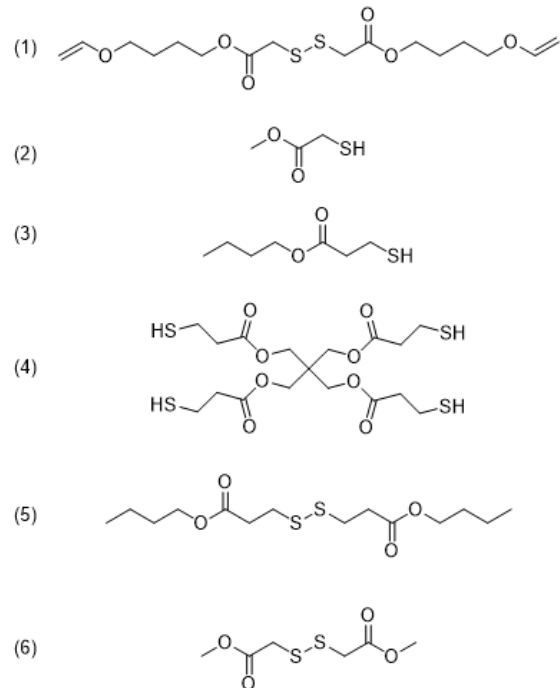
Figure 3.3: Materials used: (1) bis(butylvinylether) 2,2'-dithiodiglycolate (DSDVE). (2) methyl thioglycolate (MTG). (3) butyl-3-mercaptopropionate (BMP). (4) pentaerythritol tetrakis(3-mercaptopropionate) (PETMP). (5) bis(butyl) 3,3'-dithiobispropionate (DSMP). (6) bis(methyl) 2,2'-dithioacetate (DSMA).

3.3.1: Materials

Dithioldiglycolic acid, diisopropylcarbodiimide (DIC), 4-dimethylaminopyridine (DMAP), methylthioglycolate (MTG), butyl-3-mercaptopropionate (BMP), pentaerythritol tetrakis(3-mercaptopropionate) (PETMP), 1,4-butanediol divinyl ether, diphenyl(2,4,6-trimethylbenzoyl)phosphine oxide (TPO), and anhydrous tetrahydrofuran (THF) were all purchased from Sigma-Aldrich.

3.3.2: Experimental

NMR Spectroscopy: ^{1}*H-NMR* and ^{13}*C-NMR* spectra were recorded on a Bruker 400 MHz NMR spectrometer. Proton chemical shifts are expressed in parts per million (δ). The δ scale was referenced to deuterated solvents, as indicated in the respective measurement.

Real-Time Fourier Transform Infrared (FT-IR) Spectroscopy: Reaction kinetics were analyzed using a FTIR spectrometer (Nicolet 8700) in transmission mode to monitor real-time functional group

conversions. Samples were interposed between two NaCl windows and placed into a vertical transmission apparatus. Irradiation was performed using a mercury-lamp (Acticure 4000) with a 400-500 nm band gap filter. The light intensity was measured by a THORLABS model number PM100D radiometer. By measuring the IR peak area decreasing at 1580-1670 cm^{-1} and 2520-2620 cm^{-1}, the real-time functional group conversions of vinyl and thiol groups, respectively, were monitored and calculated as the ratio of the real-time peak area to the peak area of the initial spectra. The alkene peak was also verified by additionally measuring the IR peak area decreasing at 790-850 cm^{-1}.

Rheology: Data was collected using an Ares G2 (TA Instruments) with a 20 mm plate at 25 °C with a 0.5% strain at a frequency of 1 Hz using a photo-rheology attachment connected to an Acticure light source. Samples were irradiated *in situ* and the loss and storage moduli were monitored.

Dynamic Mechanical Analysis (DMA): DMA was performed on an RSA-G2 (TA Instruments). Samples of approximate dimensions 20mm x 5mm x 0.25mm (LxWxH) were cut, and measurements were taken using a temperature ramp rate of 3 °C/min at frequency of 1 Hz to measure the storage modulus, loss modulus, and tan(δ). The glass transition temperature (T_g) was taken to be the peak of the tan(δ) of the second temperature ramp of two temperature sweeps.

3.4: Results and Discussion

A thorough kinetic analysis was conducted to gain a better understanding of the disulfidation and thiol-ene-disulfidation polymerizations. Fundamental kinetic parameters were determined by experiments with monofunctional model compounds to avoid confounding variables (e.g. decreasing reactant mobility) that may complicate analysis of the kinetics during polymerization and crosslinking reactions. Initial studies were conducted to obtain a first estimate of the chain transfer kinetic constant for the disulfidation reaction involving only the disulfide-diene monomer. Subsequently, DSDVE was mixed and reacted with MTG at various stoichiometric ratios to obtain kinetic constants for both possible chain transfer reactions and to ascertain how fast the thiol-ene reaction is relative to disulfidation when there is only one possible thiyl

radical. Finally, DSDVE was reacted with BMP to examine the relative kinetics where a potential mixture of two types of thiyl radicals could exist. BMP was selected as a monofunctional analog of PETMP, a common multifunctional thiol used in thiol-ene polymerizations.

3.4.1: Kinetics of the Disulfidation of DSDVE

Detailed kinetic analysis of the thiol-ene-disulfidation polymerizations is crucial to controlling the material properties in a polymer network. The first step toward understanding of the evolution of the thiol-disulfide-ene networks is to evaluate the kinetics of the disulfidation polymerization of DSDVE independent of the thiol-ene reaction. We propose a model for the kinetics of the disulfidation reaction derived directly from the thiol-ene kinetics. Here, the thiols in the thiol-ene equations are replaced with disulfides because they play an analogous role to the thiol in both the propagation and chain-transfer steps.[37] Based on the mechanism in **Figure 3.2**, the governing equations used to model the disulfidation kinetics are as follows (Equations 1-4).

$$\frac{d[C=C]}{dt} = -k_p[C=C][S^\cdot] \tag{1}$$

$$\frac{d[S-S]}{dt} = -k_{ct}[S-S][C^\cdot] \tag{2}$$

$$\frac{d[S^\cdot]}{dt} = R_i - R_t(S^\cdot) + k_{ct}[S-S][C^\cdot] - k_p[C=C][S^\cdot] \tag{3}$$

$$\frac{d[C^\cdot]}{dt} = -R_t(C^\cdot) - k_{ct}[S-S][C^\cdot] + k_p[C=C][S^\cdot] \tag{4}$$

Equation 1 accounts for the concentration of the alkenes (vinyl ethers), which are consumed by the propagation of a thiyl radical through a double bond. Equation 2 accounts for the concentration of disulfides, which react via the chain transfer of a carbon-centered radical to the disulfide. Equations 3 and 4 describe the concentration of the thiyl and carbon-centered radicals, respectively, considering initiation, termination, propagation, and chain transfer events for both radical species.

The initiation and termination rates are predicted by Equations 5-7.[37] Equation 5 is the rate of initiation (R_i, M/s), where standard values for TPO were used (f = initiator efficiency (0.2), ε = molar absorption (230 L/(mol·cm))[38], [I] = initiator concentration, I_0 = light intensity, lambda = wavelength (405 nm), NA = Avogadro's number, h = Planck's constant, and c = speed of light in a vacuum). Equations 6 and 7 account for the rates of termination for carbon and thiyl radicals, respectively. For simplicity, all termination pathways are considered to be equally likely, therefore k_t (1000000 M^{-1}·s^{-1}) is assumed to be the same for each termination pathway.[37] This system of seven equations was solved numerically to model the concentration of the disulfide and alkene over time and compare the theoretical alkene concentration to experimental data. Although an analytical solution is possible for this simple set of equations given a few assumptions (i.e., pseudosteady state radical concentration and equal rates of functional group consumption)[9,37] numerical solutions using the ode45 function in MATLAB were implemented for

$$R_i = \frac{2.303 f \epsilon [I] I_0 \lambda}{N_A h c} = k_i [I] \tag{5}$$

$$R_t(C^\cdot) = 2 k_t [C^\cdot]^2 + k_t [C^\cdot][S^\cdot] \tag{6}$$

$$R_t(S^\cdot) = 2 k_t [S^\cdot]^2 + k_t [C^\cdot][S^\cdot] \tag{7}$$

consistency with subsequent modeling of the combined thiol-ene-disulfidation reaction scheme.

The conversion of the alkene during the disulfidation polymerization of DSDVE was measured via FTIR and is provided in **Figure 3.4**. The reaction was performed with 1.5 wt% TPO as a photoinitiator and was activated with 405 nm light at 14 mW/cm^2 light intensity. The inherent stoichiometry of this reaction is a 1:2 disulfide-to-alkene due to the disulfide core with two flanking vinyl ether groups. Therefore, the theoretical conversion of the alkene is 50% if every disulfide is consumed during the polymerization. There is a clear induction period during the early stage of this reaction that is attributed to oxygen inhibition.[36] Upon overcoming this inhibition, the reaction proceeds and the alkene indeed reaches approximately 50% conversion, which is assumed to correspond to complete consumption of the disulfide. The numerical model was fit to the experimental best fit value after oxygen inhibition has been overcome with k_{ct} of 8000 s^{-1}.

When the reaction is chain transfer limited as appears here, k_p is necessarily much larger than k_{ct} and its specific value does not alter the overall reaction rate significantly. Propagation kinetic constants for thiol-ene reactions in the literature between thiols and vinyl ethers are reported to be near that of chain transfer (k_p/k_{ct} = 1.2) with a k_p on the order of 130000 s^{-1} for 3-mercaptopropionates under similar conditions to those implemented here, indicating a much faster reaction than that between the disulfide and vinyl ether. As the propagation reaction between the thiyl radical and the vinyl ether should be similar regardless of whether the thiyl radical is generated from a thiol or a disulfide, this literature value of k_p = 130000 s^{-1} was used to calculate an estimate for k_p/k_{ct} for the disulfidation of DSDVE of 16.
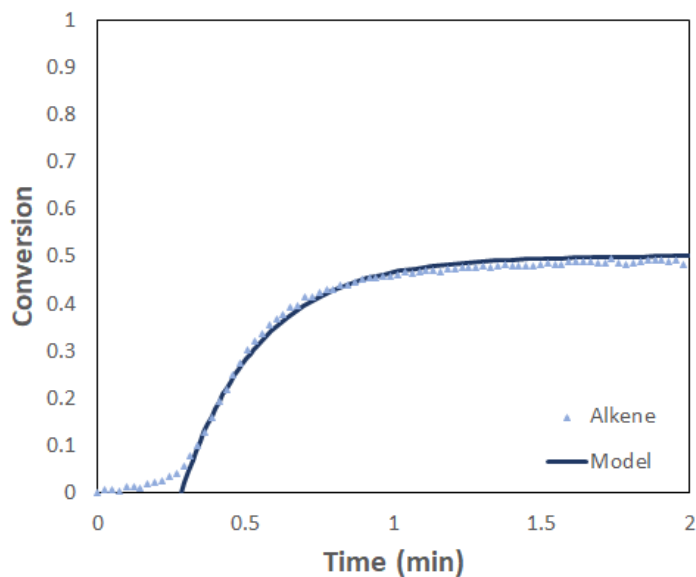
Figure 3.4: Kinetics of the disulfidation reaction of DSDVE, and the model kinetics. The reaction reaches full conversion of disulfide and 50% conversion of alkene due to the off stoichiometric ratio of the reactants (2:1 ratio alkene:disulfide). The reaction contained 1.5 wt% TPO and was reacted with 14 mW/cm^2 of light at 405nm. Full conversion is achieved after roughly one minute of irradiation time.

3.4.3: Methyl thioglycolate: Thiol-ene-disulfidation Kinetics

Introducing thiol into this reaction scheme results in two competing reaction pathways, namely the thiol-ene and disulfide-ene reactions, that share a propagation step in which the thiyl radical adds into an alkene to generate the carbon-centered radical. The chain transfer step may then proceed for either the thiol-ene reaction, by abstracting a hydrogen from a thiol, or through the disulfidation reaction by reacting with and

cleaving the disulfide (**Figure 3.5**). The more prevalent pathway at a given point in time therefore depends on both the relative chain transfer rate constants and the concentrations of thiol and disulfide. The propagating carbon radical chain transfers to a thiol or a disulfide to yield distinct products.
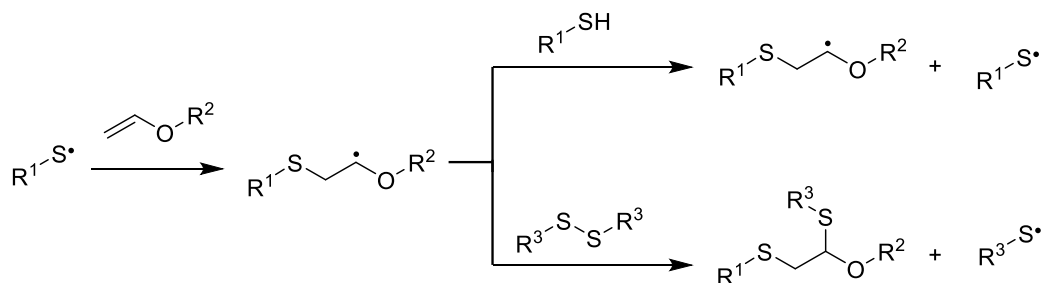
Figure 3.5: Competing reactions of a vinyl ether between the thiol-ene and disulfide-ene reactions.

Competition between these reactions was analyzed by exploring the reaction between MTG and DSDVE. Regardless of whether chain transfer occurs with a thiol or a disulfide, the reaction of either MTG or DSDVE results in a thioglycolate radical. Thus, this parallel reaction enables kinetic analysis that includes only a single type of thiyl radical. In addition to the thiol-ene reaction, introduction of thiol to this scheme also enables radical-disulfide exchange between the thiol and the disulfide during the thiol-ene stage of the reaction. This pathway is not directly accounted for in the kinetic model since the initial and final species are chemically identical but is implicitly accounted for within the chain transfer step for thiol-ene because the product of radical disulfide exchange reaction does not change the kind of thiyl radicals that are present in the reaction.

A model that also takes the thiol-ene pathway into account is presented in the species mass balances presented in Equations 8-12. The new terms introduced for the thiol-ene disulfidation model are colored blue for additional clarity. Equation 8 accounts for the thiol concentration by the chain transfer of the carbon-centered radical to the thiol. Equations 9 describes the alkene consumption and is identical to Equation 1 because both thiol-ene and disulfide-ene share the same propagation step. Equation 10 describes the disulfide consumption and is nearly identical to Equation 2, where k_{ct} has been replaced by k_{ct2} to differentiate between the two different chain transfer constants. Equations 11 and 12 account for the thiyl

27

and carbon radicals, respectively, with terms that factor in chain transfer to a thiol (k_{ct1}) and chain transfer to a disulfide (k_{ct2}). Because radical disulfide exchange is possible during the thiol-ene step of the reaction, the k_{ct1}[SH][C·] term represents the net-chain transfer rate after any disulfide exchange events occur. This system of equations was then solved numerically using the ode45 function in MATLAB and fit to experimental data.

MTG was used in a model study at three different stoichiometries of thiol-to-alkene; 0.25:1, 0.5:1, and 1:1. These stoichiometries were selected to demonstrate a robust kinetic model at different thiol, disulfide, and alkene concentrations. Mild initiation conditions, 0.5 wt% TPO photoinitiator and 7 mW/cm^2 of 405 nm light, were used to slow down the reaction such that any differences in rate could be more easily distinguished and accurately measured. For all three stoichiometries, a ratio of propagation to chain transfer kinetic constants for the thiol-ene reaction (k_p/k_{ct1}) of 1.2 was used as a previously calculated value from

$$\frac{d[SH]}{dt} = -k_{ct1}[SH][C^\cdot] \tag{8}$$

$$\frac{d[C=C]}{dt} = -k_p[C=C][S^\cdot] \tag{9}$$

$$\frac{d[S-S]}{dt} = -k_{ct2}[S-S][C^\cdot] \tag{10}$$

$$\frac{d[S^\cdot]}{dt} = R_i - R_t(S^\cdot) + k_{ct1}[SH][C^\cdot] + k_{ct2}[S-S][C^\cdot] - k_p[C=C][S^\cdot] \tag{11}$$

$$\frac{d[C^\cdot]}{dt} = -R_t(C^\cdot) - k_{ct1}[SH][C^\cdot] - k_{ct2}[S-S][C^\cdot] + k_p[C=C][S^\cdot] \tag{12}$$

the literature (Cramer et al.)[37]. Therefore, the model was fit to the data by adjusting only the ratio of the thiol-ene and disulfidation chain transfer kinetic constants (k_{ct1}/k_{ct2}).

Representative FTIR data for the thiol and alkene conversion over time for all three stoichiometries and the model fit are shown in **Figure 3.6**. A single set of kinetic parameters was used to fit all three stoichiometries where k_{ct1} = 136000 s^{-1} and k_{ct2} = 4800 s^{-1} which results in k_{ct1}/k_{ct2} = 28. The conversion over time and model fits for the 0.25:1 ratio of thiol to alkene are provided in **Figure 3.6a**. Under these

reaction conditions, there is no adequate disulfide peak in the infrared spectrum so the conversion as a function of time as predicted by the model is shown. At this stoichiometry, there are sufficient thiol and disulfides to react with a total of 75% of the vinyl ethers with 25% conversion attributed to the thiol-ene reaction and 50% conversion attributed to disulfidation. As predicted, a rapid thiol-ene reaction is observed within the first few seconds, followed by a slower disulfidation step with a transition from the thiol-ene to the disulfide-ene reaction occurring at roughly 25% conversion of the alkene, as dictated by the reaction stoichiometry. The model slightly underpredicts the rate of disulfide exchange, but accurately predicts the thiol-ene rate and the overall conversion the reaction.

Next, representative FTIR data for the thiol and alkene conversion and model prediction for the 0.5:1 ratio of thiol to alkene are provided in **Figure 3.6b**. Here, all functional groups should be consumed once both the thiol-ene and disulfidation reactions are complete, with a transition occurring around 50% conversion of the alkene. Once again two regimes are indeed observed; an initial rapid thiol-ene step, followed by a slower disulfidation step which occurs after about 50% conversion as predicted. Once again, the model accurately predicts the rate of the thiol-ene reaction, but this time overpredicts the rate of the disulfide-reaction by missing the short "ramp-up" period between the two reaction mechanisms.

Representative FTIR data for thiol and alkene conversions for the 1:1 ratio of thiol to alkene are provided in **Figure 3.6c** with their corresponding model fits. Here, only the thiol-ene reaction should occur, rapidly consuming all of the alkenes before the disulfides have a chance to react. Indeed, a single rapid reaction is observed, with 1-2% of the thiol left unreacted due to minimal conversion of the disulfides. A separate disulfidation step does not occur because nearly all of the alkenes are consumed by the thiols. In this case, the model slightly underpredicts the rate of the thiol-ene reaction relative to disulfidation by overpredicting the amount of unreacted thiol (by 2-3% conversion) due to the alkene consumption by the disulfides that was observed in the data.
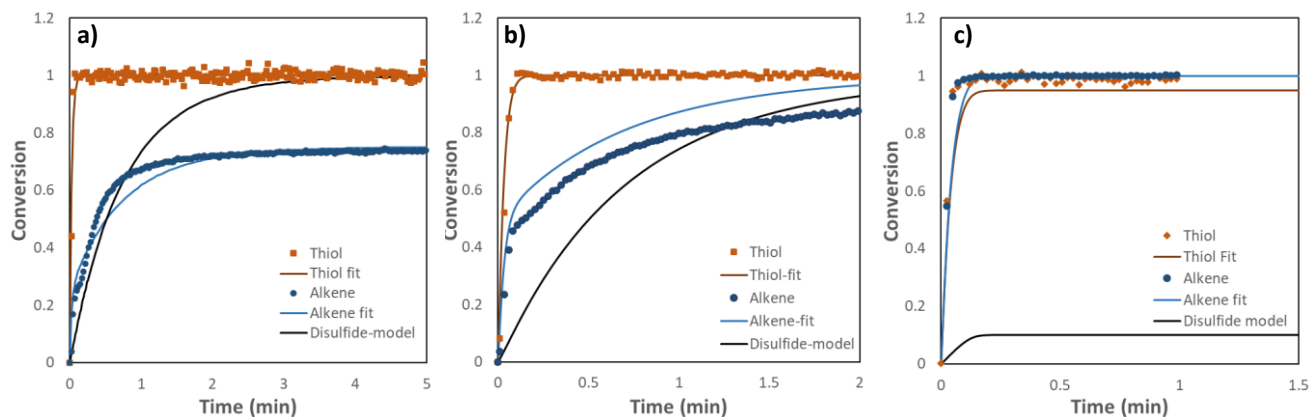
Figure 3.6: Conversion over time for the thiol and alkene for DSDVE and MTG with the overall model fits (k_P = 164000 s^{-1}, k_{ct1} = 136000 s^{-1}, k_{ct2} = 4800 s^{-1}), as well as the predicted disulfide conversion for: **a)** 0.25:1 ratio of thiol-to-alkene, **b)** 0.5:1 ratio of thiol-to-alkene, and **c)** 1:1 ratio of thiol-to-alkene. Reactions contained 0.5 wt% TPO and were initiated by 7 mW/cm^2 light at 405 nm.

The kinetic model shows reasonably good agreement with the experimental data and that the thiol-ene reaction is approximately 30 times faster than the disulfidation reaction for this system. This rate difference is largely attributed to the fact that the hydrogen atom of a thiol is significantly more sterically accessible than the disulfide bond, resulting in rapid extraction of the hydrogen atom from a thiol relative to the homolytic cleavage of the disulfide to regenerate a thiyl radical. Some discrepancies were observed across stoichiometric ratios tested; however, the model performed well overall in predicting the rate and conversion across three different stoichiometric ratios. These small discrepancies are, in part, attributed to the fact that radical-disulfide exchange is not directly accounted for in this model and differences in disulfide concentration can impact the rate differently for each stoichiometry tested. The contribution of radical-disulfide exchange for each stoichiometry will be different because the relative concentration of disulfide to thiol cannot be kept constant due to the fixed 2:1 alkene:disulfide stoichiometry imposed by the DSDVE monomer. Therefore, changing the thiol to alkene stoichiometry must also change the relative amount of disulfide and therefore the rate of the exchange. Directly accounting for radical-disulfide exchange would require knowledge of the rate constants for the addition of the thiyl radical to the disulfide and the fragmentation of that intermediate back into the radical and disulfide. These rate constants are not, as of this writing, available in literature except for a small set of purely aliphatic disulfides.[12,20,28] Additionally, the assumption of equal rates of all termination pathways also contributes to these

30

discrepancies as changes in stoichiometric ratios will alter the concentration of the various radical present in the polymerization and therefore which termination pathways predominate. Overall, this kinetic analysis shows that thiols and disulfides of the same type can be co-reacted in a controlled manner with vinyl ethers.

3.4.3: Butyl 3-mercaptopropionate: Thiol-ene-disulfidation Kinetics

Implementing thiol-ene-disulfidation polymerizations for practical applications will also involve frequently used multifunctional mercaptopropionate monomers in addition to thioglycolate-based monomers (such as PETMP), which have one additional carbon between the thiol and the carbonyl. It is therefore important to study the impact of introducing different thiyl radical species into the polymerization aside from the radicals formed by the disulfidation reaction on functional group conversions and reaction rate. This analysis is especially important because radical disulfide exchange is inherently possible during these radical polymerizations and the presence of a different thiol may impact the polymerization rate via one or both reactions. To study this impact directly, butyl 3-mercaptopropionate (BMP) was used with DSDVE to study any effects of mixed thiyl radicals on the reaction without the additional complexities of a polymerization such as increases in viscosity and crosslinking.

This study was conducted at the same three stoichiometric ratios of thiol to alkene as BMP; 0.25:1 to reach 75% alkene conversion, 0.5:1 to consume all functional groups, and 1:1 such that essentially only the thiols appreciably react with the alkenes. The conversion over time for the thiol and alkene for each functional group ratio are provided in **Figures 3.7a, 3.7b and 3.7c**, respectively.

All three stoichiometric ratios show similarities and a key difference from the experiments conducted with MTG. Overall, the temporal separation of thiol-ene and disulfidation reactions are nearly identical in terms of the conversion at which the transition occurs. For the 0.25:1 and the 0.5:1 ratio of thiol to alkene, there are distinct thiol-ene and disulfidation steps that transition at 25% and 50% alkene conversion, respectively. Likewise, the 1:1 stoichiometry shows only a thiol-ene reaction in which there is a small amount of residual, unreacted thiol due to a correspondingly small amount of disulfide consumption. However, in all three cases the thiol-ene rate of polymerization for MTG is faster than for BMP, where the transition to disulfidation

occurs after a few seconds for MTG but nearly a minute for BMP. This result is counterintuitive because, in the context of this thiol-ene reaction, the mercaptopropionate radical formed during the thiol-ene reaction with BMP should have improved chain transfer compared to MTG, due to the weakening of the SH bond by intramolecular hydrogen bonding with the carbonyl in a favored six membered ring arrangement.[39]
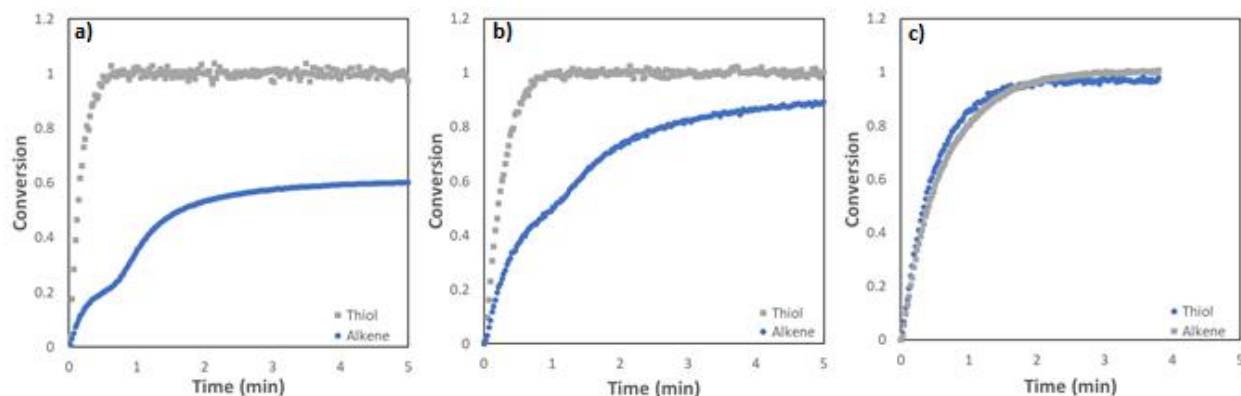
Figure 3.7: Conversion over time for the thiol and alkene for DSDVE with BMP: a) 0.25:1 ratio of thiol-to-alkene, b) 0.5:1 ratio of thiol-to-alkene, and c) 1:1 ratio of thiol-to-alkene. Reactions contained 0.5 wt% TPO, 14 mW/cm2 at 405 nm.

The explanation as to why BMP shows a slower rate of reaction than MTG in the presence of DSDVE centers on the radical disulfide exchange pathway that is expected to occur. Because the thiyl radical formed via chain transfer to BMP is different from that formed from chain transfer to MTG and DSDVE, it is not immediately clear which products of radical disulfide exchange would predominate in this context, but it is clear that the additional complexity introduced by differing thiyl radical species is impacting the rate of the thiol-ene reaction, likely due to a tendency to form the lowest energy, least reactive thiyl radical. However, there was no discernible change in the disulfidation rate with BMP compared to MTG indicating that any retardation process is only impacting the thiol-ene step of the reaction. A possible explanation is that although the BMP thiyl radical adds into the disulfide to form a radical intermediate reducing the thiyl radical concentration, the original BMP radical and disulfide reform because of the enhanced stability of the BMP radical relative to an MTG radical.
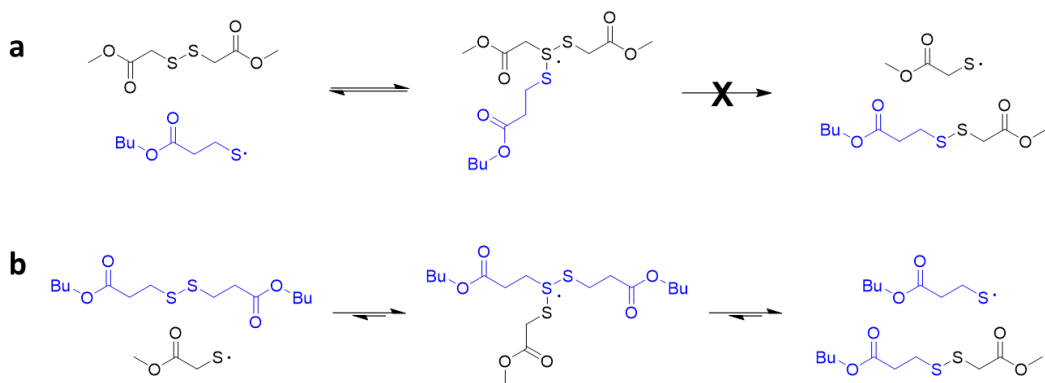
Figure 3.8: **a)** Theoretical mechanism of radical disulfide exchange between BMP thiyl radical and DSMA. Experimental reaction performed via a mixture of DSMA (1 eq) and BMP (1 eq) with 1.5 wt% TPO irradiated at 405nm at 14 mW/cm2. This reaction condition resulted in only recovery of starting compounds as detected by ^{1}H NMR. **b)** Theoretical mechanism of radical disulfide exchange between MTG thiyl radical and DSMP. Experimental reaction performed via a mixture of DSMP (1 eq) and MTG (1 eq) with 1.5 wt% TPO irradiated at 405nm at 14 mW/cm2. This reaction condition resulted in a mixture of corresponding disulfides and thiols as detected by ^{1}H NMR.

This pathway would slow the thiol-ene step by temporarily sequestering thiyl radicals without converting any symmetric dithioglycolate disulfides to a mixture of symmetric and asymmetric disulfides, leaving the disulfidation step unaffected. Furthermore, this proposed mechanism predicts that the radical intermediate formed by a BMP radical may have a longer lifetime than the intermediate formed by an MTG radical due to additional electron density associated with the additional carbon atom between the sulfur and the carbonyl, which would sequester BMP radicals longer in this intermediate state than MGT radicals specifically when DSDVE is the disulfide-containing monomer.

To investigate the cause of the change in thiol-ene rates, mixed disulfide-thiol NMR experiments were performed to probe whether the BMP radicals and dithioglycolate disulfides are in fact the favored products. Two thiol-disulfide mixtures were used in the presence of 1.5 wt% TPO photoinitiator. First, a mixture of DSMA and BMP was tested (**Figure 3.8a**), which is analogous to DSDVE-BMP because it contains the same disulfide/thiol pair. No change in the peaks or peak integration were observed after 10 minutes of irradiation at 14 mW/cm^2 . This indicates that no significant amount of new disulfides or thiols formed during the disulfide exchange process. To test this further, DSMP and MTG were mixed with the photoinitiator TPO and irradiated (**Figure 3.8b**). This mixture is the complementary pair of thiol and disulfide, where the disulfide is based on BMP instead of MTG. Here, there is a clear appearance of new

peaks after irradiation due to the formation of BMP and a mixture of disulfides due to radical thiol-disulfide exchange. These results suggest that the radical disulfide exchange does occur for these disulfides with BMP and that the BMP radical is in fact the more stable thiyl radical. Taken together, these results support the hypothesis that the thiol-ene step is slower with BMP than MTG because the exchange pathway sequesters thiyl radicals to greater extent for BMP without disulfide exchange. This lack of disulfide exchange in this system with BMP portends predictable architecture, whereas disulfide exchange with MTG may result in asymmetric disulfides and less predictable polymer architectures. In an analogous hypothetical system with a mercaptopropionate disulfide core, it would be expected that polymer architecture is less predictable with both BMP and MTG based cross-linkers. Further investigation is ongoing to explore how this phenomenon could be used to tailor polymer architecture.

3.4.5: Gelation of DSDVE

It was not immediately obvious if the polymerization of DSDVE would form a cross-linked network. A similar system based on a monomer containing a mono-thiol and mono-alkyne generates hyperbranched polymers[40]; however, polymerization of DSDVE does in fact yield an insoluble cross-linked network (**Figure 3.9**). Such an outcome could also be expected if some of the disulfides remained unreacted or the alkenes underwent a degree of homopolymerization, or both of those scenarios. However, the photoinitiated polymerization of DSDVE is difficult to evaluate via the Flory-Stockmayer relationship due
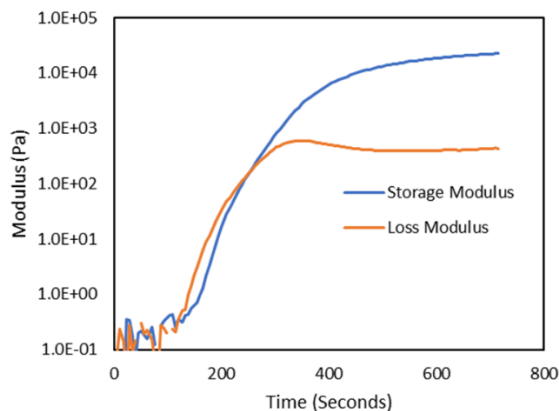
Figure 3.9: Rheology for the photopolymerization of DSDVE with 1.5 wt% TPO irradiated at 405nm at 14 mW/cm2. Data demonstrates cross-linking by the storage modulus crossing the loss modulus after roughly 2 minutes of light exposure.

to the complexities that are unique to this polymerization, namely the requirement that both reaction sites on the alkene must react during a single polymerization cycle as compared to the thiol-yne reaction where a single site may react before the second. However, it can be conceptually simplified to a reaction between difunctional and trifunctional monomers with complementary functional groups in a 2 to 1 molecular ratio (**Figure 3.10**). In such a system, under ideal and uniform reaction progress, two difunctional monomers would react with one trifunctional complement to create a heterotrifunctional compound such as the one illustrated below.

Figure 3.10: Schematic representation of the disulfide-ene reaction of DSDVE. This representation is a depiction of the fundamental reactive unit obtained after radical cleavage of the disulfide. 'A' depicts a thiyl radical and the 'B's represent the alkene that acts as a difunctional unit.

This hypothetical compound and arrangement of complementary bonds is equivalent to the fundamental reactive unit obtained by radical cleavage of the disulfide, wherein the sulfur radical is monofunctional and the vinyl ether is difunctional. According to Flory-Stockmayer[41], the critical conversion for gelation (the minimum conversion the limiting functional group must reach for network formation) is described by Equation 13.

$$p_c = \frac{1}{\left[r(f_{w,A} - 1)(f_{w,B} - 1)\right]^{1/2}} \qquad (13)$$

Where p_c is the critical conversion, r is the stoichiometric imbalance defined as the moles of limiting functional group divided by the moles of excess complementary functional group, $f_{w,A}$ is the weight averaged functionality of designated "A" functional group monomers and $f_{w,B}$ is the weight averaged functionality of the designated "B" functional group monomers (3 and 2 in this case, respectively). The stoichiometric imbalance, in this case, would be 0.75 for the three A groups divided by the four B groups, resulting in a critical conversion of 0.82, well within the range of achievable extent of reaction. It should be noted that a similar hypothetical heterotrifunctional species can be obtained by reacting a single

trifunctional A compound with a single difunctional B compound, in which case, the stoichiometric imbalance would be 2/3 and the critical conversion would be 0.87, again below the limit of 1.0. The Carothers equation for gelation[41], shown in Equation 14, where f_{avg} is defined simply as the total number of limiting functional groups divided by the total number of reactive species, yields a different result.

$$p_c = \frac{2}{f_{avg}} \qquad (14)$$

By this equation, critical gelation conversion is calculated as at or above the maximum possible conversion of 100%, indicating no gelation is possible. In practice, experimental gel point conversions frequently lie somewhere between these two simple and common predictive models. While the Flory-Stockmayer statistical treatment is typically preferred for gel point predictions, the results from the Carothers equation serve to demonstrate that this system is likely on the cusp of crosslinking, which may aid in explaining the discrepancy between the results presented herein and those reported in similar systems.

It should be noted that these comparisons with these three by two, network polymer systems rely on assumptions regarding the order and arrangement of reacted species that are most likely imperfectly reflective of the reality of the DSDVE polymerization. This analogy, however, does lend support to and does not preclude the gelation of this material. For a more in depth investigation of the heterofunctional Flory-Stockmayer characterization, Tiemersma-Thoone et al. present a detailed study.[42]

3.4.6: Co-polymerizations with PETMP

Finally, co-polymerization of the DSDVE monomer with PETMP to form insoluble cross-linked networks was investigated. The same three stoichiometric ratios between monomer and PETMP were tested as in the model studies, and rheology data and functional group conversion data were obtained (**Figure 3.11**). Rapid gelation of the material for each stoichiometric formulation of DSDVE and PETMP was achieved upon photoinitiation.
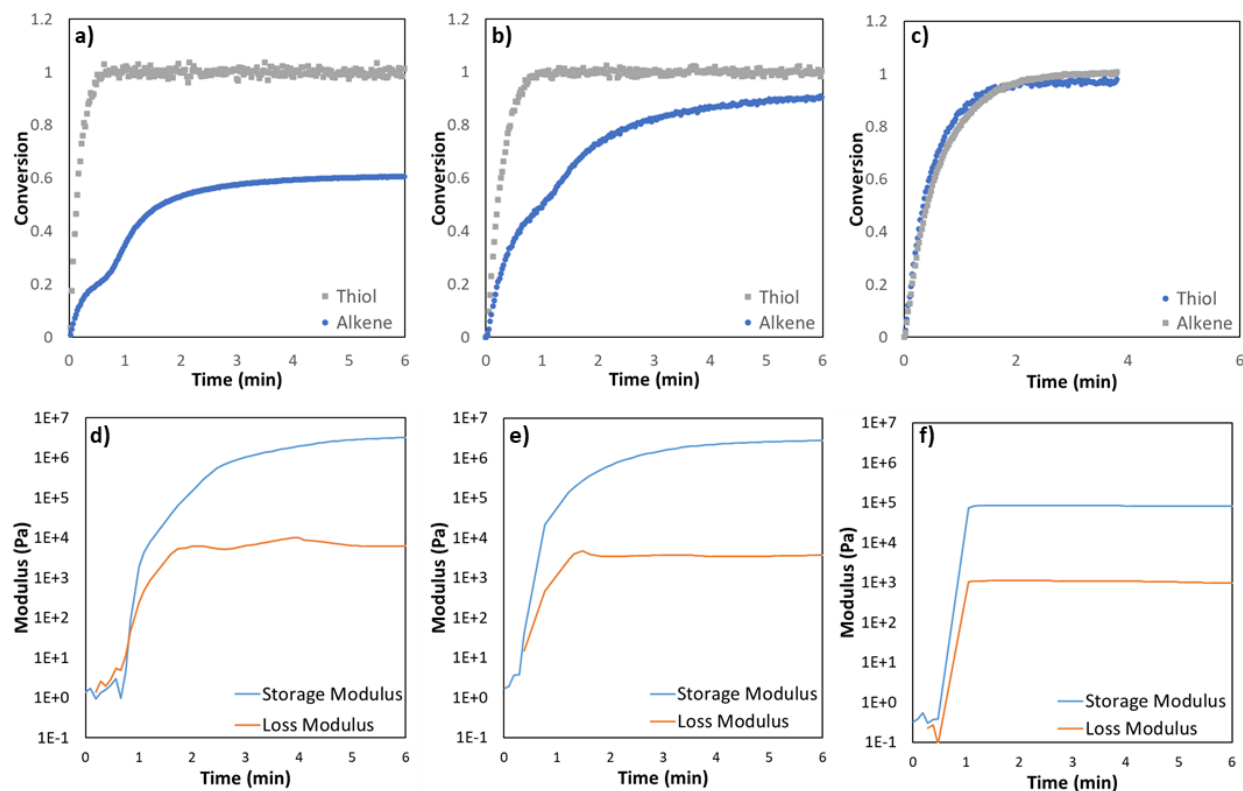
Figure 3.11: Rheology data obtained from different stoichiometric formulations of DSDVE and PETMP with 1.5wt% TPO irradiated at 405nm at an intensity of 14mW/cm2. a) Functional group conversion measured by IR versus time for a 0.25:1 stoichiometric equivalence of thiol:alkene. b) IR plot of a 0.5:1 stoichiometric equivalence of thiol:alkene. c) IR plot of a 1:1 stoichiometric equivalence of thiol:alkene. d) Storage and loss moduli as measured rheology as a function of time for a 0.25:1 stoichiometric equivalence of thiol:alkene. e) Rheology plot of a 0.5:1 stoichiometric equivalence of thiol:alkene. f) Rheology plot of a 1:1 stoichiometric equivalence of thiol:alkene.

Figure 3.11a and 3.11d are comprised of a 0.25:1 ratio of thiol to alkene, **Figure 3.11b and 11e** are comprised of a 0.5:1 ratio of thiol to alkene, and **Figure 3.11c and 3.11f** are comprised of a 1:1 ratio of thiol to alkene. The disulfidation reaction results in twice the number of cross-links compared to the thiol-ene reaction. Therefore, the formulations in which the alkene is consumed by the disulfide-ene reaction result in a nearly 100 fold increase in the storage modulus of the two formulations for which alkenes are available to react with disulfides following the thiol-ene reaction (0.25:1 and 0.5:1) compared to the 1:1 network where thiol-ene is the primary crosslinking reaction.

It was originally hypothesized, and subsequently demonstrated by the model compound kinetics, that the thiol-ene reaction being sufficiently faster than the disulfide-ene reaction would allow for sequential

and selective thiol and disulfide consumption to result in a two-step photopolymerization process. For example, the irradiation time can be used to control which polymerization chemistry occurs, where thiol-ene chemistry would proceed to completion in stage I before any significant amount of disulfidation reaction has a chance to occur (stage II). To test this hypothesis, a mixture of PETMP and DSDVE (stoichiometry of 0.5:1 thiol:alkene) was irradiated at 7 mW/cm^2 for 30 seconds. The thiol and alkene conversions were measured by IR, (**Figure 3.12a**) yielding nearly complete conversion of thiols with minimal consumption of the disulfides. Following the initial curing, a second, prolonged irradiation at 7 mW/cm^2 facilitated the disulfide-ene reaction. **Figure 3.12b** demonstrates that these temporally resolved reactions enable a dual-cure with control over crosslinking density where the thiol-ene polymerization goes to completion after stage 1 curing and can be halted by turning off irradiation, and the disulfidation polymerization proceeds once a stage 2 curing of the disulfides begins. The second stage curing process increases the storage modulus by 2-3 orders of magnitude under these conditions.
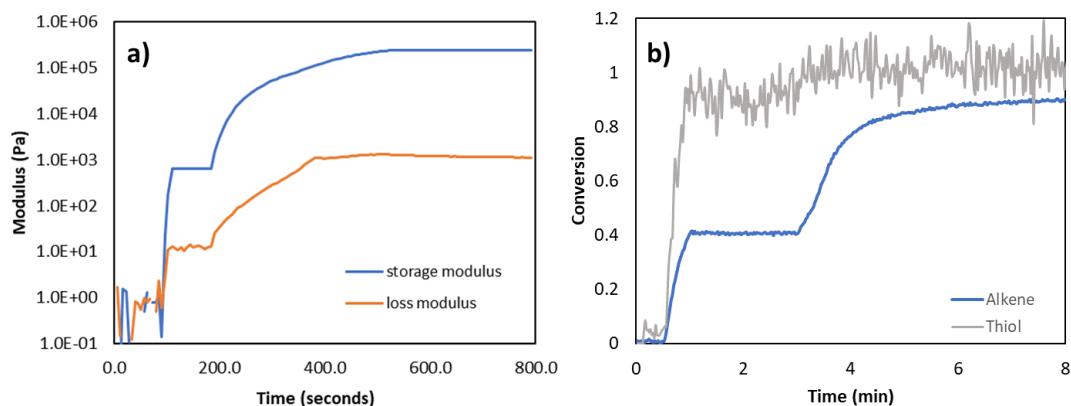
Figure 3.12: Samples prepared with DSDVE and PETMP (1:0.5 alkene:thiol stoichiometric equivalence) with 3 wt% TPO irradiated at 405nm at 7 mW/cm2. a) Storage and loss moduli as measured rheology as a function of time demonstrating control over storage modulus of the formulated network by controlling irradiation time. Light is turned on for 30 seconds demonstrating near immediate gelation via primarily thiol-ene chemistry before irradiation is stopped. After about 3 minutes light is turned back on and storage modulus continues to increase due to disulfidation chemistry starting. b) Functional group conversion measured by IR versus time demonstrating time point at which thiol reaches 100% conversion (after roughly 10 seconds of light exposure) and irradiation is stopped for two minutes. After three minutes, light is turned back on and alkene consumption continues via disulfidation.

This dual-cure system enables controlled manipulation of material properties allowing for a broader scope of potential applications for this polymerization. **Figure 3.13** demonstrates the glass transition temperatures (T_g) corresponding to the first and second stage polymerizations, with an increase of 18 ^{o}C between the first stage (T_{g1} = -36 ^{o}C) and second stage (T_{g2} = -18 ^{o}C). In addition, the high sulfur content in these polymeric systems is an attractive means to obtain materials with useful optical properties. This disulfidation reaction provides an excellent means to achieve such materials. Similar to many thiol-ene based networks, the material is optically clear in the visible light region after both curing stages.

Finally, a stage I film (same material as in Figure 12) was exposed to UV light through a photomask
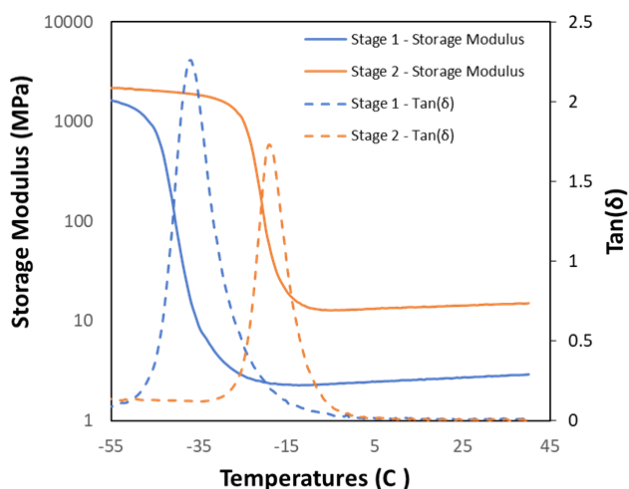
Figure 3.13: Materials consisted of PETMP and DSDVE (0.5:1 thiol:alkene stoichiometric ratio) and 3wt% TPO. Sample was cast between glass plates with 250µm spacers. Samples were irradiated at 405nm at 14 mW/cm^2 for 45 seconds for the first stage cure, and an additional 5 minutes for the second stage cure.

to create a stage II optical index gradient patterns as illustrated in **Figure 3.14**. The photopatterned features, generated as a result of a refractive index change between exposed and unexposed regions, are micrometer-sized squares of high modulus, high refractive index materials surrounded in a continuous way by a low modulus stage I matrix. As seen in the microscopic images, good feature resolution is achieved, even at relatively long exposure times (5 min) with non-collimated light. It is argued here that such an outcome was possible uniquely due to the nature of the system at hand where almost all functional groups capable

of reacting are tethered to the initial stage I network, and therefore immobilized prior to further reaction. Re-exposure in a lithographic setup breaks the disulfide crosslinks locally in the exposed areas, promoting an area-limited local reactivity increase and thiyl-vinyl coupling leading to the formation of two thioether links out of one disulfide. Overall, a spatially-restricted increase in crosslinking is achieved as well as an increase in refractive index.
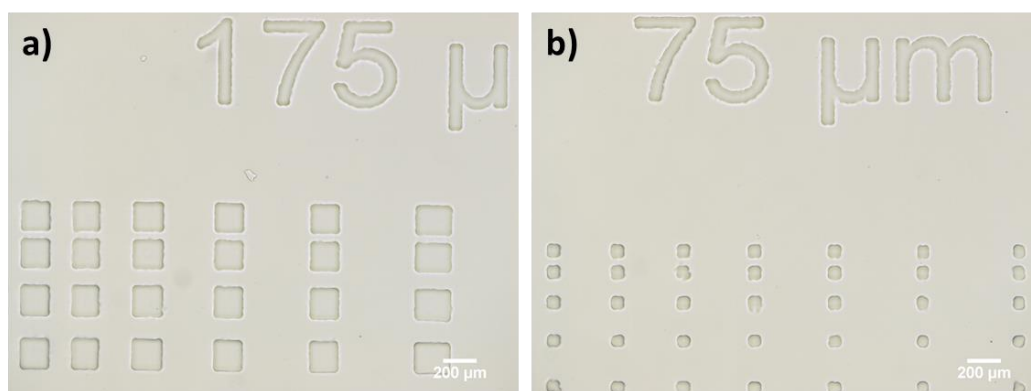
Figure 3.14: Materials consisted of PETMP and DSDVE (0.5:1 thiol:alkene stoichiometric ratio) and 3wt% TPO. Sample was cast between glass plates with 250µm spacers and irradiated with 405nm light at 14 mW/cm2 for 45 seconds for the first stage cure, and an additional 5 minutes for the second stage cure. The photopatterned features are a result of a refractive index change between exposed and unexposed regions. a) After initial UV exposure to form the cross-linked network, a secondary illumination through a photomask produced 175 µM feature patterns. b) After initial UV exposure to form the cross-linked network, a second illumination through a photomask produced 75 µM feature patterns.

3.5: Conclusions

In summary, a monomer was designed and synthesized that enables sequential photo-induced thiol-ene and disulfide-ene chemistries with appreciable rates and high overall conversions, yielding materials with a high overall sulfur content. The relative rates of the thiol-ene and disulfidation chemistries were investigated, and it was found that the thiol-ene reaction is on average approximately 30 times faster than the disulfidation reaction. This difference in rates enables spatial and temporal control over the two different chemistries allowing for a dual-cure system. The successful implementation of a two-stage photocure allows a remarkable degree of control of developing materials properties, both mechanical and optical. This work provides a new route to high sulfur containing materials and increases the scope and utility of thiol-X and disulfide-based polymerizations.

3.6: References

(1)   Mutlu, H.; Ceper, E. B.; Li, X.; Yang, J.; Dong, W.; Ozmen, M. M.; Theato, P. Sulfur Chemistry in Polymer and Materials Science. *Macromol. Rapid Commun.* **2019**, *40* (1), 1–51.

(2)   Kausar, A.; Zulfiqar, S.; Sarwar, M. I. Recent Developments in Sulfur-Containing Polymers. **2014**, *3724*.

(3)   Boyd, D. A. Sulfur and Its Role In Modern Materials Science. *Angew. Chemie - Int. Ed.* **2016**, *55* (50), 15486–15502.

(4)   Martin, R.; Rekondo, A.; De Luzuriaga, A. R.; Casuso, P.; Dupin, D.; Cabañero, G.; Grande, H. J.; Odriozola, I. Dynamic Sulfur Chemistry as a Key Tool in the Design of Self-Healing Polymers. *Smart Mater. Struct.* **2016**, *25* (8).

(5)   Hoyle, C. E.; Lowe, A. B.; Bowman, C. N. Thiol-Click Chemistry: A Multifaceted Toolbox for Small Molecule and Polymer Synthesis. *Chem. Soc. Rev.* **2010**, *39* (4), 1355–1387.

(6)   Fairbanks, B. D.; Love, D. M.; Bowman, C. N. Efficient Polymer-Polymer Conjugation via Thiol-Ene Click Reaction. *Macromol. Chem. Phys.* **2017**, *218* (18), 1–11.

(7)   Northrop, B. H.; Coffey, R. N. Thiol-Ene Click Chemistry: Computational and Kinetic Analysis of the Influence of Alkene Functionality. *J. Am. Chem. Soc.* **2012**, *134* (33), 13804–13817.

(8)   Lowe, A. B.; Hoyle, C. E.; Bowman, C. N. Thiol-Yne Click Chemistry: A Powerful and Versatile Methodology for Materials Synthesis. *J. Mater. Chem.* **2010**, *20* (23), 4745–4750.

(9)   Cramer, N. B.; Davies, T.; O'Brien, A. K.; Bowman, C. N. Mechanism and Modeling of a Thiol-Ene Photopolymerization. *Macromolecules* **2003**, *36* (12), 4631–4636.

(10)   Long, K. F.; Bongiardina, N. J.; Mayordomo, P.; Olin, M. J.; Ortega, A. D.; Bowman, C. N. Effects of 1°, 2°, and 3° Thiols on Thiol-Ene Reactions: Polymerization Kinetics and Mechanical Behavior. *Macromolecules* **2020**, *53* (14), 5805–5815.

(11)   Goethals, F.; Frank, D.; Du Prez, F. Protected Thiol Strategies in Macromolecular Design. *Prog. Polym. Sci.* **2017**, *64*, 76–113.

(12)   Pepels, M.; Filot, I.; Klumperman, B.; Goossens, H. Self-Healing Systems Based on Disulfide-Thiol Exchange Reactions. *Polym. Chem.* **2013**, *4* (18), 4955–4965.

(13)   Bang, E. K.; Lista, M.; Sforazzini, G.; Sakai, N.; Matile, S. Poly(Disulfide)S. *Chem. Sci.* **2012**, *3* (6), 1752–1763.

(14)   Fang, J.; Ye, S. H.; Wang, J.; Zhao, T.; Mo, X.; Wagner, W. R. Thiol Click Modification of Cyclic Disulfide Containing Biodegradable Polyurethane Urea Elastomers. *Biomacromolecules* **2015**, *16* (5), 1622–1633.

(15)   Gething, M.-J.; Sambrook, J. Protein Folding in the Cell. *Nature* **1992**, *355*, 33–45.

(16)   Rowan, S. J.; Cantrill, S. J.; Cousins, G. R. L.; Sanders, J. K. M.; Stoddart, J. F. *Dynamic Covalent Chemistry*.

(17)   Saito, G.; Swanson, J. A.; Lee, K. Drug Delivery Strategy Utilizing Conjugation via Reversible Disulfide Linkages : Role and Site of Cellular Reducing Activities. **2003**, *55*, 199–215.

(18)   Wojtecki, R. J.; Meador, M. A.; Rowan, S. J. Using the Dynamic Bond to Access Macroscopically Responsive Structurally Dynamic Polymers. *Nat. Mater.* **2011**, *10*, 14–27.

(19)   Meng, F.; Hennink, W. E.; Zhong, Z. Biomaterials Reduction-Sensitive Polymers and Bioconjugates for Biomedical Applications. *Biomaterials* **2009**, *30* (12), 2180–2198. https://doi.org/10.1016/j.biomaterials.2009.01.026.

(20)   Gilbert, H. F. Thiol/Disulfide Exchange Equilibria and Disulfidebond Stability. *Methods Enzymol.* **1995**, *251* (C), 8–28.

(21)   Chen, W.; Shah, L. A.; Yuan, L.; Siddiq, M.; Hu, J.; Yang, D. Polymer–Paclitaxel Conjugates Based on Disulfide Linkers for Controlled Drug Release. *R. Soc. Chem.* **2015**, *5*, 7559–7566.

(22)   Endo, K.; Múrate, K.; Otsu, T. Living Radical Polymerization of Styrene with Tetramethylene Disulfide. *Macromolecules* **1992**, *25*, 5554–5556.

(23)   Endo, K.; Shiroi, T.; Murata, K. Controlled Radical Polymerization of Styrene in the Presence of Cyclic 1,2-Disulfides. *J. Polym. Sci. Part A Polym. Chem.* **2001**, *39*, 145–151.

(24)   Chen, J.; Jiang, S.; Gao, Y.; Sun, F. Reducing Volumetric Shrinkage of Photopolymerizable Materials Using Reversible Disulfide-Bond Reactions. *J. Mater. Sci.* **2018**, *53* (23), 16169–16181.

(25)   Barcan, G. A.; Zhang, X.; Waymouth, R. M. Structurally Dynamic Hydrogels Derived from 1,2-Dithiolanes. *J. Am. Chem. Soc.* **2015**, *137* (17), 5650–5653.

(26)   Singh, R.; Whitesides, G. M. Degenerate Intermolecular Thiolate-Disulfide Interchange Involving Cyclic Five-Membered Disulfides Is Faster by ~10^3 Than That Involving Six- or Seven-Membered Disulfides. *J. Am. Chem. Soc.* **1990**, No. 10, 6304–6309.

(27)   Tong, C.; Wondergem, J. A. J.; Heinrich, D.; Kieltyka, R. E. Photopatternable, Branched Polymer Hydrogels Based on Linear Macromonomers for 3D Cell Culture Applications. *ACS Macro Lett.* **2020**, 882–888.

(28)   Fernandes, P. A.; Ramos, M. J. Theoretical Insights into the Mechanism for Thiol/Disulfide Exchange. *Chem. - A Eur. J.* **2004**, *10* (1), 257–266.

(29)   Carmine, A.; Domoto, Y.; Sakai, N.; Matile, S. Comparison of Lipoic and Asparagusic Acid for Surface-Initiated Disulfide-Exchange Polymerization. *Chem. - A Eur. J.* **2013**, *19* (35), 11558–11563.

(30)   Fairbanks, B. D.; Singh, S. P.; Bowman, C. N.; Anseth, K. S. Photodegradable, Photoadaptable Hydrogels via Radical-Mediated Disulfide Fragmentation Reaction. *Macromolecules* **2011**, *44* (8), 2444–2450.

(31)   Mavila, S.; Sinha, J.; Hu, Y.; Podg, M.; Shah, P. K.; Bowman, C. N. High Refractive Index Photopolymers by Thiol − Yne " Click " Polymerization. **2021**.

(32)   Wang, X. R.; Chen, F. Iodine-Catalyzed Disulfidation of Alkenes. *Tetrahedron* **2011**, *67* (25), 4547–4551.

(33)   Bowman, C. N.; Kloxin, C. J. Toward an Enhanced Understanding and Implementation of Photopolymerization Reactions. **2008**, *54* (11).

(34)   Usugi, S.; Yorimitsu, H.; Shinokubo, H.; Oshima, K. Disulfidation of Alkynes and Alkenes with Gallium Trichloride. **2004**, No. 5, 6–8.

(35)   Caserio, M.; Fisher, C.; Kim, J. Boron Trifluoride Catalyzed Addition of Disulfides to Alkenes. *J. Org. Chem.* **1985**, 4390–4393.

(36)   Kamps, J.; Soars, S.; Fairbanks, B.; Bowman, C. N. Photodisulfidation of Alkenes with Linear Disulfides: Reaction Scope and Kinetics. *Manuscr. Submitt. Publ.*

(37)   Cramer, N. B.; Reddy, S. K.; O'Brien, A. K.; Bowman, C. N. Thiol - Ene Photopolymerization Mechanism and Rate Limiting Step Changes for Various Vinyl Functional Group Chemistries. *Macromolecules* **2003**, *36* (21), 7964–7969.

(38)   Neumann, M. G.; Miranda, W. G.; Schmitt, C. C.; Rueggeberg, F. A.; Correa, I. C. Molar Extinction Coefficients and the Photon Absorption Efficiency of Dental Photoinitiators and Light Curing Units. *J. Dent.* **2005**, *33*, 525–532.

(39)   Hoyle, C. E.; Lee, T. A. I. Y.; Roper, T. Thiol – Enes: Chemistry of the Past with Promise for the Future. *J. Polym. Sci. Part A Polym. Chem.* **2004**, *42*, 5301–5338.

(40)   Konkolewicz, D.; Gray-Weale, A.; Perrier, S. Hyperbranched Polymers by Thiol-Yne Chemistry: From Small Molecules to Functional Polymers. *J. Am. Chem. Soc.* **2009**, *131* (50), 18075–18077.

(41)   Odian, G. *Principles of Polymerization*, 4th editio.; John Wiley & Sons, Inc., 2004.

(42)   Tiemersma-Thoone, G. P. J. M.; Scholtens, B. J. R.; Dušek, K.; Gordon, M. Theories for Network Formation in Multistage Processes. *J. Polym. Sci. Part B Polym. Phys.* **1991**, *29* (4), 463–482.

Chapter 4 – RADICAL-DISULFIDE EXCHANGE IN THIOL-ENE-DISULFIDATION POLYMERIZATIONS

4.1 Abstract

Radical-disulfide exchange reactions in thiol-ene-disulfide networks were evaluated for several structurally distinct thiol and disulfide containing monomers. A new dimercaptopropionate disulfide monomer was introduced to assess how different disulfide moieties affect the exchange process. The stress relaxation rate for the disulfides studied herein was highly tunable over a narrow range of network compositions, ranging from 50% relaxation over 10 minutes to complete relaxation over a few seconds, by changing the thiol-disulfide stoichiometry or the disulfide type in the monomer. The thiol/disulfide monomer pair was shown to have significant influence on how radical-disulfide exchange impacts the polymerization rate, where pairing a more stable radical forming thiol (e.g. an alkyl thiol) with a less stable radical-forming disulfide (e.g. a dithioglycolate disulfide) reduces the rate of the thiol-ene reaction by over an order of magnitude compared to the case where those two radicals are of the same type. The variations in rates of radical-disulfide exchange with dithioglycolate and dimercaptopropionate disulfides had a significant impact on stress relaxation and polymerization stress, where the stress due to polymerization for the final dimercaptopropionate network was about 20% of the stress in the equivalent dithiogylcolate network under the same conditions.

4.2 Introduction

Polymer networks containing dynamic bonds are a growing class of smart and responsive materials known as covalent adaptable networks (CANs)[1, 2]. A diverse and continually expanding set of applicable chemistries and dynamic bonds enable unprecedented development of materials with the viscoelastic characteristics of thermoplastics with the material properties and performance of thermosets. This vast array of dynamic bonds provides the tools to control the rheological behavior of polymer networks by tuning the particular functional groups, catalysts, and their respective concentrations, thereby determining rates of bond reconfiguration.

Disulfides, considered as one of the most common type of dynamic bonds and having been used in industrial polymer processing since the invention of vulcanized rubbers[3-5], play a crucial role in protein folding[6] and have been a known class of reconfigurable bonds since the 1950's[7]. Disulfides are responsive to a variety of stimuli and reactants including heat, light, the presence of base or nucleophiles, or free radicals which enables a host of dynamic pathways, including metathesis[8] (**Figure 4.1a**), reversible addition when radicals are generated through the homolytic cleavage and recombination of disulfides[9] (**Figure 4.1b**), reversible exchange when there are persistent thiyl radicals to facilitate bond exchange[10] (**Figure 4.1c**) or through thiolate mediated pathways[7].
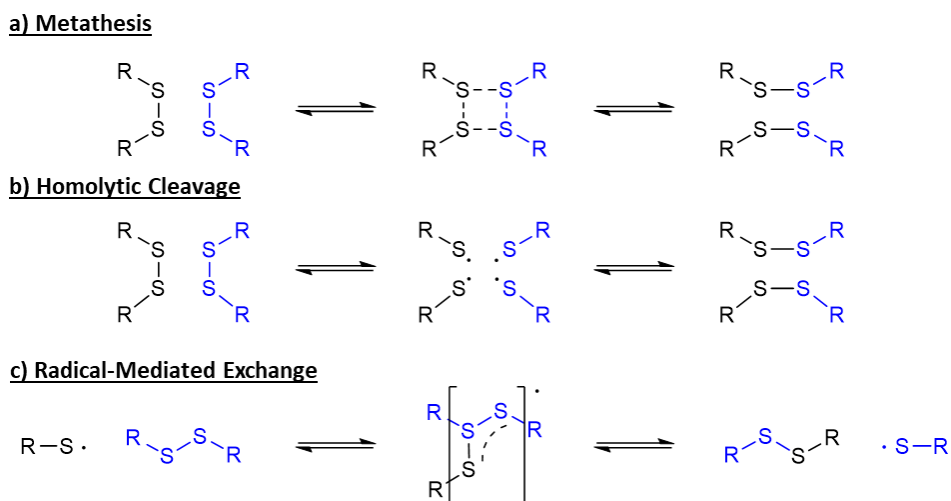
Figure 4.1 Schematic of several dynamic mechanisms of disulfide bonds: a) metatheses, b) reversible addition via homolytic cleavage and recombination of disulfide bonds, and c) radical-mediated reversible exchange between thiyl radicals and disulfides.

Numerous types of disulfide-based CANs have been fabricated, e.g. aromatic disulfide-containing polyurethane networks[8, 11], photoadaptable hydrogels[10], and epoxy resins[12]. Recently, however, a variety of disulfides have been investigated for their participation in disulfide-ene reactions in which the disulfide reacts with norbornenes[13] or vinyl ethers[14] via a step growth mechanism analogous to the thiol-ene reaction. Disulfide-ene reactions with cyclic,[15, 16] and certain linear disulfides,[14, 17] are efficient crosslinking chemistries that generate thioacetal linkages rather than the thioethers associated with thiol-ene, doubling the number of bonds formed per alkene. In addition, thiol-ene and disulfide-ene are highly compatible reactions. Both reactions share a propagation step during which a thiyl radical adds into the alkene to form

a carbon centered radical. The mechanism then diverges to thiol-ene or disulfide-ene depending on whether the carbon radical chain transfers to a thiol or to a disulfide, respectively (**Figure 4.2**).
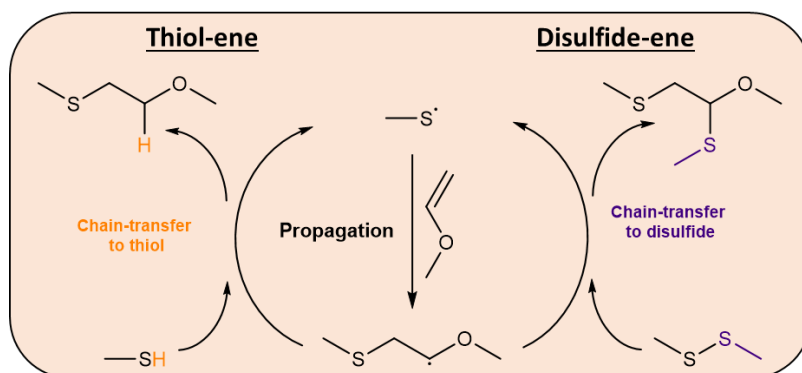
Figure 4.2: Mechanism of thiol-ene disulfidation polymerization, where both reactions share a propagation step but have distinct chain transfer pathways.

It has been demonstrated that these two reactions are effectively sequential, where the thiols are consumed about 30 times more rapidly than the disulfides. This behavior has been attributed to increased steric hindrance during the chain-transfer step associated with a disulfide compared to a thiol.[14, 17] Combining thiol-ene/disulfide-ene enables spatial and temporal control over network architecture by sequentially forming a thioether network via thiol-ene followed by an increase in crosslinking via thioacetal formation from disulfide-ene (**Figure 4.3**). This approach enables consumption of the disulfides to form
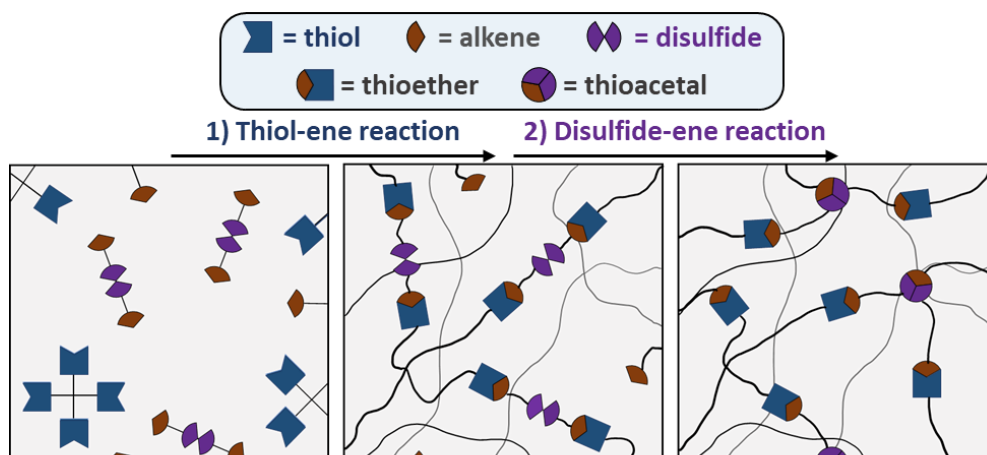
Figure 4.3: Schematic of the thiol-disulfide-ene polymerization for a multifunctional thiol with a disulfide containing divinyl ether (alkene). Polymerization proceeds, beginning with a monomer resin mixture to form a primarily thiol-ene stage 1 network made up of thioether bonds, then through the disulfide-ene reaction to form the thioacetal bonds in the stage 2 network.

additional crosslinks or leaves them available for bond exchange by manipulating the initial stoichiometry and/or the curing conditions.

Radical-disulfide exchange is an inherent feature of this polymerization because thiyl radicals and disulfides are integral to both stages of the polymerization. In their study of the kinetics of the thiol-ene-disulfidation, Soars *et al*. also demonstrated that a mix of different thiyl radicals can impact the rate of polymerization during the thiol-ene stage[17]. In their work, a divinyl ether monomer containing a thioglycolate disulfide core was co-reacted with two different thiols to elucidate whether a more stable thiyl radical should emerge after disulfide exchange events. That exchange process is expected to impact the rate of the thiol-ene polymerization. Therefore, further investigation of the impact of radical-disulfide exchange for these and similarly structured disulfides is needed to understand the impact of bond exchange both during polymerization and during post-polymerization testing.

In this work, a combined thiol-ene/disulfide-ene approach to forming radically active CANs was investigated. First, stress relaxation during photoinitiated radical-disulfide exchange was measured for networks of various thiol content of the initial resin to probe structure-property relationships between the disulfide content of the final network, crosslinking, and the ability to relax stress. In addition, the disulfide-ene polymerization has relatively slow reaction rates compared to thiol-ene and the majority of the crosslinks form during the second stage of the polymerization. Stress relaxation experiments during the second stage of the polymerization were performed to probe the effectiveness of disulfide exchange to reduce polymerization stress, and any effect on the final network structure was characterized by dynamic mechanical analysis.

Next, the impact of radical-disulfide exchange that arises from different thiol/disulfide pairs was investigated. Two divinyl ether monomers with different disulfide cores were polymerized with three multifunctional monomers yielding thiyl radicals of varied stabilities. This experimental approach enables determination of how the disulfide impacts radical-disulfide exchange during thiol-ene and subsequent

disulfide-ene polymerization, and how varying the relative thiyl radical stability of specific thiol/disulfide pairs affects disulfide exchange during polymerization.

4.3 Materials and Methods

Materials: Pentaerythritol tetrakis(3-mercaptopropionate) (PETMP), diphenyl(2,4,6-trimethylbenzoyl) phosphine oxide (TPO), 2,2-dimethoxy-2-phenylacetophenone (DMPA), tri(ethylene glycol) divinyl ether (TEG), and butyl vinyl ether (BVE) were all purchased from general suppliers (Sigma Aldrich) and used as delivered. Dithioglycolate divinyl ether (DTG), di(3-mercaptoprionate) divinyl ether (DMP), pentaerythritol tetrakis(2-mercaptoacetate) (PETTG), and silane tetrathiol (SiTSH) were synthesized according to previous literature[17, 18].

Dynamic Mechanical Analysis (DMA): Dynamic mechanical analysis was performed on an RSA-G2 (TA Instruments). Samples of approximate dimensions 20mm x 5mm x 0.25mm were cut, and measurements were taken using a temperature ramp rate of 3 °C/min at frequency of 1 Hz to measure the storage modulus, loss modulus, and tan(δ). The glass transition temperature (T_g) was taken to be the peak of the tan(δ) during the second temperature sweep.

DMA Stress Relaxation (SR): Stress relaxation was performed on a RSA-G2 (TA Instruments). Samples of approximate dimensions 20mm x 5mm x 0.25mm (LxWxH) were cut, and an 8% strain was applied while measuring the relaxation modulus. Samples were irradiated using a mercury-lamp (Acticure 4000) with a 400-500 nm or a 365 nm band gap filter to trigger the appropriate photoinitiator for the specific stress relaxation experiment.

Fourier Transform Infrared (FT-IR) Spectroscopy: Functional group conversion during two stage polymerizations was monitored using a FTIR spectrometer (Nicolet 8700) to monitor real-time functional group conversions. Monomer resin was placed between two NaCl plates and placed into a horizontal transmission apparatus. Samples were irradiated using a mercury-lamp (Acticure 4000) with a 400-500 nm band gap filter to initiate the polymerization. The light intensity was measured by an THORLABS PM100D

radiometer. Conversion of the alkene and thiol were measured by monitoring the peak area at 3100-3135 cm^{-1} and 2520-2620 cm^{-1}, respectively. Conversion was also monitored for associated stress relaxation experiments using the ATR configuration for this spectrometer, and the alkene peak at 860 cm^{-1} was monitored to determine the cure time needed to reach a plateau in alkene conversion.

4.4 Results and Discussion

4.4.1 Radical-mediated Stress Relaxation

The structures of the monomers used in this study are provided in **Figure 4.4**. The disulfide monomer, DTG, was chosen because of the relatively high reaction rates of its disulfide with vinyl ethers[14]. In addition, DTG can be effectively copolymerized with PETMP, which is a widely used and commercially available multifunctional thiol.

Previously, the dynamic behavior of thioglycolate disulfides in bulk films has been inferred based on the known behavior of disulfides when radicals are present. To study exchange with this specific disulfide directly, networks were designed such that a large number of disulfides remain to undergo bond exchange post polymerization at complete thiol and alkene conversion. Three stoichiometries were selected that vary both the amount of disulfide present and the overall structure of the network: 0.9:1, 1:1, and 1.1:1 ratios of thiol to alkene were studied.
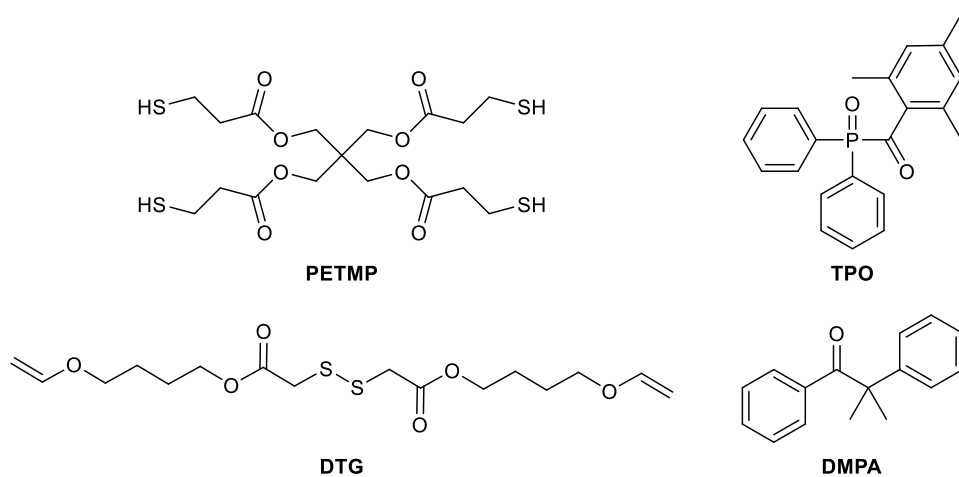
Figure 4.4: Monomers (PETMP and DTG) and photoinitiators (TPO and DMPA) used to study stress relaxation in thiol-ene disulfide networks. TPO is initiated by visible light at 405 nm and DMPA is initiated by UV light at 365 nm.

The 0.9:1 ratio was selected such that 10% of the disulfides would be consumed after the thiol-ene stage of the polymerization resulting in complete vinyl conversions. This network is the most crosslinked of the three stoichiometries due to the formation of additional crosslinks via the disulfide-ene reaction, and therefore leaving the fewest disulfide bonds available for exchange. The 1:1 ratio was chosen such that essentially all of the vinyl groups are consumed by all of the thiols with little disulfide-ene reaction. The resulting network has the maximum possible number of disulfides available for exchange but is slightly less crosslinked than the 0.9:1 stoichiometry. Lastly, the 1.1:1 ratio was selected such that 10% of the thiols remain unreacted at complete vinyl conversion. This network is the least crosslinked and the unreacted thiols can participate in the exchange process. It should be noted that the structural and compositional changes of the final networks cannot be modulated independently because the initial ratio of alkene-to-disulfide is fixed at 2:1 by the disulfide monomer structure.

Each stoichiometry was cured using 1.5 wt% TPO photoinitiator using 405 nm light at an intensity of 20 mW/cm^2 for 10 minutes (5 minutes on each side of a 250 μm sample). In addition, 3.5 wt% DMPA was included as a UV photoinitiator to induce stress relaxation post-polymerization. Each formulation was cured using FT-IR to monitor and confirm the thiol and vinyl ether conversion which were found to match well the theoretical values. Dynamic mechanical analysis (DMA) was also performed on each formulation (**Figure 4.5a**). As expected, there was a small decrease in the glass transition temperature (T_g) as the ratio of thiol to alkene increased, where the 0.9:1, 1:1, and 1.1:1 networks had T_g's of -27°C, -29°C, and -31°C, respectively. Likewise, a small decrease in the rubbery storage modulus was observed, showing a small but measurable decrease in crosslinking as the thiol content is increased.

Stress relaxation was performed on samples at each of these stoichiometries to demonstrate bond exchange as well as its dependence on the network composition. Rectangular samples (n = 3) were subjected to 8% strain for 30 seconds, then a 365 nm light of 30 mW/cm^2 was turned on for 10 minutes to induce stress relaxation (**Figure 4.5b**). Overall, both the rate and total amount of relaxation increased with increasing thiol-content in the initial resin, where the 0.9:1 thiol to alkene ratio relaxed the most slowly and
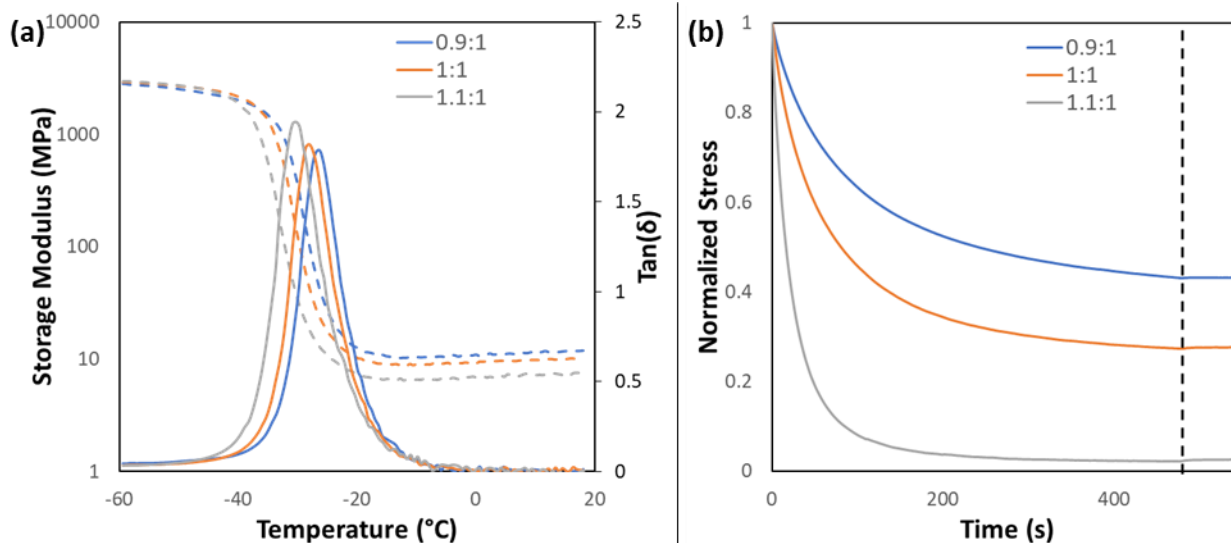
Figure 4.5: a) Dynamic mechanical analysis of the 0.9:1, 1:1, and 1.1:1 stoichiometry networks. The tan(δ) is shown as a solid line and the storage modulus is shown as a dashed line for each formation, and b) the normalized stress over time, for 0.9:1, 1:1, and 1:1 ratios of thiol to alkene with 3.5wt% DMPA as a UV photoinitiator at 15 mW/cm2. The vertical dashed line indicates the time at which the light was turned off during the experiment.

reached a final normalized stress of 43 ± 5%, followed by the 1:1 ratio which reached 27 ± 2%, then the 1.1:1 ratio which reached nearly 100% relaxation, likely near the sensitivity level of the instrument (2.5 ± 0.6%). The final normalized stress was taken after the light was turned off and the sample was allowed to equilibrate to room temperature, but no cooling effect was observed at this light intensity.

The increase in relaxation with relative thiol content of the initial resin is likely due to both the decrease in crosslinking and the increase in the content of functional groups that can participate in bond exchange. The relative contributions of crosslinking and functional group content are likely different for the increase in stress relaxation for the 0.9:1 to the 1:1 formulations, which showed an increase of 16% total relaxation, relative to the increase when comparing the 1:1 to the 1.1:1 formulations, which showed a larger increase of 25% total relaxation.

First, the structural changes for each pair of formulations were considered. In the disulfide-ene reaction, two bonds are formed for each disulfide bond that is broken. For the 0.9:1 ratio, in which the preferred reactive thiol group is limited, 10% of the alkenes necessarily react with disulfides to form additional crosslinks. Compared to the case where all of the alkenes react with thiols, this approach results in a net gain of one bond per reacted disulfide that contributes to the overall crosslinking density. For the

1:1 stoichiometry all of the unreacted functional groups, namely the disulfides, still contribute to the overall crosslinking of the network. Conversely, the 10% unreacted thiols for the 1.1:1 network don't contribute to crosslinking and instead are dangling chain ends.

Next, the role of the reactive functional groups that are present in each formulation was considered. The number of disulfides available for stress relaxation increases for the 1:1 compared to the 0.9:1 ratio because all of the disulfides are available in the 1:1 formulation but not the 0.9:1 formulation. However, every disulfide is available in both the 1:1 and 1.1:1 formulations, but 10% of thiols are unreacted for the 1.1:1 formulation and may also participate directly in thiol-disulfide exchange. Thiyl radicals should form more readily from a thiol than a disulfide due to reduced steric hinderance associated with abstracting a hydrogen compared to that same initiator fragment reacting with a disulfide bond. In addition, free thiols may also facilitate reaction-diffusion by which the thiyl radicals diffuse through the network through repeated hydrogen transfer reactions between thiols. Therefore, the effect of free thiols is likely to have a greater impact on stress relaxation than increasing the number of disulfides available for bond exchange, all else being equal. The relative importance of these structural and chemical effects is further explored later in this work.

Overall, thioglycolate disulfides effectively induce stress relaxation. The rate of relaxation can be easily manipulated by small changes in the initial stoichiometry, likely due to some combination of changes in crosslinking density and whether free thiols are present to participate in the exchange reaction.

4.4.2 Exchange During Disulfide-ene Polymerization

An important feature of this polymerization scheme is that radical-disulfide exchange is active throughout both stages of the polymerization. It is well documented that polymerizations in the presence of allyl sulfides or trithiocarbonates reduce the buildup of polymerization stress through addition-fragmentation, which is a similar radical-mediated mechanism to radical-disulfide exchange[19-21]. The impact of disulfide exchange during this polymerization is distinct for two reasons. First, the disulfides are direct participants in both the second phase of the polymerization and the exchange process itself rather

than serving as an additive designed to induce bond exchange. Second, the disulfide-ene reaction is far slower than the thiol-ene reaction, so the polymerization rate may have an outsized impact on the final polymerization stress due to the rapid radical-disulfide exchange rate.

To examine the stress buildup during the second stage of the polymerization, PETMP and DTG were used in a 0.5:1 ratio of thiol to alkene, such that 100% conversion of all functional groups is possible. A 250 µm film was cured using 3 wt% TPO at 14 mW/cm^2 for approximately 40 seconds such that the film was cured just enough to consume all thiols. Approximately 50% of the alkenes were reacted. A single photoinitiator, TPO, was used to better reflect the initiator concentration in a sample that is continuously cured to full conversion. All samples were cut from this single film to ensure that the initial vinyl ether conversion was consistent across all samples at each wavelength. Infrared spectroscopy (ATR configuration) was used to first compare the "relative conversion" over time for 5, 15, 30, and 100 mW/cm^2 light intensities (**Figure 4.6a**).

"Zero conversion" for this data corresponds to the alkene conversion achieved after the first stage thiol-ene polymerization. At each intensity, the sample was irradiated until the conversion had largely
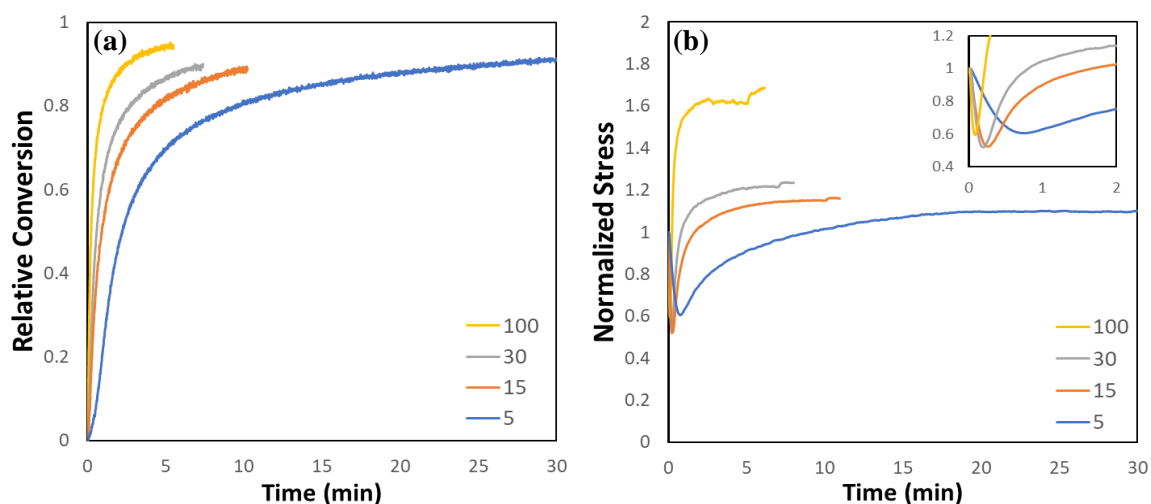
Figure 4.6: For PETMP-DTG with a 0.5:1 ratio of thiol to alkene, , a) relative conversion of alkene over time at various light intensities (mW/cm2), where zero conversion corresponds to the initial conversion reached after the first stage thiol-ene reaction, and b) the normalized stress during the disulfide-ene polymerization for samples cured through the disulfide-ene reaction at various light intensities (mW/cm2). The inset highlights the initial drop instress for each light intensity. Samples were first cured using 14 mW/cm2 405 nm light until the film was just cured enough to cut and handle

plateaued due to consumption of the disulfides and/or photoinitiator to provide a baseline to compare the final stress between intensities. The irradiation times established during FTIR experiments were subsequently used to measure stress during polymerization on samples of identical thickness. Samples at all four light intensities (5, 15, 30, and 100 mW/cm^2) reach relative conversions of approximately 90% after reacting for 30 min, 10 min, 7 min, and 5 min, respectively. In reality, 90% relative conversion corresponds to around 95% total alkene conversion because at least 50% of the alkenes were consumed during the thiol-ene stage of the polymerization. The highest light intensity, 100 mW/cm^2, reached the highest conversion overall due to the rapid polymerization rate at high light intensity.

To test the buildup of stress during the disulfide-ene step of the polymerization, samples cured through the thiol-ene stage were subjected to a constant 8% strain and irradiated at 5, 15, 30, or 100 mW/cm^2 for 30, 10, 7, or 5 min, respectively (**Figure 4.6b**). The results are summarized in **Table 4.1**.

Table 4.1: Summarized values for the irradiation time, minimum stress, and maximum stress during stress relaxation experiments

Intensity (mW/cm2)	Irradiation time (min)	Stress Min (% of initial stress)	Final Stress (% of initial Stress)
5	30	63 ± 3	107 ± 4
15	10	57 ± 4	110 ± 10
30	7	56 ± 3	130 ± 30
100	5	58 ± 4	180 ± 40

After the light was turned on, the normalized stress initially decreased, reached a minimum, then increased as the polymerization continued, reaching a plateau as the functional groups and photoinitiator were consumed. Initially, any buildup of stress due to polymerization was offset by disulfide cleavage and exchange to reduce the stress below the initially applied stress. However, as the reaction proceeded, the disulfides converted to thioacetals and the rate of shrinkage stress development outpaced the rate at which disulfide exchange could relax that stress, leading to final stresses above the applied stress in this experiment regardless of light intensity.

The minimum stress decreased only slightly as the light intensity increased and was statistically indistinguishable between the 15, 30, and 100 mW/cm^2, as highlighted in the inset of **Figure 4.6b**. This

behavior is only possible in a dynamic system because additional post-gelation polymerization in a non-dynamic network would be expected to generate significant additional stress. This behavior is advantageous for generating low-stress dual-cure materials because of the delay in gelation associated with step growth polymers and reduction in stress buildup during this stage of the polymerization due to disulfide exchange.

An increase in the final stress as light intensity increased was also observed. There was also a clear heating effect after the light was turned off that became more significant at higher light intensities. The increase in the final stress is due to more rapid consumption of the disulfides as the light intensity was increased, essentially decreasing the number of disulfide exchange events that occur before they are consumed by polymerization. This behavior is distinct from what is observed in typical addition-fragmentation systems, in which the dynamic functional group is not consumed as part of the desired polymerization (although they are subject to irreversible side reactions that may contribute to additional crosslinking). As previously mentioned, this final stress is expected to be far lower than for a comparable network structure without the capacity for bond-exchange, as evidenced by the initial decrease in stress due to bond exchange and the persistence of bond exchange throughout the polymerization.

To determine whether the difference in second stage light intensity has any impact on final network properties, DMA was performed on samples cured at all four light intensities, where 250 µm samples were irradiated for the same amount of time as the stress measurements, and each side of the sample was irradiated for half of that time. Only a small difference in the T_g was observed of 1-2 °C with virtually no difference in the storage modulus after two cycles run to 40 °C, indicating that the final network properties are largely unaffected by the rate of the second stage polymerization.

Overall, disulfide exchange during the disulfide-ene stage of the polymerization significantly reduced the polymerization stress. A non-dynamic network under the conditions tested here must experience an increase in the internal stress during polymerization. However, disulfide exchange initially reduces the stress until the disulfides are consumed an incorporated into the network faster than they can relax polymerization stress.

4.4.3 Effect of Thiol and Disulfide Type on Exchange

Radical-disulfide exchange is intrinsic to both the thiol-ene and disulfide-ene stages of the polymerization. When PETMP and DTG are polymerized, this exchange process has been shown to slow the thiol-ene step compared to the case where no disulfides are present in small molecule studies. This effect is exacerbated when the thiyl radical formed from hydrogen abstraction of the thiol is more stable than the radical formed by cleaving the disulfide[22]. It is hypothesized that the different thiol/disulfide pairs will impact the rates of both polymerization stages depending on the relative stability of the thiyl radicals that form the thiol and the disulfide.

Three monomers were synthesized to test the effect of relative radical stability. First, DMP was synthesized, containing a 3-mercaptopropionate disulfide core. The overall monomer structure is identical to DTG, except the disulfide is based on 3-mercpatopropionate rather than thioglycolate. In addition, two multifunctional thiol monomers were synthesized to vary the stability of the thiyl radicals: PETTG as the thioglycolate analogue of PETMP, and SiTSH which contains alkyl thiols. All five monomers are illustrated in **Figure 4.7a**. These two disulfides and three thiols enable a more thorough study of how disulfide exchange influences the polymerization. Specifically, measuring the conversion over time for each disulfide/thiol pair will elucidate whether disulfide exchange effects the thiol-ene polymerization under three different conditions: (1) when the radical formed by the thiol and disulfide are the same and therefore exchange cannot result in the formation of a different thiyl radical; (2) when the radical derived from the thiol is more stable than the disulfide radical and therefore little/no change in the type of thiyl radical present during thiol-ene should occur, and (3) when the disulfide radical is more stable than the thiol-derived radical and therefore asymmetric disulfides can form during the thiol-ene step, which may impact the rate of polymerization during the disulfide-ene step.

The relative stability of the thiyl radicals that form is shown in **Figure 4.7b**. The thioglycolate radical, formed from PETTG and DTG, is the most electron poor due to its proximity to the carbonyl carbon and is therefore the least stable. The next more stable is the mercaptopropionate radical, formed from
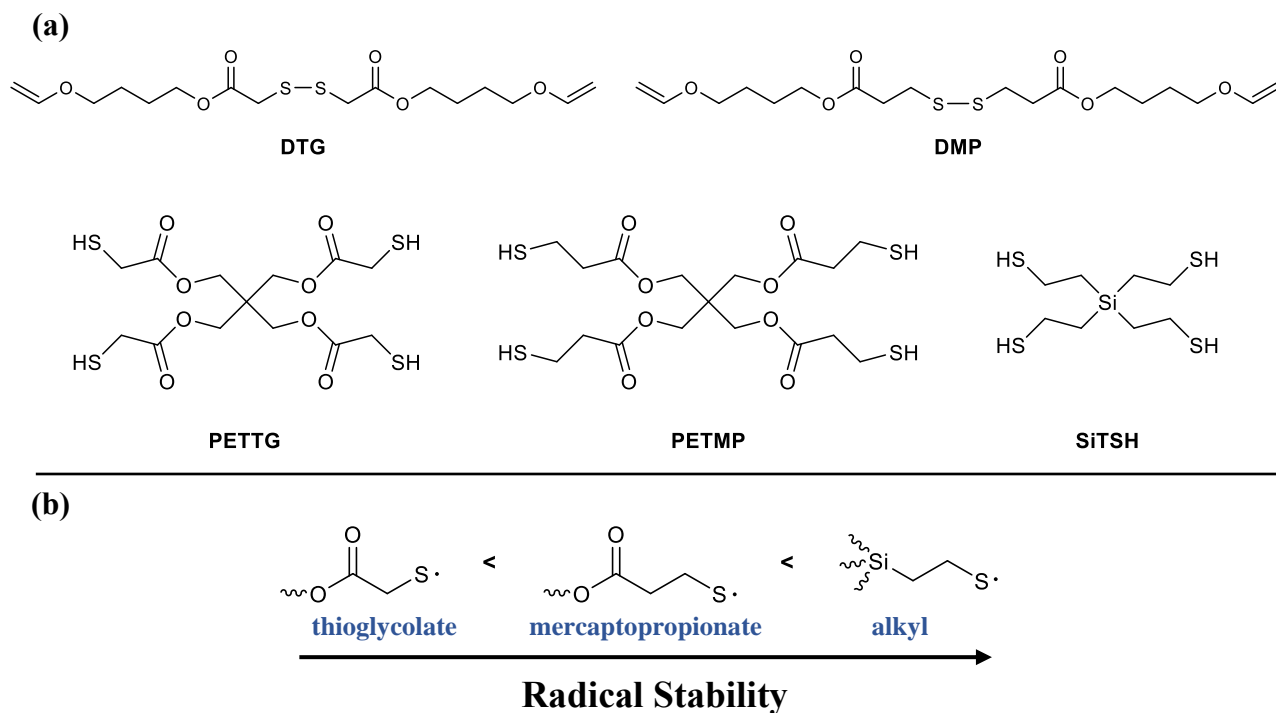
Figure 4.7: a) Monomers used to study the impact of different kinds of thiols and disulfides on thiol-ene-disulfide materials, and b) The stability of the thiyl radical derived from PETMA, PETMP, and SiTSH, respectively, going from left to right.

PETMP and DMP, because this radical is slightly more electron rich due to the extra carbon spacer between the sulfur and the carbonyl carbon. The radicals formed by SiTSH are the most electron rich because there is no electron withdrawing group making this the most stable of the three radicals that form using this monomer scope. However, the relative stability of these radicals does not necessarily correlate with thiol-ene reaction rate because although increasing thiyl radical stability may tend to increase the chain transfer rate, increased thiyl radical stability will also tend to slow down the propagation step. Given that chain transfer is only mildly rate limiting for mercaptopropionates with vinyl ethers ($k_p/k_{ct} \approx 1.2$), changing the thiol to a thioglycolate or an alkyl thiol may also change the rate limiting step, which may in turn impact how disulfide exchange influences different thiol/disulfide pairs.

To the best of our knowledge, the rate limiting step has not been established for these two thiols with vinyl ethers. As such, a kinetic analysis using FTIR was performed to determine the rate limiting step for each of these monomers with tri(ethylene glycol) divinyl ether (TEG) at three ratios of thiol to alkene:

2:1, 1:1 and 1:2. The conversion over time for the limiting reactant for each stoichiometry as well as a more thorough explanation of the procedure adapted from Cramer et al.[23] and the summary of the polymerization rate behavior is provided in **Table 4.2**. The rate limiting step for PETMP was chain transfer as previously reported[23], and the rate limiting step for both PETTG and SiTSH was propagation.

Table 4.2: For three different thiol to alkene stoichiometries, the rate of consumption of the limiting reactant for various thiol monomers, and which step, i.e., either chain transfer or propagation, is the rate limiting step. Samples were polymerized at 0.1 wt% TPO with 405 nm light at 5 mW/cm2.

Thiol-Alkene Ratio	Rate (mM/s)		
	PETMP	PETTG	SiTSH
2-1	180 ± 30	80 ± 10	13 ± 4
1-1	180 ± 10	90 ± 20	55 ± 8
1-2	109 ± 4	130 ± 20	56 ± 6
Rate Limiting step	CT	Prop	Prop

All six possible pairs of thiol/disulfide monomers were polymerized and their conversion over time measured using FTIR. Polymerization mixtures were prepared with 1.5 mol% TPO (relative to monomer present) and a 0.5:1 ratio of thiol to alkene, such that at full conversion 50% of the alkenes are consumed by the thiols and the other 50% by the disulfides. Samples were irradiated with 405 nm light at 10 mW/cm^2 for 5 minutes.

The conversion over time is shown in **Figure 4.8**, comparing the reaction rate when polymerized with either DTG or DMP for all three thiol monomers. The first feature to note is that for all three thiols the disulfide-ene rate for both disulfides is roughly the same, reaching approximately the same final conversion after 5 minutes. This outcome differs from the small molecule studies performed by Kamps et al., where the mercaptopropionate disulfide reacted approximately 10 times slower than the thioglycolate disulfide[14]. Nevertheless, the fact that the disulfide-ene rate with DMP is comparable to DTG indicates that the scope of linear disulfides that can be effectively copolymerized with thiols is not limited by their reaction rates in model reactions. In addition, the relative rate of thiol-ene polymerization for each thiol monomer aligns with the relative rates observed in the control thiol-ene reactions at the same 1:2 ratio of thiol to alkene as found in **Table 2**: PETTG was the fastest, then PETMP, then SiTSH.

As mentioned previously, significant retardation of the thiol-ene reaction has been observed with PETMP and DTG. This outcome was attributed to disulfide exchange during which the mercaptopropionate radical may add into the dithioglycolate disulfide, which then fragments preferentially to reform the same disulfide and thiyl radical. This effectively sequesters propagating radicals in a similar manner observed for additional fragmentation reactions of allyl sulfides and trithiocarbonates[24]. It was therefore hypothesized that with PETMP the thiol-ene step would be faster with DMP because both monomers would produce the same thiyl radical and reduce the slowing effect on the reaction.

Indeed, this trend was observed as shown in **Figure 4.8a**, where the alkene conversion reaches approximately 50% after a few seconds with DMP, but after 30 seconds with DTG. The initial 50% alkene
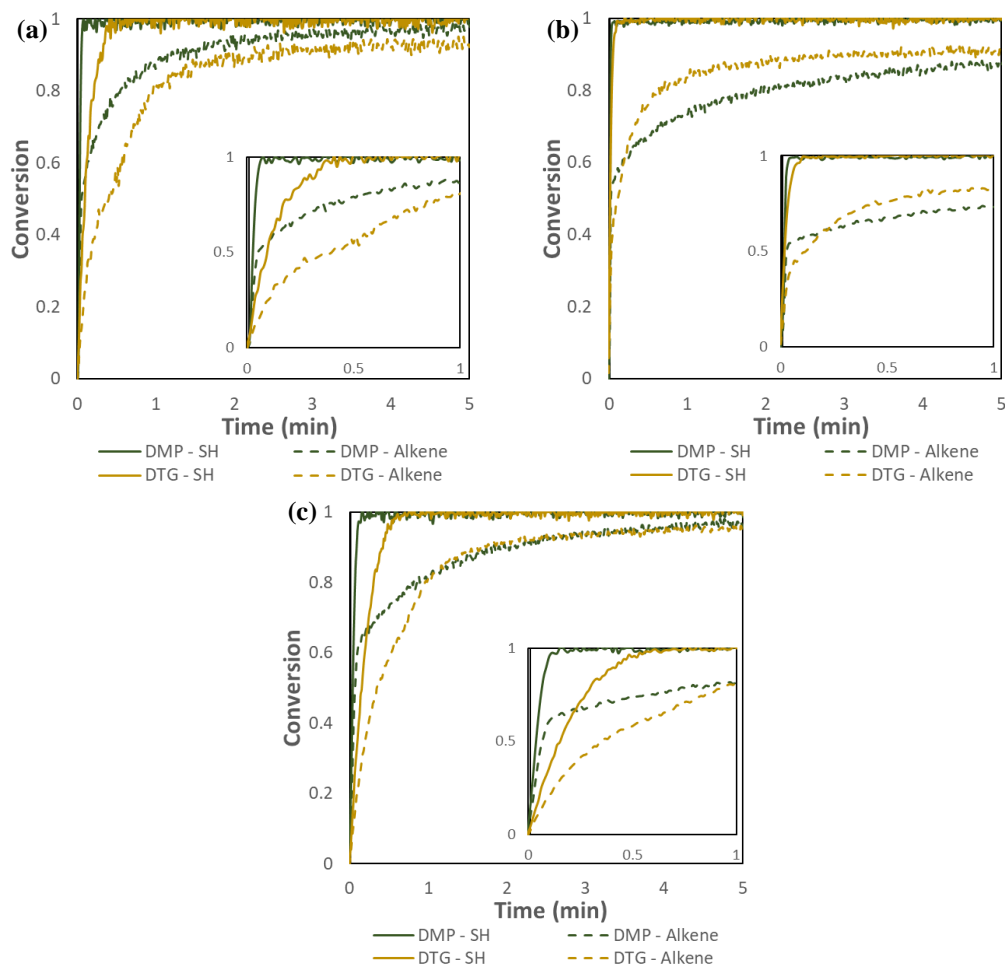
Figure 4.8: Thiol and vinyl conversion over time for the two disulfide-containing divinyl ether monomers copolymerized with thiols of different thiyl radical stability: a) PETMP, b) PETTG, and c) SiTSH. The insets show the first minute of the polymerization for each thiol to emphasize the difference in the thiol-ene rate for each thiol-disulfide pair.

conversion is almost completely attributed to the thiol-ene reaction because this conversion corresponds to complete consumption of the thiol. This is good evidence that the specific thiol/disulfide pair and the associated radical-disulfide exchange play important roles in the thiol-ene stage of the polymerization.

To test the importance of the thiol/disulfide pair further, PETTG (the thioglycolate analogue of PETMP) was copolymerized with both DMP and DTG (**Figure 4.8b**). In this case, the rates of thiol-ene are similar for both disulfides compared to the same polymerization with PETMP. However, the disulfide-ene rate with DMP is slower than with DTG. This difference is attributed to the varying thiyl radical stability for PETTG as compared to PETMP. It was hypothesized that because the thioglycolate radical is less stable, exchange events with DMP will preferentially fragment into a mercaptopropionate radical and an asymmetric disulfide. There is no such bias with PETMP to form asymmetric disulfides because the thiol itself forms the more stable radicals. This process does not result in a slower thiol-ene rate because mercaptopropionates are in fact more reactive in thiol-ene reactions than thioglycolates. However, the additional complexity of the resulting asymmetric disulfides would result in a slower disulfide-ene step compared to when DTG is used. This mechanism explains the relative polymerization rates for both PETMP and PETTG.

Lastly, SiTSH was used to probe this effect further. SiTSH forms the most stable radical of the three thiols investigated here and would therefore experience a reduced rate of thiol-ene with both disulfide monomers compared to the cases where the thiol and disulfide monomers match. Indeed, this is the case as shown in **Figure 8c**. The thiol-ene reaction is slower with DTG than for DMP, reaching 50% alkene conversion after about 25 and 4 seconds, respectively. Subsequently, the disulfide-ene step from both disulfide monomers reaches the same conversion after 5 minutes.

It should be noted that there was little difference in the material properties using these three thiols. DMA temperature sweeps of networks with PETMP, PETTG, and SiTSH copolymerized with DMP were performed and the T_g and storage moduli of all three networks were nearly identical. Using SiTSH was expected to increase the T_g compared to the other two monomers due to the shorter chains between

crosslinks, which has been observed previously in thiol-ene networks[18, 25]. The fact that SiTSH did not increase the T_g indicates that the T_g in these thiol-ene-disulfide networks is largely driven by the disulfide-ene step of the polymerization. This result is reasonable because the disulfide-ene results in twice as many bonds formed compared to thiol-ene, and the molecular weight between crosslinks of the disulfide-ene step is largely unaffected by the identity of the multifunctional thiol monomer, provided that the number of thiols-per-monomer is the same. In fact, the rate of the thiol-ene step may be independent of the material properties of the final polymer when a significant number of crosslinks are formed by the disulfide-ene step, enabling tunability of the dual-cure rate for applications in optical materials and other fields by simply changing the thiol/disulfide pair. Alternative disulfide monomer structures may also be used to further tune the T_g and dynamic moduli.

Overall, the thiol-ene-disulfide reaction proceeds quite well with all three thiols, with the only exception being PETTG with DMP during the disulfide-ene stage because of the formation of asymmetric thiols. Furthermore, using DMP instead of DTG resulted in a faster thiol-ene polymerization with all three monomers, regardless of the rate limiting step of the thiol-ene reaction. Further investigation is needed to determine if other linear disulfide cores, such as purely alkyl or sulfonate ester disulfides, are also viable in this overall reaction scheme.

4.4.4 Impact of Structure and Functional Groups on Stress Relaxation

Decoupling the impact of network structure and chemical functionality on stress relaxation is crucial to understand and tune the relaxation rates in these dynamic networks. For example, it was shown in **Figure 4.5b** that stoichiometries with excess thiol significantly decrease the relaxation time as compared to a balanced ratio of thiol to alkene and when alkene is in excess and can react with a portion of the disulfides.

To probe the relative effect of the structural impact of changing stoichiometry versus the chemical impact of having excess thiols present to participate in bond exchange, a series of control stress relaxation experiments was performed on networks with excess thiol (1.1:1 ratio of thiol to alkene) and DTG as the

disulfide monomer. First, 10 mol% butyl vinyl ether (BVE) was included to react with the excess thiols without changing the connectivity of the network, isolating the impact of the excess thiols on radical-disulfide exchange independent of the overall structure of the network. Second, controls were performed with PETTG instead of PETMP, both with and without 10 mol% BVE, to determine whether the type of thiol, specifically whether the mismatch between the mercaptopropionate radical associated with PETMP and the thioglycolate radical associated with DTG, impacts the rate of relaxation.

The DMA traces for these networks are shown in **Figure 4.9a.** Each network was initially cured with 1 wt% TPO and 405 nm light at 20 mW/cm^2 for 5 minutes on each side. For stress relaxation, 3.5 wt% DMPA was used with 365 nm light at 15 mW/cm^2 and 8 % strain. The PETMP networks with or without BVE have similar glass transition temperatures (within a degree or so), storage moduli, and molecular weight between crosslinks (1040 g/mol and 950 g/mol, respectively). The same is true for the PETTG networks with and without BVE (760 g/mol and 770 g/mol, respectively). These results indicate that BVE
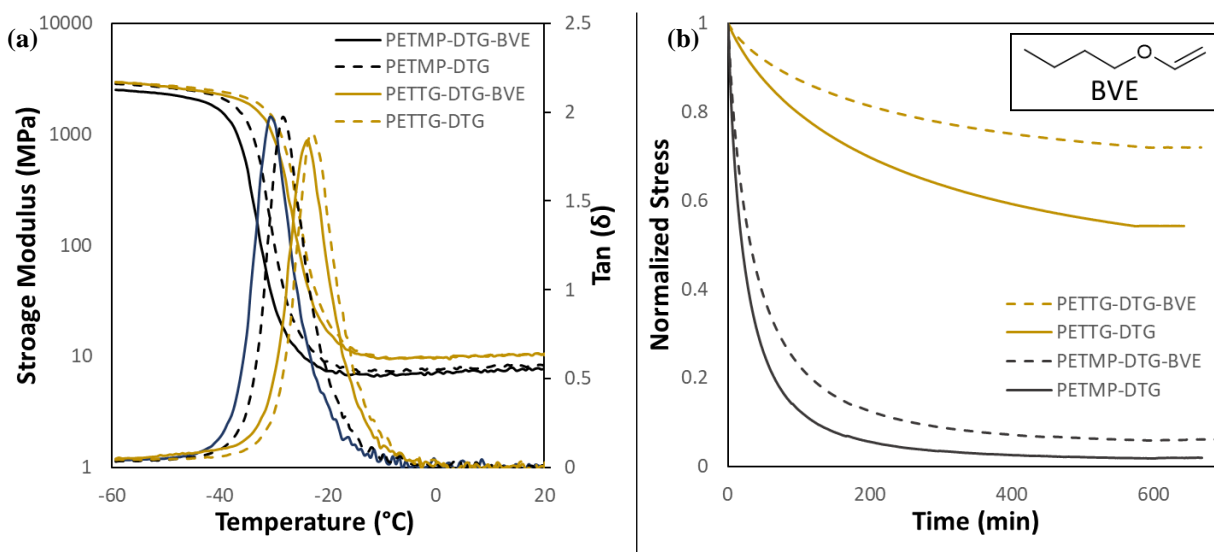
Figure 4.9: a) DMA trace and b) stress relaxation of each network, with butyl vinyl ether included in the top right. Each network was made with a 1.1:1 ratio of thiol to alkene and was cured into a 250 µm films with 1 wt% TPO irradiated with 405 nm light at 20 mW/cm2 for 5 minutes on each side. Stress relaxation was done with 3.5 wt% DMPA and 365 nm light at 15 mW/cm2 for 10 minutes at 8% strain.

did not significantly impact the network structure for either thiol monomer, but the shorter chain length associated with PETTG compared to PETMP does increase the T$_g$ and rubbery storage modulus. v

Stress relaxation behavior for these four networks is shown in **Figure 4.9b**. As expected, reacting the excess thiols with BVE resulted in slower stress relaxation compared to when free thiols were present for both thiol monomers, but this effect was more pronounced for PETTG than PETMP. This result is not surprising because kinetic analysis indicates that little productive bond exchange occurs between mercaptopropionate radicals and thioglycolate disulfides[14], meaning excess thiols should impact relaxation more for PETTG than PETMP. Interestingly, the PETMP networks relaxed stress far more rapidly than PETTG both with and without BVE though they only differ in their molecular weight between crosslinks. This indicates that while both structure and presence of reactive groups play a role in the rate of stress relaxation, the network structure also has a significant impact on the stress relaxation rate.

4.4.5 Stress Relaxation with DMP

After demonstrating the viability of DMP in thiol-ene-disulfide polymerizations, the performance of the mercaptopropionate and thioglycolate disulfides was compared in stress relaxation experiments. Two of the stoichiometries tested before, namely 0.9:1 and 1.1:1 ratios of thiol to alkene, were used to determine the exchange characteristics with and without the excess thiol. The DMP films relaxed extremely rapidly compared to films made with DTG for both stoichiometries (**Figure 4.10**). For the 0.9:1 ratio, the DTG network is two orders of magnitude slower, only reaching about 50% relaxation in 10 minutes while the DMP network achieved 50% relaxation in about 5 seconds and 100% relaxation in 1.5 minutes. The difference is less stark in systems with abundant thiols, for which DTG reached nearly complete relaxation after 10 minutes compared to 1 minute with DMP. This difference of only one order of magnitude is likely because an excess of thiol will impact the slower exchange associated with the thioglycolate disulfide more than the already rapid exchange for the mercaptopropionate disulfide.

In addition, there was only a small difference in relaxation rate between the two networks with DMP with or without thiols to participate in exchange, which again is likely because the exchange rate of this disulfide is already quite fast and therefore is not substantially enhanced by an excess of thiol. These

rapid exchange kinetics with DMP indicate that networks with far more crosslinking and fewer unreacted

disulfides are possible while maintaining fast stress relaxation capability.
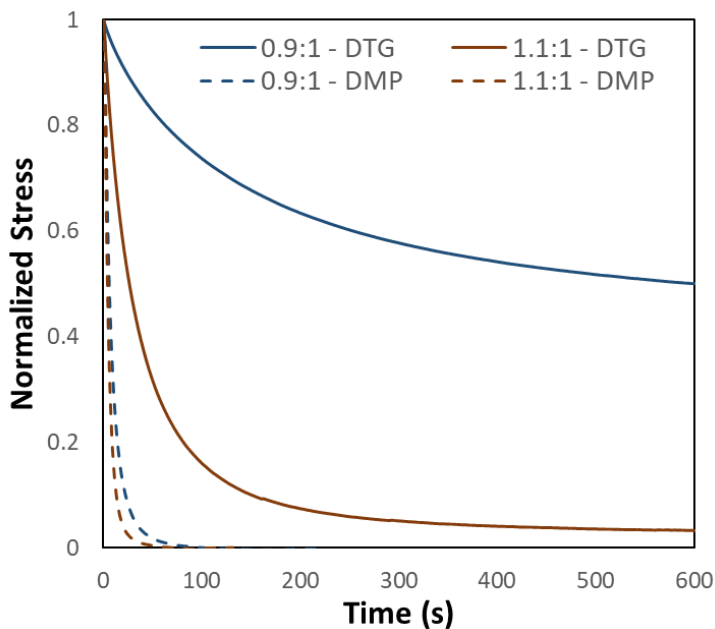
Figure 4.10: The normalized stress over time for for DTG (solid) and DMP (dashed) at two ratios of thiol to alkene. Samples were prepared with 3.5 wt% DMPA, stretch to 8% strain, and exposed to 15 mW/cm2 365 nm light.

The fact that DMP shows much faster radical-disulfide exchange also has important implications

for stress development during polymerization because faster exchange should result in lower volumetric

shrinkage stress compared to DTG. To investigate any difference in stress development during

polymerization, samples with a 0.5:1 ratio of thiol to alkene were prepared with PETMP, either DMP or

DTG, and cured with 3 wt% TPO under 14 mW/cm^2 irradiation at 405 nm to the point where the thiol-ene

reaction was complete and the samples were sufficiently polymerized to maintain integrity, i.e., 12 seconds

and 40 seconds, respectively. It should be noted that the alkene conversion between these two samples is

not coincident as these two networks experience different polymerization rates for the thiol-ene step, but in

both cases very little disulfide-ene reaction occurs before appreciable amounts of disulfide react under these

conditions. In addition, nearly all the stress that develops during polymerization should occur during the

disulfide-ene step because gelation would occur at the later stages of the thiol-ene step.

Vinyl conversion over time was measured using FTIR in an ATR configuration for the disulfide-ene reaction, and was initiated using 5, 30, or 100 mW/cm² light intensity for 305 nm light (**Figure 4.11a**).
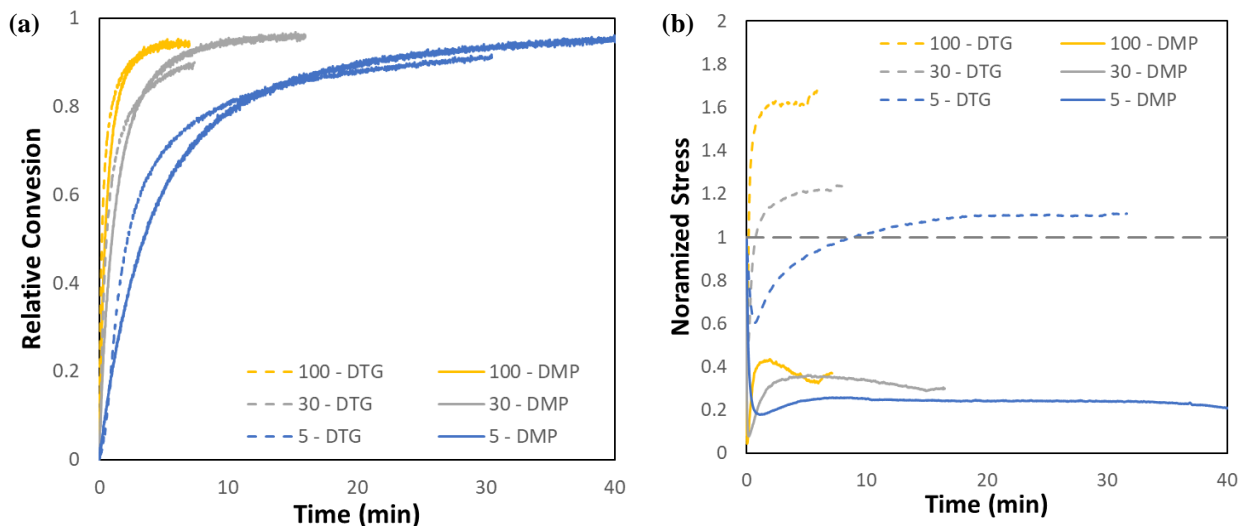
Figure 4.11: For samples of PETMP with either DTG (dashed) or DMP (solid) with a 0.5:1 ratio of thiol to alkene, ., a) relative conversion of alkene over time during the disulfide-ene polymerization at various light intensities (mW/cm2), where zero conversion corresponds to the initial conversion reached after the first stage thiol-ene reaction, and b) the normalized stress during the disulfide-ene polymerization for samples cured through the disulfide-ene reaction at various light intensities (mW/cm2). Samples were first cured using 14 mW/cm2 405 nm light until the film was just cured enough to cut and handle

The ATR configuration was used so variables such as sample thickness, and therefore light attenuation, would be identical between FTIR and stress realxation experiments. Although the polymerization rate is slightly slower for DMP compared to DTG, both networks reach similar conversions over comparable time scales at a given light intensity. Photocured samples were then subjected to 8% strain and irradiated for the same durations as determined by ATR time-conversion analysis. The stress over time was measured, shown in **Figure 4.11b**, and the results comparing the two disulfide monomers are summarized in **Table 4.3**.

For all three light intensities, DMP both reached a lower minimum stress and a lower final stress despite reaching similar or higher alkene conversion compared to DTG. As seen previously, there is an initial drop in the stress as disulfide exchange relaxes the applied stress, followed by an increase in stress as disulfides convert to thioacetals and shrinkage stress develops. However, DMP proves to be far more

Table 4.3: Summarized values for the irradiation time, minimum stress, and maximum stress during stress relaxation experiment for DMP and DTG.

Intensity (mW/cm^2)	Disulfide Monomer	Irradiation time (min)	Stress Min (% of initial stress)	Final Stress (% of initial Stress)
5	DTG	30	63 ± 3	107 ± 4
	DMP	40	13 ± 6	18 ± 8
30	DTG	7	56 ± 3	130 ± 30
	DMP	15	6 ± 3	28 ± 6
100	DTG	5	58 ± 4	180 ± 40
	DMP	6	5.0 ± .7	37 ± 1

effective at reducing stress buildup at all three light intensities. Using 5 mW/cm^2 as an example, the stress is reduced to about 13% of the initial value but remains well below the initial stress, plateauing at about 18% strain by the end of the experiment. This value is far lower than for DTG, where the initial stress only decreases to a minimum of 63% of the initial stress, but ultimately polymerization results in final stresses that are greater than the applied stress. The ultimate stress increases with light intensity for both disulfide monomers, though the final stress is far below the applied stress for DMP, while the final stress nearly doubles for DTG. This result agrees with the stress relaxation observed in **Figure 4.10**, showing that the rate of radical-disulfide exchange is faster for the mercaptopropionate-based disulfide compared to the thioglycolate-based disulfide.

Overall, thiol-ene-disulfide networks with either DTG or DMP were capable of realxation stresses both during polymerization and stress relaxation. But under identical curing and stress realxation conditions, the mercaptopropionate disulfide relaxed stress significantly faster than those based on thioglycolates. The effects of this polymerixation scheme and the impact of different disuflide cores with respect to polymerization shrinkage and shrinkage stress should be investigated further.

4.5 Conclusions

Thiol-ene-disulfide networks were investigated to better understand the role of radical disulfide exchange during network formation and stress relaxation.

Disulfides derived from mercaptopropionates were found to be nearly as efficient for the disulfide-ene polymerization as those based on thioglycolates, despite showing significantly slower rates in previous model studies. Furthermore, the thiol-ene step of the polymerization using DMP was as fast or faster, and therefore less inhibited by disulfide exchange, than DTG regardless of the type of thiol comonomer. The disulfide-ene rate was largely unaffected by the thiol/disulfide pair when the thiyl radical formed by the thiol was more stable than the radical formed by the disulfide, but slower in the opposite scheme when asymmetric disulfides could form during the thiol-ene polymerization.

Both DMP and DTG induced stress relaxation both during polymerization and during post-polymerization. However, relaxation with DMP was significantly faster than for DTG in all cases. The type of disulfide did not however greatly impact the material properties of the final networks, which is advantageous for tunability of the exchange rate independently of the mechanical properties of the network.

4.6 References

1.   Podgórski, M.; Fairbanks, B. D.; Kirkpatrick, B. E.; McBride, M.; Martinez, A.; Dobson, A.; Bongiardina, N. J.; Bowman, C. N., Toward Stimuli-Responsive Dynamic Thermosets through Continuous Development and Improvements in Covalent Adaptable Networks (CANs). *Advanced Materials* **2020,** *32* (20), 1906876.

2.   Zheng, N.; Xu, Y.; Zhao, Q.; Xie, T., Dynamic Covalent Polymer Networks: A Molecular Platform for Designing Functions beyond Chemical Recycling and Self-Healing. *Chemical Reviews* **2021,** *121* (3), 1716-1745.

3.   Craig, D., The Vulcanization of Rubber with Sulfur. *Rubber Chemistry and Technology* **1957,** *30* (5), 1291-1346.

4.   Takahashi, Y.; Tobolsky, A. V., Chemorheological study on natural rubber vulcanizates. *Polymer Journal* **1971,** *2* (4), 457-467.

5.   Tobolsky, A.; MacKnight, W.; Takahashi, M., Relaxation of disulfide and tetrasulfide polymers. *The Journal of Physical Chemistry* **1964,** *68* (4), 787-790.

6.   Wedemeyer, W. J.; Welker, E.; Narayan, M.; Scheraga, H. A., Disulfide Bonds and Protein Folding. *Biochemistry* **2000,** *39* (15), 4207-4216.

7.   Fava, A.; Iliceto, A.; Camera, E., Kinetics of Thiol-Disulfide Exchange. *Journal of the American Chemical Society* **1957,** *79*, 833-838.

8.   Martin, R.; Rekondo, A.; Ruiz de Luzuriaga, A.; Cabañero, G.; Grande, H. J.; Odriozola, I., The processability of a poly(urea-urethane) elastomer reversibly crosslinked with aromatic disulfide bridges. *Journal of Materials Chemistry A* **2014,** *2* (16), 5710-5715.

9.   Michal, B. T.; Jaye, C. A.; Spencer, E. J.; Rowan, S. J., Inherently Photohealable and Thermal Shape-Memory Polydisulfide Networks. *ACS Macro Letters* **2013,** *2* (8), 694-699.

10.   Fairbanks, B. D.; Singh, S. P.; Bowman, C. N.; Anseth, K. S., Photodegradable, Photoadaptable Hydrogels via Radical-Mediated Disulfide Fragmentation Reaction. *Macromolecules* **2011,** *44* (8), 2444-2450.

11.   Nevejans, S.; Ballard, N.; Fernández, M.; Reck, B.; Asua, J. M., Flexible aromatic disulfide monomers for high-performance self-healable linear and cross-linked poly(urethane-urea) coatings. *Polymer* **2019,** *166*, 229-238.

12.   Pepels, M.; Filot, I.; Klumperman, B.; Goossens, H., Self-healing systems based on disulfide–thiol exchange reactions. *Polymer Chemistry* **2013,** *4* (18), 4955-4965.

13.   Tong, C.; Wondergem, J. A. J.; Heinrich, D.; Kieltyka, R. E., Photopatternable, Branched Polymer Hydrogels Based on Linear Macromonomers for 3D Cell Culture Applications. *ACS Macro Letters* **2020,** *9* (6), 882-888.

14.   Kamps, J.; Soars, S.; Fairbanks, B. D.; Bowman, C. N., Photodisulfidation of Linear Disulfides and Alkenes: Reaction Scope and Kinetics (Submitted to Tetrahedron).

15.   Raeisi, M.; Tsarevsky, N. V., Radical ring-opening polymerization of lipoates: Kinetic and thermodynamic aspects. *Journal of Polymer Science* **2021,** *59* (8), 675-684.

16.	Huang, S.; Shen, Y.; Bisoyi, H. K.; Tao, Y.; Liu, Z.; Wang, M.; Yang, H.; Li, Q., Covalent Adaptable Liquid Crystal Networks Enabled by Reversible Ring-Opening Cascades of Cyclic Disulfides. *Journal of the American Chemical Society* **2021,** *143* (32), 12543-12551.

17.	Soars, S.; Bongiardina, N. J.; Fairbanks, B. D.; Podgórski, M.; Bowman, C. N., Spatial and Temporal Control of Photo Mediated Disulfide-Ene and Thiol-Ene Chemistries for Two-Stage Polymerizations. *Macromolecules (Submitted)* **2021**.

18.	Podgórski, M.; Becka, E.; Claudino, M.; Flores, A.; Shah, P. K.; Stansbury, J. W.; Bowman, C. N., Ester-free thiol–ene dental restoratives—Part A: Resin development. *Dental Materials* **2015,** *31* (11), 1255-1262.

19.	Kloxin, C. J.; Scott, T. F.; Bowman, C. N., Stress Relaxation via Addition-Fragmentation Chain Transfer in a Thiol-ene Photopolymerization. *Macromolecules* **2009,** *42* (7), 2551-2556.

20.	Park, H. Y.; Kloxin, C. J.; Abuelyaman, A. S.; Oxman, J. D.; Bowman, C. N., Stress Relaxation via Addition-Fragmentation Chain Transfer in High T-g, High Conversion Methacrylate-Based Systems. *Macromolecules* **2012,** *45* (14), 5640-5646.

21.	Park, H. Y.; Kloxin, C. J.; Abuelyaman, A. S.; Oxman, J. D.; Bowman, C. N., Novel dental restorative materials having low polymerization shrinkage stress via stress relaxation by addition-fragmentation chain transfer. *Dental Materials* **2012,** *28* (11), 3-9.

22.	Soars, S.; Bongiardina, N. J.; Podórski, M.; Bowman, C. N., Spatial and Temporal Control of Photo Mediated Disulfide-Ene and Thiol-Ene Chemistries for Two-Stage Polymerizations (to be submitted).

23.	Cramer, N. B.; Reddy, S. K.; O'Brien, A. K.; Bowman, C. N., Thiol− ene photopolymerization mechanism and rate limiting step changes for various vinyl functional group chemistries. *Macromolecules* **2003,** *36* (21), 7964-7969.

24.	Fenoli, C. R.; Wydra, J. W.; Bowman, C. N., Controllable Reversible Addition–Fragmentation Termination Monomers for Advances in Photochemically Controlled Covalent Adaptable Networks. *Macromolecules* **2014,** *47* (3), 907-915.

25.	Podórski, M.; Becka, E.; Claudino, M.; Flores, A.; Shah, P. K.; Stansbury, J. W.; Bowman, C. N., Ester-free thiol–ene dental restoratives—Part B: Composite development. *Dental Materials* **2015,** *31* (11), 1263-1270.

Chapter 5 - SUBSTITUTED THIOLS IN DYNAMIC THIOESTER REACTIONS

5.1: Abstract

The thiol-thioester reaction has emerged as a promising method for developing covalent adaptable networks (CANs) due to its ability to exchange rapidly under low temperature conditions in a number of solvents, orthogonality amongst other functional groups, and tuneability. Here, the effects of thiol substitution (i.e., primary vs secondary) were assessed with respect to their reactivity in two dynamic thioester reactions: the thiol-thioester exchange and the reversible thiol-anhydride addition. Model NMR experiments were conducted using small molecule compounds to observe how polymers of similar components would behave in thiol-thioester exchange. It was determined that the K_{eq} was near unity for mixtures of primary thiols and secondary thioesters, and vice versa, in both a polar solvent, DMSO-d_6, and at most slightly favors primary thioesters in a relatively non-polar solvent, CDCl$_3$. Dielectric spectroscopy and stress relaxation experiments were used to determine the relaxation times and activation energies of the two thioester-containing networks: thiol-ene networks, which undergo thioester exchange, displayed activation energies of 73 kJ/mol and 71 kJ/mol from dielectric measurements and 36 kJ/mol and 53 kJ/mol from stress relaxation for the primary and secondary thiols, respectively. Thiol-anhydride-ene networks, which undergo both thioester exchange and reversible thiol-anhydride addition, displayed activation energies of 94 kJ/mol and 114 kJ/mol from dielectric and 111 kJ/mol and 139 kJ/mol from stress relaxation for primary and secondary thiols, respectively. In both types of networks, the secondary thioester-based networks demonstrated slower dynamics as compared to the same primary network by at least one order of magnitude. In the anhydride network, the secondary thiol also biased the dynamics towards reversible addition.

5.2: Introduction

Covalent adaptable networks (CANs) are a class of thermosetting polymer materials that contain dynamic chemical functionalities that enable rearrangement of what would normally be considered a static network. This dynamic character combines the mechanical robustness and chemical stability of thermosets

with the processability and recyclability of thermoplastics. As such, these hybrid materials enable a unique array of material characteristics that are typically unattainable for thermosets, opening potential applications for which neither conventional thermoplastics nor thermosets are well suited.

The basic principle for producing CANs involves the incorporation of labile chemical bonds that are triggered by application of an external stimulus, such as light or heat. Depending on the choice of chemistry, the dynamic bonds either: i) break-and-reform via reversible addition, or a dissociative mechanism, as is the case for the Diels-Alder reaction[1, 2], or ii) may interconvert via a reversible exchange, or an associative mechanism, as observed for transesterification[3], disulfide exchange[4], and thiol-thioester exchange[5, 6]. In particular, thiol-thioester exchange (TTE) (**Figure 5.1**) has received increased attention because of its low activation energy threshold (~30 kJ/mol), exchange rates that are tailored by the choice and concentration of a basic or nucleophilic catalyst, and the facile incorporation of thioesters into thiol-X based materials[5-8]. This exchange moiety has shown great potential for peptide synthesis[9, 10], dissolvable sealants[11], pressure sensitive adhesives[12], and nanocomposites[12, 13].
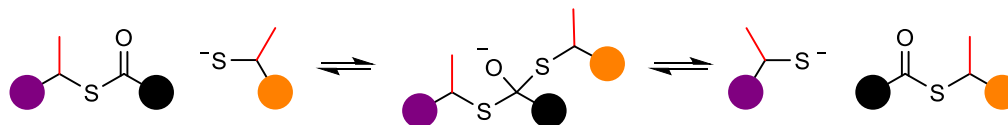
Figure 5.1: General scheme for the thiol-thioester exchange reaction for both primary and secondary (red line) thiols/thioesters.

While substantial work has been done to characterize TTE for thiols common in materials synthesis[5], the effect of substitution of the thiol on TTE has received little attention. Recently, the substitution of the thiol on various thiol-X processes has seen attention from Li and coworkers, who observed that increasingly substituted thiols have a longer shelf life and less odor than typical primary thiols[14], and Long and coworkers, who have shown that secondary and tertiary thiols can be used in thiol-ene[15] and thiol-Michael addition[16] polymerizations with minimal detrimental effects on reaction kinetics or conversion at relevant polymerization conditions while resulting in improved shelf life of the resin mixture. This outcome has important implications for many thiol-X materials that often cannot be pre-mixed and stored as a monomer resin due to their high reactivity. As such, it is also useful to understand the effects of thiol substitution on

TTE to further broaden the utility of this potent dynamic chemistry. Expanding upon classic thiol-ene systems for thioester chemistries, Podgórski and coworkers investigated dynamic thioester networks in which the thioester bonds were generated *in situ* in ring-opening thiol-anhydride additions[8, 17]. These dynamic networks were composed of thioester bonds adjacent to the carboxylic acids, formed by a ring-opening of the anhydride, and thioether bonds formed by the thiol-ene reaction. Importantly, these
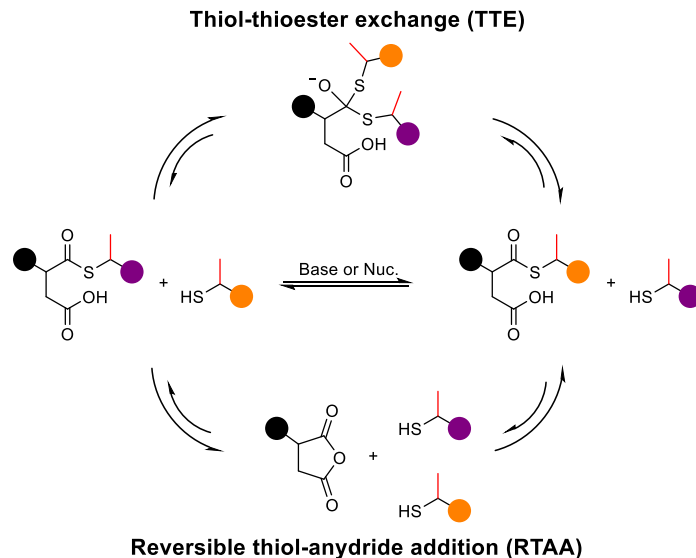
Figure 5.2: General scheme for bond rearrangement in thiol-anhydride-ene materials. Shown on top is thiol-thioester exchange and shown on bottom is reversible thiol-anhydride addition. For simplicity, both reactions are generalized by showing thiols as the exchanging species.

thioesters react both through a dissociative reaction, through reversible thiol-anhydride addition (RTAA), and an associative reaction, through TTE, depending on the amount of excess thiol, the catalyst choice and concentration, and temperature (**Figure 5.2**).

In this work, experiments were performed to assess the advantages or disadvantages of using secondary thiols in thioester-based dynamic materials, both from a mechanistic and mechanical standpoint. Small model compounds, which are analogous to the monomers used in subsequent polymer studies, were synthesized and thermodynamic equilibrium-driven reactions, similar to those described by Worrell and coworkers[5] using H^1-NMR, were conducted to determine the relative reactivity and propensity for exchange of the primary and secondary thiols of interest. The impact of the substituted thioesters was then evaluated in two different thioester-containing networks: 1) thiol-ene networks similar to those studied by Worrell and coworkers[5] and 2) thiol-anhydride-ene networks as introduced by Podgórski and coworkers[8]. The differences in the dynamic character of the primary and secondary TE-containing networks were then

evaluated using dielectric analysis (DEA) and compared to conventional mechanical measurements from dynamic mechanical analysis (DMA).

5.3: Experimental section

5.3.1: Materials

Pentaerythritol tetrakis(3-mercaptopropionate) (PETMP), methyl 3-mercaptopropionate (MMP), 1,4-diazabicyclo[2.2.2]octane (DABCO), 4-(dimethylamino)pyridine (DMAP), allyl succinic anhydride (ASA), quinuclidine (QN), 1,3,5-trimethoxybenzene (TMB), triethylamine (TEA), the phosphine oxide photoinitiator Omnicure 819, 2,2-dimethoxy-2-phenylacetophenone (DMPA), and 1,1,3,3-tetramethylguanidine (TMG) were purchased from common stock chemical suppliers (Sigma Aldrich, Fischer Scientific, TCI Chemicals) and used as delivered. Pentaerythritol tetrakis(3-mercaptobutyrate) (PETMB) was generously provided by ShowaDenko and used as delivered. Primary and secondary thioester-diene (1TE-diene and 2TE-diene respectively) and methyl 3-mercaptopropionate (MMB) were synthesized as described in Appendix 1.

5.3.2: Experimental

NMR Studies: H^1 NMR spectra were recorded in $CDCl_3$ (internal standard: 7.26 ppm) and in DMSO-d_6 (internal standard: 2.50 ppm, 1H) on a Bruker DRX-400 MHz spectrometer. See Appendix 2 for calibration curve preparation and experimental details. Chemical shifts (δ), reported in parts per million (ppm), had the following abbreviations used to identify the multiplicities: s = singlet, d = doublet, t = triplet, q = quartet, m = multiplet, b = broad.

Sample preparation for thiol-ene samples: The monomer resin was composed of a tetrathiol (1.0 equivalent PETMP or PETMB monomer), a thioester containing diene (1.0 equivalent of either 1TE-diene or 2TE-diene monomer), 1 wt.% Omnicure 819 (a phosphine oxide photoinitiator), and 4 mol% DABCO in TTE-active samples was prepared by first dissolving the photoinitiator and catalyst in the appropriate TE-diene, then mixing in the thiol. Dielectric samples were prepared on Mini-Varicon™ sensors purchased

from Lambient Technologies. Sensors were rinsed with acetone and placed in a drying oven to remove adsorbed water and solvent from the surface. The cleaned senor was placed flat on a glass slide and positioned under the curing light source with 250 µm spacers on either side, and the monomer resin was deposited on the metal electrode surface and spread over the entire metal contact surface. A glass slide was placed on top and weighted down on each side with binder clips to avoid moving the layer-up. The sample was irradiated with 405 nm at 25 mW/cm^2 for 5 minutes to activate the photoinitiator and cure the sample, which was then allowed to post cure at 60 °C for 1 hour. Samples for DMA and stress relaxation were prepared by depositing the resin between two glass slides with 250 µm spacers, after which the sample was irradiated with 405 nm at 25 mW/cm^2 for 5 minutes.

Sample preparation of thiol-ene-anhydride samples: The procedure for sample preparation was adapted from a previously reported procedure[8]. The thiol monomer (1.0 equivalent PETMP or PETMP) and allyl succinic anhydride (2.0 equivalents) were mixed. The DMPA and DABCO were then dissolved in a small amount of DCM, then mixed with the monomer mixture and allowed to rest for 0.5-1 hour. The DCM was then removed under vacuum and the sample was subsequently cast as allowed to rest for 1 hour to ensure maximum conversion of the anhydride moieties. Dielectric samples and DMA films were prepared with the same method described for the thiol-ene films. The thiol-ene reaction was then initiated by irradiation with 365 nm light at 25 mW/cm^2 for 5 minutes.

Fourier Transform Infrared Spectroscopy (FTIR): Thiol-anhydride-ene resins were prepared as described previously, and a drop of resin mixture being added between two clean salt plate before resting for 1 hour, then cured as described above. The sample was then placed in a Nicolet 8700 and allowed to equilibrate at a given temperature from 40-120 °C. Once equilibrium was achieved, as indicated by an unchanging FTIR spectrum, and the time required to equilibrate was noted for dielectric analysis before the sample was heated to the next temperature.

Dielectric Analysis (DEA): Dielectric analysis was performed on a ModuLab XM Material Test System (AMETEK Scientific Instruments, UK) at various temperatures depending on the material. Isothermal

temperature sweeps were performed over a range of 30^{-2} - 10^6 Hz under an applied sinusoidal voltage of 4500 mV in amplitude. Samples were prepared on Mini-Varicon™ sensors as described above. Thiol-ene samples were allowed to equilibrate at a given temperature for 10 minutes before a spectrum was taken. Thiol-anhydride-ene samples were allowed to equilibrate for the time needed to reach a stable anhydride concentration as determined by FTIR, as described above.

Dynamic mechanical analysis and stress relaxation: Glass transition temperature (T_g), storage modulus ($E^{'}$), and loss modulus ($E^{''}$) were measured on an RSA G2 dynamic mechanical analyzer (TA Instruments) using a temperature ramp rate of 3°C/min and a frequency of 1 Hz, with an oscillating strain of 0.03 % and a preload force of 0.40 N. Stress relaxation was performed in tension. A strain of 8% was applied and the resulting isothermal stress was measured over time at various temperatures, then normalized to the initial value.

5.4: Results and Discussion

5.4.1: Model Compound Studies

In their work on thioester exchange reaction in organic media, Worrell and coworkers[5] investigated the equilibrium constants for a variety of thiols and thioesters in a range of solvents to determine: i) the favored products at equilibrium for different thiol/thioester structures and ii) which solvents were conducive to the exchange reaction. Their approach was adopted here to determine whether primary or secondary thiol/thioester products are favored when a primary thiol reacts with a secondary thioester, and vice versa. The primary and secondary thiols and thioesters used in this study are shown in **Figure 5.3a**, and the reaction scheme used to calculate the equilibrium constant, Keq, for each mixture as well as the definition of Keq is provided in **Figure 5.1b**. Here, Keq for every mixture was calculated with the primary thioester and the secondary thiol as the reactants and the secondary thioester and primary thiol considered to be the products. This approach was used to simplify the comparison of the equilibrium constants, regardless of which thiol/thioester pair was used as the starting material. The investigation was carried out with the basic catalyst TMG (pKa = 13.6 in water), the nucleophilic catalyst QN (N = 20.5), or without any catalyst. These

catalysts were selected because of their potent catalytic activity as determined in previous studies on TTE reactions relative to other catalysts. Tests were performed directly in deuterated solvents, DMSO-d6 or CDCl$_3$, to examine the effect of solvent polarity on equilibrium. The designations "a" and "b" denote whether the initial mixture contained a primary thiol and secondary thioester or a secondary thiol and primary thioester, respectively. Calibration curves were prepared for each thiol and thioester model compound to compare the experimental thioester concentrations to an internal standard to correct for instrumental error and any solvent evaporation. Exchange reactions proceeded at room temperature until the reactions reached equilibrium – as indicated by two time points with a K$_{eq}$ difference of < 0.05 – but all reactions were stopped after 150 hours and a reaction quotient (Q) value was recorded if equilibrium had not yet been achieved, as occurred for example in the absence of any catalyst.
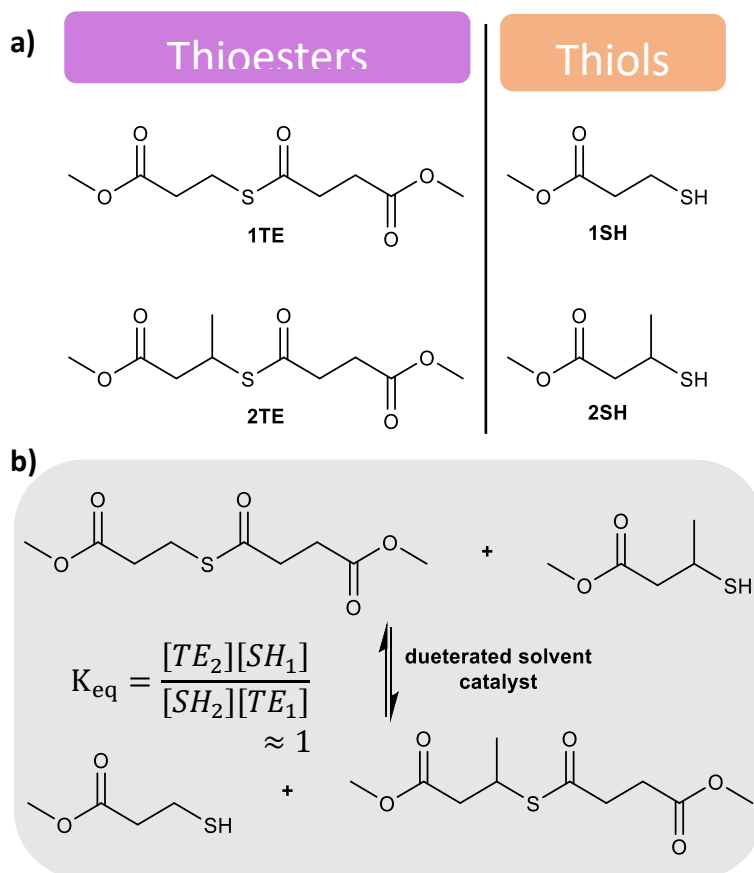
Figure 5.3: a) Model primary and secondary thiol and thioester compounds used in NMR studies, and b) Reaction scheme for exchange of primary and secondary model compounds and the definition of Keq, where the reactants and products can be either primary thiol and secondary thioester, or vice versa.

Shown in **Table 5.1** are the equilibrium constants in DMSO-d_6, the more polar of the two solvents tested. The solutions with TMG as the catalyst (2a and 2b) achieved K_{eq}'s of 1.2 ± 0.2 and 0.9 ± 0.1, respectively. The quinuclidine solutions (3a and 3b) achieved K_{eq}'s of 0.9 ± 0.2 and 0.82 ± 0.08, respectively. These equilibrium constants are approximately unity, suggesting that neither the primary or secondary thiol or thioester is significantly favored at equilibrium. Exchange also proceeded when no catalyst was present (1a and 1b) and did not reach full conversion after 150 hours, reaching reaction quotients (Q) of 0.6 ± 0.2 and 1.2 ± 0.1 in DMSO-d_6 after 150 hours while continuing to react slowly towards equilibrium.

Table 5.1: Summary of Keq values for all solutions studied, where values marked by an asterisk are reaction quotients because equilibrium was not reached by the end of experiment. Experiments were conducted in DMSO-d6 at room temperature with 10 mol % catalyst. All reactions used equimolar thiol and thioester reactants and were compared to an internal standard (1,3,5 trimethoxy benzene). Time points were taken for up to 150 hours or the achievement of equilibrium as indicated by a lack of further changes in the species concentrations.

Solution	Reactant	Product	Catalyst	K_{eq} (Q*)
1a	1° Thioester + 2° Thiol	2° Thioester + 1° Thiol	None	0.61* ± 0.1
1b	2° Thioester + 1° Thiol	1° Thioester + 2° Thiol	None	1.2 * ± 0.1
2a	1° Thioester + 2° Thiol	2° Thioester + 1° Thiol	TMG	1.2 ± .2
2b	2° Thioester + 1° Thiol	1° Thioester + 2° Thiol	TMG	0.9 ± 0.1
3a	1° Thioester + 2° Thiol	2° Thioester + 1° Thiol	quinuclidine	0.9 ± 0.2
3b	2° Thioester + 1° Thiol	1° Thioester + 2° Thiol	quinuclidine	0.82 ± 0.08

*incomplete reaction, reaction quotient (Q) given.

Equilibrium constants in the less polar solvent, CDCl$_3$, are shown in **Table 5.2**. The TMG-containing solutions (4a and 4b) achieved a K_{eq} of 0.61 ± 0.1 and 0.5 ± 0.1, respectively. The reactions with quinuclidine (5a and 5b) were incomplete after 150 hours, reaching Q's of 0.8 ± 0.1 and 0.65 ± 0.1, respectively. The equilibrium constants for the reaction catalyzed by TMG are again similar but slightly favoring the primary thioester. The quinuclidine catalyzed reactions did not reach equilibrium because solvents of lower polarity are less conducive to rapid thiol-thioester exchange. This behavior is likely due to the sterically hindered nucleophilic mechanism for which the bulky Zwitterionic intermediate will not

be as well-stabilized as in a more polar solvent. Since the TMG catalyzed reaction went to completion and slightly favored the primary, steric hindrance plays an important role in non-polar environments where thioester exchange tends to be less favorable. Because the exchange rate was significantly reduced in chloroform with catalyst, non-catalyzed exchange reactions were not performed. Even though the base and nucleophile mechanisms differ slightly, it should be noted that the K_{eq} and Q values are comparable, as expected in the context of catalysis, regardless of whether a nucleophile (quinuclidine) or base (TMG) catalyst was used and are comparable to those reported in the literature[5]. In addition, longer times were required to reach equilibrium in $CDCl_3$ compared to DMSO-d_6, not reaching equilibrium in the case of the quinuclidine catalyzed solution. This delay was expected given that thioester exchange does not occur as efficiently in non-polar media such as $CDCl_3$.

Table 5.2: Summary of Keq values for CDCl3 solutions, where values marked by an asterisk are reaction quotients because equilibrium was not reached by the end of experiment. These experiments were conducted in CDCl3 at room temperature with 10 mol % catalyst. All reactions used equimolar thiol and thioester reactants and were compared to an internal standard (1,3,5 trimethoxy benzene). Time points were taken for up to 150 hours.

Solution	Reactant	Product	Catalyst	K_{eq} (Q)
4a	1° Thioester + 2° Thiol	2° Thioester + 1° Thiol	TMG	0.61 ± 0.1
4b	2° Thioester + 1° Thiol	1° Thioester + 2° Thiol	TMG	0.5 ± 0.1
5a	1° Thioester + 2° Thiol	2° Thioester + 1° Thiol	quinuclidine	$0.8* \pm 0.1$
5b	2° Thioester + 1° Thiol	1° Thioester + 2° Thiol	quinuclidine	$0.65* \pm 0.1$

*incomplete reaction, reaction quotient (Q) given.

5.4.2: Thiol-ene materials

An important feature of any CAN is the rate of exchange when the chemistry is active. While NMR studies of model compounds show that an equilibrium mixture of primary thioester and secondary thiol, or vice versa, does not strongly favor one product, equilibrium on its own does not provide information about the exchange rates. To this end, thiol-ene networks based on previous literature5, 6 with either primary or secondary thiols/thioesters were made as shown in **Figure 5.4**. Here, DABCO was selected as a nucleophilic catalyst because of its good nucleophilicity and solubility in the monomer resins and
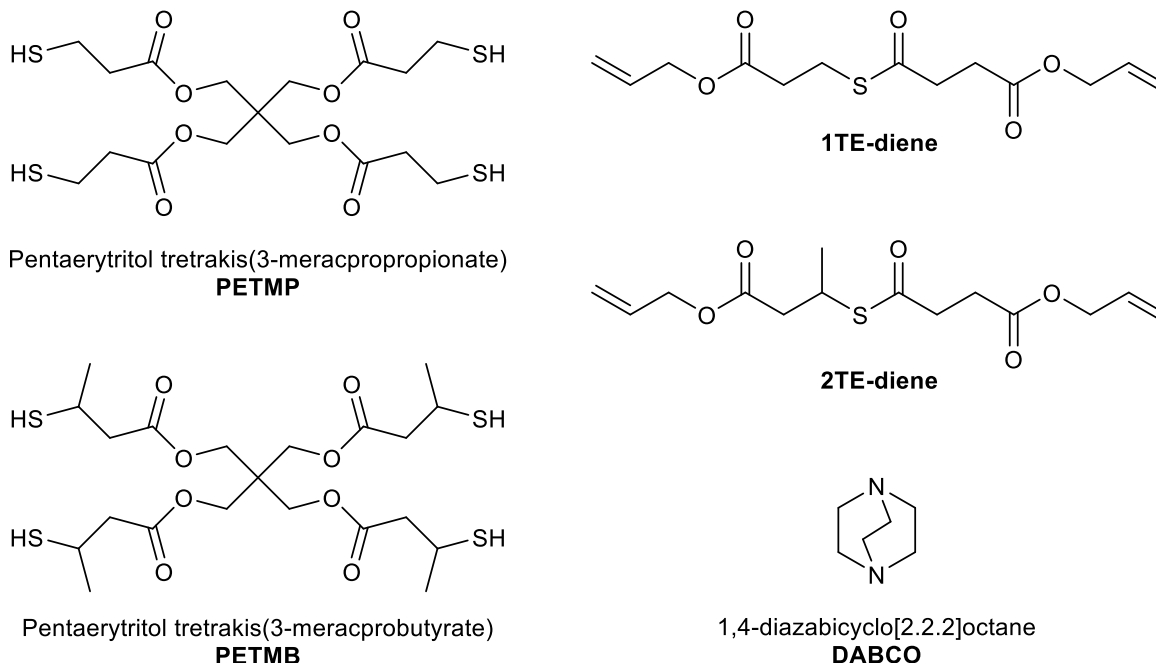
Figure 5.4: Structures of the thiols, thioesters, and nucleophilic catalyst for thiol-ene films. Samples consisted of either a 2:1 ratio of thiol-to-thioester functionality, with 1 wt% of the visible light photoinitiator I819 and were irradiated at 25 mW/cm2.

ability to remain in and remain stable over longer periods of time compared to quinuclidine. Differently from what was observed for structurally similar thiol-ene and thiol-Michael networks[15, 18], the glass transition temperatures for the secondary thiol-containing networks were slightly higher (-20 °C vs -25°C without DABCO for the primary, and -13 °C vs -14°C without catalyst for the secondary), while catalyst had little effect on the T_g. Dielectric and mechanical stress relaxation measurements were used to assess the relative effectiveness and rates of TTE for these primary and secondary thioester-based materials. It is hypothesized that due to the steric hindrance of the secondary thioester and thiol monomers, the overall dynamics are slower than for the primary system despite the comparative thermodynamic equilibria as assessed in model systems.

Dielectric Analysis of Thiol-ene networks: Dielectric analysis (DEA) is an important tool in polymer dynamics research due to its unique capability to efficiently probe different chain relaxation modes over wide temperature and frequency ranges. An oscillating electric field is applied and interacts with the permanent and induced dipole moments in the polymer. The response and relaxation of these dipoles can then be leveraged to probe the structure and properties of the material of interest. The ability to use an

oscillating electric field over a larger frequency range than mechanical analyses such as DMA (up to 10^6 Hz for DEA compared to 10^2 Hz in DMA) enables one to observe dynamics at the chain and chain-segment scale in a way that is impractical or impossible by macroscopic mechanical testing, provided that the material of interest possesses polar groups to interact with this electric field. A variety of polymer systems have been assessed using DEA, including epoxy-resin systems that are ubiquitous in materials applications[19], natural and synthetic rubbers[20, 21], dental resins[22], and composites to probe filler/resin/interface dynamics[23-25]. However, despite its appropriateness for probing molecular dynamics, there has been little work to use DEA to evaluate polymer dynamics in CANs. Moreover, DEA offers a direct approach to explore how introducing a simple structural modification, in this case the methyl groups associated with thiol/thioester substitution, on bond exchange and the overall dynamics of the network.

Here, DEA was used to assess the real (M') and loss (M'') electric moduli with respect to the α-relaxation, which is associated with segmental chain motions and the glass transition, for primary and secondary TTE networks. **Figure 5.5** shows M' and M" for primary and secondary thiol-ene networks that contain the nucleophilic catalyst DABCO (**Figure 5.5a** and **Figure 5.5b**, respectively) and those that did not contain catalyst (**Figure 5.5c** and **Figure 5.5d**, respectively). Measurements were taken over a frequency range of 30^{-2}-10^6 Hz for a temperature range of 20-60 °C. The frequency of the maximum of M" was taken to determine the relaxation time at a given temperature and was determined by a Cole-Cole fit of the modulus curves. This fit was used to accurately determine the frequency that corresponds to the peak; these relaxation times as a function of temperature are shown in **Figure 5.5e**.

For both the primary and secondary thioester networks, the α-relaxation time is faster when 4 mol% DABCO is present compared to the uncatalyzed network over the entire temperature range. The primary relaxation rate increases by a factor of two to four, while the rate for the secondary networks increases by an order of magnitude. These faster dynamics for both primary and secondary arise from increased mobility

via network rearrangement enabled by TTE when catalyst is present. Now, comparing the primary and

secondary thioester network's relaxation times with 4 mol% DABCO, the primary shows faster dynamics
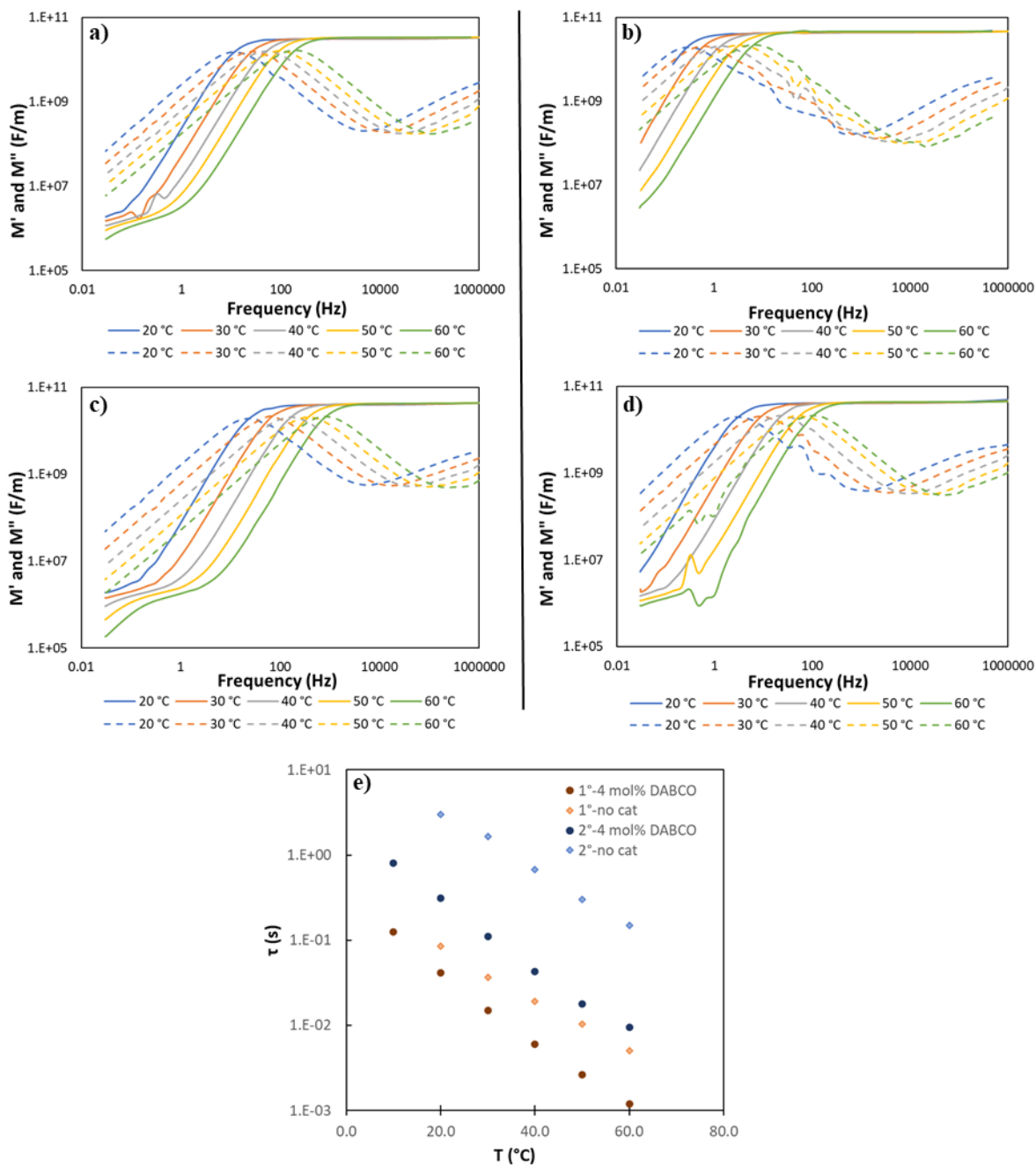
Figure 5.5: Representative dielectric spectra for thioester films taken using an interdigital sensor at various temperatures: Primary thiol/thioester sample containing no catalyst (a) and 4 mol% DABCO as a nucleophilic catalyst (c), and Secondary thiol/thioester of sample containing no catalyst (b) and 4 mol% DABCO as a nucleophilic catalyst (d). The solid lines denote the real electric modulus, and the dashed lines denote the loss electric modulus. e) The relaxation times as a function of temperature for the primary and secondary thioester films, both with and without catalyst.

at every temperature, roughly by a factor of seven. This behavior indicates that TTE is faster for primary thiols/thioesters, where steric hindrance due to the methyl substitution in the secondary thioester is likely a major contributor to slower dynamic bond rearrangement.

At the same time, when catalyst is *not* present, the relaxation times for the primary thioester are substantially faster in this dielectric measurement, by roughly a factor of 35, as compared to the equivalent secondary network, even though little dynamic covalent behavior occurs without catalyst. A possible explanation for this behavior is that the large number of methyl groups in the secondary thiols and thioesters increases steric hinderance while reducing the overall polarity of the network, which is known to decrease the rate of TTE because more polar media is conducive to the movement of charged/polar species through the material[5]. This decrease in polarity may therefore lead to a decrease in mobility, resulting in a slower relaxation time when no catalyst is present in otherwise equivalent networks. Therefore, polarity will also affect the catalyzed networks in addition to any steric effects that arise from substitution of the thiols and thioesters.

Stress Relaxation of Thiol-ene Networks: To validate DEA measurements, stress relaxation experiments were performed at constant temperatures and strain in tension (8%) to mechanically determine relaxation times due to TTE, as shown in **Figure 5.6**. The relaxation rate is significantly slower in the secondary thiol-
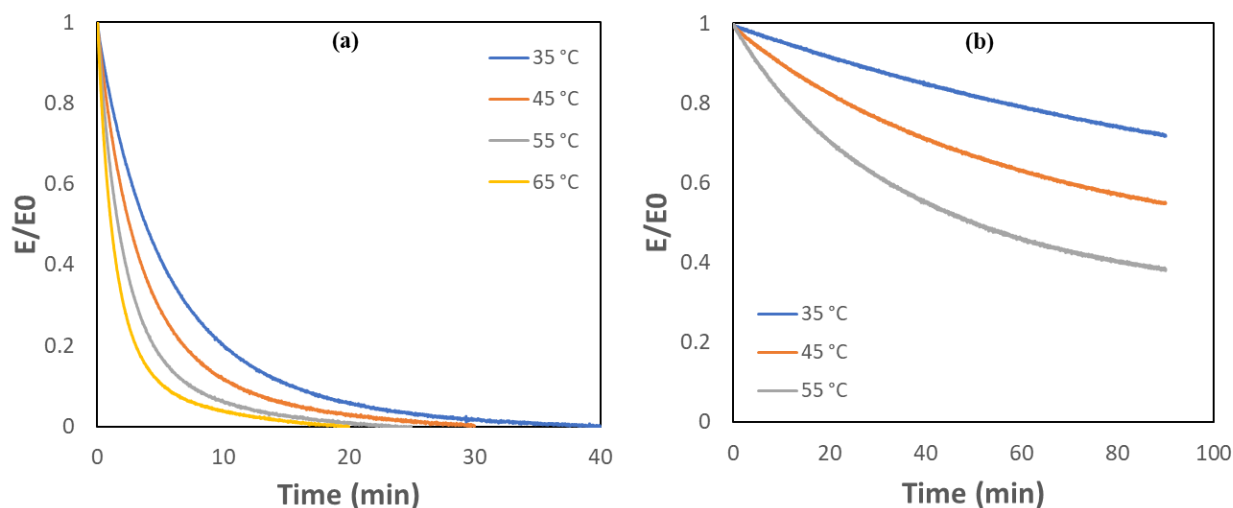
Figure 5.6: Representative stress relaxation data at various temperatures for (a) the primary thiol-thioester material and (b) the secondary thiol-thioester material.

based material. For example, the mechanical relaxation times at 35°C for the primary network relaxation times are nearly two orders of magnitude faster (~5.5 minutes) at the same catalyst concentration as compared to the secondary thioester-based network (~315 minutes). Confirming the dynamics measured by DEA, this behavior indicates that the secondary network exhibits slower covalent bond rearrangement as compared to the primary thioester network. Stress relaxation in control networks without catalyst was also evaluated at 35°C and 65°C, and only a small amount of relaxation was observed at 65°C for the primary (~5% relaxation) and none for the secondary thioester. Slower relaxation times for the secondary thioester network are attributed to a combination of steric hindrance and a decrease in polarity associated with the methyl groups.

The relaxation times from both DEA and stress relaxations were used to calculate the activation energies, all measured within the temperature range from 35°C to 65°C. Arrhenius plots of relaxation times from DEA and stress relaxation are shown in **Figure 5.7a and 5.7b**, respectively. As discussed for the dielectric measurements, the primary thiol/thioester materials exhibit fast relaxation times at all temperatures compared to their secondary counterparts, regardless of whether DABCO was included.
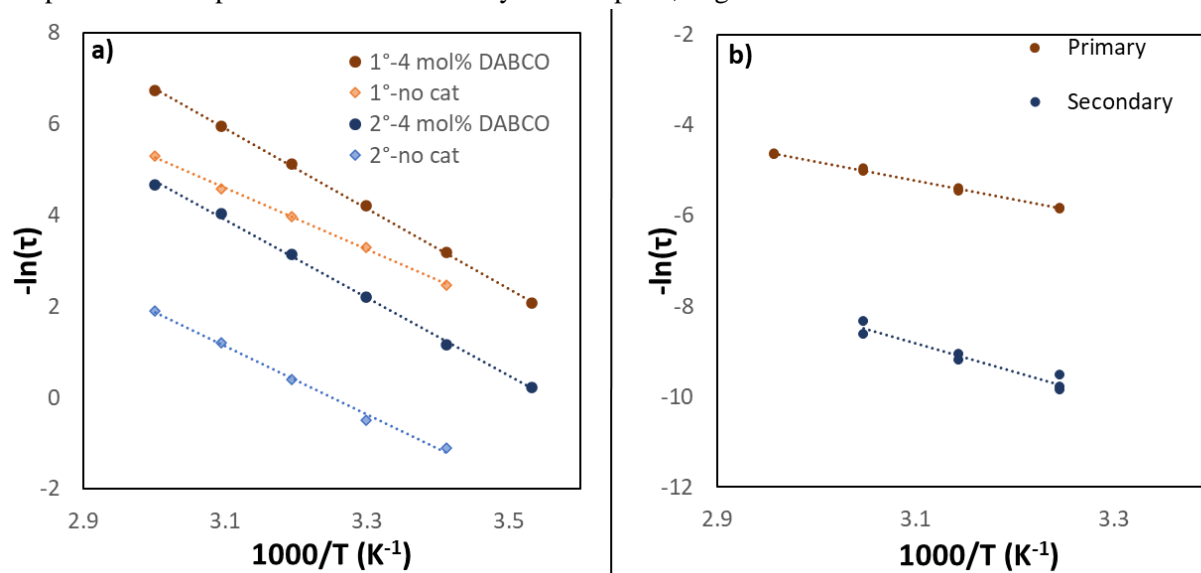
Figure 5.7: Arrhenius plots of a) the α-relaxation time from dielectric measurements for the primary and secondary thiol-ene samples, both with (diamonds) and without (circles) 4 mol% DABCO as a nucleophilic catalyst, and b) the relaxation times measured by stress relaxation with 4 mol% DABCO. Dashed lines indicate a linear fit to the data.

Mechanical stress relaxation times follow the same trend. The activation energies extracted from a linear regression of the Arrhenius plots are provided in **Table 5.3**.

The activation energies extracted from DEA for the networks containing DABCO are indistinguishable for the primary and secondary networks (73 and 71 kJ/mol, respectively) despite the slower rate at which relaxation occurs in the secondary networks. These energies differ from those extracted from the mechanical relaxation times, which were 36 and 52 kJ/mol, respectively. The discrepancy between these two measurements is likely due to inherent differences in the size scales and types of molecular motions probed by dynamic dielectric spectroscopy versus mechanical stress relaxation methodologies[26]. For example, in simultaneous DEA-DMA measurements of a curing network, DMA is able to measure the gelation point resulting from a rapid increase in the storage modulus, while DEA can measure the decrease in chain mobility after gelation that does not show up in mechanical moduli[27].

Table 5.3: Activation energies as calculated by from Arrhenius fits of the dielectric loss peaks and stress relaxation times. Errors indicated are the standard error of the regression.

	E_a (kJ/mol)	
	Primary	**Secondary**
Control (DEA)	56 ± 1	63 ± 3
4% DABCO (DEA)	72.9 ± 0.8	71 ± 1
4% DABCO (SR)	36.1 ± 0.6	52 ± 6

At the same time, control materials without catalyst show a slightly higher activation energy for the secondary network (63 versus 56 kJ/mol), although the difference is relatively small. Any difference is likely due to decreased polarity of the secondary network as discussed previously. Further, the catalyzed networks did not show the same difference in activation energy because of the increased polarity and mobility introduced by additional charged species during exchange, which is a result of the reaction of the nucleophile with thioester carbonyl groups that participate in dynamic exchange.

5.4.3: Thiol-anhydride-ene networks

a)

Pentaerytritol tretrakis(3-meracpropropionate)
PETMP

allyl succinicanhydride
ASA

Pentaerytritol tretrakis(3-meracprobutyrate)
PETMB

1,4-diazabicyclo[2.2.2]octane
DABCO

b)

1. DABCO (5 mol%)
2. DMPA (0.2 wt%))
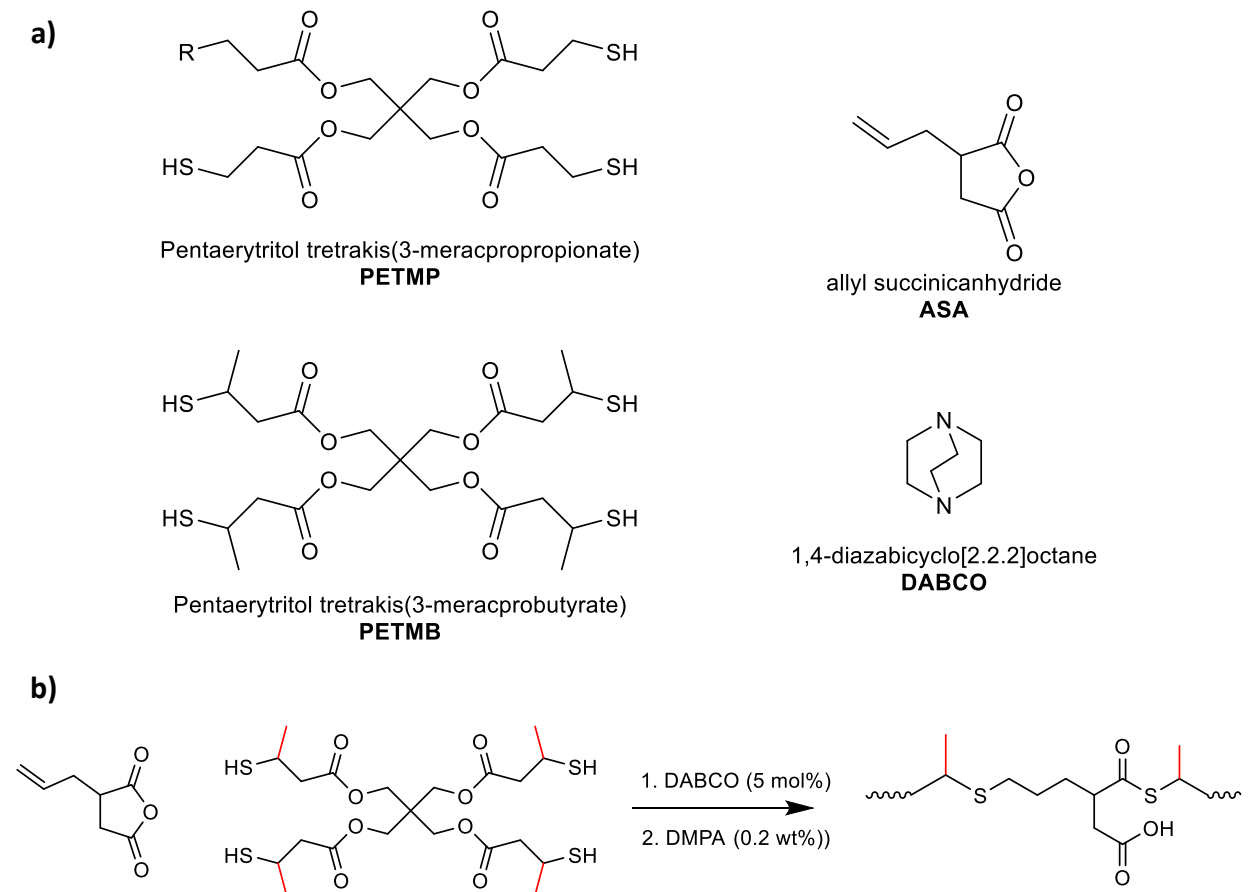
Figure 5.8: a) Structures of the thiols, anhydride, and nucleophilic catalyst for thiol-anhydride-ene films. Samples consisted of either a 2:1 ratio of thiol-to-thioester functionality, with 0.2 wt% of the UV light photoinitiator DMPA and were irradiated at 25 mW/cm2, and b) the general scheme for the thiol-anhydride-ene reaction.

Another CAN system of interest that leverages thioesters is the thiol-anhydride-based network as introduced by Podgórski and coworkers.[8] The monomers and reaction scheme are shown in **Figure 5.8a and b**, respectively. In a thiol-anhydride dynamic network, an interesting feature is introduced to the TTE paradigm because the formed thioesters are adjacent to a carboxylic acid product upon ring-opening of the anhydride by a thiol. Because this neighboring carboxylic acid is six atoms away from the sulfur in the thioester, this adduct has been shown to undergo both dynamic ring-closing/opening (dissociation) reactions as well as the TTE (association) reaction as observed in the more conventional thiol-ene materials shown previously, depending on the reaction temperature and the amount of excess thiol present in the network. Like the thiol-ene system discussed previously, it is expected that the secondary thiol-anhydride-

ene network will show slower dynamics with respect to the TTE reaction, or associative character, compared to the primary material due to steric considerations. However, steric hindrance may also increase the prevalence of the ring-closing/opening reaction pathway, or dissociative character, in the secondary thiol-thioester based material.

Dielectric Analysis of Thiol-anhydride-ene Networks: Thiol-anhydride-ene materials enable tuning of the prevalence of reversible addition versus reversible exchange by changing the temperature, catalyst type and/or catalyst concentration. Thiol substitution represents another tool through which these relative rates are tuned. Both networks possess similar glass transition temperatures around 11°C despite the secondary having a lower rubbery storage modulus. **Figure 5.9a and 5.9b** show the dielectric spectra for primary and secondary thiol-anhydride-ene materials, respectively, and **Figure 5.9e** shows the relaxation times at each temperature for both networks. As seen in **Figure 5.9e**, a clear shift to slower relaxation times is seen for the secondary thiol-based material. However, the relaxation times for both primary and secondary thioesters converge at higher temperatures, narrowing from a difference of a factor of seven at 40°C to a factor of roughly 1.8 at 120°C. Considering the slower TTE dynamics associated with secondary thiols (as observed for the thiol-ene networks discussed in the previous section), converging relaxation times suggests that the secondary thioester is reverting to the anhydride and thiol to a greater extent than the primary thioesters, which decreases crosslinking and by extension increases mobility and therefore the relaxation rate. Indeed, a greater extent of the ring closing reaction is observed in the IR spectra taken at the same temperatures as the dielectric measurements, shown in **Figures 5.9c and 5.9d**. These IR spectra are normalized to the carbonyl peak at 1740 cm^{-1}, which corresponds to the ester present in both thiol monomers, which is not expected to change with temperature.

Here, a clear increase in anhydride content is seen at 1770 cm^{-1} (highlighted in grey) for both the primary and secondary networks. However, the intensity of the anhydride peak is higher for the secondary thioester network at every temperature as compared to the primary. This behavior indicates that the secondary network has a higher propensity to undergo reversion to the thiol and anhydride rather than TTE.

86

This is most likely due to the increased steric hindrance of the secondary thiol, shifting the equilibrium toward the less sterically hindered anhydride/thiol products. As confirmation, a decrease in crosslinking at
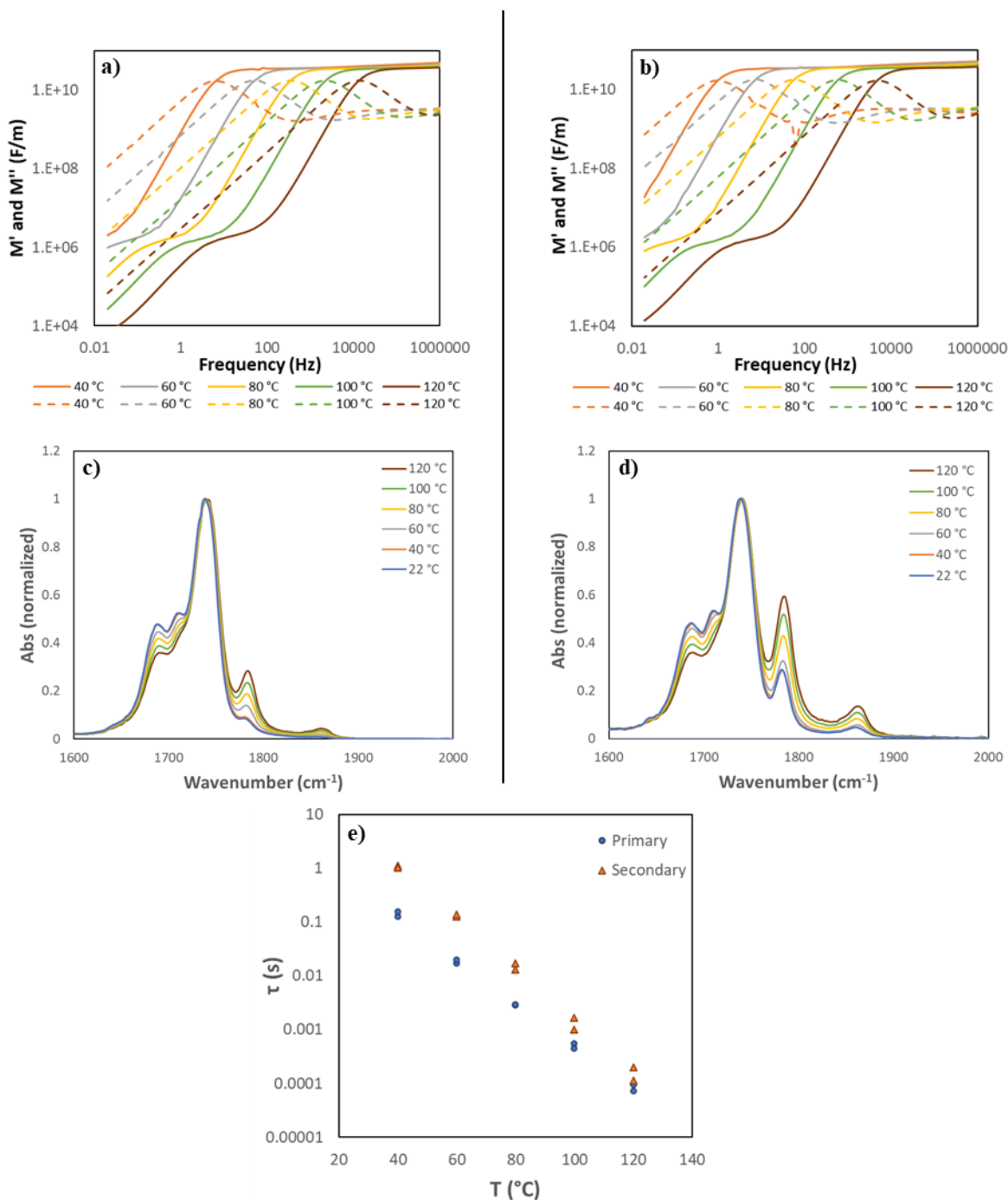
Figure 5.9: Representative dielectric spectra of a) the primary and b) secondary thiol-anhydride-ene samples at various temperatures. Dashed lines in the dielectric spectra represent the loss electric modulus (M"), and solid lines represent the real electric modulus (M'). The IR peak corresponding to the anhydride, highlighted in grey, appears at approximately 1770 cm-1, is shown for c) the primary and d) secondary thiol-anhydride-ene networks at the same temperatures as the dielectric spectra as well as room temperature. e) Relaxation time, as determined by a Cole-Cole fit, as a function of temperature for the dielectric spectra.

higher temperatures also is reflected by a drop off in rubbery storage modulus in DMA measurements at about 100 °C for the secondary as compared to the primary network at 120 °C.

Stress Relaxation of thiol-anhydride-ene materials: Stress relaxation experiments were performed (5% strain) to complement the DEA measurements as provided in **Figure 5.10a and 5.10b** for the primary and secondary thioester materials, respectively. Both materials relax stress over this temperature range. The primary network relaxes faster at 80°C with a relaxation time of 11 minutes compared to 13 minutes for the secondary. However, as the temperature increases to 120°C the secondary becomes more rapid with a relaxation time of 6 seconds compared to 14 seconds for the primary.
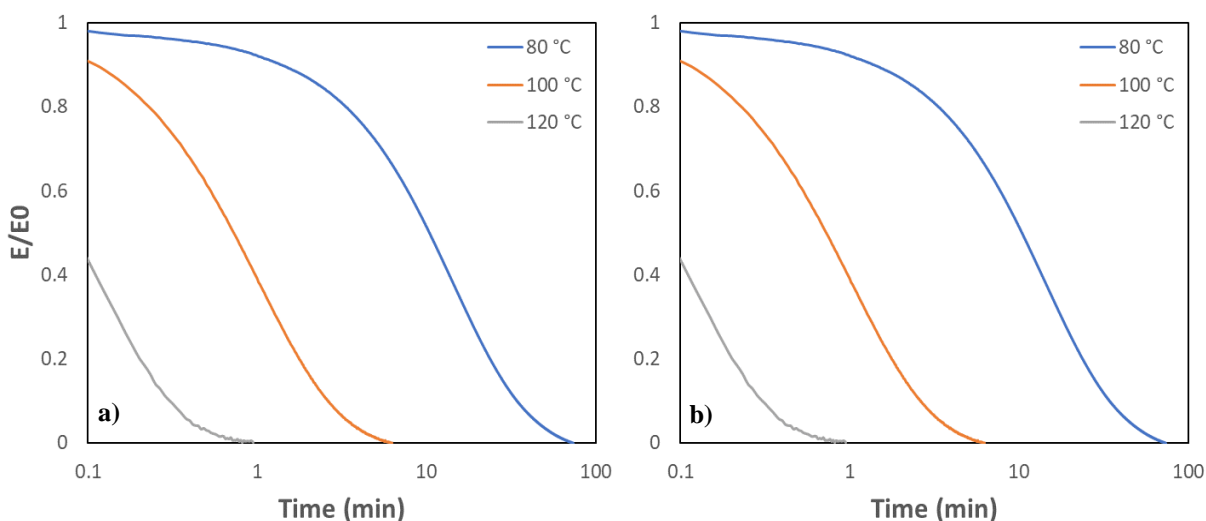
Figure 5.10: Representative stress relaxation data, given as the normalized modulus, at various temperatures for a) the primary thiol-anhydride-ene and b) the secondary thiol-anhydride-ene material.

This behavior matches well with observations in DEA and IR, discussed for **Figure 5.9**, that the secondary network has a higher propensity to undergo reversible addition at increased temperature, resulting in fewer crosslinks compared to the primary network at the same temperature and therefore faster relaxation. The ability to bias these thiol-anhydride-ene materials towards associative or dissociative rearrangement by simply increasing the substitution of the thiol is a facile tool for controlling dynamic behavior in a unique manner. The activation energies determined by linear regression of the Arrhenius plots are provided in Table 6.4.

Table 5.4: Activation energies as calculated by from Arrhenius fits of the dielectric loss peaks and stress relaxation times for the thiol-anhydride-ene materials. Errors indicated are the standard error of the regression.

	E_a (kJ/mol)	
	Primary	**Secondary**
DEA	94 ± 2	114 ± 4
Stress Relaxation	111 ± 3	139 ± 6

The activation energy of the secondary thiol is higher in both the dielectric measurement, 114 kJ/mol compared to 94 kJ/mol, and stress relaxation, 139 kJ/mol compared to 111 kJ/mol, although the primary and secondary differ more in stress relaxation than in DEA. A similar trend was observed for the thiol-ene networks, where DEA detected no significant difference in activation energy between the primary and secondary networks, but a substantial difference was measured by stress relaxation. Here, the fundamental difference is that, unlike the thiol-ene networks, reversible addition also occurs in the thiol-anhydride-ene network. This changes the network structure as temperature increases to a greater extent in the secondary network than in the primary, and DEA is capable of detecting these changes in mobility when bonds form or, in this case, break[27]. Depolymerization due to reversible addition also changes the polarity in addition to the structure because the thioesters and their adjacent carboxylic acids convert back to thiols and anhydrides. This shift in polarity may very well translate into similar trends in the activation energy for both DEA and stress relaxation. Improving our understanding of how dynamic bonds impact dielectric behavior in CANs is a continued area of interest in future investigations.

5.5: Conclusions

The substitution of the thiol in dynamic thioester reactions was shown to have a significant impact on material behavior. Model studies demonstrated that the primary thiol/thioester is not strongly favored over the secondary thiol/thioester at equilibrium in thiol-thioester exchange in media that is conducive to thioester exchange, and exchange occurs even without a base or nucleophilic catalyst, albeit much more slowly. In addition, the exchange was significantly slowed in a low polarity solvent. These same primary and secondary thioester functionalities in thiol-ene networks undergo dynamic exchange over the same temperature range, but the secondary thiol/thioester network showed far slower exchange rate in both

dielectric analysis and stress relaxation experiments due to decreases in polarity and increased steric hinderance associated with secondary thiols and thioesters. Finally, thiol-anhydride-ene networks, which enables both reversible addition and reversible thioester exchange, shows that using a secondary thiol/thioester biases exchange toward reversible addition in a stoichiometric system due to the steric hinderance of the methyl substitution. In both networks, slower exchange kinetics in the secondary materials are attributed to increased steric hindrance and a decrease in polarity associated with the methyl substitution.

5.6: References

(1) Zhang, G.; Zhao, Q.; Yang, L.; Zou, W.; Xi, X.; Xie, T., Exploring Dynamic Equilibrium of Diels–Alder Reaction for Solid State Plasticity in Remoldable Shape Memory Polymer Network. *ACS Macro Letters* **2016,** *5* (7), 805-808.

(2) Gandini, A., The furan/maleimide Diels–Alder reaction: A versatile click–unclick tool in macromolecular synthesis. *Progress in Polymer Science* **2013,** *38* (1), 1-29.

(3) Capelot, M.; Montarnal, D.; Tournilhac, F.; Leibler, L., Metal-catalyzed transesterification for healing and assembling of thermosets. *J Am Chem Soc* **2012,** *134* (18), 7664-7.

(4) Lei, Z. Q.; Xiang, H. P.; Yuan, Y. J.; Rong, M. Z.; Zhang, M. Q., Room-Temperature Self-Healable and Remoldable Cross-linked Polymer Based on the Dynamic Exchange of Disulfide Bonds. *Chemistry of Materials* **2014,** *26* (6), 2038-2046.

(5) Worrell, B. T.; Mavila, S.; Wang, C.; Kontour, T. M.; Lim, C. H.; McBride, M. K.; Musgrave, C. B.; Shoemaker, R.; Bowman, C. N., A user's guide to the thiol-thioester exchange in organic media: scope, limitations, and applications in material science. *Polymer Chemistry* **2018,** *9* (36), 4523-4534.

(6) Worrell, B. T.; McBride, M. K.; Lyon, G. B.; Cox, L. M.; Wang, C.; Mavila, S.; Lim, C. H.; Coley, H. M.; Musgrave, C. B.; Ding, Y. F.; Bowman, C. N., Bistable and photoswitchable states of matter (vol 9, 2804, 2018). *Nature Communications* **2018,** *9*.

(7) Wang, C.; Mavila, S.; Worrell, B. T.; Xi, W.; Goldman, T. M.; Bowman, C. N., Productive Exchange of Thiols and Thioesters to Form Dynamic Polythioester-Based Polymers. *Acs Macro Letters* **2018,** *7* (11), 1312-1216.

(8) Podgórski, M.; Spurgin, N.; Mavila, S.; Bowman, C. N., Mixed mechanisms of bond exchange in covalent adaptable networks: monitoring the contribution of reversible exchange and reversible addition in thiol–succinic anhydride dynamic networks. *Polymer Chemistry* **2020,** *11*, 5365-5376.

(9) Dawson, P. E.; Muir, T. W.; Clark-Lewis, I.; Kent, S. B., Synthesis of proteins by native chemical ligation. *Science* **1994,** *266* (5186), 776-9.

(10) Konieczynska, M. D.; Villa-Camacho, J. C.; Ghobril, C.; Perez-Viloria, M.; Tevis, K. M.; Blessing, W. A.; Nazarian, A.; Rodriguez, E. K.; Grinstaff, M. W., On-Demand Dissolution of a Dendritic Hydrogel-based Dressing for Second-Degree Burn Wounds through Thiol-Thioester Exchange Reaction. *Angew Chem Int Ed Engl* **2016,** *55* (34), 9984-7.

(11)   Ghobril, C.; Charoen, K.; Rodriguez, E. K.; Nazarian, A.; Grinstaff, M. W., A dendritic thioester hydrogel based on thiol-thioester exchange as a dissolvable sealant system for wound closure. *Angew Chem Int Ed Engl* **2013,** *52* (52), 14070-4.

(12)   Dobson, A. L.; Bongiardina, N. J.; Bowman, C. N., Combined Dynamic Network and Filler Interface Approach for Improved Adhesion and Toughness in Pressure-Sensitive Adhesives. *ACS Applied Polymer Materials* **2019,** *2* (3), 1053-1060.

(13)   Sowan, N.; Lu, Y.; Kolb, K.; Cox, L. M.; Long, R.; Bowman, C. N., Enhancing the toughness of composites via dynamic thiol–thioester exchange (TTE) at the resin–filler interface. *Polymer Chemistry* **2020,** *11*, 4760-4767.

(14)   Li, Q.; Zhou, H.; Hoyle, C. E., The effect of thiol and ene structures on thiol–ene networks: Photopolymerization, physical, mechanical and optical properties. *Polymer* **2009,** *8* (11).

(15)   Long, K. F.; Bongiardina, N. J.; Mayordomo, P.; Olin, M. J.; Oretega, A. D.; Bowman, C. N., Effects of 1°, 2°, and 3° Thiols on Thiol–Ene Reactions: Polymerization Kinetics and Mechanical Behavior. *Macromolecules* **2020,** *53* (14), 5805-5815.

(16)   Long, K. F.; Wang, H.; Dimos, T. T.; Bowman, C. N., Effects of Thiol Substitution on the Kinetics and Efficiency of Thiol-Michael Reactions and Polymerizations. *Macromolecules* **2021,** *54* (7), 3093-3100.

(17)   Podgórski, M.; Mavila, S.; Huang, S.; Spurgin, N.; Sinha, J.; Bowman, C. N., Thiol–Anhydride Dynamic Reversible Networks. *Angewandte Chemie International Edition* **2020,** *59* (24), 9345-9349.

(18)   Long, K. F.; Wang, H.; Dimos, T. T.; Bowman, C. N., The Effects Of Thiol Substitution On The Kinetics And Efficiency Of Thiol-Michael Reactions And Polymerizations. In Preparation, 2020.

(19)   Jilani, W.; Mzabi, N.; Gallot-Lavallée, O.; Fourati, N.; Zerrouki, C.; Zerrouki, R.; Guermazi, H., Dielectric relaxations investigation of a synthesized epoxy resin polymer. *The European Physics Journal Plus* **2015,** (130).

(20)   Carrertero-Gonzalez, J.; Ezquerra, T. A.; Amnuaypornsri, S.; Toki, S.; Verdejo, R.; Sanz, A.; Sakdapipanich, J.; Hsiao, B. S.; López–Manchado, M. A., Molecular dynamics of natural rubber as revealed by dielectric spectroscopy: The role of natural cross–linking. *Soft Matter* **2010,** (6), 3636-3642.

(21)   Hernández, M.; Grande, A. M.; van der Zwaag, S.; García, S. J., Monitoring Network and Interfacial Healing Processes by Broadband Dielectric Spectroscopy: A Case Study on Natural Rubber. *ACS Appl Mater Interfaces* **2016,** *8* (16), 10647-56.

(22)   Lovell, L. G.; Berchtold, K.; Elliot, J. E.; Lu, H.; Bowman, C. N., Understanding the kinetics and network formation of dimethacrylate dental resins. *Polym. Adv. Technol.* **2001,** *12* (6), 335-345.

(23)   Tsangaris, G. M.; Psarras, G. C.; Kouloumbi, N., Electric modulus and interfacial polarization in composite polymeric systems. *Journal of materials Science* **1998,** (33), 2027–2037.

(24)   Yang, J.; Melton, M.; Sun, R.; Yang, W.; Cheng, S., Decoupling the Polymer Dynamics and the Nanoparticle Network Dynamics of Polymer Nanocomposites through Dielectric Spectroscopy and Rheology. *Macromolecules* **2020,** *53* (1), 302-311.

(25)   Carroll, B.; Cheng, S.; Sokolov, A. P., Analyzing the Interfacial Layer Properties in Polymer Nanocomposites by Broadband Dielectric Spectroscopy. *Macromolecules* **2017,** *50* (16), 6149-6163.

(26)   Gotro, J.; Yandrasits, M., Simultaneous dielectric and dynamic mechanical analysis of thermosetting polymers. *Polymer Engineering & Science* **1989,** *29* (5), 278-284.

(27)   Shepard, D. D.; Twombly, B., Simultaneous dynamic mechanical analysis and dielectric analysis of polymers. *Thermochimica Acta* **1996,** *272*, 125-129.

Chapter 6 – DIELECTRIC SPECTROSCOPY IN COVALENT ADAPTABLE NETWORKS

6.1 - ABSTRACT

Dielectric analysis was used to evaluate relaxation dynamics in covalent adaptable networks. The electric moduli were measured for dynamic networks capable of either reversible addition (Diels-Alder), reversible exchange (thiol-thioester exchange), or a combination of both mechanisms (reversible thiol-anhydride addition and thiol-thioester exchange). At frequencies below the α-relaxation, a significant plateau in the real electric modulus for samples tested using indium-tin-oxide coated glass was observed due to interfacial polarization. For interdigit probes, only inflection points at 2-3 orders of magnitude lower intensities were observed, and measurements were much less sensitive to sample preparation and interfacial charge separation in the low frequency regime. In addition, time-temperature-superposition of the dielectric spectra was implemented. Due to the temperature dependent dynamic reactions, the spectra of reversible addition networks did not generate master curves that superimpose at frequencies above the α-relaxation. On the other hand, the spectra of reversible exchange networks superimposed quite well over the entire frequency range. These results indicate that superposition is possible when the number of crosslinks not strongly depend on temperature. To compare with the DEA results, stress relaxation in shear was implemented and the relaxation spectra were also superimposable so long as the structure is not strongly temperature dependent over the measured range.

6.2 - INTRODUCTION

Characterizing chain dynamics in polymeric materials is a significant challenge in materials science, and yet, it is one that enables a deeper understanding of macroscopic polymer behavior. An important tool for characterizing chain and segment-level dynamics in polymers is

dielectric analysis (DEA)[1, 2]. While mechanical characterization techniques like dynamic mechanical analysis (DMA) apply an oscillating strain and measure the mechanical response, DEA leverages permanent and induced dipoles along the main chain and side groups by applying an oscillating electric field across the sample and measuring the resulting dielectric response. In addition to direct measurement of chain relaxation processes, standard dielectric spectrometers can reach frequencies up to 10^6 Hz, while even high-end dynamic mechanical analyzers can only reach 10^3 Hz, and most standard DMA's can only reach 100 Hz. This issue is important because access to a larger frequency range enables the observation of a wider range of relaxation processes at a fixed temperature, thus reducing the number of measurements needed to capture chain dynamics over a given temperature range, facilitating more efficient measurement and analysis of relaxation processes. DEA has been broadly implemented to study a wide range of polymer materials including bulk relaxation of epoxy-resins[3], rubbers[4, 5], curing of dental resins[6], interfacial relaxations in composites[7-9], and hydrogen bonding in supramolecular networks[10], among others.

An important class of materials that could potentially benefit from the insights into chain dynamics provided by DEA are crosslinked polymers containing dynamic covalent chemistry within the network structure. These materials, often called covalent adaptable networks (CANs), are crosslinked networks that contain dynamic bonds which facilitate covalent bond rearrangement upon activation by a stimulus. There are a wide variety of dynamic bonds and stimuli available for CANs that generally fall into two categories: reversible addition and reversible exchange[11, 12]. Reversible addition reactions involve the reversible breaking and reforming of the dynamic bond. This results in a decrease in crosslinking due to a decrease in the equilibrium number of elastically active chains. The most well studied reversible addition chemistry is the Diels-Alder reaction[13], but other reversible chemistries include dimerization of anthracene[14] and cinnamates[15],

urethane/urea bonds[16], and thiol-Michael adducts[17]. In contrast, reversible exchange networks function via bond forming-then-breaking, in which the dynamic bond is typically attacked by an active center or catalytic species to form an intermediate which rearranges to reform the dynamic bond and the active species with a new topology. Here, the overall number of bonds is maintained and minimally temperature dependent, but the material can flow and adapt its shape under an applied stress. Some common examples of reversible exchange chemistries include addition fragmentation chain transfer of allyl sulfides and trithiocarbonates[18], transesterification[19], imine exchange[20, 21], and thiol-thioester exchange (TTE)[22-24]. There are also dynamic bonds that are capable of both reversible addition and reversible exchange depending on the reaction conditions. Such bonds include boronic esters[25, 26], disulfides[27, 28], and thiol-anhydride adducts that are capable of both thioester exchange and ring-opening/closing reactions[29, 30].

Understanding the polymer dynamics induced by these different types of dynamic bonds is of great interest to understand fundamental materials behavior. A close analogy to dynamic covalent bonds in crosslinked networks are the hydrogen bonds that make up supramolecular networks like those studied by Tress *et al.*[10] in which a peak that is directly attributed to hydrogen bonding was identified. However, no such peak has been identified in the limited number of dielectric studies of CANs[31, 32]. There has been extensive work studying rheological behavior in dynamic networks, but the narrow frequency windows associated with these techniques require large temperature windows to characterize complex dynamic systems[33].

In this work, DEA was implemented to explore the utility of this technique to understand the dynamics of these materials over a broad frequency and temperature range, and to use this in conjunction with standard rheological methods to understand better the behavior of these materials. Three types of dynamic networks were investigated: Diels-Alder based networks incorporating

furan and maleimide for reversible addition (**Figure 6.1a**), thiol-thioester exchange for reversible

exchange (**Figure 6.1b**), and the thiol-anhydride adduct which combines both types of reactions

(**Figure 6.1c**). A Cole-Cole fit of the dielectric data was implemented to characterize the relaxation

times observed in the dielectric spectra using MatLab[1].
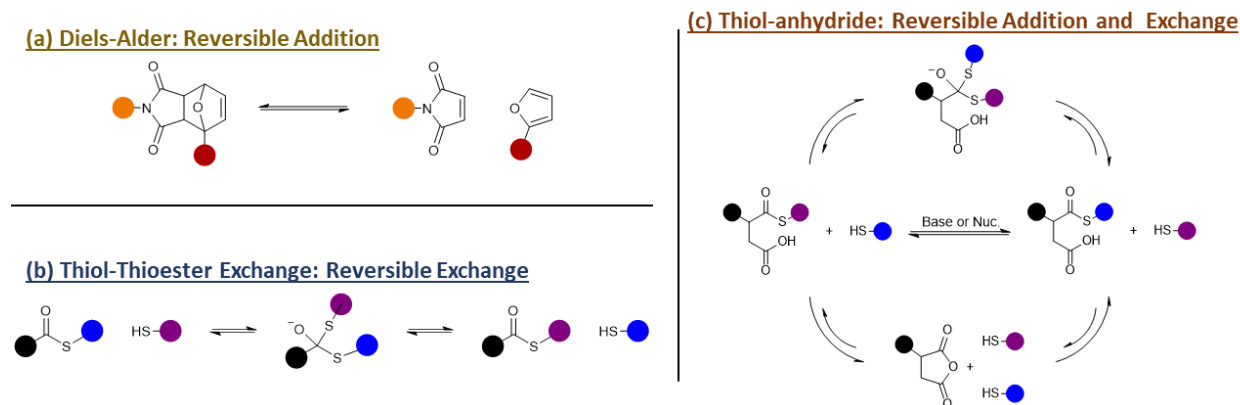
Figure 6.1: Schematics for the three dynamic bonds studied in this work: a) The Diels-Alder (DA) bond which undergoes reversible addition, b) Thiol-thioester bond which undergoes thiol-thioester exchange, and c) the thioester bond that forms from the ring opening of an anhydride by a thiol which undergoes both thiol-thioester exchange and reversible thiol-anhydride addition.

Despite the potential for DEA to probe the dynamics of CANs, there are several hurdles to its

widespread implementation, including establishment of best practices to achieve reproducible and

physically meaningful results. For example, in their work with studying thiol-anhydride networks,

Podgorski *et al.* observed significant plateaus in the electric modulus at low frequencies,

specifically frequencies below the α-relaxation. This plateau became more pronounced as the bond

rearrangement dynamics became more rapid due to either more potent catalysts or increased free

thiol content to participate in bond exchange[32]. These experiments used a parallel plate geometry

of indium-tin-oxide (ITO) coated glass to measure the dielectric response of these materials.

However, in subsequent work studying thioester and thiol-anhydride networks with substituted

thiols, Bongiardina *et al.* did not observe such a plateau and only observed an inflection point at

significantly lower intensities[31]. The key difference being that interdigit probes (IP) were utilized

rather that ITO glass to measure the dielectric response in the same thioester materials. In this

work, DEA measurements using both ITO and interdigit probes were performed to better understand whether this discrepancy is solely due to the test geometry or a combination of the test geometry and the dynamics of the network.

Time-temperature-superposition (TTS) analysis of the dielectric relaxations was implemented to understand whether DEA can observe correlations from the superposition of relaxation spectra and the type of dynamic bonding mechanism. Specifically, whether the broad frequency window afforded by DEA elucidates how the temperature dependence of relaxations differ for reversible addition (number of crosslinks changes with temperature) and reversible exchange CANs (number of crosslinks is maintained with temperature). Stress relaxation measurements in shear mode were subsequently used to verify the observations from DEA.

6.3 - EXPERIMENTAL SECTION

Materials: Pentaerythritol tetrakis(3-mercaptopropionate) (PETMP), diphenyl(2,4,6-trimethylbenzoyl) phosphine oxide (TPO), 2,2-dimethoxy-2-phenylacetophenone (DMPA), allyl succinic anhydride (ASA), 1,1'-(methylenedi-4,1-phenylene)bismaleimide (MPBM), (1,4-diazabicyclo[2.2.2]octane) (DABCO), and ethoxylated trimethylolpropane triacrylate (MW ~ 692 g/mol) were all purchased from general suppliers (Sigma Aldrich, TCI Chemicals) and used as delivered. Thioester diene (TEDE) and ethoxylated trimethylolpropane trifuran (ETMPTF) were synthesized according to previous methods[13, 34].

Dielectric analysis: Dielectric analysis was performed on a ModuLab XM Material Test System (AMETEK Scientific Instruments, UK). Isothermal temperature sweeps were performed over a range of .03 - 10^6 Hz under an applied sinusoidal voltage of 4500 mV in amplitude. Samples were prepared on Mini-Varicon[TM] sensors as described below. Diels-Alder and thiol-anhydride samples

were equilibrated at a given temperature for 30 minutes before a spectrum was taken. Thiol-ene samples were allowed to equilibrate for 10 minutes before a spectrum was taken.

Dynamic Mechanical Analysis: Glass transition temperature (T_g), storage modulus ($E^{'}$), and loss modulus ($E^{''}$) were measured on an RSA G2 dynamic mechanical analyzer (TA Instruments) using a temperature ramp rate of 3°C/min and a frequency of 1 Hz, with an oscillating strain of 0.03 % and a preload force of 0.40 N.

Stress Relaxation: Stress relaxation was performed on an ARES G2 rheometer (TA Instruments), all samples were subjected to isothermal shear strain of 10% at each temperature. Diels-Alder and thiol-anhydride samples were equilibrated at a given temperature for 30 minutes before a spectrum was taken. Thiol-ene samples were allowed to equilibrate for 10 minutes before a spectrum was taken.

Polymerization conditions:

Thiol-ene thioester samples: The alkene monomer TEDE (1 equivalent of alkene) was added to a vial followed by 1 wt% TPO photoinitiator, along with 4 mol% DABCO relative to the monomers for the dynamic samples, and the mixture was stirred until all the solids had dissolved. PETMP was then added (2 equivalents with respects to thiol) and the mixture was well stirred. Samples cast between glass slides were cured at 15 mW/cm^2 using 405 nm light for 5 minutes on each side. Interdigit samples were cured at 15 mW/cm^2 using 405 nm light for 10 minutes. Samples were then post-cured at 60°C for 1 hour to ensure full conversion.

Diels-Alder samples: The monomer ETMPTF (1.05 equivalent furan) and MPBM (1 equivalent maleimide) were mixed in a vial and heated to 150 °C for 25 minutes and were stirred using a vortex mixer. Glass slides were also heated to this temperature to facilitate sample casting. Once

mixed, samples were prepared by pouring the monomer mixture onto hot glass slides, or directly onto the interdigit probe. The sample was subsequently cooled for several seconds before the monomer mixture was sandwiched with another warm glass slide separated by 250 µm spacer. Samples were then heated to 120 °C for 20 minutes, then gradually cooled to 60 °C over the course of 1 hour and removed from the oven. This heating/cooling procedure was implemented for the ITO samples with 100 µm spacers ensure good surface contact and a known sample thickness. All samples equilibrated at room temperature for 24 hours before testing.

DEA Sample Preparation:

ITO samples preparation: ITO coated glass (Instec D256A-X000 Liquid Crystal Cells) was used to prepared dielectric samples in a parallel plate configuration. Samples were first prepared by depositing monomer mixture between two regular glass slides with 100 µm spacers. The sample was then cured according to the procedure for the appropriate monomer mixture. A 10 mm x 7 mm rectangle was then cut from this film and placed between the conductive sides of two pieces of ITO coated glass and clamped with binder clips.

Interdigit sample preparation: Interdigit samples were prepared on Mini-Varicon^{TM} sensors purchased from Lambient Technologies. The probe was attached to a glass slide with tape and 250 µm spacers on either side. The monomer resin was then deposited onto the probe and another glass slide was used to sandwich the probe and resin together. For photopolymerized resins, the samples were prepared directly under the area to be irradiated.

6.4 - RESULTS AND DISCUSSION

In order to compare the relaxation times and any distributional effects on the relaxation of various dynamic networks, a Cole-Cole fit for a single relaxation was used to determine the

frequency, and therefore relaxation time, of a given relaxation[1]. This model was selected because there was no asymmetry in the relaxations measured in this work, so a simple symmetric stretch factor was sufficient to describe the relaxation. The equation used for this fit are shown below (**Equation 1**):

$$M^* = M_\infty + \frac{\Delta M}{1+(i\omega\tau)^\beta} \tag{1}$$

Here, M* is the complex electric modulus, M_∞ is the electric modulus at $\omega = \infty$, $\Delta M = M_\infty - M_0$ is the relaxation strength, M_0 is the electric modulus at $\omega = 0$, ω is the frequency, τ is the relaxation time, and β is the symmetric stretch factor. MatLab[TM] was used to fit τ and β to experimental data using the M_∞ and ΔM that were measured experimentally. The α-relaxation, which corresponds to the segmental motions associated with the glass transition, was measured at different temperatures because this peak has been observed to shift when dynamic bonds are present in polymer networks[31, 32].

For these experiments, three chemistries with known exchange characteristics where selected. An overview of the monomers used to make three types of dynamic networks used in this work is provided in **Figure 6.2**. First, thioester containing thiol-ene networks were selected for a
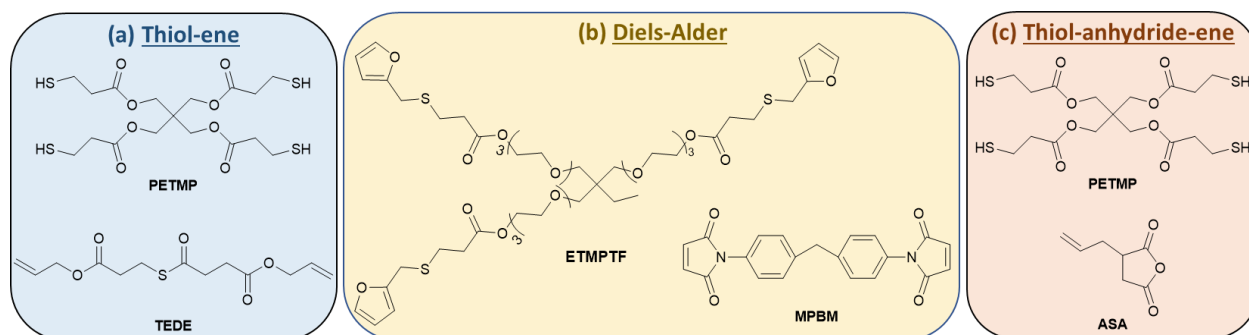
Figure 6.2: Structures for the monomers used in this study for three different dynamic network chemistries: a) Thiol-ene networks made from PETMP and TEDE that contain thioester bonds capable of thiol-thioester exchange (reversible addition only), and catalyzed using the DABCO as a nucleophile, b) Diels-alder networks from ETMPTF and MPBM (reversible addition only), and c) Thiol-anhydride-ene networks made from PETMP and ASA that contain thioester bonds capable of both thiol-thioester exchange and reversible thiol-anhydride addition (both reversible addition and reversible exchange), and catalyzed using the DABCO as a nucleophile.

network that is capable of primarily reversible exchange reactions (**Figure 6.2a**). Next, Diels-Alder networks made by directly polymerizing furan and maleimide functionalities in the network were selected for reversible addition (**Figure 6.2b**). Lastly, thiol-anhydride-ene networks were selected to form thioesters that are capable of both reversible addition and exchange (**Figure 6.2c**). Bond exchange for both thioester networks was catalyzed with a nucleophilic catalyst, DABCO[31].

6.3.2 - Comparison of ITO and Interdigit Dielectric Probes

The type of dielectric probe and sample preparation has a significant impact on the measurement, as it is crucial to have good surface contact between the conducting surface of the probe and the polymer sample. Two dielectric probe types were considered here: Indium-tin-oxide (ITO) coated glass and interdigit probes, which consist of metal electrodes on a thermally stable polymer surface. One principal difference between the parallel plate configuration for ITO coated glass (**Figure 6.3a**) and interdigit probes (**Figure 6.3b**), which have the comb-like arrangement of metal electrodes, is sample preparation and the quality of the resulting probe/polymer interface.
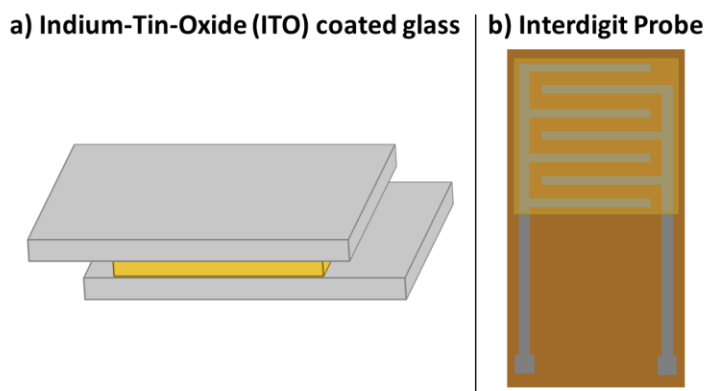
Figure 6.3: Diagram showing the sample geometries for: a) ITO coated glass, where a premade sample of known dimensions is cut and placed between the conductive sides of two ITO glass plates, and b) interdigit probe, where the liquid resin can fill the channels on the surface of the probe before being cured.

Samples prepared on ITO glass, as those prepared by Podgorski et al.[32] and in this work, are typically polymerized, cut with known dimensions, then placed between ITO plates and heat

treated to maximize interfacial contact. This process is sensitive to the consistency and quality of the ITO coating itself and how strenuously air bubbles are excluded from the interface when the sample is prepared. While it is easier to prepare samples with good surface contact for dynamic networks because the dynamic bonding can be leveraged to improve surface contact, eliminating air pockets completely is still a challenge. In contrast, samples on interdigit probes are prepared by depositing and curing the liquid resin directly onto the probe or submerging the probe in the liquid mixture. Curing the sample directly onto the probe in this manner increases the likelihood of good surface contact because the liquid resin can more easily flow into the electrode channels while minimizing likelihood of trapped air pockets between the polymer and the probe.

As stated above, discrepancies between the data from Podgorski *et al*. and Bongiardina *et al*. indicate that at low frequencies there is a significant plateau in the real electric storage modulus taken on ITO coated glass that is not observed for measurements taken on interdigit probes for similar materials[31, 32]. It is hypothesized here that these discrepancies are due, at least in part, to differences in testing geometry and the associated electrode/sample interface after sample preparation. To test this hypothesis, samples were prepared on both ITO glass and interdigit probes to verify these differences for two dynamic networks: a thioester containing thiol-ene networks with and without catalyst, and a Diels-Alder networks. This experimental design includes a non-dynamic control (thiol-ene with no catalyst), a reversible exchange network (thiol-ene with catalyst), and a reversible addition network (Diels-Alder) to determine if mechanism of dynamic bonding has any impact on the discrepancies between the types of dielectric probes.

The thioester networks made from PETMP and TEDE (**Figure 6.2a**) either with or without 4 mol% DABCO as a nucleophilic catalyst were first considered. The real (M') and loss (M") electric moduli as a function of frequency for thioester containing thiol-ene networks without

catalyst are provided in **Figure 6.4a and 6.4b**, respectively, and with catalyst in **Figure 6.4c and 6.4d**, respectively. As expected, there is a clear plateau in the M' for samples prepared on ITO coated glass, but for the interdigit samples there is slight inflection point in the same region that occurs at nearly three orders of magnitude lower intensity. The network containing catalyst to facilitate bond exchange shows a more pronounced inflection point than the network without catalyst at a given temperature. This plateau is indicative of interfacial polarization which in general occurs due to poor surface contact between the sample and the ITO surface[2]. Interfacial
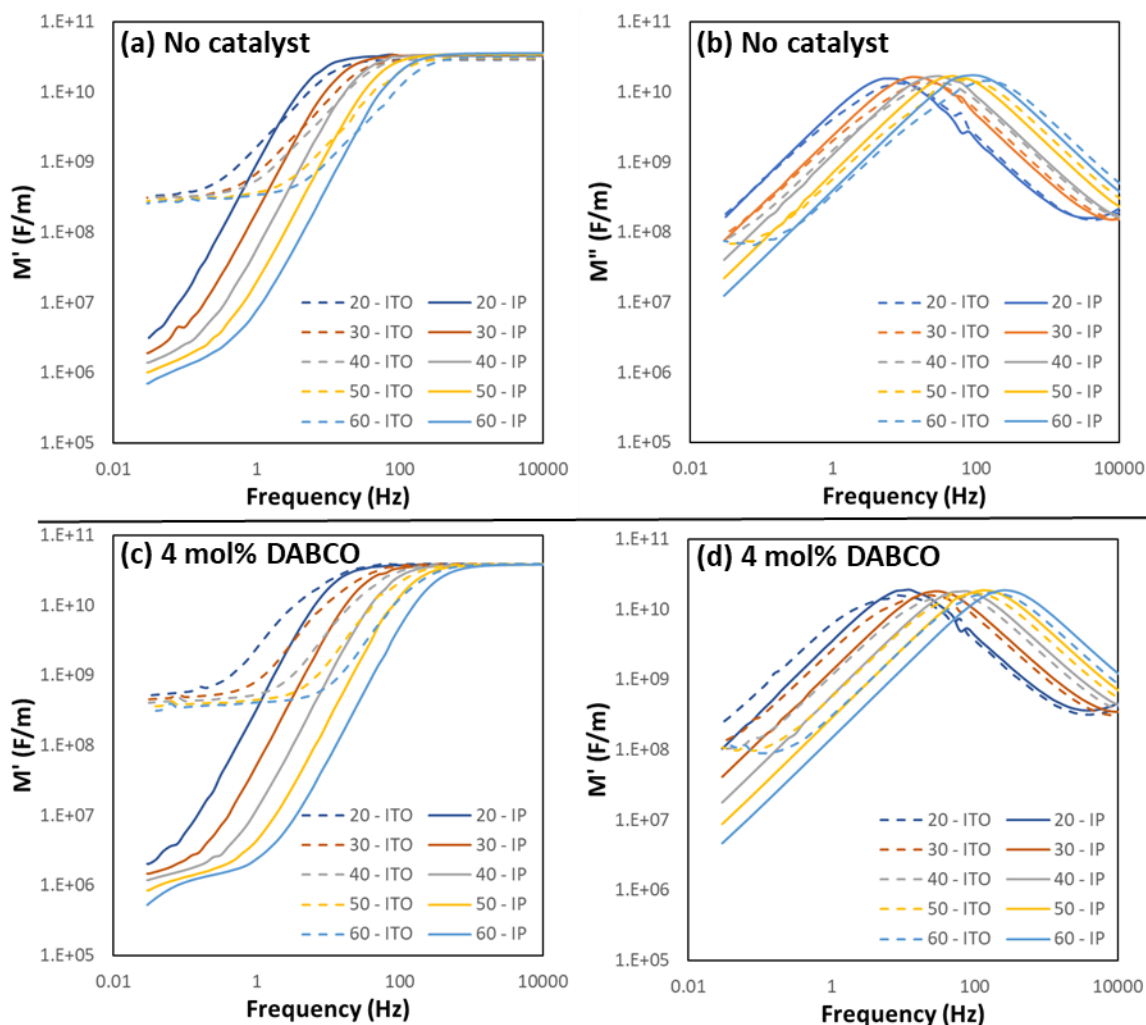
Figure 6.4: Dielectric spectra for thioester networks with a 2:1 ratio of thiol to alkene at various temperatures, where dashed lines (---) are samples taken on ITO coated glass and solid lines (—) are sample taken on the IP's. a) Real electric modulus versus frequency on samples without catalyst, b) loss electric modulus versus frequency on samples without catalyst, c) Real electric modulus versus frequency on samples with 4 mol% DABCO, b) loss electric modulus versus frequency on samples with 4 mol% DABCO.

polarization comes into play at low frequencies because there is sufficient time for charges and impurities to separate as the oscillation of the electric field slows. While observed changes in this plateau region in M' may be caused in part by the dynamics of the polymer network[32], these data suggest that the plateau is likely an artifact of interfacial polarization[2] associated with the ITO test geometry. It is only span of this plateau that is likely impacted by the rate of bond exchange, rather than caused by that bond exchange itself. It is also possible that the inflection at low frequencies observed for interdigit samples is a weaker interfacial effect that is minimized by the surface contact and elimination of trapped air pockets. In addition, there is a plateau/increase in M" at low frequencies that coincides with the plateau in M' and is associated with this interfacial charge separation[2]. This increase in more apparent at higher temperatures and occurs for samples with and without catalyst.

Additional evidence of interfacial effects, especially due to sample preparation, appeared in the symmetric stretch factor obtained from the Cole-Cole fit of these data shown in **Table 6.1**. For the interdigit probes this stretch factor is about one, which means that the relaxation behaves as a nearly ideal Debye relaxation[1]. However, a small decrease in the stretch factor is observed for the ITO samples, and this stretch factor increases one for the catalyzed samples as temperatures is increased and surface contact improves due to bond exchange. While this effect is quite small, the

Table 6.1: The symmetric stretch factor (β) from the Cole-Cole fit of the dielectric spectra the thioester networks, both with and without 4 mol% DABCO as a nucleophilic catalyst, on ITO coated glass or interdigit probes.

	Stretch Factor (β)			
	ITO Coated Glass		Interdigit Probe (IP)	
T (°C)	No Cat	DABCO	No Cat	DABCO
20	0.93	0.86	0.99	0.99
30	0.94	0.88	0.98	0.99
40	0.94	0.89	0.99	0.98
50	0.98	0.91	0.98	0.99
60	0.94	0.92	1.00	0.98

importance of sample preparation for different test geometries to obtain accurate and repeatable measurements should not be overlooked. Moreover, it is important to note that non-idealities due to interfacial interactions should not be misconstrued for network heterogeneity, which is has, for example, been observed due to heterogeneity introduced by permanent network damage in self-healing experiments[5]. Lastly, the frequency at which the relaxation occurs, denoted by a peak in M", was not significantly impacted by the test geometry.

Based on this data, it was hypothesized that improving surface contact may eliminate the plateau for ITO samples and bring them in line with the interdigit samples. A Diels-Alder network containing 5% excess furan was prepared by depolymerizing-then-repolymerizing a sample between ITO glass plates with 100 µm spacers, as well as direct polymerization onto the interdigit probe (**Figure 6.5a and 6.5b**). These spacers caused a slight decrease in the magnitude of the moduli for the ITO sample, but measurements were otherwise unaffected.
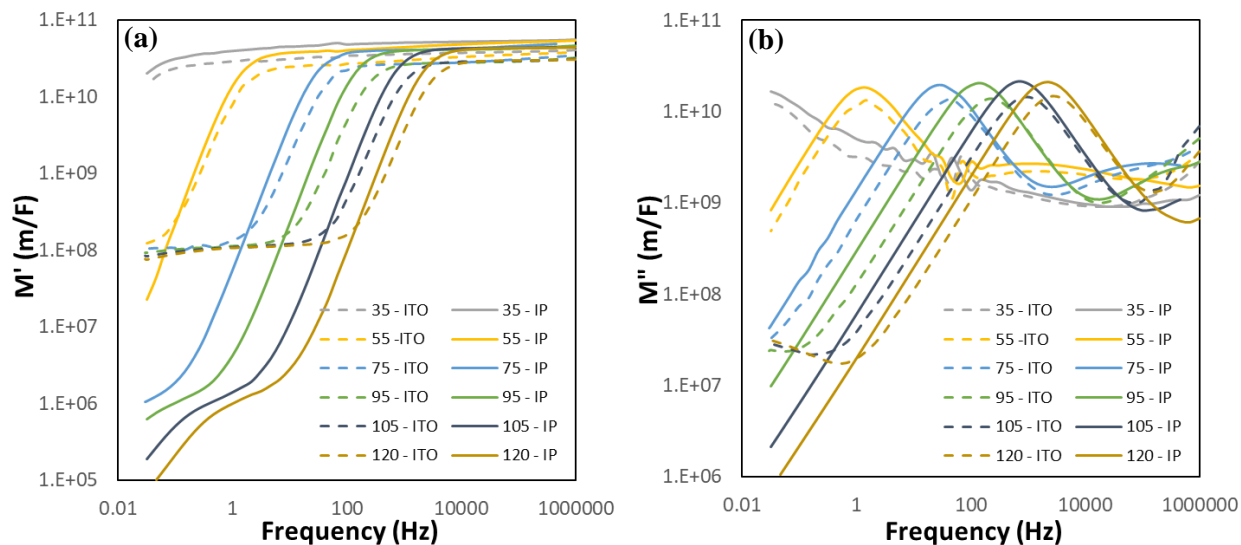
Figure 6.5: Dielectric spectra for a Diels-Alder network at various temperatures, where dashed lines (---) are samples taken on ITO coated glass and solid lines (—) are samples taken on the IP's. a) Real electric modulus versus frequency, and b) loss electric modulus versus frequency.

First, surface contact was improved as indicated by the stretch factor of nearly one for both ITO and interdigit samples at every temperature. There was no temperature effect on the stretch

factor because repolymerization the sample between the ITO plates created a well-adhered interface. However, despite the improved interface there was still a significant plateau in M' and a plateau/increase in M" at frequencies below the α-relaxation. This plateau coincides with the inflection in M' for the interdigit samples in the same manner observed for the thioester networks. This is a good indication that this plateau is inherent to the ITO configuration and not intrinsic to the dynamic networks. However, because the interfacial effects due to sample preparation have been minimized in this case, the exact reason for this low frequency behavior for this material is unclear at this time.

Nevertheless, utilizing interdigit probes is recommended to minimize the impact of sample preparation and interfacial polarization on dielectric spectra. Moreover, care should be taken to not misconstrue interfacial effects associated with the test geometry with dynamics that are intrinsic to the network, especially because these interfacial effects will also be impacted by bond dynamics.

6.4.2 - DEA and Stress Relaxation for Different Dynamic Bonding Mechanisms

To study the dielectric relaxations of CANs of differing dynamic bond mechanisms, time-temperature-superposition (TTS) was used to evaluate the temperature dependence of the dielectric spectra. In polymers, TTS is based on the principle that changes in relaxation processes shift in the same manner whether the time scale (frequency) or temperature of the measurement is varied. In the frequency domain, spectra taken at different temperatures are superimposed to generate a master curve at a reference temperature. This approach enables a description of the relaxation processes over a wider frequency range than is experimentally accessible at a given temperature for a given measurement technique. A set of spectra are superimposed using a horizontal shift factor (a_T) such that $a_T = \tau/\tau_r$. Here, τ is the characteristic relaxation time a given relaxation at a

given temperature and τ_r is the relaxation time at the reference temperature. Generating a master curve is only possible if the processes captured are relatively invariant with temperature over the measured temperature range. It has been observed in rheological measurements that CANs often do not follow time-temperature-superposition because dynamic bonds induce structural changes as temperature increases, especially for reversible addition networks[13, 35], although there is some precedent for superposition in reversible addition networks[36]. However, DEA may provide deeper insights into relaxation processes in CANs because (1) creating a master curve is not required to observe processes that occur above 100 Hz (a typical limit for rheological measurements) at a given temperature and (2) broad frequency ranges provide a more robust assessment of a potential master curve because there is more overlap between spectra at each temperature than possible through rheological measurements. All relaxation times were determined using a Cole-Cole fit in MatLab[TM].

Stress relaxation in shear mode was used as a basis of comparison to DE. Relaxation times at various temperatures were determined experimentally to be the time at which the normalized stress decreased to a value of 1/e (~0.367). TTS was then performed using an average value for a_T at a given temperature to determine whether a master curve could be constructed from the stress relaxation data.

Three dynamic network types were studied (**Figure 6.2**): i) reversible addition networks composed from Diels-Alder linkages, ii) reversible exchange networks containing thioesters, and iii) mixed mechanism networks composed of thiol-anhydride adducts.

Diels-Alder: Reversible Addition

Diels-Alder networks were utilized to study a crosslinked network that is only capable of reversible addition. The Diels-Alder reaction was used directly as the crosslinking reaction by polymerizing a trifunctional furan monomer (ETMPTF) and a difunctional maleimide (MPBM).
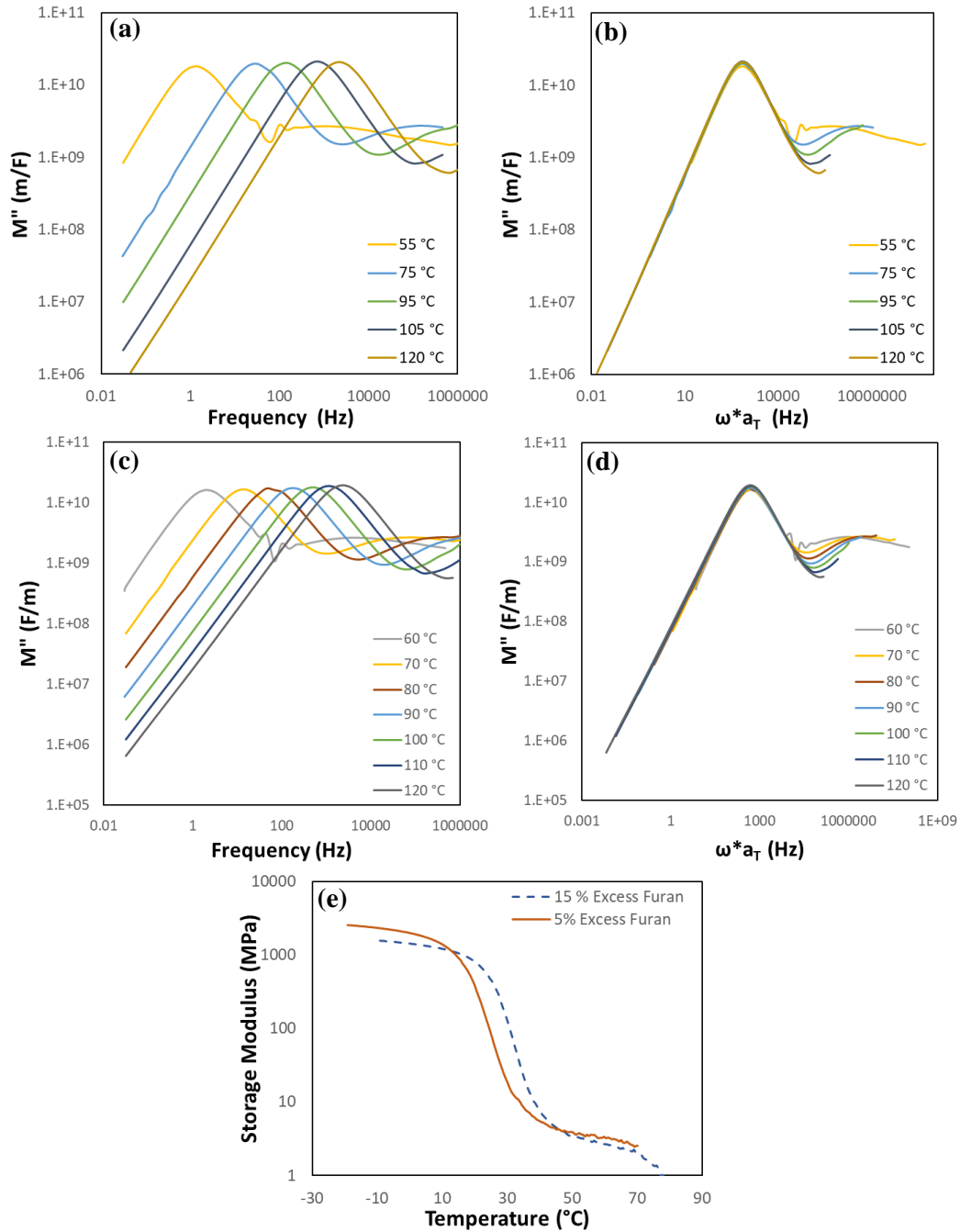
Figure 6.6: a) Dielectric spectra for the DA Network with 5% excess furan at various temperatures ,b) the master curve constructed for 5% excess furan from the loss modulus where 105 °C was used as the reference temperature, c) Dielectric spectra for the DA Network with 15% excess furan at various temperatures, d) the master curve for 15% excess furan constructed from the loss modulus where 105 °C was used as the reference temperature, and e) the storage moduli of both DA networks measured by DMA.

(**Figure 6.2b**). Monomer stoichiometries with either 5% or 15% excess furan were used to modulate the temperature at which delegation of the network would occur, where the material made with 15% excess furan is less crosslinked and will tend to de-gel at a lower temperature[37] (**Figure 6.6e**).

The electric loss moduli as a function of frequency at various temperatures for the DA networks with 5% and 15% excess furan are shown in **Figure 6.6a and 6.6c**, respectively. The relaxation times at 105 °C in each set of spectra were used as the reference to calculate a_T at each temperature, and the superimposed spectra are shown in **Figure 6.6b and 6.6d**, respectively. The α-relaxation peaks superimpose quite well at every temperature, indicating that this relaxation does not change significantly over this temperature range. However, the spectra diverge at frequencies above the α-relaxation, indicating that the α-relaxation and the higher frequency relaxations have different temperature dependencies. This trend holds for the same monomers with 15% excess furan (**Figure 6.6b**). The superposition of the relaxation itself and lack thereof at higher frequencies are consistent with shear rheology for similar DA networks investigated by Sheridan *et al.*[13] In this work, the authors observed the same divergence in the superimposed spectra at high frequencies, which they attributed to differing temperature dependences for backbone bond breakage (reversion of the DA-linkage) and small cluster diffusion[13, 35, 38].

Stress relaxation in shear mode was utilized to further study if TTS is applicable to these networks. The relaxation spectra at various temperatures for the DA networks with 5% and 15% excess furan are shown in **Figure 6.7a and 6.7c,** respectively. The relaxation times at 80 °C in each set of spectra were used as the reference to calculate a_T at each temperature, and the superimposed spectra are shown in **Figure 6.7b and 6.7d**, respectively. Instrumentation constraints limited the high temperature range to 95°C. Here, the difference in gelation temperature
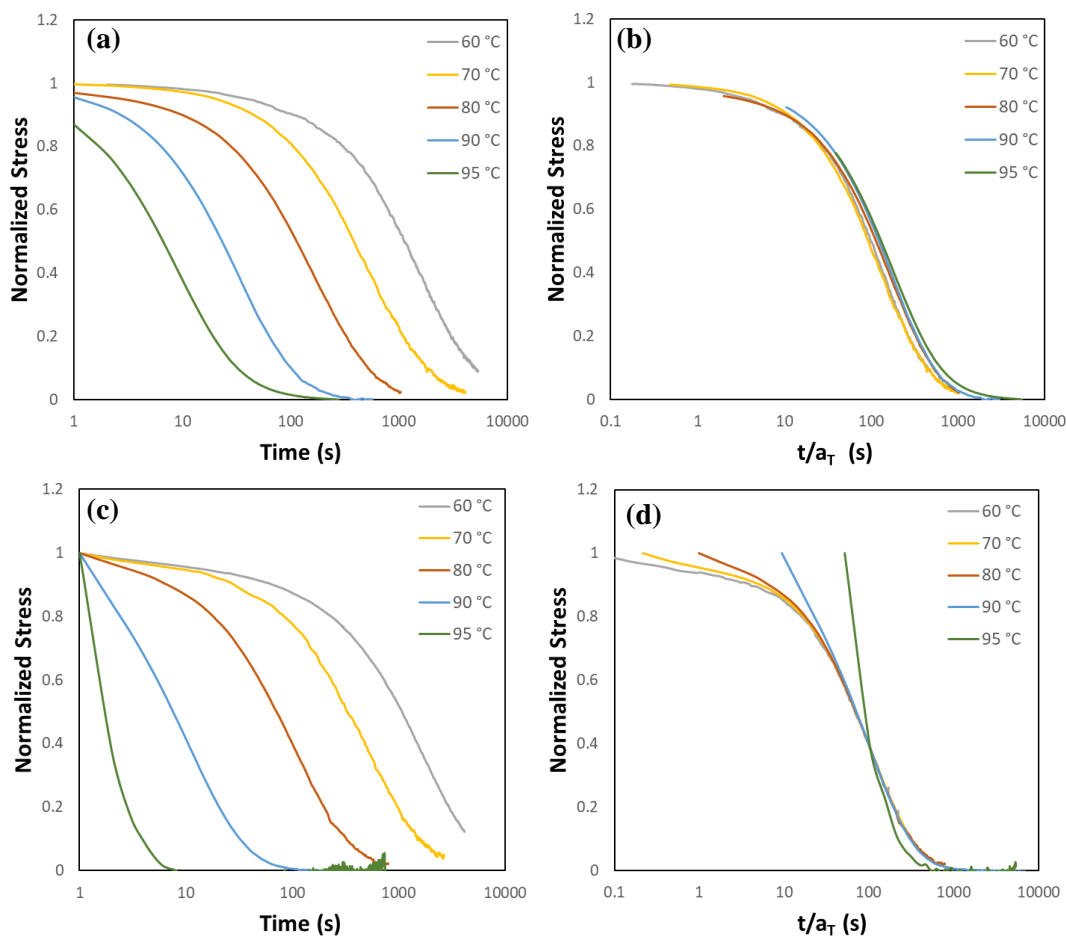
Figure 6.7: a) Normalized stress as a function of time with 5% excess furan and b) the master curve constructed from the stress relaxation with 5% excess furan data where 80 °C was used as the reference temperature to calculate the horizontal shift factor, a_T, c) Normalized stress as a function of time with 15% excess furan and b) the master curve constructed from the stress relaxation with 15% excess furan data where 80 °C was used as the reference temperature.

between these two stoichiometries becomes apparent. The network made with 5% excess furan relaxes more slowly, especially at higher temperatures. This behavior results because the network is more crosslinked and has fewer free furan groups at any given temperature to facilitate network rearrangement than the materials with 15% excess furan. In turn, the relaxation spectra superimpose relatively well because the network behaves more as a crosslinked network over this temperature range. In contrast, the spectra with 15% excess furan do not superimpose well and become progressively less superimposable as temperature increases and the material is behaving

110

more as a liquid than a crosslinked polymer. Overall, TTS from both DEA and stress relaxation qualitatively support prior observations that superposition is not suited to describe temperature-dependent structure over the entire temperature-frequency range.

Thiol-Thioester Exchange: Reversible Exchange

Next, a thiol-ene network containing thioester bonds from a tetrafunctional thiol (PETMP) and a thioester containing diene (TEDE) was utilized to study a thioester containing network that is only capable of reversible exchange (**Figure 6.2a**). A 2:1 ratio of thiol to alkene was used such that free thiol was present to facilitate in bond exchange. A control without catalyst which should be a non-dynamic network and a dynamic network with a nucleophilic catalyst, DABCO, were made to compare static and dynamic networks.

The electric loss moduli at various temperatures for networks with and without 4 mol% DABCO are shown in **Figure 6.8a and 6.8c**, respectively. The relaxation time at 50 °C was used as the reference to calculate a_T at each temperature, and the superimposed spectra are shown in **Figure 6.8b and 6.8d**, respectively. These networks have identical glass transition temperatures and the network with catalyst has a slightly lower rubbery storage modulus (**Figure 6.8e**), which is typically observed for thioester networks with moderate catalyst loading[39]. As expected for a non-dynamic crosslinked polymer, the network without catalyst superimposes well at all frequencies over this temperature range. However, the entire spectra for samples with active dynamic bonds also superimposes quite well, even at frequencies above the α-relaxation. This behavior is likely because the thiol-thioester exchange does not significantly change the number of bonds in the network as temperature increases, only the topology. Although the rate of bond exchange is certainly sensitive to temperature, the overall number of thioester bonds present in the network is not. In other words, the dynamic thioester network does not have a temperature-

dependent structure in the same manner as the reversible addition Diels-Alder system over this temperature range. The notion that reversible addition networks can be superimposed has been observed in rheological analyses of PDMS[36]. Stress relaxation measurements in shear confirm that
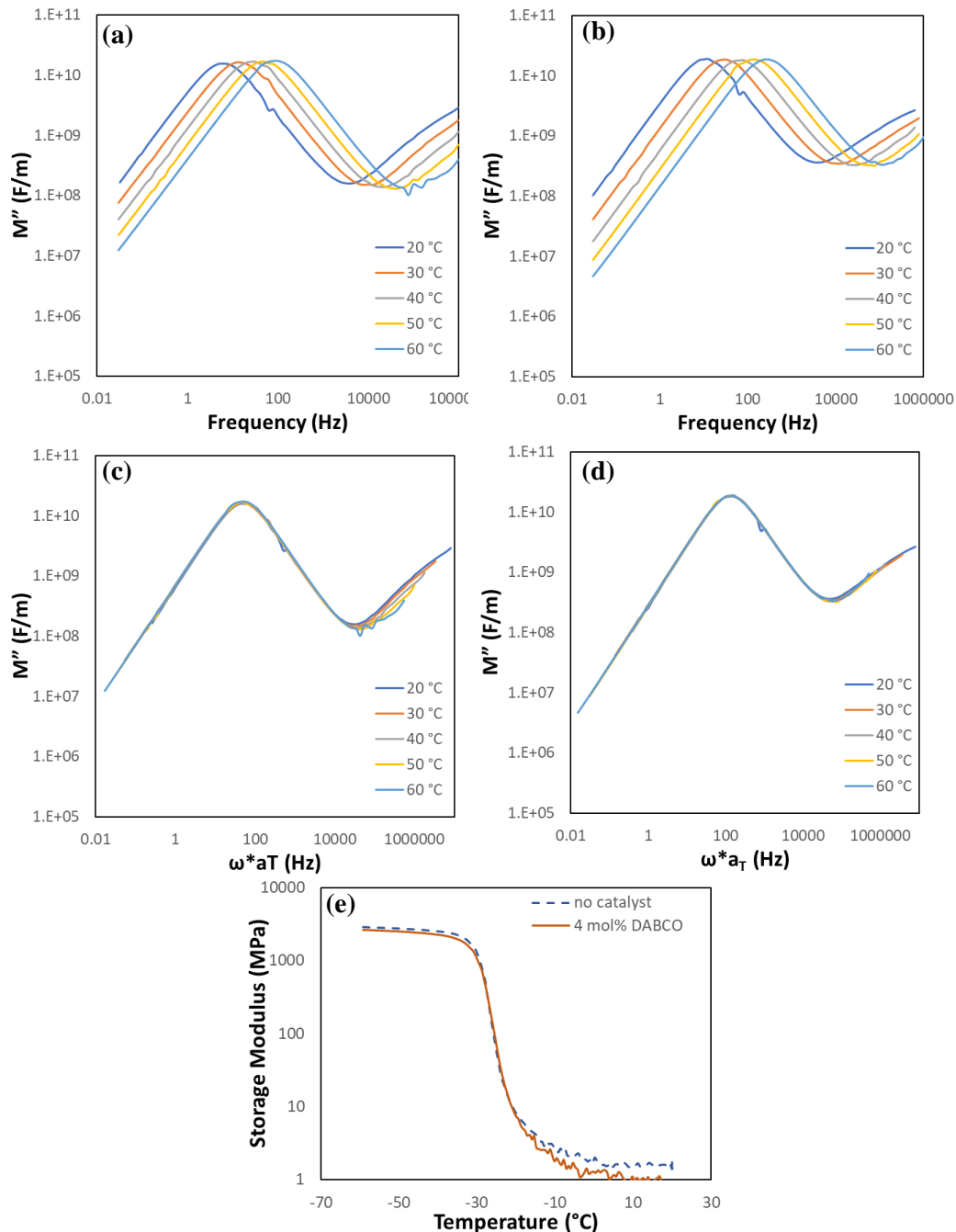
Figure 6.8: a) Loss modulus spectra for the thioester network without catalyst at various temperatures, b) the master curve constructed from the loss modulus for the thioester network without catalyst where 50 °C was used as the reference temperature, c) loss spectra for the thioester network with 4 mol% DABCO at various temperatures , d) the master curve constructed from the loss modulus for the thioester network with 4 mol% DABCO where 50 °C was used as the reference temperature, and e) the storage moduli of thioester networks measured by DMA.

these thioester networks do not undergo a change in the number of crosslinks with temperature, shown with catalyst present in **Figure 6.9**. Indeed, the relaxation spectra (**Figure 6.9a**)
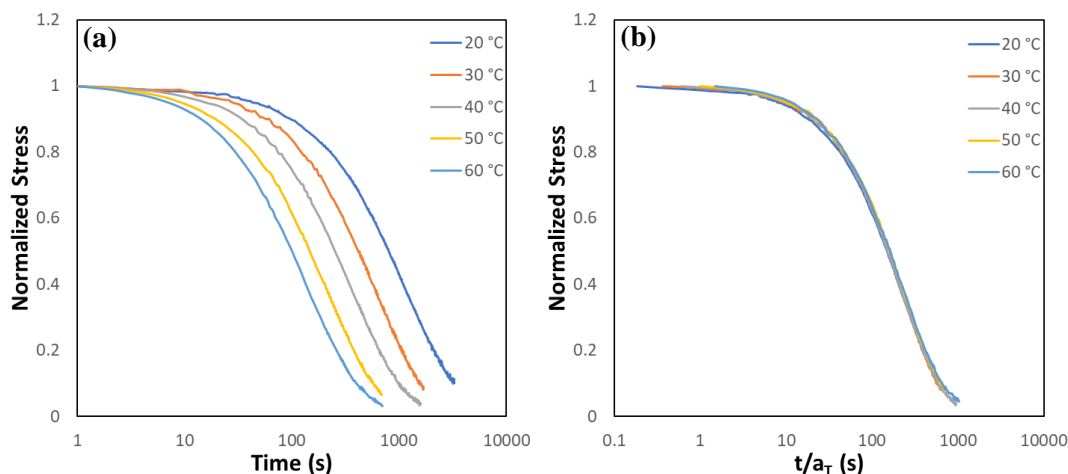
Figure 6.9: a) Normalized stress versus time for thioester networks with 4 mol% DABCO, and b) superimposed of the normalized stress for thioester networks at various temperatures. The relaxation time at 50 °C was used at the reference to calculate the horizontal shift factor (a_T).

superimpose nearly perfectly (**Figure 6.9b**), indicating that there is not a strong difference between the temperature dependence of the stress relaxation and the number of crosslinks over this temperature range. These thioester networks do not significantly relax stress without a catalyst being present[23]

Thiol-anhydride adducts: Reversible Addition and Exchange

Finally, thiol-anhydride-ene networks were utilized by polymerizing PETMP and allyl succinic anhydride (ASA), (**Figure 6.2c**) via thiol-anhydride and thiol-ene reactions. Networks made with 5% excess anhydride and 50% excess thiol were made to bias the system toward either reversible addition (due to a lack of thiols to participate in thioester exchange at lower temperatures) or reversible exchange (due to the large excess of free thiol), respectively[32]. Finally, 5 mol% DABCO was used to catalyze the thiol-anhydride addition and both dynamic mechanisms.

The electric loss moduli at various temperatures for networks with and without 4 mol% DABCO are shown in **Figure 6.10a and 6.10c**, respectively. The superimposed loss moduli for

networks with and without 5% excess anhydride and 50% excess thiol are shown in **Figure 6.10b and 6.10c**, respectively, with a reference temperature of 80°C. As observed for both the Diels-Adler networks and the exchange thioester network, the relaxation itself overlaps quite well for
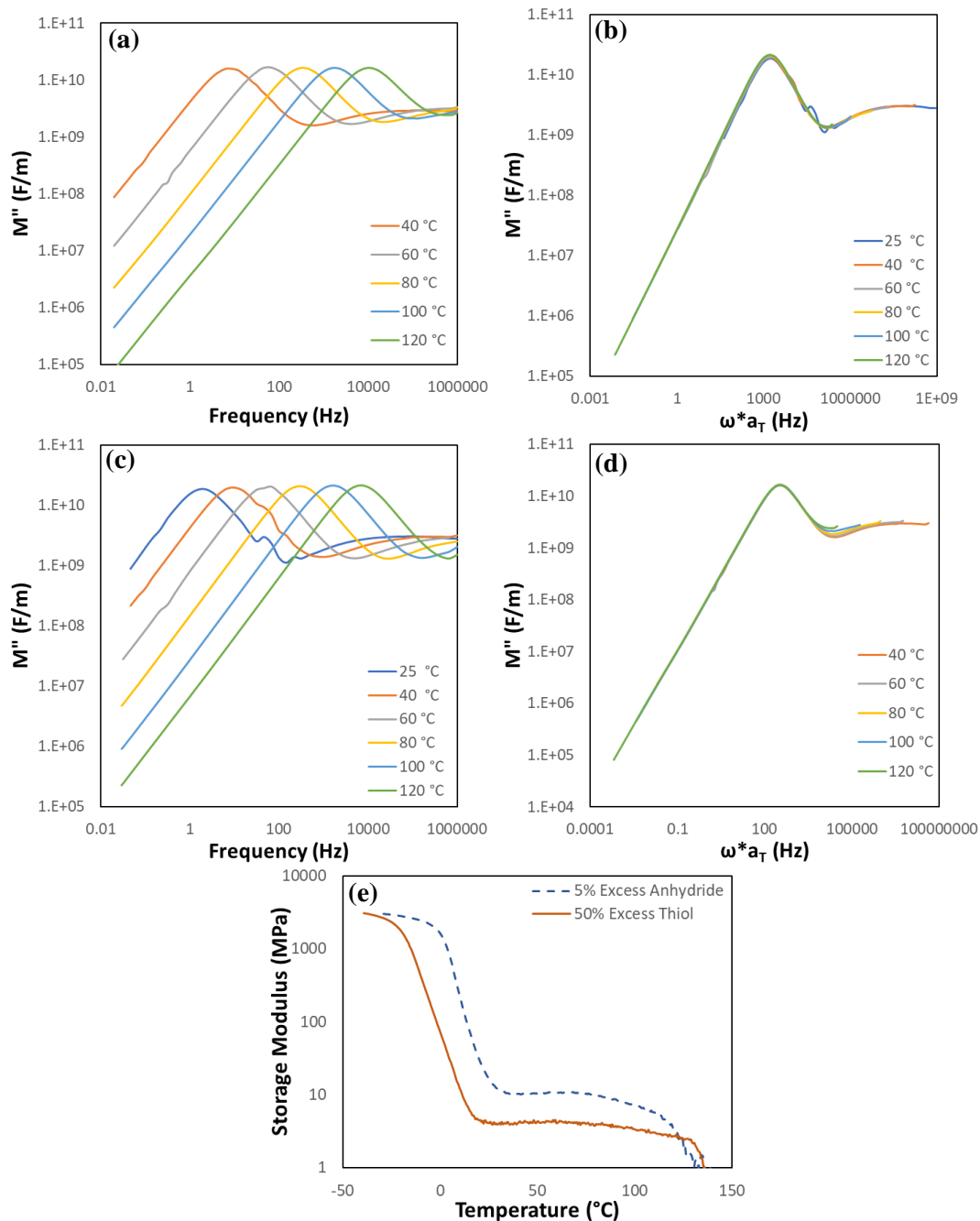
Figure 6.10: a) Loss modulus spectra for the thiol-anhydride network with 5% excess anhydride at various temperatures, b) the master curve constructed from the loss modulus for the thiol-anhydride network with 5% excess anhydride, where 80 °C was used as the reference temperature, c) loss spectra for the for the thiol-anhydride network with 50% excess thiol at various temperatures , d) the master curve constructed from the loss modulus the thiol-anhydride network with 50% excess thiol, where 80 °C was used as the reference temperature, and e) the storage moduli of thioester networks measured by DMA.

both stoichiometries, regardless of which mechanism is preferred. However, the spectra for the 5% excess anhydride material did not perfectly superimpose at higher frequencies, which is expected for a reversible addition CAN whose structure depends on temperature. The divergence at higher frequencies was less pronounced than for the Diels-Alder systems. This behavior arises because at higher temperatures thioester exchange also becomes faster due to the increased thiol concentration, meaning relaxation is occurring due to both mechanisms in this system. On the other hand, spectra for the 50% excess thiol material overlap almost perfectly across the entire frequency range. This result corresponds with behavior in the pure thioester exchange networks, likely because the large excess of thiol strongly biases thiol-anhydride reaction toward the thioester product and bond rearrangement toward exchange. Indeed, the storage modulus as measured by DMA for the sample with 5% excess anhydride begins to drop around 95°C and continues to drop more precipitously that the network with excess thiol (**Figure 6.10e**).

Stress relaxation data for both stoichiometries is shown in **Figure 6.11a** and **6.11b** for 5% excess anhydride and 50% excess thiol, respectively, up to 95°C, and the superimposed spectra are provided in **Figure 6.11a** and **6.11b,** respectively. Both sets of spectra superimpose quite well over this temperature range. The upper temperature range of the instrument is limiting to observe possible deviations from a master curve for the 5% excess anhydride material. However, the relaxation times with 50% excess thiol are significantly faster at every temperature. For example, at 70 °C the average relaxation time for excess anhydride is 2900 seconds compared to 1100 seconds with excess thiol. The fact that the dielectric spectra for this stoichiometry superimpose despite significantly faster relaxation times supports the hypothesis that CANs that undergo reversible exchange do not undergo significant changes in the total number of crosslinks, and that overall network topology is maintained. However, because the changes in network structure were

not readily observable until about 95°C, the upper limit of the instrument range, data at higher temperatures is required to make any further judgements about these mixed mechanism thiol-anhydride systems.
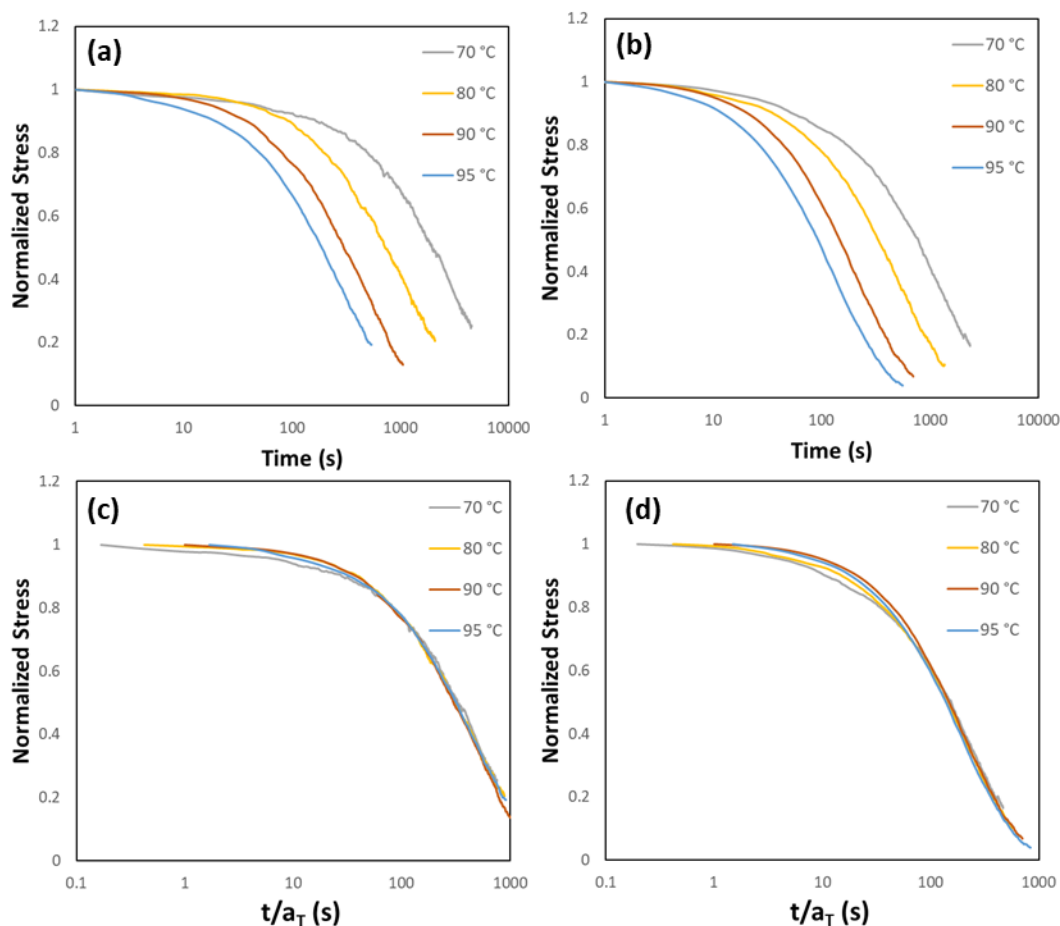
Figure 6.11: a) Normalized stress as a function of time with 5% excess anhydride and b) the master curve constructed from the stress relaxation with 5% excess anhydride data where 80 °C was used as the reference temperature to calculate the horizontal shift factor, a_T, c) Normalized stress as a function of time with 50% excess thiol and b) the master curve constructed from the stress relaxation with 50% excess thiol data where 80 °C was used as the reference temperature.

There are some general considerations to take into account. It should be noted that each of these network types have distinct mechanical properties and temperatures for which their dynamic behavior arises. To account for these differences, measurements were taken in the rubbery state and over a relatively narrow temperature range in some cases. Indeed, the temperature range for some of the stress relaxation measurements was limited by the instrument, and temperatures above

100 °C were not accessible for the Diels-Alder and thiol-anhydride networks. Access to even higher temperatures for both DEA and stress relaxation measurements would be useful to fully explore these temperature dependences. While this works aimed to probe a broad range of dynamic bonding mechanisms, expanding the scope of the dynamic bonds tested using this methodology is necessary to build a complete picture of the impact of bond dynamics on network structure.

Overall, DEA provides a platform studying relaxations in CANs that are limited for conventional DMA analysis using time-temperature-superposition. The broad frequency windows associated with DEA facilitates observation more relaxations directly at a given temperature. Superposition of those spectra were then be used to determine whether those relaxations have different temperature dependencies because there is more overlap between frequency sweeps taken at different temperatures. In CANs for which the overall topology and number of crosslinks changes with temperature (reversible addition), poor superposition at frequencies above the α-relaxation were observed because as temperature increases the network becomes less crosslinked. While the spectra for CANs that largely maintained their topology with temperature (reversible exchange) superimposed quite well at all frequencies because crosslinking does not have a different temperature dependency from the segmental relaxation processes. It would not be possible to observe whether lower temperature spectra superimpose with the high temperature without access to the additional 4 orders of magnitude in frequency compared to standard DMA techniques.

6.5 - Conclusions

Dielectric analysis was implemented to explore the utility of this technique to understand the dynamics over a broad frequency range. Three types of covalent adaptable networks were

examined using a combination of dielectric spectroscopy and stress relaxation to determine how the type of dynamic bonding mechanism impacts dielectric measurements.

Interfacial effects were observed at low frequencies for both ITO and interdigit probes. These effects present as a significant plateau region on ITO glass and a relatively weak inflection for interdigit probes. While measurements in this regime are impacted by dynamic bonding, care should be taken not to misconstrue these low frequency interfacial effects as relaxations are intrinsic to the dynamic network. Measurements using interdigit probes were also less sensitive to sample preparation.

Time-temperature-superposition of the dielectric spectra corresponded well with prior literature using rheological measurements, indicating that the spectra superimpose well when the network structure does not depend on temperature. The spectra for the Diels-Alder network, which follows a reversible addition mechanism, did not superimpose at frequencies above the α-relaxation. The same was true for the thiol-anhydride network with excess anhydride, which also tends toward reversible addition. On the other hand, spectra of the thiol-ene network and the thiol anhydride network with excess thiol, which both follow reversible exchange mechanisms superimposed quite well. Time-temperature-superposition of stress relaxation data of each of these networks agreed with the observations from dielectric analysis.

6.6 - References:

1. Kremer, F.; Schönhals, A., *Broadband dielectric spectroscopy*. Springer Science & Business Media: 2002.

2. Vassilikou-Dova, A.; Kalogeras, I. M., Dielectric analysis (DEA). *Thermal analysis of polymers, fundamentals and applications* **2009**, 497-613.

3. Jilani, W.; Mzabi, N.; Gallot-Lavallée, O.; Fourati, N.; Zerrouki, C.; Zerrouki, R.; Guermazi, H., Dielectric relaxations investigation of a synthesized epoxy resin polymer. *The European Physics Journal Plus* **2015,** (130).

4. Carrertero-Gonzalez, J.; Ezquerra, T. A.; Amnuaypornsri, S.; Toki, S.; Verdejo, R.; Sanz, A.; Sakdapipanich, J.; Hsiao, B. S.; López–Manchado, M. A., Molecular dynamics of natural rubber as revealed by dielectric spectroscopy: The role of natural cross–linking. *Soft Matter* **2010,** (6), 3636-3642.

5. Hernández, M.; Grande, A. M.; van der Zwaag, S.; García, S. J., Monitoring Network and Interfacial Healing Processes by Broadband Dielectric Spectroscopy: A Case Study on Natural Rubber. *ACS Appl Mater Interfaces* **2016,** *8* (16), 10647-56.

6. Lovell, L. G.; Berchtold, K.; Elliot, J. E.; Lu, H.; Bowman, C. N., Understanding the kinetics and network formation of dimethacrylate dental resins. *Polym. Adv. Technol.* **2001,** *12* (6), 335-345.

7. Tsangaris, G. M.; Psarras, G. C.; Kouloumbi, N., Electric modulus and interfacial polarization in composite polymeric systems. *Journal of materials Science* **1998,** (33), 2027–2037.

8. Yang, J.; Melton, M.; Sun, R.; Yang, W.; Cheng, S., Decoupling the Polymer Dynamics and the Nanoparticle Network Dynamics of Polymer Nanocomposites through Dielectric Spectroscopy and Rheology. *Macromolecules* **2020,** *53* (1), 302-311.

9. Carroll, B.; Cheng, S.; Sokolov, A. P., Analyzing the Interfacial Layer Properties in Polymer Nanocomposites by Broadband Dielectric Spectroscopy. *Macromolecules* **2017,** *50* (16), 6149-6163.

10. Tress, M.; Xing, K.; Ge, S.; Cao, P.; Saito, T.; Sokolov, A., What dielectric spectroscopy can tell us about supramolecular networks⋆. *The European Physical Journal E* **2019,** *42* (10), 133.

11. Podgórski, M.; Fairbanks, B. D.; Kirkpatrick, B. E.; McBride, M.; Martinez, A.; Dobson, A.; Bongiardina, N. J.; Bowman, C. N., Toward Stimuli-Responsive Dynamic Thermosets through Continuous Development and Improvements in Covalent Adaptable Networks (CANs). *Advanced Materials* **2020,** *32* (20), 1906876.

12. Khan, A.; Ahmed, N.; Rabnawaz, M., Covalent Adaptable Network and Self-Healing Materials: Current Trends and Future Prospects in Sustainability. *Polymers* **2020,** *12* (9), 2027.

13. Sheridan, R. J.; Bowman, C. N., A Simple Relationship Relating Linear Viscoelastic Properties and Chemical Structure in a Model Diels–Alder Polymer Network. *Macromolecules* **2012,** *45* (18), 7634-7641.

14. Chandross, E. A.; Ferguson, J.; McRae, E. G., Absorption and Emission Spectra of Anthracene Dimers. *The Journal of Chemical Physics* **1966,** *45* (10), 3546-3553.

15. Egerton, P. L.; Hyde, E. M.; Trigg, J.; Payne, A.; Beyton, P.; Mijovic, M. V.; Reiser, A., PhotocycloadditioninLiquidEthylCinnamateandinEthylCinnamateGlasses.ThePhotoreactionasaProbeintotheMicromorphologyoftheSolid. *Journal of the American Chemical Society* **1981,** *103*, 3859-3863.

16.   Ying, H.; Zhang, Y.; Cheng, J., Dynamic urea bond for the design of reversible and self-healing polymers. *Nature Communications* **2014,** *5* (1), 3218.

17.   Zhang, B.; Digby, Z. A.; Flum, J. A.; Chakma, P.; Saul, J. M.; Sparks, J. L.; Konkolewicz, D., Dynamic Thiol–Michael Chemistry for Thermoresponsive Rehealable and Malleable Networks. *Macromolecules* **2016,** *49* (18), 6871-6878.

18.   Fenoli, C. R.; Wydra, J. W.; Bowman, C. N., Controllable Reversible Addition–Fragmentation Termination Monomers for Advances in Photochemically Controlled Covalent Adaptable Networks. *Macromolecules* **2014,** *47* (3), 907-915.

19.   Montarnal, D.; Capelot, M.; Tournilhac, F.; Leibler, L., Silica-Like Malleable Materials from Permanent Organic Networks. *Science* **2011,** *334* (6058), 965-968.

20.   Lei, X. F.; Jin, Y. H.; Sun, H. L.; Zhang, W., Rehealable imide-imine hybrid polymers with full recyclability. *Journal of Materials Chemistry A* **2017,** *5* (40), 21140-21145.

21.   Liu, Y. J.; Tang, Z. H.; Chen, Y.; Wu, S. W.; Guo, B. C., Programming dynamic imine bond into elastomer/graphene composite toward mechanically strong, malleable, and multi-stimuli responsive vitrimer. *Composites Science and Technology* **2018,** *168*, 214-223.

22.   Wang, C.; Mavila, S.; Worrell, B. T.; Xi, W. X.; Goldman, T. M.; Bowman, C. N., Productive Exchange of Thiols and Thioesters to Form Dynamic Polythioester-Based Polymers. *Acs Macro Letters* **2018,** *7* (11), 1312-1316.

23.   Worrell, B. T.; Mavila, S.; Wang, C.; Kontour, T. M.; Lim, C. H.; McBride, M. K.; Musgrave, C. B.; Shoemaker, R.; Bowman, C. N., A user's guide to the thiol-thioester exchange in organic media: scope, limitations, and applications in material science. *Polymer Chemistry* **2018,** *9* (36), 4523-4534.

24.   Worrell, B. T.; McBride, M. K.; Lyon, G. B.; Cox, L. M.; Wang, C.; Mavila, S.; Lim, C. H.; Coley, H. M.; Musgrave, C. B.; Ding, Y. F.; Bowman, C. N., Bistable and photoswitchable states of matter (vol 9, 2804, 2018). *Nature Communications* **2018,** *9*.

25.   Cash, J. J.; Kubo, T.; Bapat, A. P.; Sumerlin, B. S., Room-Temperature Self-Healing Polymers Based on Dynamic-Covalent Boronic Esters. *Macromolecules* **2015,** *48* (7), 2098-2106.

26.   Smithmyer, M. E.; Deng, C. C.; Cassel, S. E.; LeValley, P. J.; Sumerlin, B. S.; Kloxin, A. M., Self-Healing Boronic Acid-Based Hydrogels for 3D Co-cultures. *ACS Macro Letters* **2018,** *7* (9), 1105-1110.

27.   Martin, R.; Rekondo, A.; Ruiz de Luzuriaga, A.; Cabañero, G.; Grande, H. J.; Odriozola, I., The processability of a poly(urea-urethane) elastomer reversibly crosslinked with aromatic disulfide bridges. *Journal of Materials Chemistry A* **2014,** *2* (16), 5710-5715.

28.   Michal, B. T.; Jaye, C. A.; Spencer, E. J.; Rowan, S. J., Inherently Photohealable and Thermal Shape-Memory Polydisulfide Networks. *ACS Macro Letters* **2013,** *2* (8), 694-699.

29.   Podgórski, M.; Mavila, S.; Huang, S.; Spurgin, N.; Sinha, J.; Bowman, C. N., Thiol–Anhydride Dynamic Reversible Networks. *Angewandte Chemie International Edition* **2020,** *59* (24), 9345-9349.

30.   Podgórski, M.; Spurgin, N.; Mavila, S.; Bowman, C. N., Mixed mechanisms of bond exchange in covalent adaptable networks: monitoring the contribution of reversible exchange and reversible addition in thiol–succinic anhydride dynamic networks. *Polymer Chemistry* **2020,** *11*, 5365-5376.

31.   Bongiardina, N. J.; Long, K. F.; Podgórski, M.; Bowman, C. N., Substituted Thiols in Dynamic Thiol–Thioester Reactions. *Macromolecules* **2021,** *54* (18), 8341-8351.

32.   Podgórski, M.; Spurgin, N.; Mavila, S.; Bowman, C. N., Mixed mechanisms of bond exchange in covalent adaptable networks: monitoring the contribution of reversible exchange and reversible addition in thiol–succinic anhydride dynamic networks. *Polymer Chemistry* **2020**.

33.   Porath, L. E.; Evans, C. M., Importance of Broad Temperature Windows and Multiple Rheological Approaches for Probing Viscoelasticity and Entropic Elasticity in Vitrimers. *Macromolecules* **2021,** *54* (10), 4782-4791.

34.   Worrell, B. T.; McBride, M. K.; Lyon, G. B.; Cox, L. M.; Wang, C.; Mavila, S.; Lim, C. H.; Coley, H. M.; Musgrave, C. B.; Ding, Y. F.; Bowman, C. N., Bistable and photoswitchable states of matter. *Nature Communications* **2018,** *9*.

35.   Peterson, A. M.; Palmese, G. R., Reaction Kinetics and Thermodynamic Aspects of Thermoreversibly Cross-Linked Polymer Networks. *Macromolecular Chemistry and Physics* **2013,** *214* (16), 1798-1805.

36.   Porath, L. E.; Evans, C. M., Importance of Broad Temperature Windows and Multiple Rheological Approaches for Probing Viscoelasticity and Entropic Elasticity in Vitrimers. *Macromolecules* **2021**.

37.   Adzima, B. J.; Aguirre, H. A.; Kloxin, C. J.; Scott, T. F.; Bowman, C. N., Rheological and Chemical Analysis of Reverse Gelation in a Covalently Cross-Linked Diels−Alder Polymer Network. *Macromolecules* **2008,** *41* (23), 9112-9117.

38.   Pratchayanan, D.; Yang, J.-C.; Lewis, C. L.; Thoppey, N.; Anthamatten, M., Thermomechanical insight into the reconfiguration of Diels–Alder networks. *Journal of Rheology* **2017,** *61* (6), 1359-1367.

39.   Dobson, A. L.; Bongiardina, N. J.; Bowman, C. N., Combined Dynamic Network and Filler Interface Approach for Improved Adhesion and Toughness in Pressure-Sensitive Adhesives. *ACS Applied Polymer Materials* **2019,** *2* (3), 1053-1060.

Chapter 7 - FLORY-HUGGINS PARAMETERS FOR THIOL-ENE NETWORKS USING HANSEN SOLUBILITY PARAMETERS

7.1: Abstract

Thiol-ene networks based on polar and non-polar monomers at various crosslinking densities were subjected to swelling in organic solvents to measure the Flory-Huggins interaction parameter. To the best of our knowledge, this is the first example of Flory-Huggins measurements for thiol-ene networks in organic media. Experimentally determined values were compared to those predicted using the Hansen solubility parameter approach with the assistance of the HSPiP software, which is used industrially to determine the miscibility. It was shown that the polymer suite in this software does not adequately account for the thioether bonds by underpredicting the dispersive Hansen parameter by roughly 5 MPa$^{0.5}$ when corrected to experimental thiol-ene swelling data. Even with corrections for the thioether bonds, HSPiP and Hansen solubility parameters in general lack the ability to account for structural factors that impact polymer/solvent interaction parameters, especially for crosslinked polymer networks.

7.2: Introduction

Understanding the solubility and swelling of polymer materials through solubility parameters has enabled numerous industrial application processes such as coatings,[1] paints,[2] membrane casting and formation,[3] fiber spinning[4], and in pharmaceutical fields[5]. All these processes are based on the principle that species with similar solubility parameters will exhibit miscibility, resulting in the dissolution or swelling of polymers in a given solvent or solvent system. The intended applications of the polymers require an understanding of polymer solution properties at different processing conditions, which are mainly affected by the interactions between the polymer and solvent. To analyze polymer-solvent interactions, a series of different models have been developed such as Flory-Huggins theory,[6, 7] the UNIFAC-FV formalism,[8] the Sanchez-Lacombe equation of state,[9-11] and statistical associating fluid theory[9, 12]. Due to the simplicity of Flory-Huggins theory, it continues to be the most prominent method for understanding and interpreting the thermodynamics and phase behavior of polymer and polymer/solvent mixtures[13, 14].

The Flory-Huggins interaction parameter (χ) is an estimate of the favorability of the interactions between two substances. Predicting χ for a given solvent/polymer pair is often difficult because it requires knowledge of the specific interactions of the two species for which miscibility is to be determined, especially for novel polymer/solvent pairs. Therefore, a theoretical framework for determining χ for an arbitrary pair of species has been of great interest. One such approach has been to estimate solubility parameters that account for different kinds of intermolecular interactions [15-17]. The concept of a solubility parameter was first introduced by Hildebrand and Scott in 1950[18] and was defined as the square root of the cohesive energy density for each species, which therefore can be determined without the knowledge of how a pair of molecules may interact. The Hildebrand solubility parameter is, however, limited to non-polar polymers and non-polar solvents wherein Van Der Waals interactions are primarily responsible for miscibility or lack thereof. Consequently, Hansen in 1967 extended this theory to account for other kinds of interactions, which are recognized as Hansen solubility parameters.[19, 20] The Hansen model utilizes three solubility parameters derived from three types of intermolecular forces: dispersive (or Van Der Waals) interactions (δ_d), polar interactions (δ_p), and hydrogen-bonding interactions (δ_h) which, when appropriately combined, enable a direct calculation of χ for a given polymer-solvent pair.[21-23] Attempts have been made to accurately measure the interaction parameter using swelling[24, 25], inverse gas chromatography[26-28], and intrinsic viscosity[29-31]. Overall, the most convenient experimental technique for determination of the χ parameter for polymer networks is the measurement of equilibrium swelling.

The most extensively studied crosslinked polymers are based on (meth)acrylates due to their widespread industrial application. For example, Bahar et al. studied poly(2-hydroxyethyl methacrylate) gels with various cross-link densities swollen to equilibrium in the diethylene glycol as solvent to estimate the polymer-solvent interaction. The swelling experiments were used to determine the effective cross-link density.[32] Various other crosslinked polymers have been subjected to swelling behavior in appropriate solvents to determine the polymer-solvent interaction parameter and investigated at different temperature, pH and chemical composition to explore the effect on the interaction parameter for materials such as

crosslinked ethylene–propylene–diene[24], styrene butadiene rubber copolymer[33-35], and cinnamoyloxy ethyl methacrylate with dodecyl acrylate[36]. The Flory-Huggins polymer-solvent interaction parameter has been also utilized as a predictive tool to explain gelation behavior in hydrogels[37, 38] and organogels[39, 40].

Thiol-ene chemistry has emerged as an efficient photopolymerization approach, for example in films, coatings, surface modification, biomaterials, etc. However, our understanding of the interactions between solvents and thioether-based crosslinked polymers obtained using step growth thiol-X polymerizations has been limited. In contrast, the most studied crosslinked polymers, i.e., those used generally for the model-based prediction of interaction parameters, are based on acrylates, isocyanates, and styrene. Very recently, Akalp et al. employed a self-learning model to determine the χ value for PEG hydrogels formed from a step-growth mechanism between an eight-arm PEG functionalized with norbornene and the crosslinker PEG dithiol. [41] However, these materials were largely based on PEG in water, and to date, there are limited studies predicting polymer-solvent interaction parameters of bulk thiol-ene networks in organic solvents.

Indeed, easy access to an estimation of the solubility of thioether-based polymers in organic solvents and polymer-solvent interactions would ease the selection of appropriate material to implement thiol-ene chemistry cost-effectively and at industrial scales. As such, attention here was focused on four different thiol-ene network polymers with varying crosslink density formed from a step-growth reaction between multifunctional thiols and alkenes to obtain the Flory-Huggins interaction parameters (χ) using equilibrium swelling measurements. To the best of our knowledge, this work is the first report on the estimation of the Flory-Huggins interaction parameter for thiol-ene network polymers in organic solvents. Three "polar" and one "non-polar" thiol-ene network were swollen to measure the interaction parameter (χ_m) for comparison to the predicted interaction parameters (χ_p) using the Hansen Solubility Parameters in Practice (HSPiP) software, which is used industrially to predict the miscibility. This approach served two purposes: to measure χ directly and determine the efficacy of HSPiP to predict χ for thiol-ene networks.

7.3: Materials and Methods

Materials:

Pentaerythritol tetrakis(3-mercaptopropionic acid) (PETMP), trimethylolpropane tris(3-mercaptopropionoic acid) (TMPTMP), ethylene glycol di(3-mercaptopropionic acid) (GDMP), 1,9-nonanedithiol (NDT), triallyl-1,3,5-triazine-2,4,6-trione (TTT), diphenyl(2,4,6)-trimethylbenzoyl) phosphine oxide (TPO) were purchased from Sigma Aldrich. Hexanes, toluene, acetone, ethyl acetate, isopropanol (IPA), tetrahydrofuran (THF), dichloromethane (DCM), dimethyl sulfoxide (DMSO), dimethylformamide (DMF), ethylene glycol diethyl ether (EGDE), acetic acid, γ-butyrolactone (GBL), and aniline were purchased from Fisher scientific. Trimethylolpropane triallyl ether (TMPTAE) was synthesized according to a previously reported procedure.[42]All chemicals were of reagent grade and used without further purification.

Experimental:

Sample Preparation: Three different polar thiol-ene network polymers with varying crosslink densities were prepared from a 1:1 stoichiometric multifunctional thiol monomer, PETMP, TMPTMP and GDMP, with multifunctional alkene, TTT, (per functional group concentration) in the presence of 2 wt% TPO as a photoinitiator to conduct equilibrium swelling experiments. The polymer films were prepared by injecting monomers between two glass slides with 0.25 mm thickness spacers. Mixtures of thiols and alkenes were photopolymerized by the photoinitiator, TPO, using an Acticure 4000 light source with 405 nm bandpass filter with light intensity of 20 mW/cm^2. Irradiation times of 5 minutes on each side resulted in the network polymers PETMP-TTT, TMPTMP-TTT, and GDMP-TTT. All samples were post-cured at 60°C for over an hour to ensure the highest conversion attainable. The same procedure was used to obtain a non-polar thiol-ene network polymer using NDT as the thiol and TMPTAE as the alkene.

Swelling Measurements: The post-cured samples were punched out into 21 mm (using a 5/6" tool) disks, and each disk was weighed and immersed in 15 mL acetone to extract any residual sol-fraction due to impurities present in the monomers and from latent initiator fragments at room temperature for 4 days until

equilibrium was attained. The acetone was then removed, and the samples were dried in an oven at 60 °C for 24 h. The sol fraction was found to be between 1-3 wt% for all four networks. All the polymer samples (3 per test) were first weighed for the initial weight (m_0), then immersed in various types of organic solvents until arriving at equilibrium swelling. The mass uptake was recorded until an equilibrium final weight (m_f) was achieved.

Equilibrium Swelling experiments: The massed polymer sample with their sol-fraction removed were placed in 20 mL scintillation vials. For the polar thiol-ene networks, to each vial was added 15 mL of one of the following solvents: hexanes, toluene, acetone, ethyl acetate, IPA, THF, DCM, DMSO, DMF, EGDE, acetic acid, GBL, or aniline. Triplicate samples were prepared for each solvent, with each replicate in its own vial. Wet masses were taken each day for the first three consecutive days, then every other day until a constant wet mass (m_f) was found in two sequential measurements. The volume fraction (ϕ) of the polymer and swelling ratio (λ) for each sample were calculated according to equations 1 and 2, respectively:

$$\phi = \frac{\dfrac{m_p}{\rho_p}}{\dfrac{m_p}{\rho_p} + \dfrac{m_s}{\rho_s}} \ (Eq \ 1)$$

$$\lambda = \frac{m_f - m_0}{m_0} \ (Eq \ 2)$$

Where $m_p = m_0$ is the mass of the polymer, $m_s = m_f - m_0$ is the mass of the solvent, and ρ_p and ρ_s are the polymer and solvent densities, respectively. All equilibrium swelling was performed at room temperature. The affine Flory-Rhener equation (Equation 3) was then used to calculate the Flory-Huggins interaction parameter from the swelling data[43].

$$\chi_m = \frac{1}{\phi^2}\left(\frac{\rho V_1}{M_c}\left(1 - \frac{2}{f}\right)\phi^{2/3} + ln(1 - \phi) + \phi\right) \ (Eq \ 3)$$

Here, ρ is the density of the polymer, V_1 is the molar volume of the solvent, f is the average functionality of the crosslinker, and M_c is the molecular weight between crosslinks.

Solubility Parameter: The calculation of the Hansen Solubility Parameters was performed with the Hansen Solubility Parameter in Practice (HSPiP) software package (5th Edition 5.3.06, developed by Abbott, Hansen and Yamamoto). The three types of intermolecular forces: dispersive interactions (δ_d), polar interactions (δ_p), and hydrogen-bonding interactions (δ_h) were obtained from HSPiP and used to calculate the solubility parameters (δ_t) of the all the organic solvents utilized for equilibrium swelling using the following equation 4.

$$\delta_t = \sqrt[2]{\delta_d^2 + \delta_p^2 + \delta_h^2} \ (Eq\ 4)$$

Table 7.1 lists the Hansen parameters (δ_d, δ_p, and δ_h) derived from HSPiP for the solvents and polymer networks.

Table 7.1 Hansen solubility parameters determined from HSPiP for the polymer networks and solvents tested in swelling experiments.

	δ_d	δ_p	δ_h
PETMP-TTT	18.6	8.4	4.1
TMPTMP-TTT	18.6	8.5	4.2
GDMP-TTT	18.7	8.7	4.3
NDT-TMPTE	18.4	2.4	2
Hexanes	14.9	0	0
toluene	18	1.4	2
acetone	15.5	10.4	7
ethyl acetate	15.8	5.3	7.2
IPA	15.8	6.1	16.4
THF	16.8	5.7	8
DCM	17	7.3	7.1
DMSO	18.4	16.4	10.2
DMF	17.4	13.7	11.3
EGDE	15.4	6.3	6
acetic acid	14.5	8	13.5
γ-butyrolactone	18	16.6	7.4
Aniline	20.1	5.8	11.2

Estimated Flory-Huggins, χ_p, interaction parameter: The solubility parameters (**Table 7.1**) were directly used to estimate the Flory-Huggins interaction parameter (χ_p) for each solvent/polymer pair. Equation 5 shows the formulation for the Flory-Huggins, χ_p, interaction parameter.

$$\chi_p = 0.6\frac{V_1}{RT}\left[(\delta_{d1} - \delta_{d2})^2 + 0.25(\delta_{p1} - \delta_{p2})^2 + 0.25(\delta_{h1} - \delta_{h2})^2\right] \ (Eq\ 5)$$

where V_1 is the molar volume of the solvent (cm^3/mol), R is the gas constant (8.314 J/(mol·K)), T is the temperature (in K), δ_{d1} is dispersive interactions, δ_{p1} is polar interactions, and δ_{h1} is hydrogen-bonding interactions of the solvent in MPa$^{0.5}$. Similarly, δ_{d2}, δ_{p2}, and δ_{h2} correspond to the dispersive interaction, polar interaction, and hydrogen-bonding interaction of the polymer in MPa$^{0.5}$, respectively. While a variety of solvents were employed in this study, too few non and borderline solvents were included to determine an overall Hansen Sphere.

Dynamic Mechanical Analysis (DMA): The glass transition temperature (T_g) and the rubbery storage modulus (E_r) were measured on an RSE G2 dynamic mechanical analyzer (TA Instruments) in multifrequency strain, using a temperature ramp rate of 3°C/min and a frequency of 1 Hz, with an oscillating strain of 0.03 % and a preload force of 0.40 N. Samples were cut into rectangles with approximate dimensions of 20 mm x 5 mm x 0.25 mm (LxWxH). DMA was measured for samples as cured and after removal of the sol-fraction.

The storage modulus within the rubbery plateau (E_r) was used to evaluate M_c, defined as the molecular weight between crosslinks. The E_r correlates with M_c according to the following equation 6.

$$M_c = \frac{3RT\rho}{E_r} \ (Eq \ 6)$$

where E_r is the rubbery storage modulus measured by DMA at 40°C above the T_g for each network after the sol-fraction was removed, r is the density of the polymer (1.2 g/cm^3), and R is the ideal gas constant (8.314 J/(mol*K)).

7.4 Results and Discussion

The monomers used to synthesize the three polar and one non-polar network are presented in **Figure 7.1**. The polar thiol-ene network polymers obtained from the three different mercaptopropionate thiols (GDMP, TMPTMP, PETMP) with varying number of thiol functional groups and triallyl-1,3,5-triazine-2,4,6-trione (TTT) were employed to systematically vary the crosslinking density. The
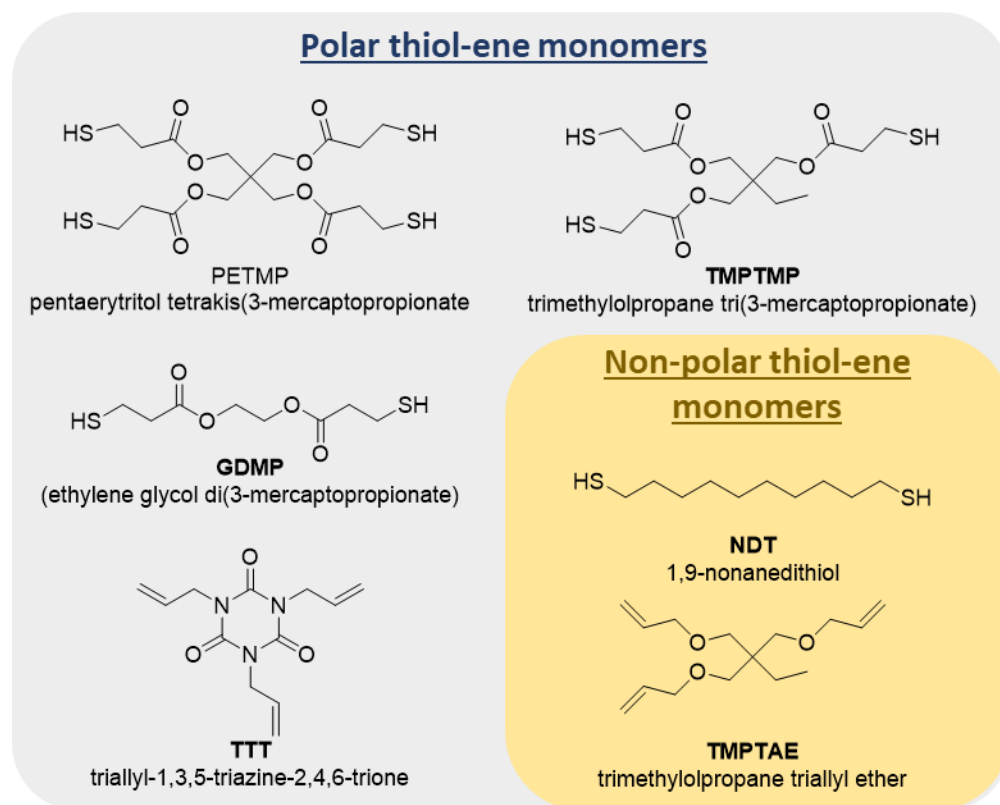
Figure 7.1: Structures of the monomer used to predict and measure interaction parameters. One set (grey) was used to produce polar thiol-ene networks, and the other (yellow) was used to produce a non-polar thiol-ene network. Lucirin TPO was used a visible light photoinitiator with 405 nm light at an intensity of 20 mW/cm^3.

mercaptopropionate-based thiol derivatives have an ester functional group and the alkene derivative has a triazine-trione as the core moiety, which greatly contributes to the polar nature of the formed network polymer. To obtain a non-polar thiol-ene network polymer, 1,9-nonanedithiol (NDT) and trimethylolpropane triallyl ether (TMPTAE) were utilized. The presence of long alkyl chains and an allyl ether results in a substantially less polar crosslinked system.

The equilibrium swelling of the network polymer is expected to be influenced by the polarity of the functional group present and the crosslink density. Hence, the thiol-ene networks with either varied number of functional groups or less polar functional groups would introduce both structural and the chemical factors that affect swelling in solvents with differing polarity index. It is expected that the analysis of the three polar networks with systematic variation in the crosslink density would enable control of the network structure without substantially changing the chemical interactions or environment. Simultaneously,

inclusion of a less polar network is expected to enable a more direct focus on the thioether group contribution due to the predominancy of dispersive interactions over polar and hydrogen bonding interactions. These key variations would represent a basis to predict solubility parameters for thioether containing networks.

7.4.1: Solubility Parameters from HSPiP:

To quantify polymer-solvent affinity and compatibility, the Hansen model utilizes three parameters; one for dispersive interactions (δ_d), one for polar interactions (δ_p), and one for hydrogen-bonding interactions (δ_h). The Hansen total solubility parameter was calculated using **Equation 4**. A systematic study was conducted with a wide range of solvents to span a variety of polarities and Hansen parameters, and therefore represent different combinations of high and low values for each Hansen parameter. The chosen set of organic solvents comprise different functional groups, such as halogens, alcohols, amines, ethers, and sulfoxides to cover polar, non-polar, protic, and aprotic solvents which results in different intermolecular interactions. Different intermolecular interactions could be interpreted from the three Hansen parameters which would then guide to the quantification of good and poor polymer/solvent affinities. For example, ethyl acetate and IPA have an identical δ_d (15.8 MPa$^{0.5}$), similar δ_p (5.3 and 6.1 MPa$^{0.5}$, respectively), but very a different δ_h (7.2 and 16.4 MPa$^{0.5}$, respectively), while GBL exhibits Hansen parameters of 18, 16.6, and 7.4 MPa$^{0.5}$, respectively.

Similarly, using HSPiP the Hansen parameters for all three of the network polymers were predicted. The predicted Hansen parameters for all the three polar network polymers were extremely similar with only slight variation, with values as follows: δ_d of 18.6 MPa$^{0.5}$, δ_p of 8.5 MPa$^{0.5}$, and δ_h of 4.2 MPa$^{0.5}$. This slight variation could be attributed to the presence of nearly chemically identical mercaptopropionate monomers. It is worth noting that an increase in crosslinking density would have negligible effect on the solubility parameter predicted by HSPiP because it is calculated from chemical group contributions. Furthermore, the non-polar network resulted in much lower predicted polar and hydrogen bonding Hansen parameters (2.4 and 2 MPa$^{0.5}$, respectively) and a very similar dispersion parameter (18.4 MPa$^{0.5}$) compared to the polar

networks. The polar and hydrogen bonding parameters are, as expected, driven down by a lack of polar groups and hydrogen bond donors. Interestingly, all the thiol-ene polymers exhibit similar dispersion parameters (δ_d) irrespective of polar and non-polar nature of the polymer. These dispersive forces arise because of temporary dipoles induced in atoms or molecules.[44, 45] In the polymeric systems under study the triazine-trione, ester, and ether groups are more polar than methylene and thioether groups due to the comparable electronegativity of sulfur relative to oxygen. However, the thioether group contribution to the dispersive component is quite high due to polarizability of the sulfur atom when compared to triazine-trione, ester, and ether groups. Overall, the net effect of temporary dipoles occurring due to the presence of -CH_2-, -SCH_2-, -N-, and C=O groups in the polar systems and -CH_2-, -SCH_2-, and -COC- group in the non-polar system might be very similar, resulting in similar dispersive component, δ_d.

It should be noted that practically speaking, HSPiP is, at best, designed to directly model linear polymers. Therefore, these networks were modeled as branched linear structures containing the correct proportion of fragments from each monomer to achieve the stoichiometric ratio in the actual monomer resins.

7.4.2: Equilibrium Swelling:

The equilibrium swelling experiments were performed to measure the amount of each solvent taken up by each polymer network in order to experimentally determine χ_m for each polymer/solvent pair. The molecular weight between crosslinks used to calculate the swelling ratios were determined by DMA for each network were determined to be: 350 g/mol for PETMP, 540 g/mol for TMPTMP, and 1020 g/mol for GDMP all with TTT, and 1020 g/mol for NDT with TMPTAE. The swelling ratios and measured interaction parameters from swelling studies as well as the predicted interaction parameters for all four thiol-ene

networks obtained from either PETMP, TMPTMP, or GMDP with TTT or NDT with TMPTAE as the multifunctional alkene are provided in **Tables 7.2 and 7.3**.

Table 7.2: Table 2: Swelling ratio (λ, the Flory-Huggins Parameter (χ_m, MPa$^{0.5}$), measured swelling experiments, and Flory-Huggins parameter predicted by HSPiP (χ_p, MPa$^{0.5}$) for the three polar networks made PETMP, TMPTMP, and GDMP with TTT. A red X (X) denotes that the network did not swell in that solvent. All errors represented are the standard deviation. *only one sample survived swelling, no standard deviation possible.

Solvent	PETMP-TTT			TMPTMP-TTT			GDMP-TTT		
	λ	χ_m	χ_p	λ	χ_m	χ_p	λ	χ_m	χ_p
hexanes	X	X	1.1	X	X	1.1	X	X	1.2
toluene	X	X	0.35	0.16 ± 0.04	1.0 ± 0.1	0.36	0.223 ± 0.003	0.971 ± 0.006	0.39
acetone	0.156 ± 0.002	0.931 ± 0.007	0.22	0.19 ± 0.02	0.95 ± 0.07	0.22	0.288 ± 0.008	0.86 ± 0.01	0.23
ethyl acetate	0.068 ± 0.009	1.4 ± 0.1	0.30	0.21 ± 0.01	0.89 ± .02	0.30	0.315 ± 0.005	0.833 ± 0.008	0.32
IPA	X	X	0.87	X	X	0.86	0.030 ± 0.006	2.29 ± 0.2	0.86
THF	0.255 ± 0.008	0.69 ± 0.02	0.26	0.36 ± 0.004	0.66 ± 0.01	0.26	0.39 ± 0.04	0.78 ± 0.05	0.28
DCM	0.303 ± 0.005	0.91 ± 0.01	0.08	0.32 ± 0.07	1.01 ± 0.1	0.07	0.39 ± 0.06	1.00 ± 0.07	0.08
DMSO	0.36 ± 0.01	0.58 ± 0.02	0.50	0.400 ± 0.003	0.690 ± 0.005	0.49	0.67 ± 0.02	0.62 ± 0.01	0.46
DMF	0.316 ± 0.006	0.59 ± 0.01	0.40	0.37 ± 0.02	0.67 ± 0.03	0.39	0.62 ± 0.05	0.59 ± 0.03	0.38
EGDE	0.15 ± 0.01	0.86 ± .04	0.31	0.217 ± 0.001	0.84 ± 0.003	0.31	0.21 ± 0.02	1.00 ± 0.04	0.33
acetic acid	0.149 ± 0.02	1.2 ± 0.1	0.54	0.231 ± 0,003	1.05 ± 0.01	0.54	0.33 ± 0.01	0.96 ± 0.01	0.54
GBL	0.36 ± 0.02	0.63 ± 0.04	0.37	0.470 ± .002	0.64 ± 0.002	0.36	1.08 ± 0.01	0.42 ± 0.006	0.34
aniline	0.41*	0.37*	0.37	0.70 ± .01	0.27 ± .01	0.36	1.18 ± 0.06	0.25 ± 0.03	0.35

Table 7.3: Swelling ratio (λ, the Flory-Huggins Parameter (χ_m, MPa$^{0.5}$), measured swelling experiments, and Flory-Huggins parameter predicted by HSPiP (χ_p, MPa$^{0.5}$), for the non-polar network NDT-TMPTAE. All errors represented are the standard deviation.

Solvent	NDT-TMPTAE		
	λ	χ_m	χ_p
hexanes	0.14 ± 0.01	1.05 ± 0.05	0.47
acetone	0.14 ± 0.02	1.23 ± 0.07	0.54
DMSO	0.044 ± 0.009	2.3 ± 0.2	1.30
acetic acid	0.155 ± 0.004	1.36 ± 0.01	0.57
GBL	0.086 ± 0.02	1.76 ± 0.01	1.07

For the three polar networks, the swelling ratio as a function of δ_d, δ_p, and δ_h for all solvents are provided in **Figure 7.2a, 7.2b and 7.2c**, respectively, to explore why different solvents were able to swell these networks. The polar and/or protic solvents were expected to exhibit favorable intermolecular interactions with the polar functional groups in these networks. Indeed, the degree of swelling for the polar systems was highest in the high polarity solvents, such as DMSO and DMF, and was lowest in the low polarity solvents, such as toluene (for which swelling occurred for GDMP-TTT and TMPTMP-TTT, but
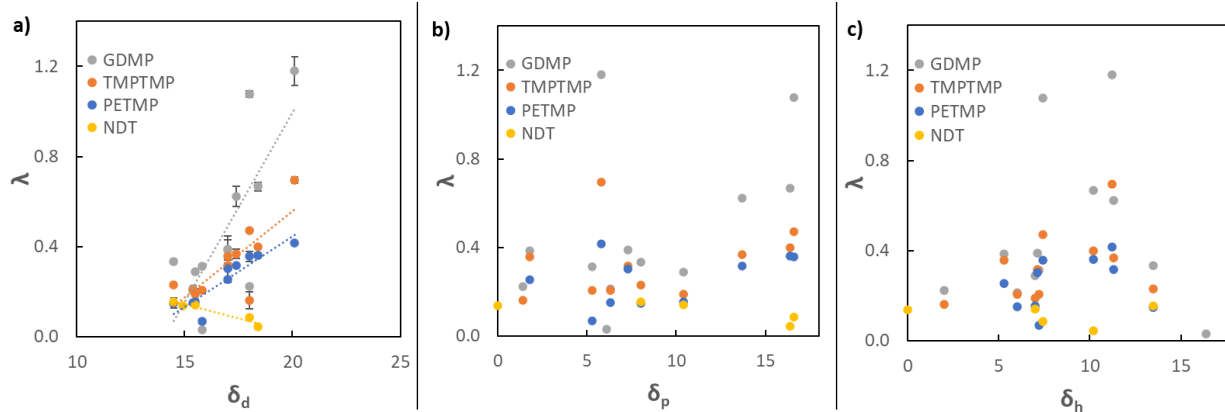
Figure 7.2: The swelling ratio λ as a function of: a) the dispersion Hansen parameter where the dashed lines indicate the trend observed for each network polymer, where the polar networks exhibit an upward trend (higher swelling) and the non-polar network shows a downward trend (less swelling) as δ_d increases, b) the polar Hansen parameter for which none of the networks exhibit a trend, and c) the hydrogen bonding Hansen parameter for which none of the networks exhibit a trend. Error bars for λ are the standard deviation and are indicated in "a".

not PETMP-TTT) and hexanes (which did not swell any of the polar networks). The degree of swelling increased with decreasing crosslinking density in all solvents, where the GDMP-TTT network showed the greatest degree of swelling, followed by TMPTMP-TTT, then PETMP-TTT. This behavior is due to greater elastic constraints on the network at higher crosslinking densities which prevents solvent molecules from displacing polymer chains and occupying space inside the network.

The non-polar network NDT-TMPTAE, was subjected to equilibrium swelling studies in five of the solvents, such as hexane, acetone, DMSO, acetic acid and γ-butyrolactone. These solvents were selected to cover the full range of solubility parameters represented by the entire set. The non-polar NDT-TMPTAE network exhibited the least degree of swelling in the set, despite possessing a similar molecular weight between crosslinks as GMDP-TTT (1020 g/mol). This could be attributed to a significant decrease in polarity which reduces affinity for most of the relatively polar solvents selected for this study. In addition, the network was expected to exhibit high intermolecular interaction with non-polar solvents. Indeed, swelling was observed in hexanes which was completely immiscible with the polar networks.

Subsequently χ_m, a measure of interaction between polymer and solvent was calculated using the affine Flory-Rhener equation, as shown in Equation 3. It was previously demonstrated that the polymer-solvent χ parameter can be utilized to determine the extent of solubility of a polymer in solvent. Generally,

a liquid is considered as a non-solvent if, $\chi > 1$, a plasticizer/solvent, if $0.5 < \chi < 1$, or a good solvent if, $\chi < 0.5$.[46] In other words, the polymer-solvent interaction becomes more favorable when χ_m is lower for polymer/solvent pairs.

Looking to the predicted polar and hydrogen bonding Hansen parameters (**Figures 7.2b and 7.2c**), there is little to no correlation between δ_p or δ_h and the amount of swelling observed for all four materials. However, there is a strong correlation between the swelling ratio and the dispersion parameter (**Figure 7.2a**), represented by a dashed line for each network. The three polar networks show an increase in the swelling ratio as the dispersion parameter increases. Using the GDMP-TTT network to illustrate this trend, aniline ($\delta_d = 20.1$ MPa$^{0.5}$) exhibited far greater swelling with $\lambda = 1.18$ than ethyl acetate ($\delta_d = 15.8$ MPa$^{0.5}$) with $\lambda = 0.32$, while the non-polar network showed a small decrease in swelling as the dispersion parameter of the solvent increases. Taken together, the dispersion parameter is the only Hansen parameter that correlates to the amount of swelling for this set of solvents and will prove to be important for understanding the quality of the HSPiP predictions of the polymer solubility parameters and therefore χ_p.

7.4.3: Comparing Experimental χ to Theoretical χ:

Comparing the experimental and predicted Flory-Huggins Parameters is crucial to determining: i) the reliability of the predicted polymer solubility parameter and ii) the origin for any deviations. Plots of the χ_m vs. χ_p denoted by either polymer network for all solvents or by solvent for all polymer networks are provided in **Figure 7.3a** and **7.3b**, respectively. The dashed black line on both plots indicates the case for which $\chi_m = \chi_p$, is provided to clearly indicate deviations between χ_m and χ_p. Overall, the measured and predicted χ values do not show good agreement for any of the four polymer networks examined in **Figure 7.3** by systematically underpredicting the interaction parameter

Although the predicted values are systematic underestimates, there is not an obvious trend that can be used to create a simple, direct relationship between χ_m and χ_p based on this data that would easily correct for that underestimate. Some solvents show better agreement than others. For instance, solvents like aniline,
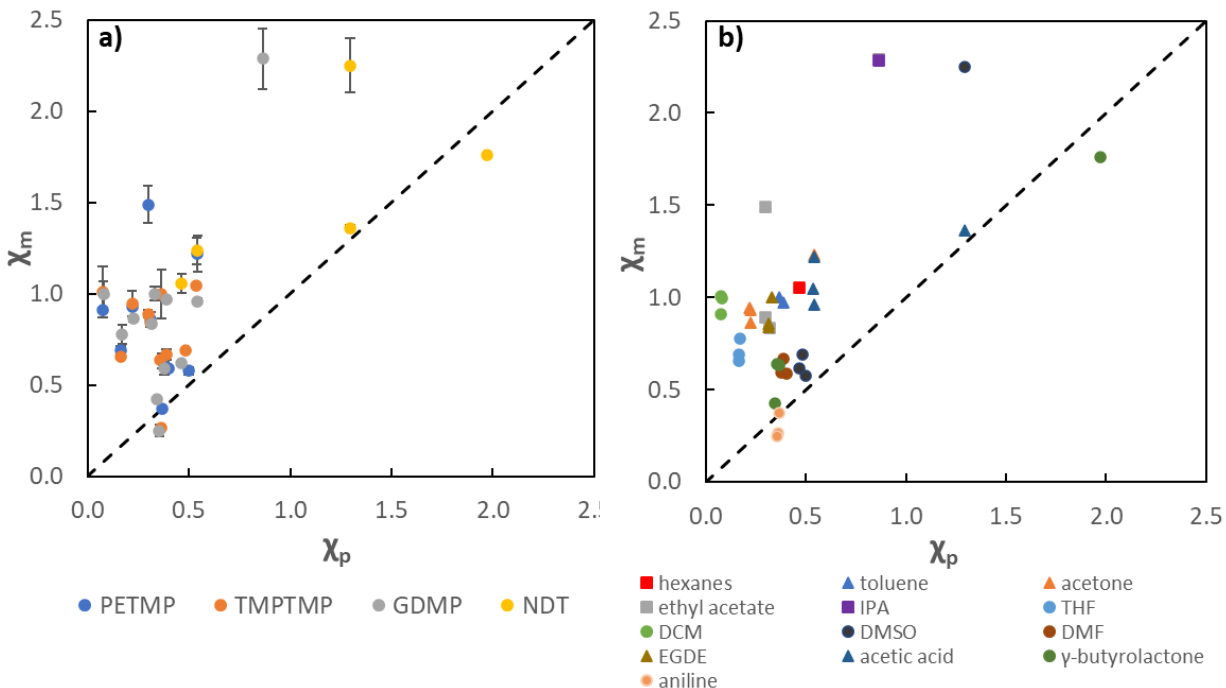
Figure 7.3: Plots of the measured Flory-Huggins parameter (χ_m) compared to the predicted Flory-Huggin parameter as determined by HSPiP, a) categorized by the identity of the polymer network for all solvents and b) categorized by the solvent across all 4 polymer networks. Points that lay closer to the dashed black line indicate predicted and measured values that agree.

DMSO, and GBL show much closer agreement than solvents like EGDE, acetone, and ethyl acetate. Hence, it is evident that individual solubility parameters influence the quality of these HSPiP predictions.

To understand the influence of individual solubility parameters on the quality of the HSPiP prediction, the solvents used for equilibrium swelling were categorized as "great", "good" and "poor" based on the degree of swelling. Here, "great swelling" was defined as solvents that resulted in a swelling ratio greater than 0.2 (THF, DMSO, DMF, GBL, DCM, and aniline), "good swelling" gave a swelling ratio between 0.05-0.2 (EDGE, acetic acid, acetone, and toluene), and "poor swelling" exhibited a swelling ratio below 0.05 (hexanes, ethyl acetate, and IPA) for the PETMP-TTT networks. This categorization was selected with PETMP-TTT as the reference because this network exhibited the lowest degree of swelling, with essentially zero swelling for the three poor solvents.

This grouping is shown graphically according to this categorization on a plot of the polar vs. dispersion and hydrogen bonding vs. dispersion solubility parameters in **Figure 7.4a and 7.4b**,

respectively, to demonstrate the correlation between this grouping and solubility parameters. For these solvents, a dispersive parameter greater than 16 MPa$^{0.5}$ resulted in "great" swelling (grouped in green) regardless of the polar or hydrogen bonding parameter. Toluene is the only exception that did not swell into the PETMP-TTT network despite swelling the other two polar networks and the non-polar network relatively well. Solvents with dispersion parameters below 16 MPa$^{0.5}$ but sufficiently high polar solubility parameter (greater than 6.3 MPa$^{0.5}$) still showed "good" swelling (points grouped in yellow). For the hydrogen bonding parameter, the "good" solvents land at intermediate hydrogen bonding parameters, again with toluene being the exception. Finally, the "poor" solvents had lower dispersion (less than 16 MPa$^{0.5}$) and polar parameters (less than 6.3 MPa$^{0.5}$). There is not a strong trend in the hydrogen bonding parameter among the "poor" solvents as they span the entire range from completely non-hydrogen bonding (hexanes) to high degrees of hydrogen bonding (IPA). A specific case of interest that occurs at the boundary of "good" and "poor" solvents in **Figure 7.4b** is comparing IPA and EDGE which have nearly identical δ_d and δ_p but EDGE is a good solvent and IPA did not swell the PETMP-TTT or TMPTMP-TTT networks at all. The reason for divergence in miscibility becomes more evident when comparing their respective δ_h, for which IPA has a very large value (16.4 MPa$^{0.5}$) and EDGE has a relatively small value (6 MPa$^{0.5}$). This difference
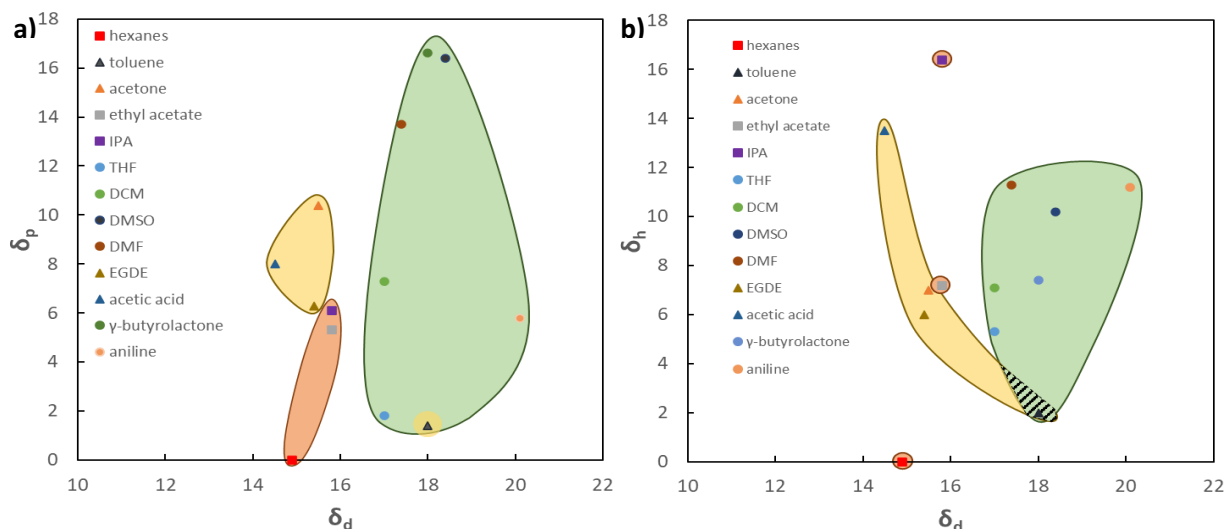
Figure 7.4: a) Plot of the polar solubility parameter (δ_p) vs. the dispersion solubility parameter (δ_d) and b) Plot of the hydrogen bonding solubility parameter (δ_h) vs. the dispersion solubility parameter. For both plots the quality of the solvent swelling is indicated as "great", highlighted in green, "good" highlighted in yellow, or "poor", highlighted in red.

is likely because IPA is both a strong hydrogen bond donor and acceptor, resulting in poor compatibility with these thiol-ene networks.

Overall, the nature of these thiol-ene networks is reflected in the swelling data for this set of solvents; the higher the dispersion component, the higher the affinity of the solvent for the network, but lower δ_d solvent with some degree of polarity may still swell these networks, which can likely be attributed to the presence of esters groups and triazine-trione rings present in the PETMP-TTT, TMPTMP-TTT, and GDMP-TTT networks.

Toluene is also an interesting case because although it did not swell the PETMP-TTT network, it did swell the other three networks tested. In fact, NDT-TMPTAE network exhibited such high degree of swelling in toluene that the samples became too delicate to handle in order to measure the solvent uptake. This behavior likely arises from a high δ_d and low δ_p and δ_h associated with the aromatic ring of the toluene being highly compatible with the highly non-polar network.

With the understanding that the dispersion parameter is driving solvent compatibility of these thiol-ene networks, it is possible to begin to assess the disagreement between the measured and predicted interaction parameters, specifically whether any one Hansen parameter is responsible for this disagreement. The difference in the predicted and measured interaction parameters (χ_p-χ_m) versus δ_d, δ_p, and δ_h are shown in **Figure 7.5a, 7.5b, and 7.5c,** respectively. As noted above, in essentially every case the predicted interaction parameter is higher than the parameter measured by swelling, and the dispersion parameter of the solvent increases the agreement between the predicted and measured χ improves somewhat at δ_d values greater than 16 MPa$^{0.5}$. At the same time, there is no correlation between χ_p-χ_m and δ_p or δ_h across all solvents, indicating that the dispersive character is driving the inability of HSPiP to accurately predict the Hansen parameters and therefore interaction parameters of these thiol-ene systems compared to experimental data.
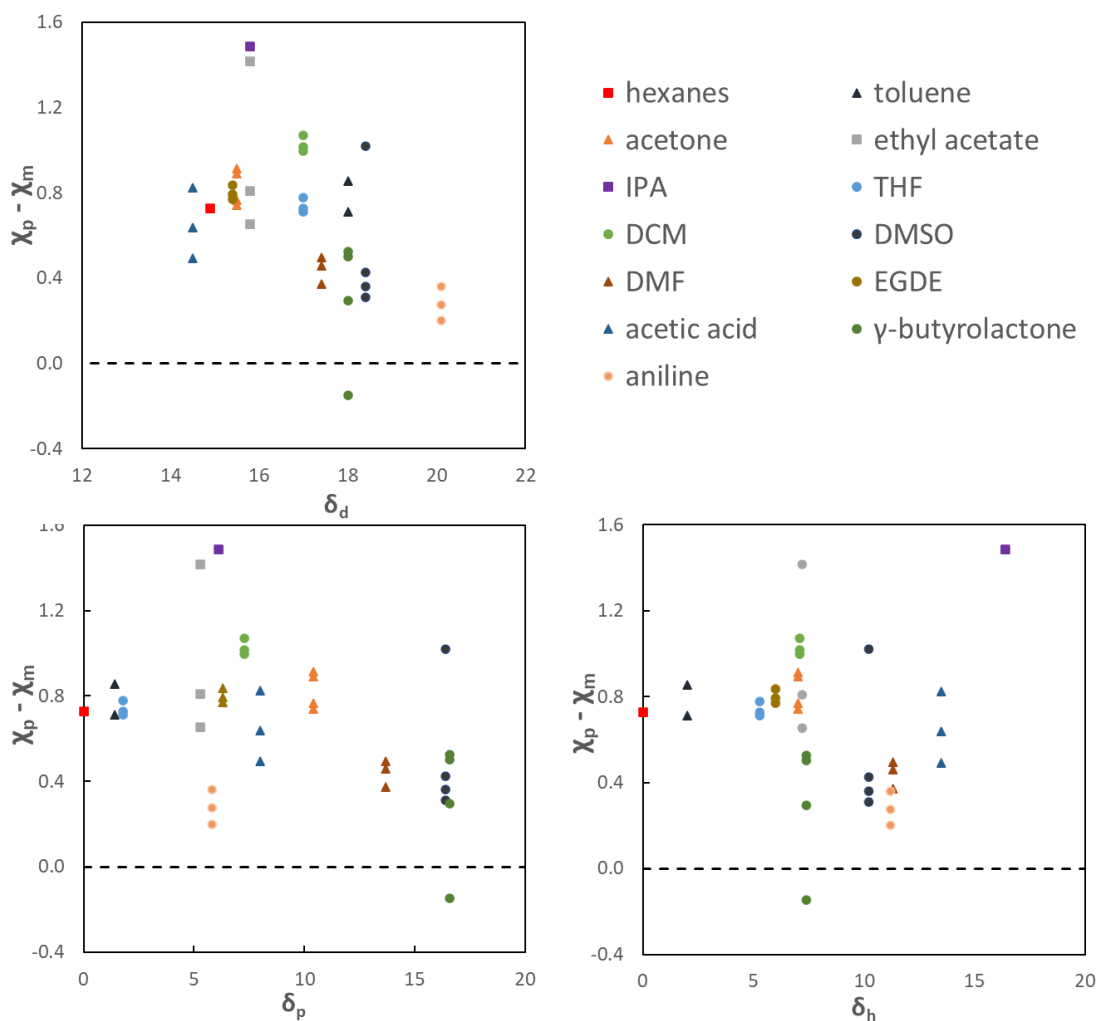
Figure 7.5: The difference in the predicted and measured interaction parameters as a function of each solubility parameter of the solvent for a) the dispersion Hansen parameter, b) the polar Hansen parameter, and c) the hydrogen bonding Hansen parameter.

7.4.4: Fitting δ_d to Experimental data:

The dispersion parameter has been identified as the most important factor that is not properly accounted for in these thiol-ene networks based on which the solubility parameters are correlated with the difference in the predicted and measured interaction parameters. We hypothesize that the disparity is due to an improper accounting for the extremely prevalent thioether bonds present in the network, which are not common in the polymer types for which HSPiP is calibrated to predict Hansen parameters. In fact, HSPiP predictions did not change when the sulfur atoms are replaced with carbon, indicating that the thioether bonds are not actually accounted for in the polymer prediction suite in the software. This is a crucial oversight because the large and polarizable electron cloud in a thioether bond should contribute significantly to δ_d compared

138

to a carbon atom at the same position. At the same time, a thioether should have a comparable δ_p and δ_h to carbon since sulfur has a similar electronegativity to carbon (2.55 for carbon and 2.58 for sulfur) and is a poor hydrogen bond acceptor, meaning that any lack of accounting for the thioether in the prediction should not significantly affect these two Hansen parameters compared to the dispersion parameter. To test the impact of accounting for thioether bonds improves the quality of the predictions, the dispersion parameter for each network was independently fit to **Equation 4** using a least-squares fit to minimize χ_P- χ_m without changing the other two Hansen parameters. The HSPiP and fitted values are provided in **Table 7.4**.

Table 7.4: Values for the dispersion Hansen parameter predicted by HSPiP and the value from fitting δ_d to the experimental swelling data.

	HSPiP	Fit
PETMP-TTT	18.60	23.25
TMPTMP-TTT	18.60	22.89
GDMP-TTT	18.70	22.16
NDT-TMPTE	18.40	22.28

The fitted dispersion parameters are all in the range of about 22-23 MPa$^{0.5}$ and are extremely similar for all four networks despite being fit independently of each other. These values are significantly higher than the values around 18.7 MPa$^{0.5}$ predicted with HSPiP. The interaction parameters calculated from the fitted dispersion parameters improve the agreement between the measured and predicted interaction parameters by changing just one of the three solubility parameters, shown in **Figure 7.6**.

Because the square of the difference between the Hansen parameters is considered when calculating χ_P and the dispersion parameter is weighed four times heavier in **Equation 5** than the other two parameters, it is reasonable that a large error between the true and predicted dispersion parameter is driving the underestimate in the predicted interaction parameters when using HSPiP to predict interaction parameters for thiol-ene networks. This error is likely due to the lack of available data in the software to accurately predict the dispersion parameter for thioether-containing polymers. There are likely additional corrections that can be made for the polar and hydrogen bonding parameters as well. However, thioether bonds are of low polarity and are poor hydrogen bond acceptors and δ_p and δ_h are not as heavily weighted in predicting the Flory-Huggins parameter and therefore do not contribute as significantly. It is important to note that
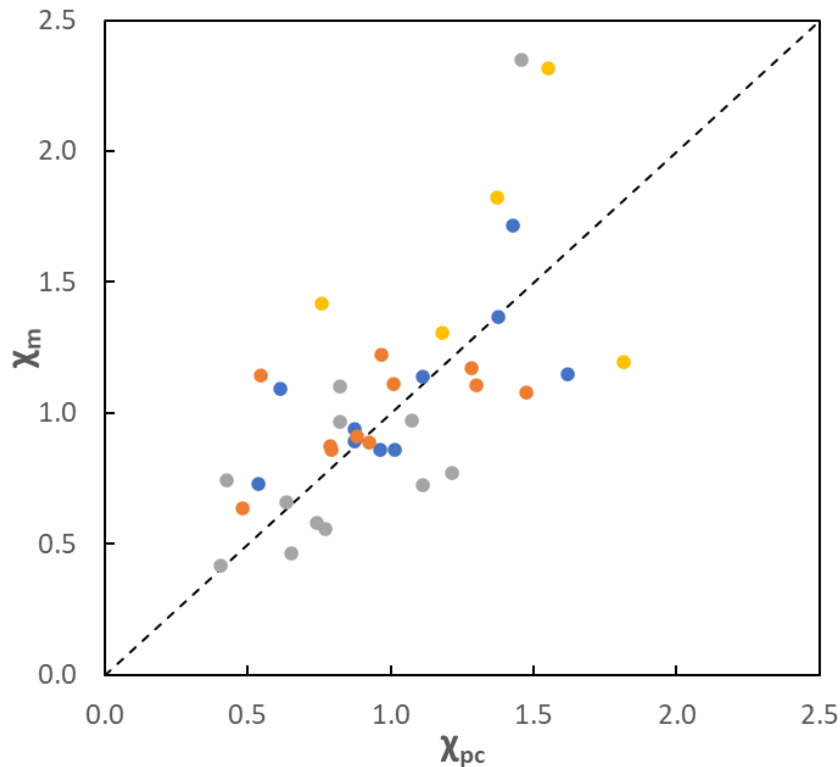
Figure 7.6: Plot of the measured Flory-Huggins interaction parameter versus the corrected parameter that was determined by a least-squares fit of the dispersion parameter to the experimental data.

while this fitting procedure did eliminate the bias toward underpredicting the interaction parameter, the overall correlation between χ_P and χ_m is still poor. HSPiP does very little to account for how crosslinking density or structural factors such as molecular weight or branching impact the interaction parameter. Polymer informatics, which takes both chemical and structural features of polymers and polymer networks into account, offers a possible alternative to Hansen parameters for predicting polymer properties.[47] This approach requires aggregation of a large amount of polymer property data and the use of machine learning tools to predict polymer properties and may prove to be a better tool for predicting such properties such as solubility in the future.[48] At this time, the field of data driven materials science is still relatively young, and improvements to data sharing and standardization, completeness, and analysis are required to fully realize this approach.[49]

Lastly, **Figure 7.7** shows χ_m versus polymer volume fraction (ϕ), and implies that the increase of χ_m is larger at higher polymer content in the swollen state. Extrapolation of χ_m to $\phi = 0$ is found to be 0.49 for the range of $\phi = 0$ to 0.15, which is consistent with the findings of Sakurada et al. and Peppas et al. [50, 51]
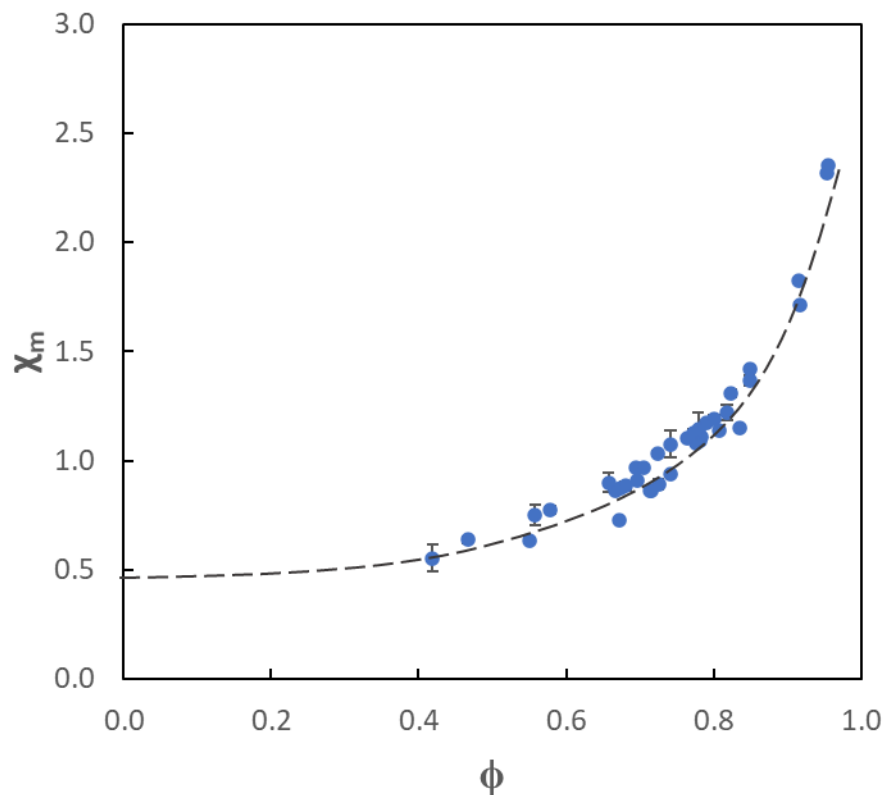
Figure 7.7: Plot of the measured Flory-Huggins interaction parameter versus the polymer volume fraction of the thiol-ene networks at room temperature. The dashed line is the extrapolation of the data to $\phi = 0$.

7.5: Conclusions

The Flory-Huggins interaction parameters were measured for thiol-ene networks of varying crosslinking density and polarity in a variety of organic solvents. These measurements were used to assess how effectively HSPiP can predict the interaction parameter for thiol-ene networks using the Hansen solubility parameter method.

The degree of swelling was measured and the affine Flory-Rhener equation was implemented to calculate the interaction parameter for each polymer/solvent pair, and the solvents were categorized as

"poor", "good", or "great" based on how effectively each solvent was able to swell the most crosslinked network, PETMP-TTT. This analysis revealed that a dispersion parameter above 16 MPa$^{0.5}$ results in excellent solubility for a wide range of polar and hydrogen bonding Hansen parameters, which is largely driven by the thioether bonds that predominate in thiol-ene networks. For the more polar networks, lower dispersion parameters are possible if the polar Hansen parameter is above 6.3 MPa$^{0.5}$ and the hydrogen bonding parameter is not too high.

Lastly, it was shown that HSPiP significantly underpredicts the dispersion Hansen parameter in these thiol-ene networks because the software neglects to account for the thioether bonds for its polymer predictions. Correcting for this disparity significantly for each network improves the overall correlation between the predicted and measured interaction parameters, removing the bias toward underprediction of χ. However, HSPiP currently lacks the ability to account for structural considerations such as crosslinking, molecular weight, and branching which are needed to accurately predict of solvent-polymer miscibility and swelling, and therefore utility of HSPiP for polymer materials.

7.6: References

1.   Sorensen, P. A.; Kiil, S.; Dam-Johansen, K.; Weinell, C. E., Anticorrosive coatings: a review. *Journal of Coatings Technology and Research* **2009,** *6* (2), 135-176.

2.   Moodley, K.; Mabaso, M.; Bahadur, I.; Redhi, G. G., Industrial application of ionic liquids for the recoveries of spent paint solvent. *Journal of Molecular Liquids* **2016,** *219*, 206-210.

3.   Xing, P. X.; Robertson, G. P.; Guiver, M. D.; Mikhailenko, S. D.; Wang, K. P.; Kaliaguine, S., Synthesis and characterization of sulfonated poly(ether ether ketone) for proton exchange membranes. *Journal of Membrane Science* **2004,** *229* (1-2), 95-106.

4.   Subramanian, C.; Weiss, R. A.; Shaw, M. T., Electrospinning and characterization of highly sulfonated polystyrene fibers. *Polymer* **2010,** *51* (9), 1983-1989.

5.   Vay, K.; Scheler, S.; Friess, W., Application of Hansen solubility parameters for understanding and prediction of drug distribution in microspheres. *International Journal of Pharmaceutics* **2011,** *416* (1), 202-209.

6.   Flory, P. J., Thermodynamics of high polymer solutions. *Journal of Chemical Physics* **1942,** *10* (1), 51-61.

7.   Huggins, M. L., Some properties of solutions of long-chain compounds. *Journal of Physical Chemistry* **1942,** *46* (1), 151-158.

8.   Fredenslund, A.; Jones, R. L.; Prausnitz, J. M., GROUP-CONTRIBUTION ESTIMATION OF ACTIVITY-COEFFICIENTS IN NONIDEAL LIQUID-MIXTURES. *Aiche Journal* **1975,** *21* (6), 1086-1099.

9.   Sanchez, I. C.; Lacombe, R. H., ELEMENTARY MOLECULAR THEORY OF CLASSICAL FLUIDS - PURE FLUIDS. *Journal of Physical Chemistry* **1976,** *80* (21), 2352-2362.

10.   Sanchez, I. C.; Lacombe, R. H., STATISTICAL THERMODYNAMICS OF POLYMER-SOLUTIONS. *Macromolecules* **1978,** *11* (6), 1145-1156.

11.   Sato, Y.; Fujiwara, K.; Takikawa, T.; Sumarno; Takishima, S.; Masuoka, H., Solubilities and diffusion coefficients of carbon dioxide and nitrogen in polypropylene, high-density polyethylene, and polystyrene under high pressures and temperatures. *Fluid Phase Equilibria* **1999,** *162* (1-2), 261-276.

12.   Huang, S. H.; Radosz, M., EQUATION OF STATE FOR SMALL, LARGE, POLYDISPERSE, AND ASSOCIATING MOLECULES. *Industrial & Engineering Chemistry Research* **1990,** *29* (11), 2284-2294.

13.   Lacombe, R. H.; Sanchez, I. C., STATISTICAL THERMODYNAMICS OF FLUID MIXTURES. *Journal of Physical Chemistry* **1976,** *80* (23), 2568-2580.

14.   Chapman, W. G., PREDICTION OF THE THERMODYNAMIC PROPERTIES OF ASSOCIATING LENNARD-JONES FLUIDS - THEORY AND SIMULATION. *Journal of Chemical Physics* **1990,** *93* (6), 4299-4304.

15.   Hansen, C. M., UNIVERSALITY OF SOLUBILITY PARAMETER. *Industrial & Engineering Chemistry Product Research and Development* **1969,** *8* (1), 2-&.

16.   Barton, A. F. M., SOLUBILITY PARAMETERS. *Chemical Reviews* **1975,** *75* (6), 731-753.

17.   Venkatram, S.; Kim, C.; Chandrasekaran, A.; Ramprasad, R., Critical Assessment of the Hildebrand and Hansen Solubility Parameters for Polymers. *Journal of Chemical Information and Modeling* **2019,** *59* (10), 4188-4194.

18.   Hildebrand, J. a. S., R.L, *The Solubility of Nonelectrolytes*. 3rd ed.; Reinhold Pub Corp.: New York, 1950.

19.   Hansen, C. M., *Hansen Solubility Parameter a User's Handbook* 2nd ed.; CRC Press: Boca Raton, 2007.

20.   Miller-Chou, B. A.; Koenig, J. L., A review of polymer dissolution. *Progress in Polymer Science* **2003,** *28* (8), 1223-1270.

21.   Hansen, C. M., The three dimensional solubility parameter-key to paint component affinities: II. Dyes, emulsifiers, mutual solubility and compatibility, and pigments, . *J. Paint Technol* **1967,** *39* (511), 505-510.

22.   Hansen, C. M., The three dimensional solubility parameter-key to paint component affinities: III. Independent calculation of the parameters components *J. Paint Technol.* **1967,** *39* (511), 511-514.

23.   Hansen, C. M., The three dimensional solubility parameter-key to paint component affinities I. Solvents, plasticizers, polymers, and resins *J. Paint Technol* **1967,** *39* (505), 104-117.

24.   HrnjakMurgic, Z.; Jelencic, J.; Bravar, M.; Marovic, M., Influence of the network on the interaction parameter in system EPDM vulcanizate-solvent. *Journal of Applied Polymer Science* **1997,** *65* (5), 991-999.

25.   Ferrell, W. H.; Kushner, D. I.; Hickner, M. A., Investigation of Polymer-Solvent Interactions in Poly(styrene sulfonate) Thin Films. *Journal of Polymer Science Part B-Polymer Physics* **2017,** *55* (18), 1365-1372.

26.   Sanchez, I. C., RELATIONSHIPS BETWEEN POLYMER INTERACTION PARAMETERS. *Polymer* **1989,** *30* (3), 471-475.

27.   Jankovic, S.; Tsakiridou, G.; Ditzinger, F.; Koehl, N. J.; Price, D. J.; Ilie, A.-R.; Kalantzi, L.; Kimpe, K.; Holm, R.; Nair, A.; Griffin, B.; Saal, C.; Kuentz, M., Application of the solubility parameter concept to assist with oral delivery of poorly water-soluble drugs - a PEARRL review. *Journal of Pharmacy and Pharmacology* **2019,** *71* (4), 441-463.

28.   Liu, Y.; Shi, B., Determination of Flory interaction parameters between polyimide and organic solvents by HSP theory and IGC. *Polymer Bulletin* **2008,** *61* (4), 501-509.

29.   Segarceanu, O.; Leca, M., Improved method to calculate Hansen solubility parameters of a polymer. *Progress in Organic Coatings* **1997,** *31* (4), 307-310.

30.   Bustamante, P.; Navarro-Lupion, J.; Escalera, B., A new method to determine the partial solubility parameters of polymers from intrinsic viscosity. *European Journal of Pharmaceutical Sciences* **2005,** *24* (2-3), 229-237.

31.   Ovejero, G.; Perez, P.; Romero, M. D.; Guzman, I.; Diez, E., Solubility and Flory Huggins parameters of SBES, poly(styrene-b-butene/ethylene-b-styrene) triblock copolymer, determined by intrinsic viscosity. *European Polymer Journal* **2007,** *43* (4), 1444-1449.

32.   Bahar, I.; Erbil, H. Y.; Baysal, B. M.; Erman, B., DETERMINATION OF POLYMER SOLVENT INTERACTION PARAMETER FROM SWELLING OF NETWORKS - THE SYSTEM POLY(2-HYDROXYETHYL METHACRYLATE)-DIETHYLENE GLYCOL. *Macromolecules* **1987,** *20* (6), 1353-1356.

33.   Marzocca, A. J., Evaluation of the polymer-solvent interaction parameter chi for the system cured styrene butadiene rubber and toluene. *European Polymer Journal* **2007,** *43* (6), 2682-2689.

34.   Marzocca, A. J.; Rodriguez Garraza, A. L.; Mansilla, M. A., Evaluation of the polymer-solvent interaction parameter chi for the system cured polybutadiene rubber and toluene. *Polymer Testing* **2010,** *29* (1), 119-126.

35.   Chu, H. Z.; Liu, D.; Cui, Z. W.; Wang, K.; Qiu, G. X.; Liu, G. Y., Effect of crosslink density on solubility parameters of styrene butadiene rubber and the application in pre-screening of new potential additives. *Polymer Testing* **2020,** *81*.

36.   Atta, A. M.; El-Ghazawy, R. A. M.; Farag, R. K.; Abdel-Azim, A. A.-A., Swelling and network parameters of oil sorbers based on alkyl acrylates and cinnamoyloxy ethyl methacrylate copolymers. *Journal of Polymer Research* **2006,** *13* (4), 257-266.

37.   Yagi, Y.;   Inomata, H.; Saito, S., SOLUBILITY PARAMETER OF AN N-ISOPROPYLACRYLAMIDE GEL. *Macromolecules* **1992,** *25* (11), 2997-2998.

38.   Mah, C. H.; Wu, Q.; Deen, G. R., Effect of nature of chemical crosslinker on swelling and solubility parameter of a new stimuli-responsive cationic poly(N-acryloyl-N'-propyl piperazine) hydrogel. *Polymer Bulletin* **2018,** *75* (1), 221-238.

39.   Bentz, K. C.; Walley, S. E.; Savin, D. A., Solvent effects on modulus of poly(propylene oxide)-based organogels as measured by cavitation rheology. *Soft Matter* **2016,** *12* (22), 4991-5001.

40.   Gao, J.; Wu, S.; Rogers, M. A., Harnessing Hansen solubility parameters to predict organogel formation. *Journal of Materials Chemistry* **2012,** *22* (25), 12651-12658.

41.   Akalp, U.; Chu, S.; Skaalure, S. C.; Bryant, S. J.; Doostan, A.; Vernerey, F. J., Determination of the polymer-solvent interaction parameter for PEG hydrogels in water: Application of a self learning algorithm. *Polymer* **2015,** *66*, 135-147.

42.   Song, H. B.; Baranek, A.; Worrell, B. T.; Cook, W. D.; Bowman, C. N., Photopolymerized Triazole-Based Glassy Polymer Networks with Superior Tensile Toughness. *Advanced Functional Materials* **2018,** *28* (22), 9.

43.   Flory, P. J., *Principles of polymer chemistry*. Cornell University Press: 1953.

44.   A.L. Companion , S. E., Chemical Bonding. Secoond ed.; McGraw-Hill Inc.: 1979.

45.   Adamska, K.; Voelkel, A., Hansen solubility parameters for polyethylene glycols by inverse gas chromatography. *Journal of Chromatography A* **2006,** *1132* (1-2), 260-267.

46.   Sudduth, R. D., A review of the similarities and differences between five different polymer-solvent interaction coefficients. *Pigment & Resin Technology* **2013,** *42* (6), 394-405.

47.   Kim, C.; Chandrasekaran, A.; Huan, T. D.; Das, D.; Ramprasad, R., Polymer Genome: A Data-Powered Polymer Informatics Platform for Property Predictions. *The Journal of Physical Chemistry C* **2018,** *122* (31), 17575-17585.

48.   Chandrasekaran, A.; Kim, C.; Venkatram, S.; Ramprasad, R., A Deep Learning Solvent-Selection Paradigm Powered by a Massive Solvent/Nonsolvent Database for Polymers. *Macromolecules* **2020,** *53* (12), 4764-4769.

49.   Himanen, L.; Geurts, A.; Foster, A. S.; Rinke, P., Data-driven materials science: status, challenges, and perspectives. *Advanced Science* **2019,** *6* (21), 1900808.

50.   Sakurada, I.; Nakajima, A.; Fujiwara, H., VAPOR PRESSURES OF POLYMER SOLUTIONS .2. VAPOR PRESSURE OF THE POLY(VINYL ALCOHOL)-WATER SYSTEM. *Journal of Polymer Science* **1959,** *35* (129), 497-505.

51.   Peppas, N. A.; Merrill, E. W., DETERMINATION OF INTERACTION PARAMETER-CHI-1 FOR POLYVINYL-ALCOHOL) AND WATER IN GELS CROSSLINKED FROM SOLUTIONS. *Journal of Polymer Science Part a-Polymer Chemistry* **1976,** *14* (2), 459-464.

Chapter 8 – CONCLUSIONS AND FUTURE DIRECTIONS

8.1 Conclusions

Covalent Adaptable Networks have become an important class of polymer materials, for reprocesable and responsive polymer materials. This thesis aims to add to the toolbox of polymerization chemistries for making CANs and expand the scope of characterization techniques for studying their dynamic behavior. First, the kinetics thiol-ene disulfidation polymerization were studied to incorporate disulfides into thiol-x networks. The relative rates of the thiol-ene and disulfide-ene polymerizations were measured and modeled for dual cure applications. Furthermore, the dynamic characteristics imbued by the disulfides that both participate in the polymerization and bond exchange were studied for different disulfide/thiol combinations. Next, dielectric analysis was implemented to investigate dynamic behavior in CANs. The impact of thiol/thioester substitution in thiol-ene and thiol-anhydride-ene networks was investigated to determine how steric hinderance and polarity effect rates of exchange and stress relaxation. In addition, DEA was used to evaluate how time-temperature-superposition analysis can be applied to CANs that rearrange bond through different dynamic bonding mechanisms. The sections that follow summarize the findings of this work and recommend future directions for these lines of research.

8.1.1 Thiol-ene-disulfides Polymerizations

A thorough kinetics analysis was undertaken to evaluate polymerization rates in thiol-ene disulfide-polymerizations. Reaction rates were measured experimentally using FTIR for systems of increasing complexity. First, the kinetics disulfidation polymerization of the disulfide-containing divinyl ether monomer were measured and was shown to be effectively modeled using a modified version of the thiol-ene kinetics equations. Next, this disulfide monomer was co-reacted with monofunctional thiols to model the reaction by accounting for both thiol-ene and disulfide-ene kinetics, and it was found that the thiol-ene reaction is on average approximately 30 times faster than the disulfidation reaction. The final disulfide content of the network and overall crosslinking could then be controlled by the initial stoichiometry of the monomer mixture. The difference in rates also enables spatial and temporal control over the two different

polymerization chemistries, which were leveraged to demonstrate that a dual-cure approach is possible with this scheme. Indeed, two-stage photopolymerization was used to generate a stage-one thiol-ene network, and optical features were written using a stage-two disulfide-ene reaction. This work provides a new route to high sulfur containing materials and increases the scope and utility of thiol-X and disulfide-based polymerizations.

8.1.2 Radical Disulfide Exchange in Thiol-ene-disulfide Networks

Thiol-ene-disulfide networks, whose kinetics were investigated in the previous section, were studied as covalent adaptable networks. This reaction scheme propagates though free radicals, which will also induce radical-disulfide exchange throughout both stages of the polymerization. Bond exchange introduces an alternative pathway through which radicals may react during the polymerization, which was shown to relax stress both during and after polymerization

A disulfide monomer derived from mercaptopropionates was introduced to study how the type of thiyl radicals present during the reaction impact the polymerization, and it was found to be nearly as efficient for the disulfide-ene polymerization as those based on thioglycolates during the second stage. These disulfides were then polymerized with multifunctional thiols of different radical stability and rate limiting steps. The thiol-ene step of the polymerization using the mercaptopropionate core was as fast or faster than the thioglycolate core, regardless of the type of thiol comonomer. The disulfide-ene rate was largely unaffected by the thiol/disulfide pair when the thiyl radical formed by the thiol was more stable than the radical formed by the disulfide, but slower in the opposite scheme when asymmetric disulfides could form during the thiol-ene polymerization.

Both disulfide cores effectively induced stress relaxation both during polymerization and during post-polymerization stress relaxation. However, relaxation with mercaptopropionate core was significantly faster than for thioglycolate core. However, the disulfide core did not have a significant impact the material properties of the final networks, which enable independent tuning of the rates of relaxation and network properties.

8.1.3 Substituted Thiols in Thioester Reactions

Substituted thiol/thioester were implemented to study the impacts of substitution on dynamic thioester reactions. Model NMR studies demonstrated that, in terms of equilibrium of thiol-thioester exchange, primary thiol/thioesters are not strongly favored over the secondary thiol/thioesters, and exchange occurs even without a base or nucleophilic catalyst, albeit much more slowly.

Monomer containing the same primary and secondary thioester functionalities were then used to make thiol-ene networks that undergo thiol-thioester exchange over the same temperature range. Dielectric analysis and stress relaxation experiments showed that the secondary thiol/thioester network showed relax slower than their primary analogues due to decreases in polarity and increased steric hinderance associated with the methyl group. In addition, thiol-anhydride-ene networks, which are capable of both reversible addition and reversible thioester exchange, showed that secondary thiol/thioesters bias dynamic bonding toward reversible addition, also due to the steric hindrance of the methyl substitution. In both thiol-ene and thiol-anhydride-ene networks, the secondary thiols/thioester showed slower exchange rates and relaxation times, which was attributed to a combination of increased steric hindrance and a decrease in polarity associated with the methyl substitution.

8.1.4 Dielectric Analysis for Covalent Adaptable Networks

Dielectric analysis was implemented to explore the utility this technique to understand the dynamics of CANs over a broader frequency window than is accessible for mechanical measurements. Measurements using two types of dielectric probes were compared to determine whether the test method significant impact the measurements. Next, three types of covalent adaptable networks were examined using a combination of dielectric spectroscopy and stress relaxation to determine how the type of dynamic bonding mechanism impacts dielectric measurements.

Interfacial effects due to charge polarization the were observed at low frequencies for both ITO and interdigit probes. These effects present as a significant plateau region on ITO glass and a relatively weak

inflection for interdigit probes. While measurements in this regime are impacted by dynamic bonding as seen in previous literature, care should be taken not to misconstrue these low frequency interfacial effects as relaxations are intrinsic to the dynamic network. Measurements using interdigit probes were also less sensitive to sample preparation overall.

Time-temperature-superposition of the dielectric spectra corresponded well with prior literature using rheological measurements, indicating that the spectra superimpose well when the network structure does not depend on temperature. The spectra for the Diels-Alder network, which follows a reversible addition mechanism, did not superimpose at frequencies above the α-relaxation. The same was true for the thiol-anhydride network with excess anhydride, which also tended toward reversible addition. On the other hand, spectra of the thiol-ene network and the thiol anhydride network with excess thiol, which both follow reversible exchange mechanisms, superimposed quite well. Time-temperature-superposition of stress relaxation data of each of these networks agreed with the observations from dielectric analysis, although access to higher temperatures in rheology is required to draw broader conclusions.

8.1.5 Flory-Huggins Parameters of Thiol-ene Networks

Flory-Huggins interaction parameters were measured for thiol-ene networks of varying crosslinking density and polarity. These measurements were used to determine how well Hansen solubility parameters can be used to predict which thiol-ene networks will swell in the presence of various organic solvents. The degree of swelling was measured for each polymer/solvent pair, and the solvents were categorized as "poor", "good", or "great" based on how much each solvent was able to swell these networks. It was determined that solvents with a dispersion parameter above 16 $MPa^{0.5}$ results in excellent solubility for a wide range of polar and hydrogen bonding Hansen parameters. This trend was largely driven by the thioether bonds that are permeate thiol-ene materials. For networks of greater polarity, lower dispersion parameters are still amenable to swelling if the polar Hansen parameter is higher than 6.3 $MPa^{0.5}$ and the hydrogen bonding parameter is not too high.

Lastly, it was shown that the software used to implement the Hansen method in this study, HSPiP, neglects to account for the thioether bonds for polymers and therefore significantly underpredicts the dispersion parameter. Correcting for this disparity improves the overall correlation between the predicted and measured Floty-Huggins parameters. However, HSPiP cannot to account for structural considerations such as crosslinking, molecular weight, and branching which are needed to accurately predict the amount of swelling for polymer networks.

8.2 Future Directions

8.2.1 Further Expand the Scope of Thiol-ene-disulfide Polymerizations

The findings of this thesis demonstrate that the scope of the thiol-ene-disulfide reaction is broader than was initially hypothesized[1], specifically with respect to the viability of disulfide cores other than those derived from thioglycolates. This warrants the development of disulfide monomers (**Figure 8.1**) with (1) alternative disulfide cores (monomers 1-3) to modulate the rate of disulfide exchange and (2) modifying the flanking functional groups to have greater substitution and/or more rigid substituents (monomers 4 and 5) to modulate the materials properties and relaxation rates. Studies that aim to better understand why certain disulfides and alkenes are more reactive in disulfidation reactions would also be useful to better understand what factors improve this reaction.
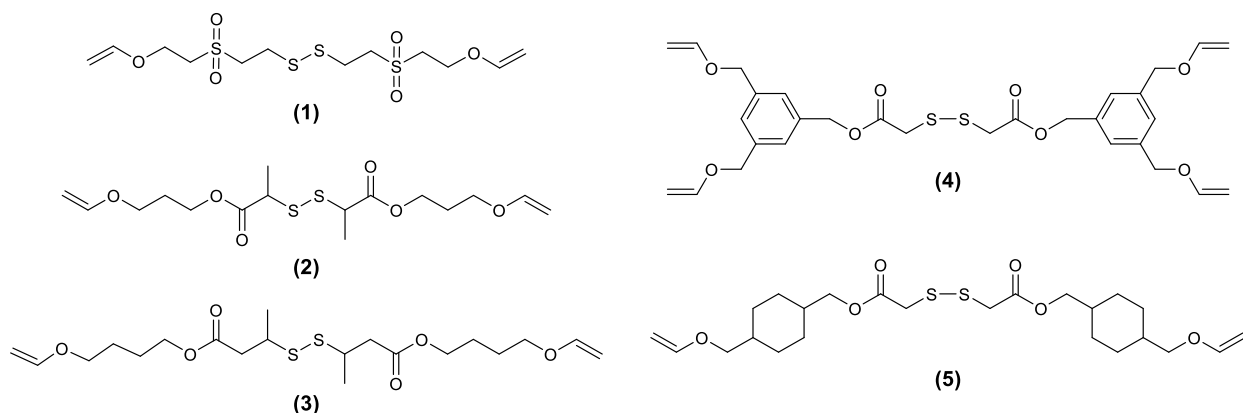
Figure 8.1: A selection of potential disulfide-containing alkene monomers. Monomers (1), (2), and (3) represent different disulfide core structures. Monomer (4) represents an approach to increase the rigidity and functionality of the disulfide monomer, and monomer (5) would increase only the rigidity.

In addition to disulfide-ene approach that has been explored so far, it is also worth exploring similar reaction pathways to generate disulfide-containing networks. For instance, cyclic disulfides have been used to make polydisulfide[2] networks and for the disulfidation of norbornenes[3] to make hydrogels, but further investigation of cyclic disulfides for in thiol-ene-disulfide scheme is also warranted due to their high reactivity and potential for shrinkage stress reduction.

One of the advantages of the thiol-ene-disulfide approach is that more crosslinking per functional group is achieved for disulfide-ene compared to thiol-ene. It is also possible that disulfides react in a similar manner with alkynes to increase crosslinking even further, as proposed in **Figure 8.2**. This reaction scheme is analogous to the thiol-yne reaction[4] in the same manner than the reaction with alkenes is analogous to
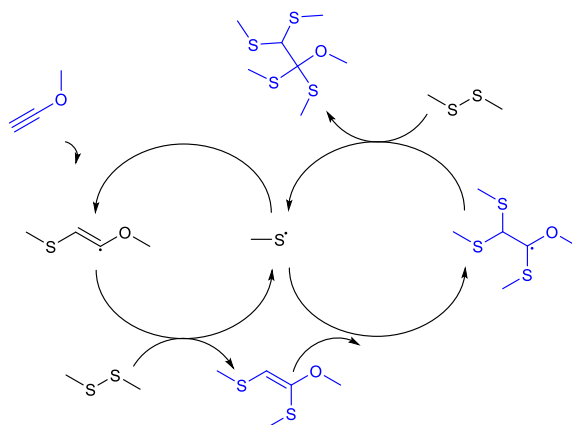
Figure 8.2: Proposed mechanism for a disulfide-yne reaction, which is analogous to the thiol-yne reaction.

Figure 8.3: Proposed mechanism for a disulfide-yne reaction, which is analogous to the thiol-yne reaction.

the thiol-ene reaction. If either the single or the double addition into the alkyne occurs, this approach could yield even more highly crosslinked materials with functionalizable or even degradable linkages. This may work with either linear or cyclic disulfide groups.

8.2.1 Continued Exploration Dielectric Analysis in CANs

This thesis has also demonstrated the potential utility of dielectric analysis for characterizing dynamic behavior in CANs. Expanding this analysis to a larger scope of dynamic bonds and polymer

network properties is needed to draw more robust and generalizable conclusions about the impact of different dynamic bonding mechanisms on chain dynamics. Inclusion of dynamic bonds that are activated by different of stimuli, over different temperature ranges, and in networks of a wider range of mechanical

Disulfide exchange[6-8]	Reversible Addition or Exchange Heat, radicals, bases, nucleophiles Wide temperature ranges
Transesterification[9]	Reversible Addition or Exchange Heat, radicals, bases, nucleophiles Wide temperature ranges
Urea-amine exchange[10]	Reversible Exchange Base/lewis acids > 150 °C
Aldehyde-amine condensation and imine exchange[11]	Reversible Exchange (primarily) as low as 37 °C, > 100 °C
Boronic/boronate ester condensation + hydroxyl exchange[12]	Reversible Addition or Exchange Acids Wide temperature ranges

Figure 8.4: Examples of dynamic networks that can be studied by dielectric analysis.

properties will build a more complete picture as to DEA as a tool for evaluating CANs. For instance, investigating vitrimers in the transition from their non-dynamic to dynamic states with increasing temperature. This is especially interesting for exploring differences between associative and dissociative networks that exhibit vitrimeric behavior. Some examples of common dynamic bonds are provided in **Figure 8.3**, this list is by was adapted from a more comprehensive lost compiled by Podgorski *et al*.[5] and is by no means exhaustive. These reactions include disulfide exchange reactions including those described in the thesis[6-8], transesterification[9], urea-amine exchange[10], imine exchange[11], and boronic exters[12]. Expanding into other types of dynamic polymers that single-phase amorphous polymers, such as composites with dynamic interfaces and liquid crystal elastomers.

8.3 References

1.   Kamps, J.; Soars, S.; Fairbanks, B. D.; Bowman, C. N., Photodisulfidation of Linear Disulfides and Alkenes: Reaction Scope and Kinetics (Submitted to Tetrahedron).

2.   Huang, S.; Shen, Y.; Bisoyi, H. K.; Tao, Y.; Liu, Z.; Wang, M.; Yang, H.; Li, Q., Covalent Adaptable Liquid Crystal Networks Enabled by Reversible Ring-Opening Cascades of Cyclic Disulfides. *Journal of the American Chemical Society* **2021,** *143* (32), 12543-12551.

3.   Tong, C.; Wondergem, J. A. J.; Heinrich, D.; Kieltyka, R. E., Photopatternable, Branched Polymer Hydrogels Based on Linear Macromonomers for 3D Cell Culture Applications. *ACS Macro Letters* **2020,** *9* (6), 882-888.

4.   Lowe, A. B.; Hoyle, C. E.; Bowman, C. N., Thiol-yne click chemistry: A powerful and versatile methodology for materials synthesis. *Journal of Materials Chemistry* **2010,** *20* (23), 4745-4750.

5.   Podgórski, M.; Fairbanks, B. D.; Kirkpatrick, B. E.; McBride, M.; Martinez, A.; Dobson, A.; Bongiardina, N. J.; Bowman, C. N., Toward Stimuli-Responsive Dynamic Thermosets through Continuous Development and Improvements in Covalent Adaptable Networks (CANs). *Advanced Materials* **2020,** *32* (20), 1906876.

6.   Chen, J.; Jiang, S.; Gao, Y.; Sun, F., Reducing volumetric shrinkage of photopolymerizable materials using reversible disulfide-bond reactions. *Journal of Materials Science* **2018,** *53* (23), 16169-16181.

7.   Matxain, J. M.; Asua, J. M.; Ruipérez, F., Design of new disulfide-based organic compounds for the improvement of self-healing materials. *Physical Chemistry Chemical Physics* **2016,** *18* (3), 1758-1770.

8.   Michal, B. T.; Jaye, C. A.; Spencer, E. J.; Rowan, S. J., Inherently Photohealable and Thermal Shape-Memory Polydisulfide Networks. *ACS Macro Letters* **2013,** *2* (8), 694-699.

9.   Montarnal, D.; Capelot, M.; Tournilhac, F.; Leibler, L., Silica-Like Malleable Materials from Permanent Organic Networks. *Science* **2011,** *334* (6058), 965-968.

10.   Erice, A.; Ruiz de Luzuriaga, A.; Matxain, J. M.; Ruipérez, F.; Asua, J. M.; Grande, H.-J.; Rekondo, A., Reprocessable and recyclable crosslinked poly(urea-urethane)s based on dynamic amine/urea exchange. *Polymer* **2018,** *145*, 127-136.

11.   Taynton, P.; Yu, K.; Shoemaker, R. K.; Jin, Y. H.; Qi, H. J.; Zhang, W., Heat- or Water-Driven Malleability in a Highly Recyclable Covalent Network Polymer. *Advanced Materials* **2014,** *26* (23), 3938-3942.

12.   Cash, J. J.; Kubo, T.; Bapat, A. P.; Sumerlin, B. S., Room-Temperature Self-Healing Polymers Based on Dynamic-Covalent Boronic Esters. *Macromolecules* **2015,** *48* (7), 2098-2106.

BIBLIOGRAPHY

1.   Giles Jr, H. F.; Mount III, E. M.; Wagner Jr, J. R., Extrusion: the definitive processing guide and handbook. William Andrew: 2004.

2.   Rosato, D. V.; Rosato, M. G., Injection molding handbook. Springer Science & Business Media: 2012.

3.   Parker, L. A Whopping 91 Percent of Plastic Isn't Recycled. https://www.nationalgeographic.org/article/whopping-91-percent-plastic-isnt-recycled/.

4.   Podgórski, M.; Fairbanks, B. D.; Kirkpatrick, B. E.; McBride, M.; Martinez, A.; Dobson, A.; Bongiardina, N. J.; Bowman, C. N., Toward Stimuli-Responsive Dynamic Thermosets through Continuous Development and Improvements in Covalent Adaptable Networks (CANs). Advanced Materials 2020, 32 (20), 1906876.

5.   Khan, A.; Ahmed, N.; Rabnawaz, M., Covalent Adaptable Network and Self-Healing Materials: Current Trends and Future Prospects in Sustainability. Polymers 2020, 12 (9), 2027.

6.   Kloxin, C. J.; Scott, T. F.; Adzima, B. J.; Bowman, C. N., Covalent Adaptable Networks (CANs): A Unique Paradigm in Cross-Linked Polymers. Macromolecules 2010, 43 (6), 2643-2653.

7.   Gandini, A., The furan/maleimide Diels–Alder reaction: A versatile click–unclick tool in macromolecular synthesis. Progress in Polymer Science 2013, 38 (1), 1-29.

8.   Chen, X.; Dam, M. A.; Ono, K.; Mal, A.; Shen, H.; Nutt, S. R.; Sheran, K.; Wudl, F., A Thermally Re-mendable Cross-Linked Polymeric Material. Science 2002, 295 (5560), 1698-1702.

9.   Chandross, E. A.; Ferguson, J.; McRae, E. G., Absorption and Emission Spectra of Anthracene Dimers. The Journal of Chemical Physics 1966, 45 (10), 3546-3553.

10.   Egerton, P. L.; Hyde, E. M.; Trigg, J.; Payne, A.; Beyton, P.; Mijovic, M. V.; Reiser, A., PhotocycloadditioninLiquidEthylCinnamateandinEthylCinnamateGlasses.ThePhotoreactionasaProbeintotheMicromorphologyoftheSolid. Journal of the American Chemical Society 1981, 103, 3859-3863.

11.   Jin, B.; Song, H.; Jiang, R.; Song, J.; Zhao, Q.; Xie, T., Programming a crystalline shape memory polymer network with thermo- and photo-reversible bonds toward a single-component soft robot. Science Advances 2018, 4 (1), eaao3865.

12.   Ying, H.; Zhang, Y.; Cheng, J., Dynamic urea bond for the design of reversible and self-healing polymers. Nature Communications 2014, 5 (1), 3218.

13.   Velankar, S.; Pazos, J.; Cooper, S. L., High-performance UV-curable urethane acrylates via deblocking chemistry. Journal of applied polymer science 1996, 62 (9), 1361-1376.

14.   Zhang, B.; Digby, Z. A.; Flum, J. A.; Chakma, P.; Saul, J. M.; Sparks, J. L.; Konkolewicz, D., Dynamic Thiol–Michael Chemistry for Thermoresponsive Rehealable and Malleable Networks. Macromolecules 2016, 49 (18), 6871-6878.

15.   Van Herck, N.; Maes, D.; Unal, K.; Guerre, M.; Winne, J. M.; Du Prez, F. E., Covalent Adaptable Networks with Tunable Exchange Rates Based on Reversible Thiol–yne Cross-Linking. Angewandte Chemie 2020, 132 (9), 3637-3646.

16.   Fenoli, C. R.; Wydra, J. W.; Bowman, C. N., Controllable Reversible Addition–Fragmentation Termination Monomers for Advances in Photochemically Controlled Covalent Adaptable Networks. Macromolecules 2014, 47 (3), 907-915.

17.   Sowan, N.; Cox, L. M.; Shah, P. K.; Song, H. B.; Stansbury, J. W.; Bowman, C. N., Dynamic Covalent Chemistry at Interfaces: Development of Tougher, Healable Composites through Stress Relaxation at the Resin-Silica Nanoparticles Interface. Advanced Materials Interfaces 2018, 5 (18).

18.   Montarnal, D.; Capelot, M.; Tournilhac, F.; Leibler, L., Silica-Like Malleable Materials from Permanent Organic Networks. Science 2011, 334 (6058), 965-968.

19.   Wang, C.; Mavila, S.; Worrell, B. T.; Xi, W. X.; Goldman, T. M.; Bowman, C. N., Productive Exchange of Thiols and Thioesters to Form Dynamic Polythioester-Based Polymers. Acs Macro Letters 2018, 7 (11), 1312-1316.

20.   Worrell, B. T.; Mavila, S.; Wang, C.; Kontour, T. M.; Lim, C. H.; McBride, M. K.; Musgrave, C. B.; Shoemaker, R.; Bowman, C. N., A user's guide to the thiol-thioester exchange in organic media: scope, limitations, and applications in material science. Polymer Chemistry 2018, 9 (36), 4523-4534.

21.   Worrell, B. T.; McBride, M. K.; Lyon, G. B.; Cox, L. M.; Wang, C.; Mavila, S.; Lim, C. H.; Coley, H. M.; Musgrave, C. B.; Ding, Y. F.; Bowman, C. N., Bistable and photoswitchable states of matter (vol 9, 2804, 2018). Nature Communications 2018, 9.

22.   Sowan, N.; Lu, Y.; Kolb, K.; Cox, L. M.; Long, R.; Bowman, C. N., Enhancing the toughness of composites via dynamic thiol–thioester exchange (TTE) at the resin–filler interface. Polymer Chemistry 2020.

23.   Lei, X. F.; Jin, Y. H.; Sun, H. L.; Zhang, W., Rehealable imide-imine hybrid polymers with full recyclability. Journal of Materials Chemistry A 2017, 5 (40), 21140-21145.

24.   Liu, Y. J.; Tang, Z. H.; Chen, Y.; Wu, S. W.; Guo, B. C., Programming dynamic imine bond into elastomer/graphene composite toward mechanically strong, malleable, and multi-stimuli responsive vitrimer. Composites Science and Technology 2018, 168, 214-223.

25.   Park, H. Y.; Kloxin, C. J.; Abuelyaman, A. S.; Oxman, J. D.; Bowman, C. N., Stress Relaxation via Addition-Fragmentation Chain Transfer in High T-g, High Conversion Methacrylate-Based Systems. Macromolecules 2012, 45 (14), 5640-5646.

26.   Park, H. Y.; Kloxin, C. J.; Abuelyaman, A. S.; Oxman, J. D.; Bowman, C. N., Novel dental restorative materials having low polymerization shrinkage stress via stress relaxation by addition-fragmentation chain transfer. Dental Materials 2012, 28 (11), 3-9.

27.   Park, H. Y.; Kloxin, C. J.; Fordney, M. F.; Bowman, C. N., Stress relaxation of trithiocarbonate-dimethacrylate-based dental composites. Dental Materials 2012, 28 (8), 888-893.

28.   Denissen, W.; Winne, J. M.; Du Prez, F. E., Vitrimers: permanent organic networks with glass-like fluidity. Chemical science 2016, 7 (1), 30-38.

29.   Taynton, P.; Ni, H. G.; Zhu, C. P.; Yu, K.; Loob, S.; Jin, Y. H.; Qi, H. J.; Zhang, W., Repairable Woven Carbon Fiber Composites with Full Recyclability Enabled by Malleable Polyimine Networks. Advanced Materials 2016, 28 (15), 2904-2909.

30.   Taynton, P.; Yu, K.; Shoemaker, R. K.; Jin, Y. H.; Qi, H. J.; Zhang, W., Heat- or Water-Driven Malleability in a Highly Recyclable Covalent Network Polymer. Advanced Materials 2014, 26 (23), 3938-3942.

31.   Zhu, C. P.; Xi, C.; Doro, W.; Wang, T. Y.; Zhang, X.; Jin, Y. H.; Zhang, W., Tuning the physical properties of malleable and recyclable polyimine thermosets: the effect of solvent and monomer concentration. Rsc Advances 2017, 7 (76), 48303-48307.

32.   Cui, C.; Chen, X.; Ma, L.; Zhong, Q.; Li, Z.; Mariappan, A.; Zhang, Q.; Cheng, Y.; He, G.; Chen, X.; Dong, Z.; An, L.; Zhang, Y., Polythiourethane Covalent Adaptable Networks for Strong and Reworkable Adhesives and Fully Recyclable Carbon Fiber-Reinforced Composites. ACS Applied Materials & Interfaces 2020, 12 (42), 47975-47983.

33.   Elling, B. R.; Dichtel, W. R., Reprocessable Cross-Linked Polymer Networks: Are Associative Exchange Mechanisms Desirable? ACS Central Science 2020, 6 (9), 1488-1496.

34.   Podgórski, M.; Mavila, S.; Huang, S.; Spurgin, N.; Sinha, J.; Bowman, C. N., Thiol–Anhydride Dynamic Reversible Networks. Angewandte Chemie International Edition 2020, 59 (24), 9345-9349.

35.   Podgórski, M.; Spurgin, N.; Mavila, S.; Bowman, C. N., Mixed mechanisms of bond exchange in covalent adaptable networks: monitoring the contribution of reversible exchange and reversible addition in thiol–succinic anhydride dynamic networks. Polymer Chemistry 2020, 11, 5365-5376.

36.   Cash, J. J.; Kubo, T.; Bapat, A. P.; Sumerlin, B. S., Room-Temperature Self-Healing Polymers Based on Dynamic-Covalent Boronic Esters. Macromolecules 2015, 48 (7), 2098-2106.

37.   Smithmyer, M. E.; Deng, C. C.; Cassel, S. E.; LeValley, P. J.; Sumerlin, B. S.; Kloxin, A. M., Self-Healing Boronic Acid-Based Hydrogels for 3D Co-cultures. ACS Macro Letters 2018, 7 (9), 1105-1110.

38.   Martin, R.; Rekondo, A.; Ruiz de Luzuriaga, A.; Cabañero, G.; Grande, H. J.; Odriozola, I., The processability of a poly(urea-urethane) elastomer reversibly crosslinked with aromatic disulfide bridges. Journal of Materials Chemistry A 2014, 2 (16), 5710-5715.

39.   Michal, B. T.; Jaye, C. A.; Spencer, E. J.; Rowan, S. J., Inherently Photohealable and Thermal Shape-Memory Polydisulfide Networks. ACS Macro Letters 2013, 2 (8), 694-699.

40.   Wedemeyer, W. J.; Welker, E.; Narayan, M.; Scheraga, H. A., Disulfide Bonds and Protein Folding. Biochemistry 2000, 39 (15), 4207-4216.

41.   Craig, D., The Vulcanization of Rubber with Sulfur. Rubber Chemistry and Technology 1957, 30 (5), 1291-1346.

42.   Green, M. S.; Tobolsky, A. V., A NEW APPROACH TO THE THEORY OF RELAXING POLYMERIC MEDIA. Journal of Chemical Physics 1946, 14 (2), 80-92.

43.   Takahashi, Y.; Tobolsky, A. V., Chemorheological study on natural rubber vulcanizates. Polymer Journal 1971, 2 (4), 457-467.

44.   Tobolsky, A.; MacKnight, W.; Takahashi, M., Relaxation of disulfide and tetrasulfide polymers. The Journal of Physical Chemistry 1964, 68 (4), 787-790.

45.   Matxain, J. M.; Asua, J. M.; Ruipérez, F., Design of new disulfide-based organic compounds for the improvement of self-healing materials. Physical Chemistry Chemical Physics 2016, 18 (3), 1758-1770.

46.   Pepels, M.; Filot, I.; Klumperman, B.; Goossens, H., Self-healing systems based on disulfide–thiol exchange reactions. Polymer Chemistry 2013, 4 (18), 4955-4965.

47.   Huang, S.; Shen, Y.; Bisoyi, H. K.; Tao, Y.; Liu, Z.; Wang, M.; Yang, H.; Li, Q., Covalent Adaptable Liquid Crystal Networks Enabled by Reversible Ring-Opening Cascades of Cyclic Disulfides. Journal of the American Chemical Society 2021, 143 (32), 12543-12551.

48.   Zhang, X.; Waymouth, R. M., 1,2-Dithiolane-Derived Dynamic, Covalent Materials: Cooperative Self-Assembly and Reversible Cross-Linking. Journal of the American Chemical Society 2017, 139 (10), 3822-3833.

49.   Liu, Y.; Jia, Y.; Wu, Q.; Moore, J. S., Architecture-Controlled Ring-Opening Polymerization for Dynamic Covalent Poly(disulfide)s. Journal of the American Chemical Society 2019, 141 (43), 17075-17080.

50.   Sakai, N.; Matile, S., Stack Exchange Strategies for the Synthesis of Covalent Double-Channel Photosystems by Self-Organizing Surface-Initiated Polymerization. Journal of the American Chemical Society 2011, 133 (46), 18542-18545.

51.   Choi, C.; Self, J. L.; Okayama, Y.; Levi, A. E.; Gerst, M.; Speros, J. C.; Hawker, C. J.; Read de Alaniz, J.; Bates, C. M., Light-Mediated Synthesis and Reprocessing of Dynamic Bottlebrush Elastomers under Ambient Conditions. Journal of the American Chemical Society 2021, 143 (26), 9866-9871.

52.   Tong, C.; Wondergem, J. A. J.; Heinrich, D.; Kieltyka, R. E., Photopatternable, Branched Polymer Hydrogels Based on Linear Macromonomers for 3D Cell Culture Applications. ACS Macro Letters 2020, 9 (6), 882-888.

53.   Suzuki, T.; Nambu, Y.; Endo, T., Radical Copolymerization of Lipoamide with Vinyl Monomers. Macromolecules 1989, 23, 1579-1582.

54.   Cramer, N. B.; Reddy, S. K.; O'Brien, A. K.; Bowman, C. N., Thiol− ene photopolymerization mechanism and rate limiting step changes for various vinyl functional group chemistries. Macromolecules 2003, 36 (21), 7964-7969.

55.   Cramer, N. B.; Davies, T.; O'Brien, A. K.; Bowman, C. N., Mechanism and modeling of a thiol− ene photopolymerization. Macromolecules 2003, 36 (12), 4631-4636.

56.   Ge, J.; Trujillo-Lemon, M.; Stansbury, J. W., A mechanistic and kinetic study of the photoinitiated cationic double ring-opening polymerization of 2-methylene-7-phenyl-1, 4, 6, 9-tetraoxa-spiro [4.4] nonane. Macromolecules 2006, 39 (26), 8968-8976.

57.   Kamps, J.; Soars, S.; Fairbanks, B. D.; Bowman, C. N., Photodisulfidation of Linear Disulfides and Alkenes: Reaction Scope and Kinetics (Submitted to Tetrahedron).

58.   Porath, L. E.; Evans, C. M., Importance of Broad Temperature Windows and Multiple Rheological Approaches for Probing Viscoelasticity and Entropic Elasticity in Vitrimers. Macromolecules 2021.

59.   Liu, W.; Schmidt, D. F.; Reynaud, E., Catalyst selection, creep, and stress relaxation in high-performance epoxy vitrimers. Industrial & Engineering Chemistry Research 2017, 56 (10), 2667-2672.

60.   Chen, M.; Zhou, L.; Wu, Y.; Zhao, X.; Zhang, Y., Rapid stress relaxation and moderate temperature of malleability enabled by the synergy of disulfide metathesis and carboxylate transesterification in epoxy vitrimers. ACS Macro Letters 2019, 8 (3), 255-260.

61.   Amamoto, Y.; Kamada, J.; Otsuka, H.; Takahara, A.; Matyjaszewski, K., Repeatable photoinduced self-healing of covalently cross-linked polymers through reshuffling of trithiocarbonate units. Angew Chem Int Ed Engl 2011, 50 (7), 1660-3.

62.   Jilani, W.; Mzabi, N.; Gallot-Lavallée, O.; Fourati, N.; Zerrouki, C.; Zerrouki, R.; Guermazi, H., Dielectric relaxations investigation of a synthesized epoxy resin polymer. The European Physics Journal Plus 2015, (130).

63.   Carrertero-Gonzalez, J.; Ezquerra, T. A.; Amnuaypornsri, S.; Toki, S.; Verdejo, R.; Sanz, A.; Sakdapipanich, J.; Hsiao, B. S.; López–Manchado, M. A., Molecular dynamics of natural rubber as revealed by dielectric spectroscopy: The role of natural cross–linking. Soft Matter 2010, (6), 3636-3642.

64.   Hernández, M.; Grande, A. M.; van der Zwaag, S.; García, S. J., Monitoring Network and Interfacial Healing Processes by Broadband Dielectric Spectroscopy: A Case Study on Natural Rubber. ACS Appl Mater Interfaces 2016, 8 (16), 10647-56.

65.   Lovell, L. G.; Berchtold, K.; Elliot, J. E.; Lu, H.; Bowman, C. N., Understanding the kinetics and network formation of dimethacrylate dental resins. Polym. Adv. Technol. 2001, 12 (6), 335-345.

66.   Tsangaris, G. M.; Psarras, G. C.; Kouloumbi, N., Electric modulus and interfacial polarization in composite polymeric systems. Journal of materials Science 1998, (33), 2027–2037.

67.   Yang, J.; Melton, M.; Sun, R.; Yang, W.; Cheng, S., Decoupling the Polymer Dynamics and the Nanoparticle Network Dynamics of Polymer Nanocomposites through Dielectric Spectroscopy and Rheology. Macromolecules 2020, 53 (1), 302-311.

68.   Tress, M.; Xing, K.; Ge, S.; Cao, P.; Saito, T.; Sokolov, A., What dielectric spectroscopy can tell us about supramolecular networks⋆. The European Physical Journal E 2019, 42 (10), 133.

69.   Zheng, N.; Xu, Y.; Zhao, Q.; Xie, T., Dynamic Covalent Polymer Networks: A Molecular Platform for Designing Functions beyond Chemical Recycling and Self-Healing. Chemical Reviews 2021, 121 (3), 1716-1745.

70.   Scheutz, G. M.; Lessard, J. J.; Sims, M. B.; Sumerlin, B. S., Adaptable Crosslinks in Polymeric Materials: Resolving the Intersection of Thermoplastics and Thermosets. Journal of the American Chemical Society 2019, 141 (41), 16181-16196.

71.   Podgórski, M.; Spurgin, N.; Mavila, S.; Bowman, C. N., Mixed mechanisms of bond exchange in covalent adaptable networks: monitoring the contribution of reversible exchange and reversible addition in thiol–succinic anhydride dynamic networks. Polymer Chemistry 2020.

72.   Long, K. F.; Wang, H.; Dimos, T. T.; Bowman, C. N., Effects of Thiol Substitution on the Kinetics and Efficiency of Thiol-Michael Reactions and Polymerizations. Macromolecules 2021.

73.   Long, K. F.; Bongiardina, N. J.; Mayordomo, P.; Olin, M. J.; Oretega, A. D.; Bowman, C. N., Effects of 1°, 2°, and 3° Thiols on Thiol–Ene Reactions: Polymerization Kinetics and Mechanical Behavior. Macromolecules 2020, 53 (14), 5805-5815.

74.   Fava, A.; Iliceto, A.; Camera, E., Kinetics of Thiol-Disulfide Exchange. Journal of the American Chemical Society 1957, 79, 833-838.

75.   Fairbanks, B. D.; Singh, S. P.; Bowman, C. N.; Anseth, K. S., Photodegradable, Photoadaptable Hydrogels via Radical-Mediated Disulfide Fragmentation Reaction. Macromolecules 2011, 44 (8), 2444-2450.

76.   Nevejans, S.; Ballard, N.; Fernández, M.; Reck, B.; Asua, J. M., Flexible aromatic disulfide monomers for high-performance self-healable linear and cross-linked poly(urethane-urea) coatings. Polymer 2019, 166, 229-238.

77.   Raeisi, M.; Tsarevsky, N. V., Radical ring-opening polymerization of lipoates: Kinetic and thermodynamic aspects. Journal of Polymer Science 2021, 59 (8), 675-684.

78.   Soars, S.; Bongiardina, N. J.; Fairbanks, B. D.; Podgórski, M.; Bowman, C. N., Spatial and Temporal Control of Photo Mediated Disulfide-Ene and Thiol-Ene Chemistries for Two-Stage Polymerizations. Macromolecules (Submitted) 2021.

79.   Podgórski, M.; Becka, E.; Claudino, M.; Flores, A.; Shah, P. K.; Stansbury, J. W.; Bowman, C. N., Ester-free thiol–ene dental restoratives—Part A: Resin development. Dental Materials 2015, 31 (11), 1255-1262.

80.   Kloxin, C. J.; Scott, T. F.; Bowman, C. N., Stress Relaxation via Addition-Fragmentation Chain Transfer in a Thiol-ene Photopolymerization. Macromolecules 2009, 42 (7), 2551-2556.

81.   Soars, S.; Bongiardina, N. J.; Podgórski, M.; Bowman, C. N., Spatial and Temporal Control of Photo Mediated Disulfide-Ene and Thiol-Ene Chemistries for Two-Stage Polymerizations (to be submitted).

82.   Podgórski, M.; Becka, E.; Claudino, M.; Flores, A.; Shah, P. K.; Stansbury, J. W.; Bowman, C. N., Ester-free thiol–ene dental restoratives—Part B: Composite development. Dental Materials 2015, 31 (11), 1263-1270.

83.   Zhang, G.; Zhao, Q.; Yang, L.; Zou, W.; Xi, X.; Xie, T., Exploring Dynamic Equilibrium of Diels–Alder Reaction for Solid State Plasticity in Remoldable Shape Memory Polymer Network. ACS Macro Letters 2016, 5 (7), 805-808.

84.   Capelot, M.; Montarnal, D.; Tournilhac, F.; Leibler, L., Metal-catalyzed transesterification for healing and assembling of thermosets. J Am Chem Soc 2012, 134 (18), 7664-7.

85.   Lei, Z. Q.; Xiang, H. P.; Yuan, Y. J.; Rong, M. Z.; Zhang, M. Q., Room-Temperature Self-Healable and Remoldable Cross-linked Polymer Based on the Dynamic Exchange of Disulfide Bonds. Chemistry of Materials 2014, 26 (6), 2038-2046.

86.   Wang, C.; Mavila, S.; Worrell, B. T.; Xi, W.; Goldman, T. M.; Bowman, C. N., Productive Exchange of Thiols and Thioesters to Form Dynamic Polythioester-Based Polymers. Acs Macro Letters 2018, 7 (11), 1312-1216.

87.   Dawson, P. E.; Muir, T. W.; Clark-Lewis, I.; Kent, S. B., Synthesis of proteins by native chemical ligation. Science 1994, 266 (5186), 776-9.

88.   Konieczynska, M. D.; Villa-Camacho, J. C.; Ghobril, C.; Perez-Viloria, M.; Tevis, K. M.; Blessing, W. A.; Nazarian, A.; Rodriguez, E. K.; Grinstaff, M. W., On-Demand Dissolution of a Dendritic Hydrogel-based Dressing for Second-Degree Burn Wounds through Thiol-Thioester Exchange Reaction. Angew Chem Int Ed Engl 2016, 55 (34), 9984-7.

89.   Ghobril, C.; Charoen, K.; Rodriguez, E. K.; Nazarian, A.; Grinstaff, M. W., A dendritic thioester hydrogel based on thiol-thioester exchange as a dissolvable sealant system for wound closure. Angew Chem Int Ed Engl 2013, 52 (52), 14070-4.

90.   Dobson, A. L.; Bongiardina, N. J.; Bowman, C. N., Combined Dynamic Network and Filler Interface Approach for Improved Adhesion and Toughness in Pressure-Sensitive Adhesives. ACS Applied Polymer Materials 2019, 2 (3), 1053-1060.

91.   Sowan, N.; Lu, Y.; Kolb, K.; Cox, L. M.; Long, R.; Bowman, C. N., Enhancing the toughness of composites via dynamic thiol–thioester exchange (TTE) at the resin–filler interface. Polymer Chemistry 2020, 11, 4760-4767.

92.   Li, Q.; Zhou, H.; Hoyle, C. E., The effect of thiol and ene structures on thiol–ene networks: Photopolymerization, physical, mechanical and optical properties. Polymer 2009, 8 (11).

93.   Long, K. F. B., N. J.; Mayordomo, P.; Olin, M. J.; Oretega, A. D.; Bowman, C. N., Effects of 1°, 2°, and 3° Thiols on Thiol–Ene Reactions: Polymerization Kinetics and Mechanical Behavior. Macromolecules 2020, 53 (14), 5805-5815.

94.   Long, K. F.; Wang, H.; Dimos, T. T.; Bowman, C. N., Effects of Thiol Substitution on the Kinetics and Efficiency of Thiol-Michael Reactions and Polymerizations. Macromolecules 2021, 54 (7), 3093-3100.

95.   Long, K. F.; Wang, H.; Dimos, T. T.; Bowman, C. N., The Effects Of Thiol Substitution On The Kinetics And Efficiency Of Thiol-Michael Reactions And Polymerizations. In Preparation, 2020.

96.   Carrertero-Gonzalez, J. E., T. A.; Amnuaypornsri, S.; Toki, S.; Verdejo, R.; Sanz, A.; Sakdapipanich, J.; Hsiao, B. S.; López–Manchado, M. A., Molecular dynamics of natural rubber as revealed by dielectric spectroscopy: The role of natural cross–linking. Soft Matter 2010, (6), 3636-3642.

97.   Carroll, B.; Cheng, S.; Sokolov, A. P., Analyzing the Interfacial Layer Properties in Polymer Nanocomposites by Broadband Dielectric Spectroscopy. Macromolecules 2017, 50 (16), 6149-6163.

98.   Gotro, J.; Yandrasits, M., Simultaneous dielectric and dynamic mechanical analysis of thermosetting polymers. Polymer Engineering & Science 1989, 29 (5), 278-284.

99.   Shepard, D. D.; Twombly, B., Simultaneous dynamic mechanical analysis and dielectric analysis of polymers. Thermochimica Acta 1996, 272, 125-129.

100.   Kremer, F.; Schönhals, A., Broadband dielectric spectroscopy. Springer Science & Business Media: 2002.

101.   Vassilikou-Dova, A.; Kalogeras, I. M., Dielectric analysis (DEA). Thermal analysis of polymers, fundamentals and applications 2009, 497-613.

102.   Sheridan, R. J.; Bowman, C. N., A Simple Relationship Relating Linear Viscoelastic Properties and Chemical Structure in a Model Diels–Alder Polymer Network. Macromolecules 2012, 45 (18), 7634-7641.

103.   Bongiardina, N. J.; Long, K. F.; Podgórski, M.; Bowman, C. N., Substituted Thiols in Dynamic Thiol–Thioester Reactions. Macromolecules 2021, 54 (18), 8341-8351.

104.   Porath, L. E.; Evans, C. M., Importance of Broad Temperature Windows and Multiple Rheological Approaches for Probing Viscoelasticity and Entropic Elasticity in Vitrimers. Macromolecules 2021, 54 (10), 4782-4791.

105.   Worrell, B. T.; McBride, M. K.; Lyon, G. B.; Cox, L. M.; Wang, C.; Mavila, S.; Lim, C. H.; Coley, H. M.; Musgrave, C. B.; Ding, Y. F.; Bowman, C. N., Bistable and photoswitchable states of matter. Nature Communications 2018, 9.

106.   Peterson, A. M.; Palmese, G. R., Reaction Kinetics and Thermodynamic Aspects of Thermoreversibly Cross-Linked Polymer Networks. Macromolecular Chemistry and Physics 2013, 214 (16), 1798-1805.

107.   Adzima, B. J.; Aguirre, H. A.; Kloxin, C. J.; Scott, T. F.; Bowman, C. N., Rheological and Chemical Analysis of Reverse Gelation in a Covalently Cross-Linked Diels−Alder Polymer Network. Macromolecules 2008, 41 (23), 9112-9117.

108.   Pratchayanan, D.; Yang, J.-C.; Lewis, C. L.; Thoppey, N.; Anthamatten, M., Thermomechanical insight into the reconfiguration of Diels–Alder networks. Journal of Rheology 2017, 61 (6), 1359-1367.

109.   Sorensen, P. A.; Kiil, S.; Dam-Johansen, K.; Weinell, C. E., Anticorrosive coatings: a review. Journal of Coatings Technology and Research 2009, 6 (2), 135-176.

110.   Moodley, K.; Mabaso, M.; Bahadur, I.; Redhi, G. G., Industrial application of ionic liquids for the recoveries of spent paint solvent. Journal of Molecular Liquids 2016, 219, 206-210.

111.   Xing, P. X.; Robertson, G. P.; Guiver, M. D.; Mikhailenko, S. D.; Wang, K. P.; Kaliaguine, S., Synthesis and characterization of sulfonated poly(ether ether ketone) for proton exchange membranes. Journal of Membrane Science 2004, 229 (1-2), 95-106.

112.   Subramanian, C.; Weiss, R. A.; Shaw, M. T., Electrospinning and characterization of highly sulfonated polystyrene fibers. Polymer 2010, 51 (9), 1983-1989.

113.   Vay, K.; Scheler, S.; Friess, W., Application of Hansen solubility parameters for understanding and prediction of drug distribution in microspheres. International Journal of Pharmaceutics 2011, 416 (1), 202-209.

114.   Flory, P. J., Thermodynamics of high polymer solutions. Journal of Chemical Physics 1942, 10 (1), 51-61.

115.   Huggins, M. L., Some properties of solutions of long-chain compounds. Journal of Physical Chemistry 1942, 46 (1), 151-158.

116.   Fredenslund, A.; Jones, R. L.; Prausnitz, J. M., GROUP-CONTRIBUTION ESTIMATION OF ACTIVITY-COEFFICIENTS IN NONIDEAL LIQUID-MIXTURES. Aiche Journal 1975, 21 (6), 1086-1099.

117.   Sanchez, I. C.; Lacombe, R. H., ELEMENTARY MOLECULAR THEORY OF CLASSICAL FLUIDS - PURE FLUIDS. Journal of Physical Chemistry 1976, 80 (21), 2352-2362.

118.   Sanchez, I. C.; Lacombe, R. H., STATISTICAL THERMODYNAMICS OF POLYMER-SOLUTIONS. Macromolecules 1978, 11 (6), 1145-1156.

119.   Sato, Y.; Fujiwara, K.; Takikawa, T.; Sumarno; Takishima, S.; Masuoka, H., Solubilities and diffusion coefficients of carbon dioxide and nitrogen in polypropylene, high-density polyethylene, and polystyrene under high pressures and temperatures. Fluid Phase Equilibria 1999, 162 (1-2), 261-276.

120.   Huang, S. H.; Radosz, M., EQUATION OF STATE FOR SMALL, LARGE, POLYDISPERSE, AND ASSOCIATING MOLECULES. Industrial & Engineering Chemistry Research 1990, 29 (11), 2284-2294.

121.   Lacombe, R. H.; Sanchez, I. C., STATISTICAL THERMODYNAMICS OF FLUID MIXTURES. Journal of Physical Chemistry 1976, 80 (23), 2568-2580.

122.   Chapman, W. G., PREDICTION OF THE THERMODYNAMIC PROPERTIES OF ASSOCIATING LENNARD-JONES FLUIDS - THEORY AND SIMULATION. Journal of Chemical Physics 1990, 93 (6), 4299-4304.

123.   Hansen, C. M., UNIVERSALITY OF SOLUBILITY PARAMETER. Industrial & Engineering Chemistry Product Research and Development 1969, 8 (1), 2-&.

124.   Barton, A. F. M., SOLUBILITY PARAMETERS. Chemical Reviews 1975, 75 (6), 731-753.

125.   Venkatram, S.; Kim, C.; Chandrasekaran, A.; Ramprasad, R., Critical Assessment of the Hildebrand and Hansen Solubility Parameters for Polymers. Journal of Chemical Information and Modeling 2019, 59 (10), 4188-4194.

126.   Hildebrand, J. a. S., R.L, The Solubility of Nonelectrolytes. 3rd ed.; Reinhold Pub Corp.: New York, 1950.

127.   Hansen, C. M., Hansen Solubility Parameter a User's Handbook 2nd ed.; CRC Press: Boca Raton, 2007.

128.   Miller-Chou, B. A.; Koenig, J. L., A review of polymer dissolution. Progress in Polymer Science 2003, 28 (8), 1223-1270.

129.   Hansen, C. M., The three dimensional solubility parameter-key to paint component affinities: II. Dyes, emulsifiers, mutual solubility and compatibility, and pigments, . J. Paint Technol 1967, 39 (511), 505-510.

130.   Hansen, C. M., The three dimensional solubility parameter-key to paint component affinities: III. Independent calculation of the parameters components J. Paint Technol. 1967, 39 (511), 511-514.

131.   Hansen, C. M., The three dimensional solubility parameter-key to paint component affinities I. Solvents, plasticizers, polymers, and resins J. Paint Technol 1967, 39 (505), 104-117.

132.   HrnjakMurgic, Z.; Jelencic, J.; Bravar, M.; Marovic, M., Influence of the network on the interaction parameter in system EPDM vulcanizate-solvent. Journal of Applied Polymer Science 1997, 65 (5), 991-999.

133.   Ferrell, W. H.; Kushner, D. I.; Hickner, M. A., Investigation of Polymer-Solvent Interactions in Poly(styrene sulfonate) Thin Films. Journal of Polymer Science Part B-Polymer Physics 2017, 55 (18), 1365-1372.

134.   Sanchez, I. C., RELATIONSHIPS BETWEEN POLYMER INTERACTION PARAMETERS. Polymer 1989, 30 (3), 471-475.

135.   Jankovic, S.; Tsakiridou, G.; Ditzinger, F.; Koehl, N. J.; Price, D. J.; Ilie, A.-R.; Kalantzi, L.; Kimpe, K.; Holm, R.; Nair, A.; Griffin, B.; Saal, C.; Kuentz, M., Application of the solubility parameter concept to assist with oral delivery of poorly water-soluble drugs - a PEARRL review. Journal of Pharmacy and Pharmacology 2019, 71 (4), 441-463.

136.   Liu, Y.; Shi, B., Determination of Flory interaction parameters between polyimide and organic solvents by HSP theory and IGC. Polymer Bulletin 2008, 61 (4), 501-509.

137.   Segarceanu, O.; Leca, M., Improved method to calculate Hansen solubility parameters of a polymer. Progress in Organic Coatings 1997, 31 (4), 307-310.

138.   Bustamante, P.; Navarro-Lupion, J.; Escalera, B., A new method to determine the partial solubility parameters of polymers from intrinsic viscosity. European Journal of Pharmaceutical Sciences 2005, 24 (2-3), 229-237.

139.   Ovejero, G.; Perez, P.; Romero, M. D.; Guzman, I.; Diez, E., Solubility and Flory Huggins parameters of SBES, poly(styrene-b-butene/ethylene-b-styrene) triblock copolymer, determined by intrinsic viscosity. European Polymer Journal 2007, 43 (4), 1444-1449.

140.   Bahar, I.; Erbil, H. Y.; Baysal, B. M.; Erman, B., DETERMINATION OF POLYMER SOLVENT INTERACTION PARAMETER FROM SWELLING OF NETWORKS - THE SYSTEM POLY(2-HYDROXYETHYL METHACRYLATE)-DIETHYLENE GLYCOL. Macromolecules 1987, 20 (6), 1353-1356.

141.   Marzocca, A. J., Evaluation of the polymer-solvent interaction parameter chi for the system cured styrene butadiene rubber and toluene. European Polymer Journal 2007, 43 (6), 2682-2689.

142.   Marzocca, A. J.; Rodriguez Garraza, A. L.; Mansilla, M. A., Evaluation of the polymer-solvent interaction parameter chi for the system cured polybutadiene rubber and toluene. Polymer Testing 2010, 29 (1), 119-126.

143.   Chu, H. Z.; Liu, D.; Cui, Z. W.; Wang, K.; Qiu, G. X.; Liu, G. Y., Effect of crosslink density on solubility parameters of styrene butadiene rubber and the application in pre-screening of new potential additives. Polymer Testing 2020, 81.

144.   Atta, A. M.; El-Ghazawy, R. A. M.; Farag, R. K.; Abdel-Azim, A. A.-A., Swelling and network parameters of oil sorbers based on alkyl acrylates and cinnamoyloxy ethyl methacrylate copolymers. Journal of Polymer Research 2006, 13 (4), 257-266.

145.   Yagi, Y.; Inomata, H.; Saito, S., SOLUBILITY PARAMETER OF AN N-ISOPROPYLACRYLAMIDE GEL. Macromolecules 1992, 25 (11), 2997-2998.

146.   Mah, C. H.; Wu, Q.; Deen, G. R., Effect of nature of chemical crosslinker on swelling and solubility parameter of a new stimuli-responsive cationic poly(N-acryloyl-N'-propyl piperazine) hydrogel. Polymer Bulletin 2018, 75 (1), 221-238.

147.   Bentz, K. C.; Walley, S. E.; Savin, D. A., Solvent effects on modulus of poly(propylene oxide)-based organogels as measured by cavitation rheology. Soft Matter 2016, 12 (22), 4991-5001.

148.   Gao, J.; Wu, S.; Rogers, M. A., Harnessing Hansen solubility parameters to predict organogel formation. Journal of Materials Chemistry 2012, 22 (25), 12651-12658.

149.   Akalp, U.; Chu, S.; Skaalure, S. C.; Bryant, S. J.; Doostan, A.; Vernerey, F. J., Determination of the polymer-solvent interaction parameter for PEG hydrogels in water: Application of a self learning algorithm. Polymer 2015, 66, 135-147.

150.   Song, H. B.; Baranek, A.; Worrell, B. T.; Cook, W. D.; Bowman, C. N., Photopolymerized Triazole-Based Glassy Polymer Networks with Superior Tensile Toughness. Advanced Functional Materials 2018, 28 (22), 9.

151.   Flory, P. J., Principles of polymer chemistry. Cornell University Press: 1953.

152.   A.L. Companion , S. E., Chemical Bonding. Secoond ed.; McGraw-Hill Inc.: 1979.

153.   Adamska, K.; Voelkel, A., Hansen solubility parameters for polyethylene glycols by inverse gas chromatography. Journal of Chromatography A 2006, 1132 (1-2), 260-267.

154.   Sudduth, R. D., A review of the similarities and differences between five different polymer-solvent interaction coefficients. Pigment & Resin Technology 2013, 42 (6), 394-405.

155.   Kim, C.; Chandrasekaran, A.; Huan, T. D.; Das, D.; Ramprasad, R., Polymer Genome: A Data-Powered Polymer Informatics Platform for Property Predictions. The Journal of Physical Chemistry C 2018, 122 (31), 17575-17585.

156.   Chandrasekaran, A.; Kim, C.; Venkatram, S.; Ramprasad, R., A Deep Learning Solvent-Selection Paradigm Powered by a Massive Solvent/Nonsolvent Database for Polymers. Macromolecules 2020, 53 (12), 4764-4769.

157.   Himanen, L.; Geurts, A.; Foster, A. S.; Rinke, P., Data-driven materials science: status, challenges, and perspectives. Advanced Science 2019, 6 (21), 1900808.

158.   Sakurada, I.; Nakajima, A.; Fujiwara, H., VAPOR PRESSURES OF POLYMER SOLUTIONS .2. VAPOR PRESSURE OF THE POLY(VINYL ALCOHOL)-WATER SYSTEM. Journal of Polymer Science 1959, 35 (129), 497-505.

159.   Peppas, N. A.; Merrill, E. W., DETERMINATION OF INTERACTION PARAMETER-CHI-1 FOR POLYVINYL-ALCOHOL) AND WATER IN GELS CROSSLINKED FROM SOLUTIONS. Journal of Polymer Science Part a-Polymer Chemistry 1976, 14 (2), 459-464.

160.   Lowe, A. B.; Hoyle, C. E.; Bowman, C. N., Thiol-yne click chemistry: A powerful and versatile methodology for materials synthesis. Journal of Materials Chemistry 2010, 20 (23), 4745-4750.

161.   Chen, J.; Jiang, S.; Gao, Y.; Sun, F., Reducing volumetric shrinkage of photopolymerizable materials using reversible disulfide-bond reactions. Journal of Materials Science 2018, 53 (23), 16169-16181.

162.   Erice, A.; Ruiz de Luzuriaga, A.; Matxain, J. M.; Ruipérez, F.; Asua, J. M.; Grande, H.-J.; Rekondo, A., Reprocessable and recyclable crosslinked poly(urea-urethane)s based on dynamic amine/urea exchange. Polymer 2018, 145, 127-136.